THE UNIVERSITY
of EDINBURGH

Cortical circuit and behavioural pathophysiology in rodent models of *SYNGAP1* haploinsufficiency

Danai Katsanevaki, BSc, MSc

A thesis submitted for the degree of Doctor of Philosophy
at the University of Edinburgh

September 2017

Declaration

This work was carried out in the Centre for Integrative Physiology, School of Biomedical Sciences at the University of Edinburgh. I hereby declare that this thesis is entirely my own work, with the exception of the following:

- Ms Joanna Smith and Ms Natasha Anstey contributed to data collection for some of the spontaneous exploration tasks or the 3-chamber task; data analysis was performed by the author.
- Matlab and Python scripts used for two-photon analysis were written and developed by members of the Rochefort lab. Some alterations have been made by the author to fit specific analysis needs.
- Statistical analysis using mixed models used for analysis of grouped two-photon data was developed and performed by Dr. Owen Dando.
- Mr Mark Patrizio often carried out genotyping for the mouse mutant lines. Later on, all genotyping was processed externally by Transnetyx, Inc, USA.
- All contributions from colleagues, such as experiments, figures and diagrams are explicitly referenced in the text.

The work in this thesis has not been submitted for any other degree or professional qualification.

Signed ……. Date…….....

Acknowledgements

First and foremost, I would like to thank my two supervisors Peter Kind and Nathalie Rochefort for allowing me to pursue projects that I found most interesting. Peter, thank you for your patience, support and continuous enthusiasm for research. I greatly appreciate the commitment to your students, your willingness to collaborate and share ideas and your confidence in my abilities, especially when I did not have any. Nathalie, thank you for your encouragement and attention to detail, which has pushed me to perform better experiments every time.

I would also like to thank Oliver Hardt who taught me how to do behaviour. I will always be grateful for your guidance and the long conversations which started with behaviour and usually ended up discussing sociology or evolution. Furthermore, thank you Emma Wood for always being there when I had questions, helping me with behaviour planning and sharing the equipment of your lab. Thank you, David Wyllie, for your always level headed comments; I do greatly appreciate all your detailed feedback that has been a big contributor to my continuous effort to improve my critical thinking and presentation skills. I would also like to acknowledge Edinburgh Neuroscience. With your generosity, I was able to visit Dr. Albrecht Stroh's lab in Germany and learn how to perform the initial *in vivo* experiments. Regarding my time in Mainz, I would like to thank Albrecht who welcomed me in his lab and all his lab members who taught me surgeries and helped me along the way.

I thank my friends and co-workers in the Kind and Rochefort lab (and adjacent labs-since we are a big happy family) for their support, energy, and good humour. In particular, I would like to thank Sally Till, Sam Booker, Evelyn Dylda, Antonis Asiminas, Janelle Pakan, Adam Jackson, and Aleks Domanski for all the hands-on help along the way. Thank you, Joanna Smith, for helping me run some of the really, really long behaviour. Thank you Owen Dando for spending so much time developing and running mixed models for my data. Especially when you had to do it again (and again, and again) every time something changed. Furthermore, thank you Christina McClure, Stephanie Barnes, Sophie Thomson, Sarah Scullion, Sang Soo Seo, Mel

Chiang, Susana Louros, Melania Muscas, Max Whittaker, Philip Hasel, Sean McKay, Sonal Kedia, Liz Davenport, Anna Toft, Jini Basu, Lindsay Mizen, Katie Marwick, Natasha Anstey and Laura Oliveira (phew!) for all the fun around the labs. And thank you Laura Butterworth for your never-ending encouragement and friendship.

A very special thank you to Kevin and my sister, Mara, for their tremendous support and patience the last years. I am indeed very lucky. And my parents, Despoina and Yiannis, for always allowing me to do whatever I (stubbornly) pursued and never doubting me… even though they did not agree with (most of) my decisions. Finally, to Marc-Andre, who I can't thank in person, your friendship is something I will forever cherish.

Scientific Abstract

SYNGAP1 haploinsufficiency is one of the most common monogenic causes of nonsyndromic moderate to severe intellectual disability (NSID) and autism (Hamdan *et al*., 2009; Pinto *et al*., 2010). *De novo* truncating or frameshift mutations in the *SYNGAP1* gene lead to the loss of the encoded protein *Syn*aptic *G*TPase *a*ctivating *p*rotein (SynGAP), one of the most abundant of postsynaptic proteins (Hamdan *et al*., 2011). SynGAP, present at excitatory and inhibitory synapses (Kim *et al*., 1998), acts as a key regulator of highly conserved signaling pathways linked to AMPA- and NMDA-receptor dependent plasticity at the post synaptic density (Krapivisky *et al*., 2004; Vazquez *et al*., 2004).

The *Syngap* mouse model has been extensively used to understand the pathophysiology underlying abnormal SynGAP-mediated signaling. *Syngap* heterozygous (het) mice demonstrate a range of physiological and behavioural abnormalities from development to adulthood (Komiyama *et al.,* 2002; Muhia *et al.,* 2010). However, recent advances in techniques for genome manipulation have allowed for the generation of rat models of neurodevelopmental disorders, including *Syngap*; enabling phenotypes to be validated across species and to address cognitive and social dysfunction, using paradigms that are more difficult to assess in mice.

In this study, we examined the pathophysiology associated with a heterozygous deletion of the C2 and catalytic GAP domain of the protein, in Long-Evans rats (het). In contrast with het mice, het rats do not present with hyperactivity and can be habituated to an open field environment. To examine associative recognition memory, we tested the rats in five spontaneous exploration tasks for short-term and long-term memory, object-recognition (OR), object-location (OL), object-place (OP), object-context (OC) and object-place-context (OPC). Both groups were able to perform short-term memory tasks, but only wild type rats performed above chance in OL with a 24hour delay, suggesting deficits in long- term spatial memory. We also tested if partial loss of the GAP domain in SynGAP affects social behaviour in rats and we found that het rats exhibited impaired short- term social memory, with no signs of

social isolation. These findings do not fully recapitulate previous abnormalities reported in the mouse model of *SYNGAP1* haploinsufficiency, suggesting that some key behavioural phenotypes may be species-specific.

Furthermore, based on physiological deficits that *Syngap* het mice exhibit, such as alterations in mEPSC/mIPSC amplitude and frequency and evoked cortical hyperexcitability *in vitro* (Guo *et al.,* 2009; Ozkan *et al.,* 2014), we also aimed to test if *in vivo* neuronal activity and circuit properties are altered. Using two-photon calcium imaging in awake mice, we focused on two areas of the cortex; a primary sensory area, the binocular region of the visual cortex (V1), and an association area, the medial posterior parietal cortex (PPC). Both areas have been found to maintain activity during visual discrimination tasks but to present with divergent activity trajectories (Harvey *et al*., 2012; Goard *et al*., 2016). We found preliminary evidence that neurons in layer 2-3 of the PPC of *Syngap* mice are hypoactive in basal conditions when animals are still in the dark, compared to wild type controls. When we assessed whether that changes when animals are running, we found that during locomotion neurons of both genotypes increase their activity, consistent with previous findings in wild type mice (McGinley *et al*., 2015; Pakan *et al*., 2016). However, this response gain is exaggerated in *Syngap* het neurons of the PPC. In contrast to above findings in PPC, results in V1 show that layer 2-3 neurons are hyperactive during both behavioural states, suggesting seemingly different computations of these two cortical areas.

This work provides the first evidence for a dysregulated neuronal circuit *in vivo* in both visual and parietal cortex of *Syngap* mice, two areas critical for sensory processing that has been found to be affected in individuals with NSID and autism (Joosten and Bundy, 2010). We also provide first evidence of the effect of loss of SynGAP activity in behaviour of rats, complimenting existing data in the literature in a species-specific manner and providing greater insight into sensory and cognitive dysfunction associated with dysregulation in SynGAP-mediated signaling.

Lay Summary

The human brain consists of hundreds of billions of neurons and non-neuronal cells which play a crucial role in the sensory, cognitive and social experiences that shape us. Neuronal cells in the brain process and transmit information in the form of electrical signals, through specialised junctions called synapses. Mutations that cause neurodevelopmental disorders are often found in genes composing proteins that regulate synaptic function. One such protein, *Syn*aptic *G*TPase *a*ctivating *p*rotein (SynGAP), is the study of this thesis. Several mutations in the gene that encodes SynGAP are found to cause intellectual disability, comorbid with autism and childhood epilepsy.

Due to their sporadic nature and clinical importance, mutations that cause the loss of SynGAP have been studied using the mouse model of the disorder that lacks the same protein as affected humans. One major part of research so far has focused on the structure and function of the synapses themselves, in brain slices taken from the animals. However, less is known about the activity of the affected neurons in the intact brain. In this thesis, we monitored the activity of entire neuronal cell populations in different areas of the brain, in real time, in awake animals. We found changes in the activity of cells in multiple brain areas of the Syngap mouse that are involved in behaviours associated with sensory processing and decision making.

A second part of the research in the field has been focusing on behavioural modeling of the disorder in the mouse. However, recent technological advancements have made it possible to generate rat models of neurodevelopmental disorders. Rats are larger, have more flexible behaviours and are the preferred animal model used by pharmaceutical companies as they respond to drugs in a more similar way to humans. We found that some behavioural phenotypes, such as cognitive impairments in long-term spatial memory and social memory, are also present in the Syngap rat. However, other core phenotypes such as hyperactivity are not shared between mice and rats, suggesting species-specific differences.

Overall this work highlights important findings in both the mouse and the rat model of loss of SynGAP, that will provide valuable knowledge for future work on understanding underlying mechanisms of neurodevelopmental disorders and potentially developing precise pharmacological interventions to help alleviate symptoms in human patients.

Contents

List of figures

List of tables

Abbreviations

(h)Syn	(human) Synapsin
3CT	3-chamber task
AAV	Adeno-associated virus
AC	Auditory cortex
Ach	Acetylcholine
AIC	Akaike's information goodness-of-fit criterion
AMPAR	A-amino-3-hydroxy-5-methyl-4-isoxazolepropionic acid receptor
ASD	Autism spectrum disorders
BIC	Bayesian information goodness-of-fit criterion
BLA	Basolateral amygdala
C2	Protein kinase C conserved
CaMKII	calcium/calmodulin-dependent protein kinase II
CaN	Calcineurin
ChR2	Channelrhodopsin-2
CNV	Copy number variation
CS	Conditioned stimulus
DBD	Developmental brain disorders
DDD	Deciphering developmental disorders
DG	Dentate gyrus
DHPG	(S)-3,5-Dihydroxyphenylglycine
DSI	Direction selectivity index
ECoG	Optical encephalogram
E/I	Excitation/Inhibition
EE	Epileptic encephalopathy
EEG	Electroencephalogram
eF-1a	Elongation factor – 1 alpha
Fmr1	Fragile X mental retardation 1 gene
FMRP	Fragile X mental retardation protein
FOV	Field of view
FXS	Fragile X Syndrome
GABAR	Gamma-aminobutyric acid receptor
GABRA2	Gamma-aminobutyric acid type A receptor Alpha-2 subunit gene
GCaMP	Genetically encoded calcium indicators (or GECI)
GLMM	Generalised linear mixed model
$H_{(n)}$	Habituation

HC	Hippocampus
I/O	Input/output relationship
ICA	Principle component analysis
ID	Intellectual disability
ILA	Infralimbic area of mPFC
IP3	Inositol triphosphate
IQ	Intelligence quotient
ITI	Inter-trial interval
LA	Lateral amygdala
LMI	Locomotion modulation index
LMM	Linear mixed model
LTD	Long-term depression
LTP	Long-term potentiation
MAPK	Mitogen-activated protein kinase
mEPSC	miniature excitatory postsynaptic currents
mGluR	Metabotropic glutamate receptor
mIPSC	miniature inhibitory postsynaptic currents
mPFC	medial Prefrontal cortex
MUPP1	Multi-PDZ domain protein 1
MWM	Morris watermaze
NAc	Nucleus accumbens
nAchR	Nicotinic acetylcholine receptor
NDD	Neurodevelopmental disorders
NE	North-East
NF1	Neurofibromatosis type-1 gene
NMDAR	N-methyl-D-aspartate receptor
NOR	Novel object recognition
NSID	Nonsyndromic intellectual disability
NW	North-West
OC	Object-context
OF	Open field
OGB1-AM	Oregon-Green 488 Bapta AM
OL	Object location
OP	Object-place
OPC	Object-place-context
OSI	Orientation selectivity index
PET	Positron emission tomography

PFC	Prefrontal cortex
PH	Pleckstrin homology
phMRI	Pharmacological magnetic resonance imaging
PI3K	Phosphoinositide 3-kinase
PKA	Protein kinase A
PKC	Protein kinase C
PL	Prelimbic area of mPFC
PLC	Phospholipase C
PMT	Photomultiplier tube
PPC	Posterior parietal cortex
PPI	Pre-pulse inhibition
PSD	Postsynaptic density
PSD-95	Postsynaptic density protein 95 (or SAP90)
PV	Parvalbumin
RL	Rostromedial parietal cortex
RM	Reference memory
ROI	Region of interest
rsfMRI	Resting-state functional magnetic resonance imaging
S1	Somatosensory area 1
SAP102	Synapse-associated protein 102
SCZ	Schizophrenia
SE	South-East
SF	Spatial frequency
SSp	Somatosensory cortex
SST	Somatostatin (or SOM)
st-fMRI	Stimulus-induced functional magnetic resonance imaging
SW	South-West
SynGAP	Synaptic GTPase activating protein
tdTom	tdTomato, a red fluorescent protein
TF	Temporal frequency
TSC1/2	Tuberous sclerosis-1/2 gene
US	Unconditioned stimulus
USVs	Ultrasonic vocalisations
V1	Primary visual cortex
VIP	Vasoactive-intestinal peptide
VSD	Voltage sensitive dye
VTA	Ventral tegmental area

Chapter 1

Introduction

1.1 Intellectual Disability

There has been a growing appreciation in recent years for the importance of identifying and treating causes of genetic disorders of childhood neurodevelopment. While the discovery of predominately phenotype-driven monogenic mutations associated with neurodevelopmental disorders has increased dramatically, there are still many cases where the underlying genetic cause is unknown. However, the introduction of studies of copy number variation (Itsara *et al*., 2009; Mefford *et al*., 2009) and whole exome sequencing of the human genome (O'Roak *et al*., 2011; Iossifov *et al*., 2012; Chahrour *et al*., 2012), have increased the number of identified single genes associated with cognitive and behavioural dysfunction (Barkovich *et al*., 2005).

A genotype-driven project which started in the UK recruiting children with severe and extreme developmental phenotypes for systematic genomic analysis (Firth & Wright, 2011; Fitzgerald *et al*., 2014), called Deciphering Developmental Disorders (DDD) project recently identified another 12 novel genes associated with neurodevelopmental disorders by screening 1133 affected children. The inclusion criteria for the DDD study have been neurodevelopmental disorder, congenital anomalies, abnormal growth parameters, dysmorphic features, unusual behavioural phenotypes and currently unknown genetic disorders of significant impact (Firth & Wright, 2011). In addition, another database has been recently developed which includes neuropsychiatric disorders of the brain that result from neuronal dysfunctions in early life (Mirzaa *et al*., 2014). This has been defined as the developmental brain disorders database (DBDB) and it includes numerous genes associated with the most common developmental brain disorders (DBDs); intellectual disability (ID), autism spectrum disorders (ASD), schizophrenia (SCZ), and childhood epilepsy. Nonetheless, while more and more mutations in single genes are being discovered, multigenic causes due to combinatorial factors, i.e. in cases when disease results from combined mutations in more than one gene, are still poorly understood due to the lack of extensive datasets acquired from populations of typical individuals and the lack of effective deep sequencing analysis to handle such datasets.

Intellectual disability (ID), is a complex neurodevelopmental disorder that is characterised by substantial cognitive impairment and has estimated prevalence of 1-3% in Western countries (Leonard & Wen, 2002; Ropers, 2010). With onset of manifestation usually in childhood (Save, 2000), it represents the most frequent cause of handicap in children, contributing to overall low levels of cognition, motor skills and adaptive functions, such as language, communication and social abilities (Ropers, 2008; Van Bokhoven, 2011).

1.1.1 Diagnosis and Symptoms of Intellectual Disability

Clinical diagnosis of ID has been based on standardised intelligence testing in early childhood. Intelligence quotient (IQ) of two standard deviations below the general population mean (IQ<70) accompanied with significant deficits of adaptive and functional skills has historically been characterised as ID. Severity classes based on IQ range from mild to profound; 50-69 for mild, 35-49 for moderate, 20-34 for severe and IQ<20 for profound. Recently, according to the DSM-5 (Diagnostic and Statistical Manual of Mental Disorders; American Psychiatric Association, 2013) criteria for ID has now been revised and severity is based on assessment of conceptual, social and practical deficits, to encourage a more comprehensive view of the individual. Other diagnostic criteria include childhood developmental delays, such as speech and motor (National Academies of Sciences, Engineering and Medicine, 2015), and evidence that the mental manifestations began before adulthood (van Bokhoven, 2011).

Typically, ID coexists with other psychiatric symptoms, such as ASD, epilepsy, cerebral palsy, hyperactivity, attention-deficit, motor coordination and control disorders, anxiety, sleep disorders and abnormal responses to sensory stimuli (Huguet *et al*., 2013). In fact, more than 40% of patients with mild to severe ID have met diagnostic criteria for other disorders, with significantly increased rates of ASD, attention deficit, as well as other psychiatric problems, such as schizophrenia and depression (Gillberg *et al*., 1986; Bouras, 1999l; Simonoff *et al*., 2008). Incidence of

epilepsy amongst the ID population is also very high, ranging from 16 to 50% (van Blarikom *et al*., 2006).

Despite the prevalence of ID within the general population it is very difficult to provide successful therapeutic interventions, mainly due to lack of understanding, the variability and the complexity of the underlying mechanisms causing ID. Treatments generally can be classified in the following categories (National Academies of Sciences, Engineering and Medicine, 2015):

> Early cognitive and behavioural treatment, through several strategies such as special education programs, human development training, habilitation and life skills training (Dulcan & Kaplan, 2006; Harris, 2006).
>
> Treatment to reduce medical symptoms, for eg. diet restrictions for patients that have phenylketonuria (Fitzgerald *et al*., 2000).
>
> Treatment to alleviate comorbid physical and psychiatric disorders with the aim to improve quality of life of the patient, such as medication with antidepressants, antipsychotics or anxiolytics (Harris, 2006).
>
> Targeted therapy, such as pharmacological trials on children with Fragile X Syndrome (FXS), the most common inherited form of ID and autism (Berry-Kravis, 2014; Hagerman & Polussa, 2015).

1.1.2 Causes and underlying genetics of Intellectual Disability

The wide span of symptoms can be explained by the variable causes, penetrance and expressivity of ID. Indeed, heterogeneity of aetiological factors can be attributed to genetic (single gene mutations or interactions with other genes, aneuploidies, microdeletions), environmental (eg. exposure to toxic substances, brain radiation,

infections, fetal alcohol syndrome), and epigenetic causes (Chelly & Mandel, 2001; San Martín & Pagani, 2014).

Genetic factors play a major role in ID; Inlow & Restifo in 2004 proposed 282 ID-contributing genes, and ever since this number has increased to estimations of about a 1000 (Van Bokhoven, 2011). Genetic forms of ID are divided into two main categories:

> *Syndromic ID* coexisting with physical, clinical and metabolic features, for eg. Tuberous schlerosis, Fragile X syndrome, neurofibromatosis.
>
> *Nonsyndromic ID* (NSID) with no other co-morbid clinical manifestation, for eg. mutations in *SYNGAP1*, *STXBP1*, *SHANK3*.

A significant gender bias has been reported based on epidemiological evidence. A greater number of male children, than female, seem to be affected by monogenic causes of ID (Leonard & Wen, 2002), suggesting that a great number of genes that are implicated in cognition are located on the X-chromosome. While it is possible that X-linked mutations are easier to map, studies have identified 16% of ID genes to be located on the X-chromosome, which is interesting since only 4% of all known genes are in that location (Inlow & Restifo, 2004; Ropers, 2010).

The difficulty in establishing a genetic cause is more prominent in affected individuals with NSID, possibly due to locus heterogeneity, where a single disorder is caused by mutations in genes at different chromosomal loci (i.e. only one mutant locus is needed for phenotypic manifestation). In addition, as procreation from affected individuals is less likely, the typical genetic mapping strategies for autosomal dominant forms of ID, such as linkage analysis and positional cloning, have been less successful (Kaufman *et al*., 2010). The introduction of high-density microarrays and the use of next-generation sequencing however, have recently allowed for identification of a large number of *de novo* point mutations, deletions and insertions in patients with NSID (Vissers *et al*., 2010; Cooper *et al*., 2011; Rauch *et al*., 2012), which explain the largely sporadic nature of the disorder.

Finally, despite decades of research, the exact cause of ID has still only been established in about 50% of children with more moderate to severe ID and therefore many cases of ID in the population, including milder forms, remain of unknown aetiology (Roy *et al*., 2016). Particularly challenging remain those cases where affected individuals present with severe undiagnosed disorders of variable clinical manifestations, due to environmental or multigenic causes.

The focus of this thesis is one monogenic cause of ID and autism, mutations in *Syn*aptic *G*TPase-*A*ctivating *P*rotein 1 (*SYNGAP1*) gene.

1.2 *SYNGAP1* haploinsufficiency linked to Intellectual Disability

While the conventional distinction into syndromic and non-syndromic forms of ID is still very useful from a clinical perspective, more recent phenotype-genotype studies in humans and animal models are aiming to further characterize ID/ASD-related encoded proteins into functional categories. Distinct subclasses have been proposed, based on the contributing factor underlying phenotypic manifestation (Chelly *et al*., 2006):

> transmembrane proteins, microtubule and actin-associated proteins, synaptic plasticity-associated proteins (Figure 1.1), chromatin-remodeling factors, regulators and effectors of Ras/Rho-GTPase pathways and transcription and translation proteins.

One protein that is a key mediator of synaptic plasticity and a regulator of GTPase pathways is SynGAP, which is encoded by the *SYNGAP1* gene in humans. Several rare pathogenic *de novo* mutations in the *SYNGAP1* gene (located on chromosome 6-6p21.3) have been identified in individuals with NSID that are predicted to lead to haploinsufficiency, loss of function of one copy of *SYNGAP1*. Although reported cases of *SYNGAP1* haploinsufficiency are not as prevalent as other gene mutations, such as *Fmr1*, *MeCP2* or *NF1*, continuing genome sequencing studies of families report

increasing number of *de novo* mutations which could be as high as 4% of non-syndromic forms of ID (Hamdan *et al*., 2011). A more recent review based on 11 studies that report 2368 *de novo* mutations from a total 2358 probands and 600 *de novo* mutations from 731 controls, reported that *SYNGAP1* is one of 8 recurrently mutated and overlapping genes with *de novo* mutations in ID, ASD, epileptic encephalopathy (EE) and schizophrenia (SCZ) (Hoischen *et al*., 2014). Finally, in the DDD study, *SYNGAP1* was identified as one of the top 5 recurrently mutated genes in individuals with genetically-undefined DBDs, with no pathogenic *SYNGAP1* mutations in over 1000 control cases (Fitzgerald *et al*., 2014).

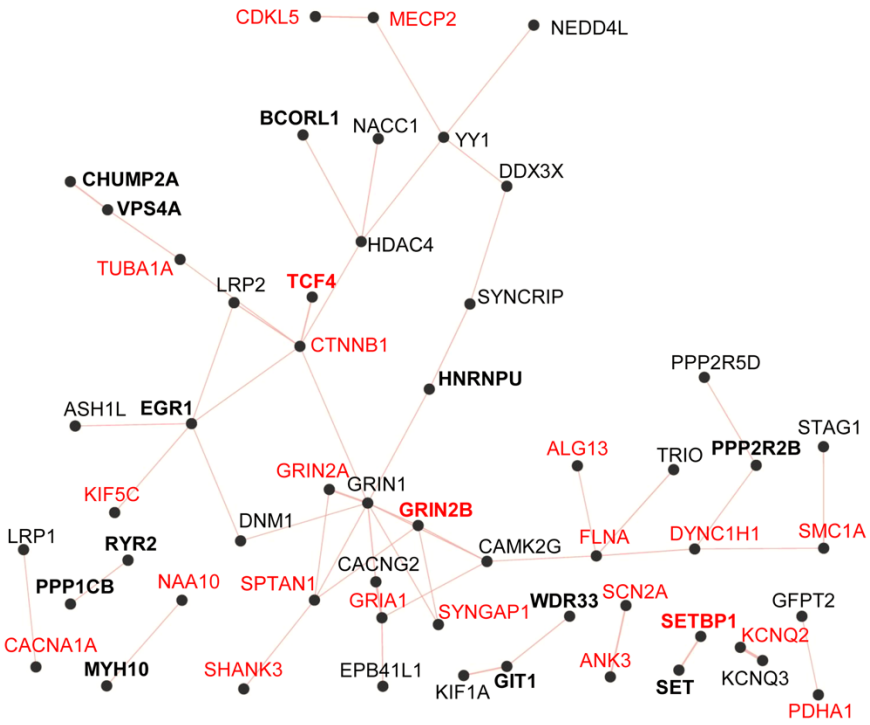

Figure 1.1 Physical protein-protein interaction network implicated in glutamate receptor signalling pathway. Generated by Hamdan *et al* (2014) in a Gene Ontology molecular function network based on candidate to that study (bold) and known ID genes with reported predicted-damaging *de novo* mutations from other studies (red).

1.2.1 Pathogenic autosomal *de novo* mutations in *SYNGAP1*

The first study included children of 4-11 years with mixed ethnicity and gender and similar clinical features for NSID (Hamdan *et al*., 2009) and identified three novel rare mutations in *SYNGAP1* (K138X, R579X, L813RFSX22). Of the three patients, two were heterozygous for nonsense mutations and one for a frameshift producing a premature stop codon; all proposed to be pathogenic because they truncated the encoded protein, SYNGAP. The R579X mutation was found in the RasGAP domain of the protein, while K138X and L813RFSX22 were found in amino-terminus (N-) and SH3 domain respectively. Interestingly, all mutations were absent from parental DNA (non-consanguineous parents) and therefore were characterised as *de novo*.

Since the Hamdan *et al* (2009) study, a wide number of mutations in the *SYNGAP1* gene have been, and continue to be, identified in patients with varying degrees of ID (see Appendix1 Table1). Most of the mutations identified are nonsense or frameshift mutations, predicted to truncate the protein, while other mutations include: splice mutations (Vissers *et al*., 2010; Hamdan *et al*., 2011; de Ligt *et al*., 2012; Rauch *et al*., 2012), microdeletions in chromosome region 6p21.3 encompassing *SYNGAP1* (Krepischi *et al*., 2010; Zollino *et al*., 2011; Writzl & Knegt, 2013), a balanced translocation between chr6 and 22 (also truncating; Klitten *et al*., 2011). All pathogenic truncating mutations abolish the carboxyl-terminus (C-) domains that are required for SYNGAP to interact with post-synaptic density protein 95 (PSD95) and other membrane-associated guanylate kinase scaffold proteins (MAGUKs) at the post synaptic density (PSD; Kim *et al*., 1998; Berryer *et al*., 2013). However, there are also at least 7 pathogenic *de novo* missense mutations in the *SYNGAP1* gene (Berryer *et al*., 2013; O'roak *et al*., 2014; Parker *et al*., 2015; Mignot *et al*., 2016; DECIPHER), including at least 3 point mutations in the active GAP domain and at least 2 point mutations in the C2 domain. For the majority of those pathogenic mutations, it is not entirely clear how the remaining protein is affected. Finally, Berryer *et al* (2013) identified one patient with a base duplication whose father was mosaic for this mutation.

Damaging *SYNGAP1* mutations are also causally linked to other neuropsychiatric disorders. Several studies have found pathogenic *SYNGAP1* mutations in ASD patients (De Rubeis *et al*., 2014; O'Roak *et al*., 2011, 2014; Iossifov *et al*., 2014), including a large-scale copy number variant (CNV) study on ASD patients that reported a CNV loss in one individual overlapping the entire gene (Pinto *et al*., 2010). Epilepsy is a frequent comorbidity, with *SYNGAP1* patients exhibiting epileptic seizures early on during childhood, with an age onset from 3 months to 4 years of life (Hamdan *et al*., 2009; Pinto *et al*., 2010; Zollino *et al*., 2011, Berryer *et al*., 2012; Klitten *et al*., 2011). Furthermore, several patients with epileptic encephalopathy, a debilitating form of epilepsy with poor diagnosis due to refractory seizures and cognitive arrest, were found to carry *de novo* truncating mutations in *SYNGAP1* (Carvill *et al*., 2013).

While Hamdan *et al* (2009) found no *de novo* mutations in *SYNGAP1* in 143 probands with schizophrenia (SCZ), a post-mortem study by Funk *et al* (2009) reported reduced levels of SYNGAP, PSD-95 and Multiple PDZ domain protein (MUPP1) in SCZ patients that received no treatment 6months prior to death, compared to treated patients and control individuals, although it is uncertain if this is a causal or secondary effect. Following this however, a more convincing study in a very large cohort of 2543 SCZ patients, also reported damaging *de novo* mutations in *SYNGAP1* (Purcell *et al*., 2014).

In line with all the evidence arising from past and current studies, the Simons Foundation Autism Research Initiative (sfari.org) has listed *SYNGAP1* as one of 23 high confidence autism risk genes (Figure 1.2 and Appendix1 Table1 illustrate the pathogenic and likely pathogenic mutations in *SYNGAP1* mentioned above).

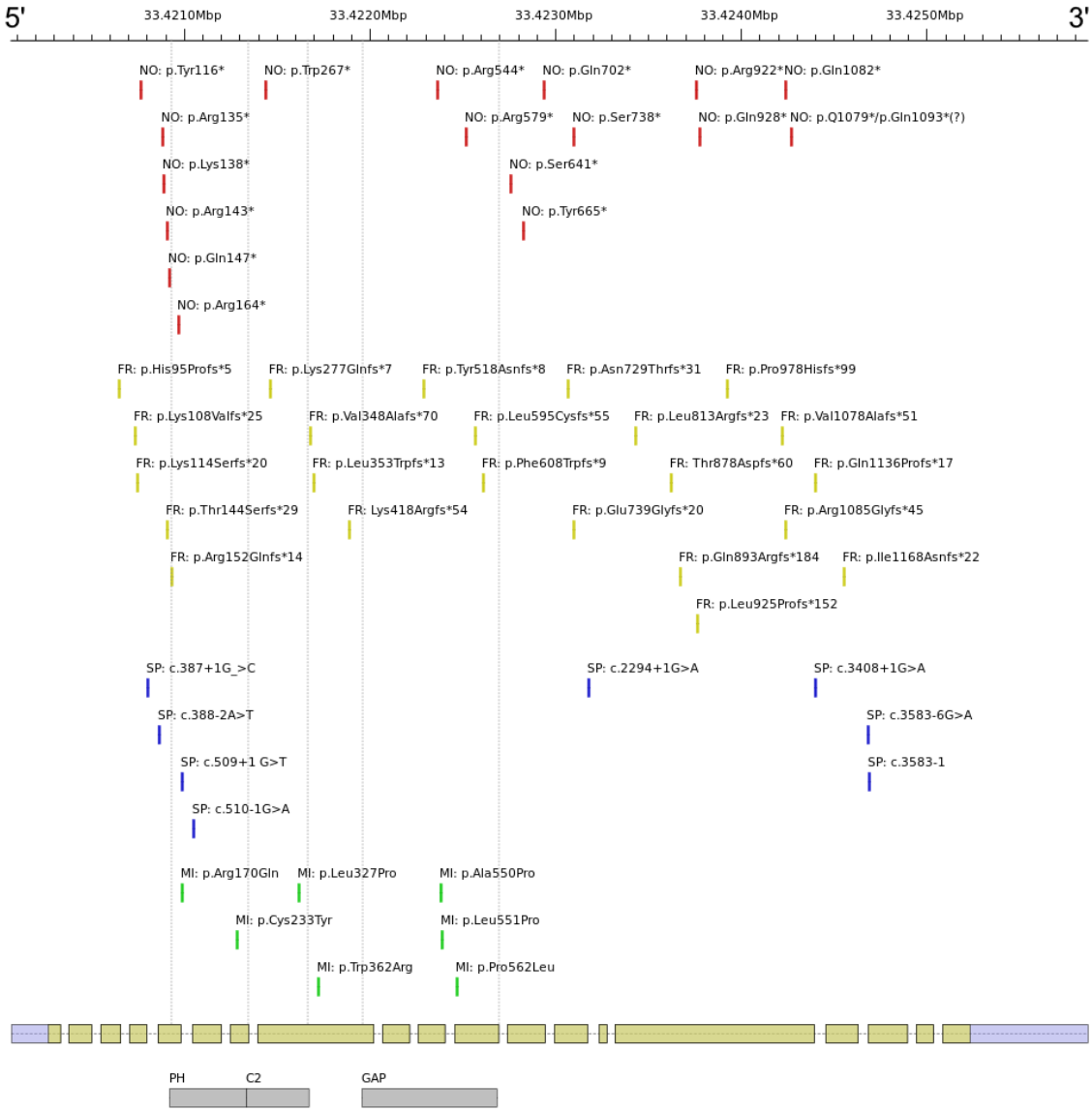

Figure 1.2 **Diagram of SYNGAP mutations.** Generated by Dr. Owen Dando this figure collectively demonstrates mutations reported in the following publications: Hamdan *et al* (2009, 2011), Vissers *et al* (2010), O'Roak *et al* (2011), Xu *et al* (2012), de Ligt *et al* (2012), Rauch *et al* (2012), Berryer *et al* (2013), Carvill *et al* (2013), Redin *et al* (2014), Parker *et al* (2015), Mignot *et al* (2016). For a full list refer to Appendix1 Table 1. *Red*, nonsense mutations; *Yellow*, frameshift; *Blue*, splice sites; *Green*, missense. Domains mentioned: Pleckstrin homology (PH), Protein kinase C conserved (C2), RasGAP (GAP). PH domain amino acid peptide range: 27-253, C2 domain: 263-362, GAP domain: 392-729, SH3-binding domain: 770-823, Coiled-coil domain: 1188-1272, α1 isoform has a QTRV motif is the terminal sequence (tail) at the end of 3'. Positions of domains were defined through Ensembl genome browser (Yates *et al*., 2015; Aken *et al*., 2016).

1.2.2 Symptoms of *SYNGAP1* haploinsufficiency

As DBDs have high symptomatic overlap (Maski *et al*., 2011), symptomatology associated with *SYNGAP1* haploinsufficiency also varies in severity. While birth weight is normal, some children are underweight during development and almost all patients appear to miss developmental milestones, therefore presenting with global psychomotor and expressive language (if developed at all) delay. Facial appearance of some affected children revealed that most common shared facial dysmorphisms are almond-shaped palpebral fissures slanting downwards that get more pronounced with age. Some patients also exhibit mild microcephaly (Parker *et al*., 2015).

Most of the patients develop moderate-to-severe ID, while milder forms are rarer (also see Appendix1 Table1). High comorbidity with ASD and other abnormal behaviours, including attention deficit, depression, mood instability, aggressiveness, tantrums, general hyperexcitability, and disturbed sleep patterns (Berryer *et al*., 2013; Parker *et al*., 2015). Some patients also present with oversensitivity to certain sensory stimuli, such as sounds (Prchalova *et al*., 2017). Seizures are often comorbid in *SYNGAP1* patients, most commonly complex and generalised, including myoclonic, drop attacks and absences (Pinto *et al*., 2010; Carvill *et al*., 2013; Parker *et al*., 2015). Furthermore, Parker *et al* (2015) reported 'normal' magnetic resonance tomography of the brain in all the patients (seven) that had undergone neurological examination of that kind.

Finally, while SYNGAP1 haploinsufficiency has been characterised as nonsyndromic, some patients exhibit features of syndromic nature. These include strabismus, constipation, hip dysplasia, kyphosis or kyphoscoliosis, while one patient with a 6p21.3 deletion presented with apparent connective tissue abnormalities (Krepischi *et al*., 2010), similar to ones observed in several patients with FXS, challenging the current clinical separation of ID in syndromic and nonsyndromic nature.

1.2.3 SynGAP: protein structure and function

SynGAP, a ~140 kDa protein encoded by the *Syngap* gene, was originally identified by Kim *et al* (1998) and Chen *et al* (1998) as a protein associated with a large complex of NMDAR, PSD-95 and SAP102, by cloning *Syngap* cDNA and identifying *Syngap* α1. Four different amino-terminal isoforms have been identified since then, arising from alternative transcription start sites: A, B, C, and E (Li *et al*., 2001). Alternative splicing of *Syngap* mRNA also gives rise to distinct carboxyl-terminus isoforms α1, α2, β1, β2, β3, β4, and γ (McMahon *et al*., 2012).

1.2.3.1 SynGAP protein structure

SynGAP protein contains several functional domains (Figure 1.3), the catalytic domain is a highly conserved GAP domain that activates the GTPase activity of Ras (Chen *et al*., 1998) and was also later found to be critical for synaptic transmission (Rumbaugh *et al*., 2006). The calcium/lipid domain (C2) serving as a calcium-dependent membrane binding protein (Chen *et al*., 1998) is also shared by all isoforms. The pleckstrin homology domain (PH) for phospholipid binding is complete in only SynGAP A, B, and E isoforms, and truncated in C. The PH domain has been found to be critical for protein-protein interactions and membrane trafficking (Li *et al*., 2001).

The carboxyl-terminus contains phosphorylation sites, which are targeted by Ca^{2+}/calmodulin-dependent protein kinase (CamKII) and protein tyrosine kinases (Chen *et al*., 1998). It has been also highlighted as a potential classical SH3 binding domain, usually mediating assembly of specific protein complexes (proline-rich region at positions 770-800; Cohen *et al*., 1995). The most studied isoforms are α1 and α2, due to their association with the PDZ-binding domain of PSD-95 at the synapse.

Interestingly, only SynGAP α1 possesses a PDZ binding domain (QTRV motif) enabling it to directly bind to PSD-95, which is suggested to be the binding mediator of SynGAP to the PSD (Chen *et al*., 1998; Kim *et al*., 1998). Yet, SynGAP β, lacking

a QTRV motif, is also isolated at the PSD fraction, suggesting that there is an additional binding partner. Furthermore, through a set of experiments where Vazquez *et al* (2004) introduced a mutation of the QTRV motif in the C-terminus of SynGAP, authors demonstrated that the mutation did not alter the targeting of recombinant protein to the spines, therefore suggesting that PSD-95 binding is not crucial from anchoring SynGAP to the synapse.

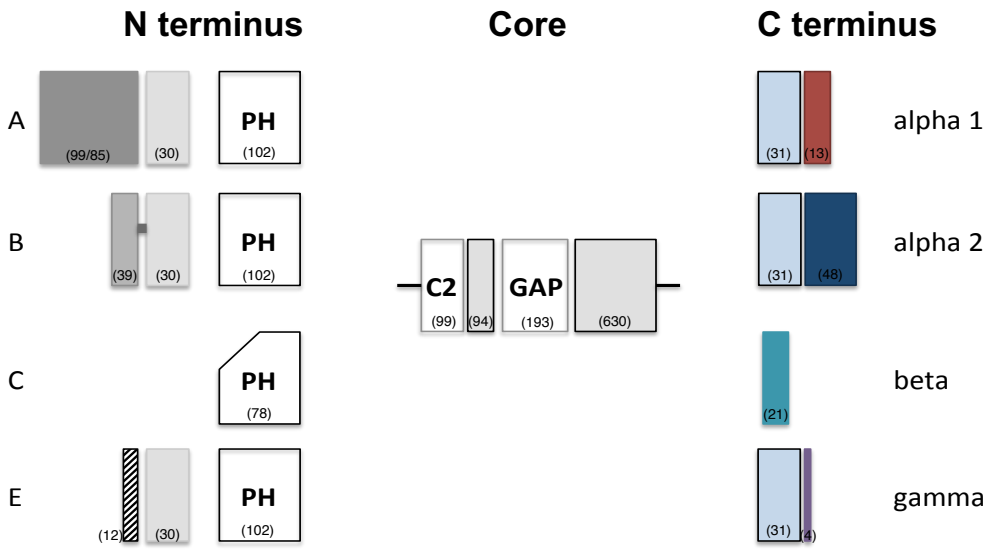

Figure 1.3 Schematic of the protein domain structure of SynGAP isoforms. The core part of SynGAP consists of a C2 and a GAP domain. Different N-terminal peptides contain unique peptide sequence and full PH domain arising from different transcription start sites. SynGAP C is shorted with a truncated PH domain. Different C-terminal tails (α1, α2, β, γ) arise from alternative mRNA splicing. In parentheses, amino acid peptide lengths; diagram not to scale. Image adjusted from Aoife McMahon, thesis. See Appendix1 Figure 1.1 (A, B) for SynGAP amino acid sequence and evolutionary conservation proposed by Kim *et al.,* 1998.

1.2.3.2 SynGAP localisation

SynGAP is enriched at the PSD but not in presynaptic terminals (Barnett *et al*., 2006) and is expressed in glutamatergic (Kim *et al*., 1998; Chen *et al*., 1998; Knuesel *et al*., 2005; Clement *et al*., 2012; Clement *et al*., 2013; Ozkan *et al*., 2014) but also in GABAergic neurons (Zhang *et al*., 1999; Moon *et al*., 2008; Ozkan *et al*., 2014; Berryer *et al*., 2016).

SynGAP isoforms have been found to be differentially distributed in neurons. SynGAP α1 was found solely in excitatory cells of neuronal cultures and homogenates (Kim *et al*., 1998; Moon *et al*., 2008), while SynGAP β was detected in both excitatory and inhibitory neurons (Moon *et al*., 2008). Both isoforms have been found to be highly enriched in the dendritic spines of cultured neurons (co-localisation with PSD-95), but also at the dendritic shaft. A larger number of SynGAP β clusters relative to α1 has been found distributed along the dendritic tree in cultures (Moon *et al*., 2008). Finally, SynGAP α2 and γ isoforms appear to be less abundant, at least at the level of mRNA (Li *et al*., 2001).

Localisation of SynGAP to the spines has also been shown to be regulated in an activity-dependent manner. Yang *et al* (2011) demonstrated redistribution of SynGAP protein away from the membrane and towards a region of high concentration of CaMKII, upon depolarization. In addition, Araki *et al* (2015), also demonstrated rapid dispersion of SynGAP from spines during and after chemical LTP induction, following phosphorylation of CaMKII.

1.2.3.3 Other SynGAP interactions

PSD-95 interacts with the GluN2B subunit of the NMDA receptor through a PDZ-binding motif at the C-terminal tail of GluN2B. Therefore, through its association with PSD-95, SynGAP is also linked to the GluN2B subunit (Kim *et al*., 1998; Figure 1.4). Stimulation of neurons with NMDA has been shown to cause an increase in the

phosphorylation of SynGAP in cultures, further supporting its regulation in an activity-dependent manner. In a study by Wang *et al* (2013), genetic knockout of GluN2B in neurons showed enhanced AMPAR-mediated synaptic transmission and increased protein synthesis rates, like in SynGAP knock-down cultures. Overexpression of SynGAP in GluN2B knockout neurons corrected enhanced mEPSC amplitude, while when SynGAP was knocked-down in GluN2B knockout neurons, it did not further increase it, suggesting that SynGAP acts downstream of GluN2B to both regulate the same pathway providing a possible therapeutic target.

While SynGAP α1 localises to the synapse through binding to PSD-95 and potentially other MAGUKs, SynGAP β localised to the PSD fraction by directly interacting with the α subunit of CaMKII (Li *et al*., 2001). Interaction of these two proteins has been suggested to be regulated in an activity-dependent manner, as SynGAP β and CaMKII interaction is lost following autophosphorylation of CaMKII α subunit.

SynGAP has also been shown to interact with another large ubiquitously expressed scaffolding protein, MUPP1. MUPP1, through its multiple PDZ domains, interacts with the α subunit of SynGAP, bringing it to physical interaction with CaMKII, and therefore anchoring it to the GluN2B subunit of the NMDA receptor signalling complex (Krapivinsky *et al*., 2004). However, MUPP1-SynGAP interactions are not required for SynGAP binding to the PSD. In addition, disruption of MUPP1-SynGAP complex dephosphorylates SynGAP, inactivates p38 MAP kinase and increases the number of synapses containing functioning AMPA receptors, presented through an increase in frequency and amplitude of AMPAR-mediated mEPSCs (Krapivinsky *et al*., 2004; Rama *et al*., 2008).

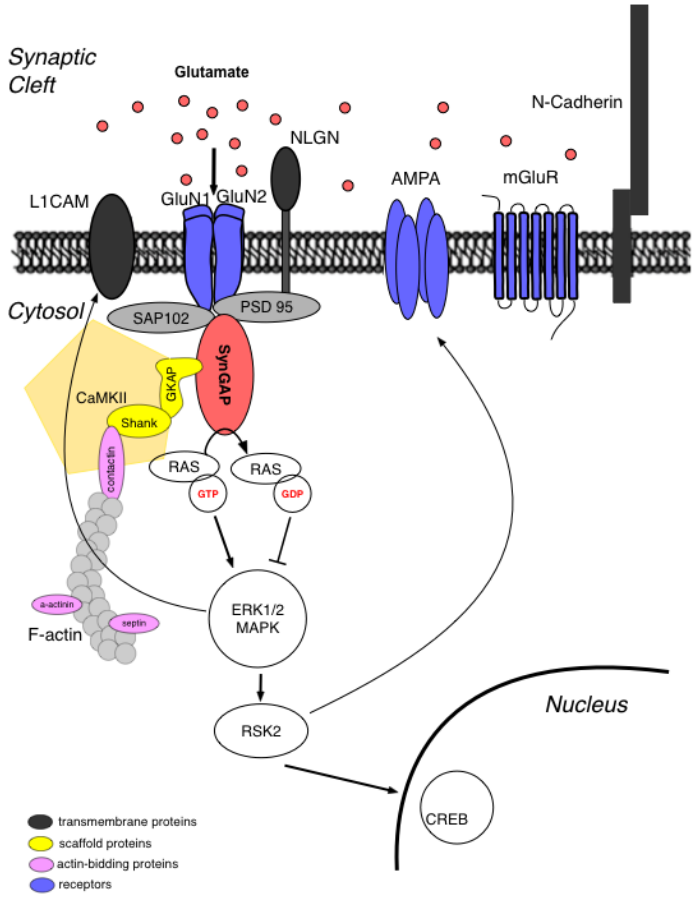

Figure 1.4 Schematic illustration of SynGAP interactions with the Ras/ERK pathway. NMDA receptors are linked to MAGUK proteins PSD-95 and SAP102, which are directly associated with SynGAP, therefore regulating the Ras/ERK pathway. This pathway regulates transcription via CREB and cell adhesion via L1CAM. It also regulates AMPA receptor trafficking and localization to the PSD through the ERK1/2-MAPK downstream signaling pathway, therefore being key regulator of synaptic plasticity. SynGAP also regulates cytoskeletal morphology through interaction with F-actin. Only major PSD families are shown. Scaffold and actin-binding proteins are colour-coded (bottom left). Schematic is simplified, not to scale, and represents established interactions.

1.2.4 SynGAP expression

During embryonic development, SynGAP expression starts at embryonic day (E) 8.5 (Porter *et al*., 2005). Expression at the cortex, basal ganglia and thalamus starts at E10.5, while expression in subcortical regions such as the hippocampus and hypothalamus starts later at E16.5 (Figure 1.5). SynGAP is also expressed throughout the neural tube, somites and heart during development (Chen *et al*., 1998; Porter *et al*.,

2005). SynGAP expression levels peak in the first postnatal weeks, during the rodent critical window for synaptogenesis and synaptic plasticity (~P14), before declining into adulthood for most areas, except for the hippocampus. In adulthood (>6 weeks) SynGAP is detected in the hippocampus, cortex (mostly layer 2/3 and the boundary between layer 4 and 5), striatum, amygdala and olfactory bulbs, but not in the cerebellum, thalamus, midbrain, or brain stem (Kim *et al*., 1998; Porter *et al*., 2005). While Figure 1.5 below shows expression of SynGAP through β-gal immunostaining; Barnett *et al* (2006) reproduced these findings in adult mice by reporting a comparable profile of protein expression in the cortex by using the anti-pan-SynGAP antibody.

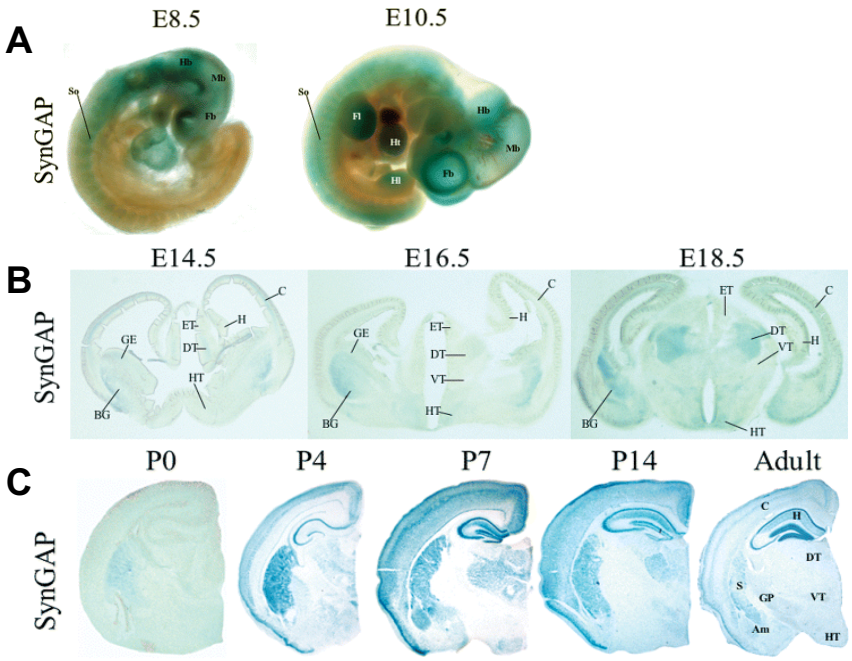

Figure 1.5 Differential expression of SynGAP during mouse development. (A) X-gal staining for SynGAP expression at E8.5 (left) and E10.5 (right) in whole mount embryos. (B) E14.5, E16.5, and E18.5 coronal brain sections. (C) Coronal brain section at postnatal day 0 through to 6 weeks. For comparison purposes, images are adjusted to a similar size to the adult. *Am*, amygdala; *BG*, basal ganglia; *C*, cortex; *CP*, cortical plate; *DT*, dorsal thalamus; *ET*, epithalamus; *Fb*, forebrain; *F,* forelimb bud; *GE*, ganglionic eminence; *GP*, globus pallidus; *H*, hippocampus; *Hb*, hindbrain; *Hl*, hindlimb bud; *Ht*, heart; *HT*, hypothalamus; *IC*, internal capsule; *Mb*, midbrain; *MZ*, marginal zone; *Nt*, neural tube; *S*, striatum; *So,* somites; *SP*, subplate; *VT*, ventral thalamus; *VZ*, ventricular zone. *E*, embryonic day; *P*, postnatal day. Image adjusted from Porter *et al.,* (2005).

1.2.5 Signalling cascades regulated by SynGAP

Forming part of the NMDA receptor complex at the PSD, SynGAP couples NMDAR activation to downstream signalling cascades (Chen *et al*., 1998). CaMKII phosphorylation of SynGAP occurs at multiple sites, is reversible, and increases its GAP activity by 70-95% (Oh *et al*., 2004).

CaMKII can be activated through two mechanisms; either by Ca^{2+} entry to the PSD predominantly through NMDAR activation, or from autophosphorylation providing a Ca^{2+}-independent mechanism (Coultrap & Bayer, 2012). In wild type cortical cultures, transfection of constitutively active CaMKII (T286D) leads to reduction in AMPAR-mediated mEPSC amplitude. Wang *et al* (2013) then showed that in SynGAP knockout neurons (all isoforms), elevated mEPSC amplitude cannot be corrected through transfection of T286D, suggesting that SynGAP is downstream of CaMKII and that CaMKII cannot regulate AMPAR-mediated synaptic transmission if SynGAP is absent.

Following phosphorylation by CaMKII, activated SynGAP specifically facilitates GTP hydrolysis to GDP, therefore negatively regulating the Ras family of small G-proteins, such as Ras, Rap1 and Rap2 (Chen *et al*., 1998; Kim *et al*., 1998; Ye & Carew, 2010). The family of G-proteins cycles through active (GTP-bound) and inactive (GDP-bound) states, due to regulation from GAP proteins and guanine nucleotide exchange factors (GEF) proteins, ultimately assuring precise activation levels of neurons and regulation of synaptic strength and plasticity (Bos *et al*., 2007). Therefore, SynGAP being a critical element in the control of Ras activity, also prevents further activation of downstream targets of Ras including the ERK1/2-MAPK, P13K-Akt-mTor and p38-MAPK signalling cascades. These Ras-mediated parallel signalling pathways are critical for expression of certain forms of synaptic plasticity by mediating AMPA receptor insertion to the PSD (Stornetta & Zhu, 2011). In cultures, overexpression of SynGAP (α1 isoform only) decreased the number of surface AMPAR receptors (Rumbaugh *et al*., 2006) and heterozygous or full knockout lead to an increased number of AMPA receptor clusters relative to wild type (Kim *et al*., 2003; Araki *et al*., 2015). In addition, *Syngap* HET mice display deficits in

NMDAR-dependent LTP in the hippocampus in a Ras-ERK1/2-dependent manner (Komiyama *et al*., 2002) and elevated levels of basal protein synthesis (Barnes *et al*., 2015). Furthermore, SynGAP has also been shown to regulate baseline levels of Rac activity and downstream PAK1-3 kinase cascade which leads to the phosphorylation of cofilin (Carlisle & Kennedy, 2005; Carlisle *et al*., 2008). Cofilin inactivated by phosphorylation was shown to be prevented from binding to F-actin and severing its activity and that transient regulation of cofilin by treatment with NMDA is also dysregulated in *Syngap* heterozygous mice (Carlisle *et al*., 2008). This study therefore provided direct evidence of SynGAP regulating the steady-state morphology of spine cytoskeleton in an NMDAR-dependent manner.

Finally, a study by Walkup *et al* (2015) also reported that recombinant (r-)SynGAP (lacking 102 residues at the amino-terminus) can be phosphorylated by cyclin-dependent kinase 5 (CDK5) as well as CaMKII. Authors showed that phosphorylation of r-SynGAP by CDK5 increased its Ras GAP activity by 98% and Rap1 GAP activity by 20%, whereas phosphorylation by CaMKII increased its Ras GAP activity by 25% and Rap1 GAP activity by 76%. The above study demonstrates how activation of r-SynGAP shifts the ratio of its GAP activity depending its phosphorylation partner.

1.2.6 Activity-dependent regulation of SynGAP

More recent studies have identified different N-terminal isoforms (Li *et al*., 2001) and found that their expression is regulated in an activity-dependent manner (McMahon *et al*., 2012). McMahon *et al* (2012) investigated the regulation of different isoforms through activity in cortical mouse cultures and found *Syngap* B and C mRNA was upregulated and A was downregulated when increasing network activity, while the total mRNA levels remained unchanged (also see Appendix1 Figure 1.1C). These activity-dependent changes of relative mRNA abundance were abolished by inhibition of network activity through TTX wash-on. Increased network activity did not have an effect in C-terminal isoforms α1 and α2.

In the same study, forebrain neurons were transfected with plasmids containing a combination of N- and C- terminal isoforms. SynGAP A or B with α2-tail had no effect on proportion of silent synapses, while SynGAP A, B or C containing the α1 C-tail increased their number. It is still unknown what combination of isoforms exists in neurons, but C-terminal isoforms (α1 and a2) exist in the cortex and hippocampus (Yang *et al*., 2013). Yang *et al* (2013) also illustrated that α1 and α2 isoforms localise to PSD, suggesting that α1 associates with the PDZ domain of PSD-95 to block association with other proteins. In addition, upon NMDA receptor activation both isoforms move out of the PSD (Yang *et al*., 2011; Yang *et al*., 2013) to either change the access of Ras and induce activity-dependent synaptic morphological modifications (spine enlargement) or to create an empty slot for the association of an AMPAR (Yang *et al*., 2013; Araki *et al*., 2015). Indeed, overexpression of α1 reduces AMPA receptor-mediated mEPSCs, while overexpression of a2 enhances them (McMahon *et al*., 2012). The above studies illustrate the opposing effects different SynGAP isoform combinations can induce and their importance in synaptic plasticity mediated events. Finally, in SynGAP heterozygous mice different isoform levels have been found to be comparable to WT at the level of mRNA (relative to total SynGAP expression; Shinjini Basu, unpublished data).

1.2.7 Mouse model of *SYNGAP1* haploinsufficiency

Animal models of human psychiatric disorders are traditionally valued based on three basic criteria: construct, face, and predictive validity (Willner, 1984; Belzung & Lemoire, 2011; Sztainberg & Zoghbi, 2016).

> *Construct validity* represents the ability to recapitulate the aetiology of human disorder in an animal model, for eg. causing a genetic mutation or pharmacological and environmental perturbation that mimics the one that has been observed in human patients.
>
> *Face validity* refers to the animal model's resemblance to core features of the disorder, such as physiological or behavioural phenotypes. Face validity can be argued on the basis of whether rodent endophenotypes have phenomenological similarity between them and the human behaviour aimed to be modelled (eg. social behaviour in rodents and social isolation in autistic patients).
>
> *Predictive validity* covers the translatability of pharmacological interventions to affected individuals. This is based on the presumption that human patients will respond similarly to certain interventions and those will therefore be considered of high effectiveness (currently no drugs for *SYNGAP1* haploinsufficiency).

For decades, the common mouse, *Mus Musculus*, has been the laboratory animal of choice focusing on modelling highly penetrant monogenic disorders that cause ID and ASD in humans. There are many reasons behind this rodent model preference. First and foremost, the genetic access that has been available for decades. With 95-98% of mouse genes having a correspondent to the human genome (Su *et al*., 2002), the ability to genetically manipulate mice to selectively knock in and out genes in a global or cell-type specific manner has given the opportunity for precise interrogation of pathophysiology associated with dysregulated neuronal circuits in ID and ASD. Mammalian animal models of pathogenic mutations in *SYNGAP1*, which is the focus

of this thesis, have been so far restricted to the mouse. Homozygous deletion of SynGAP in mice leads to early postnatal lethality, due to extensive cortical apoptosis triggered by loss of SynGAP (Knuesel *et al*., 2005). *Syngap* null mice exhibit small body size and brain, reduced movement and feeding and die shortly after birth around P2 to P4 (Komiyama *et al*., 2002; Vazquez *et al*., 2004). *Syngap* HET mice, however, are viable and fertile and by adulthood they present with typical physical appearance. There is a small window during development (P28-P32) when body size appears decreased (Dr. Stephanie Barnes, thesis) but they soon catch up to size comparable to WT littermate controls.

Notably, targeted mutations in the *Syngap* gene for generation of mutant lines include not only the full germline mutation ($Syngap^{+/-}$) which has excellent construct validity, but also a conditional knock-out line ($Syngap^{+/fl}$; $Syngap1^{tm1.Geno}$/*RumbJ*) and a conditional rescue line ($Syngap^{+/lx\text{-}st}$; $Syngap1^{tm2Geno}$/*RumbJ*). These provide invaluable information about the cell-type specific function of SynGAP protein but have no construct validity.

The following paragraphs present a literature review on the pathophysiology associated with loss of SynGAP in the mouse.

1.2.8 SynGAP in the development of barrel cortex

The role of SynGAP in the lamination of the primary somatosensory cortex (SSp) was first assessed by Barnett *et al* (2006). *Syngap* KO mice presented with a complete loss of cellular segregation into barrels, while thalamocortical axon afferents (TCA) terminate to rows of layer 4 but not in a barrel-like pattern. Incomplete segregation of TCAs in *Syngap* KO brains was also observed in the barreloids of the thalamus, but not in the brainstem (Barnet *et al*., 2006). *Syngap* HET mice present with reduced segregation of TCAs into barrels, as reflected by a reduction in the ratio of cells in the barrel wall relative to hollow.

1.2.9 SynGAP regulating dendritic spines

The functional significance of dendritic spine formation and regulation has been studied extensively as the vast majority of the excitatory synapses in the brain are located onto spines (Carlisle & Kennedy, 2005). As a physical protrusion from the dendritic tree, spine initial formation, morphology and turnover dynamics are tightly dependent to the cytoskeletal protein F-actin, which is in turn regulated by major signaling pathways that recruits Ras and Rac- GTPase activity (Nimchinsky *et al*., 2002). In addition, F-actin dynamics are altered by interaction with N-Cadherin, whose presence has been found to be enhanced by the GluR2 subunit of the AMPA receptor (Saglietti *et al*., 2007). However, while actin regulation and dynamics can control both AMPAR trafficking (physiological effect) and changes in the architecture of spines, such as shape, size, and dynamics (morphological effect), the two can be distinct events (Wang *et al*., 2007).

As it would be expected, altered levels of SynGAP expression can result in changes in structural changes of synaptic sites which can be illustrated as altered dendritic spine number, morphology and dynamics. Following results from Vazquez *et al* (2004) in cultured neurons which suggested that *Syngap* HET neurons present with a higher number of spines and increased spine head morphology, Carlisle *et al* (2008) and Clement *et al* (2012) both examined spine morphology in slices using confocal or multiphoton microscopy. Both studies that examined hippocampal CA1 neurons or hippocampal dentate gyrus cells, reported an increase in dendritic spine head. Conversely, another study by Barnes *et al* (2015), found no differences in spine number or spine head width in CA1 pyramidal neurons of *Syngap* HET mice using stimulated emission depletion (STED) microscopy. Spines of HET mice exhibited slightly longer neck length and narrower neck width, which resulted in an increased compartmentalisation factor on a population and mean animal level. Compartmentalisation factor, which is used to predict the impact of morphological changes on diffusional coupling (Yuste, 2013), was calculated as the head volume multiplied by the head neck length and then divided by the cross-sectional area of the spine neck (Wijetunge *et al*., 2014). Barnes *et al* (2015) reported increased

compartmentalisation in *Syngap* HET mice, which indicates that SynGAP reduction alters the biochemical coupling of spines to their dendritic shaft.

The discrepancies in dendritic spine morphology (increased head diameter) could be due to many factors; first, different ages of animals used, different cell type of the hippocampus, as well as differentiation between type of dendrite included in each dataset (apical or basal). Second, and possibly the main reason, is due to the separation of spines into specific categories, i.e. 'mushroom', 'filopodia', 'stubby' spines. While spines have been shown to represent a continuum (Tønnesen *et al*., 2014; Wijetunge *et al*., 2014), both Carlisle *et al* (2008) and Clement *et al* (2012) are using the old categorisation criteria and reported subtle changes only in the 'mushroom' type spine shape. It is therefore unclear whether these differences between WT and HET mice would still remain if categorisation is removed. A third reason, which applies to the study performed by Carlisle *et al* (2008) is the inappropriate use of statistics. Authors in this study used n as number of spines for comparisons between genotypes, which was ranging from 2383 to 2788, therefore treating spines as independent measurements (when in fact they are interdependent to the animal) resulting in exaggerating statistical significance. Finally, both studies included measurements below 200 nm in their analysis, which is beyond the lowest limit for resolution of regular confocal and multiphoton microscopy (for tissue).

A transient increase in spine density, accompanied by changes in pyramidal cell morphology was also reported in a neocortical region of *Syngap* HET mice. In a study by Aceti *et al* (2015) investigating neuronal morphology of layer 5 pyramidal cells of the SSp *in vitro*, authors reported increased length and volume of the dendritic tree, as well as increased number of dendritic spines, at P21, which by P60 (young adulthood) returned to levels comparable to WT. Spine turnover was also assessed *in vivo* through sequential time-lapse imaging of dendrites of primary somatosensory cortex (SSp) in anaesthetised mice. Spines of *Syngap* HET mice presented with a decreased turnover index compared to WT, from P21 to P23 and from P30 to P32 (Aceti *et al*., 2015). Findings from this study suggest that reduced levels of SynGAP promote early maturation of layer 5 SSp neurons in a postnatal critical period of somatosensory processing. Conversely, a transient increase in spine motility has been demonstrated

in cells of the dentate gyrus of P14 *Syngap* HET slices (Clement *et al*., 2012), indicating that reported spine dynamics abnormalities happen during critical developmental periods but have differential outcomes in distinct brain regions.

1.2.10 Synaptic transmission affected by reduced levels of SynGAP

Originally, basal levels of synaptic activity of AMPA receptors in the CA1 of the hippocampus of adult *Syngap* HET mice were found to be intact and comparable to WT controls (Komiyama *et al*., 2002; Kim *et al*., 2003). However, based on the role of SynGAP in regulating glutamatergic signalling and previous findings about altered AMPA receptor content in neuronal cultures (Vazquez *et al*., 2004; Rumbaugh *et al*., 2006), Clement *et al* (2012) investigated AMPAR-mediated synaptic strength during various time points of mouse development. By assessing input/output (I/O) relationship and AMPA/NMDA receptor currents in cells at the medial perforant pathway and the Schaffer collateral pathway of the hippocampus, authors reported that basal levels of synaptic transmission of *Syngap* HET mice are intact at earlier ages (P9), but at P14 both I/O relationship and AMPA/NMDA ratios were increased, suggesting increased levels of incorporation of AMPA receptors to the PDS. However, and in line with previous results, this was only a transient finding, as after P21 basal synaptic transmission of *Syngap* HET mice returned to the same levels as WT. The above suggests that partial loss of SynGAP can result in premature acceleration of synaptic strength. Whether that can then affect adult synaptic plasticity or underlie hippocampus-dependent behavioural deficits in adulthood is more difficult to assess, especially since studies in hippocampus-dependent memory tasks in *Syngap* HET mice show weak deficits (Komiyama *et al*., 2002; Muhia *et al*., 2012).

In contrast to the hippocampus, findings in mPFC suggest gradual development of deficits in excitatory and inhibitory synaptic function. Ozkan *et al* (2014) showed that while basal synaptic transmission at P14 remains unaffected in *Syngap* HET mice, at adulthood mEPSC amplitude and frequency was significantly increased. This was accompanied by a reduction of miniature inhibitory currents (mIPSC), reduced firing

frequency of PV neurons and reduced amplitude of PV mEPSCs in mPFC slices from adult *Syngap* HET mice. Interestingly, basic intrinsic and synaptic properties of SST neurons of HET mice remained unaffected. The above findings suggest a progressive exacerbation of synaptic transmission deficits (E/I imbalance) in layer 2/3 of mPFC when SynGAP levels are reduced.

1.2.11 Synaptic plasticity in *Syngap* heterozygous mice

Long-term potentiation (LTP) or depression (LTD) are mechanisms of synaptic changes that have been characterised as sustained modification after periods of repetitive synaptic activity following some sort of electrical or chemical stimulus (Kandel *et al*., 2000). Ras and Rac- mediated signalling cascades have been shown to play a predominant role in LTP, mainly through ERK1/2 and MAPK (Carlisle & Kennedy, 2005; Kennedy *et al*., 2005), and in LTD (Li *et al*., 2006) by modulating the trafficking of AMPA receptors to the PSD surface.

1.2.11.1 Long-term potentiation (LTP)

In the CA1 of the hippocampus, decreased levels of LTP have been described in *Syngap* HET mice in numerous studies (Komiyama *et al*., 2002; Kim *et al*., 2003; Ozkan *et al*., 2014) by using different paradigms such as application of high frequency stimulation or theta-burst stimulation to the Schaffer-collateral pathway. Interestingly, basal synaptic transmission was unaffected, as shown by extracellularly recorded fEPSPs, paired pulse ratio, and NMDA/AMPA EPSC ratios (Komiyama *et al*., 2002), suggesting that while basal properties of AMPA receptors are unaffected in CA1 neurons of *Syngap* HET mice, their recruitment to the synapse upon LTP stimulation is ineffective. Komiyama *et al* (2002) reported further increase of, already upregulated at basal state, (phospho) pERK1/2 levels following chemical NMDAR activation. Conversely, Ozkan *et al* (2014) reported that activation state did not further increase

after LTP induction (theta burst stimulation), suggesting a saturated Ras-ERK1/2 pathway in the CA1 of the hippocampus. It is unclear why those discrepancies arise, although the two NMDAR stimulation protocols are very different. In addition, SynGAP has been shown to rapidly disperse from synaptic sites during and after LTP following phosphorylation by CaMKII and that dispersion activated Ras and predicts the maintenance of potentiated synapses (Araki *et al*., 2015), suggesting inhibition of lasting LTP due to reduction of SynGAP in heterozygotes. Importantly, adult reversal of the pathogenic mutation using Tm1(Cre/ERT); *Syngap*$^{+/lx\text{-}st}$ and delivering tamoxifen at 8 weeks of age, completely rescued both the LTP deficit and the levels of Ras and pERK (Ozkan *et al*., 2014). However, this was not the case for behavioural phenotypes as discussed later on in section 1.2.13.

Similar deficits in LTP to those seen in the hippocampus were also apparent in the cortex. In layer 4 stellate cells of SSp, Clement *et al* (2013) reported early maturation of thalamocortical synapses, as illustrated by the significantly increased AMPA/NMDA ratio of cells from P5 *Syngap* HET mice relative to WT controls. This was accompanied by an absence of LTP in slices from P5 HET mice, while WTs had robust LTP induction which disappeared at P8. After directly measuring the number of silent synapses for each genotype, through minimal stimulation experiments, they suggested that the failure to induce LTP in stellate cells of the SSp in *Syngap* HET mice is due to premature accumulation of AMPA receptors (‘unsilencing’) which therefore altered the window of synaptic plasticity of barrel cortex.

1.2.11.2 Long-term depression (LTD)

The role of SynGAP protein in NMDAR-mediated forms of LTD in the CA1 of the hippocampus appears to be specific to the induction protocol. Chemical NMDAR-dependent LTD induction, through acute application of NMDA in slices showed impaired LTD in the CA1 of *Syngap* HET mice (and increased level of p-Cofilin), while experiments using paired pulse low frequency stimulation (with NBQX to

inhibit AMPA, and no Mg^{2+}; only NMDAR component) find LTD of HET mice intact (Kim *et al*., 2003; Carlisle *et al*., 2008).

Furthermore, SynGAP has been found to regulate another distinct form of glutamate receptor-dependent form of synaptic plasticity. Barnes *et al* (2015) demonstrated that in the CA1 of the hippocampus, DHPG application (selective group1 mGluR agonist) induced a significant increase in the magnitude of LTD in slices from *Syngap* HET mice relative to WT littermate controls. Finally, while LTD was enhanced in HET mice, the head size of dendritic spines remained unaffected, suggesting that these two parameters are not functionally linked.

1.2.12 Circuit defects caused by the loss of SynGAP

Major alterations of functional properties of glutamatergic synapses, such as mechanisms that prevent activity-dependent synaptic plasticity, can greatly influence cellular and circuit hyperexcitability. However, less effort has been put into investigating circuit deficits arising from pathogenic *Syngap* mutations, which can provide a bridge of information linking the dendritic and synaptic pathophysiology directly to symptoms associated with the disorder.

Excitability at the circuit level has been assessed in two different brain regions of *Syngap* heterozygote mice. Clement *et al* (2012) investigated the propagation of voltage-sensitive dye (VSD) signals to uncaging glutamate at the dentate gyrus (DG). They reported that slices from P16 *Syngap* HET mice presented with a dramatically amplified propagation of VSD-signals through the hippocampus. The mPFC is another region where deficits in VSD-signal propagation have been reported. Ozkan *et al* (2014) showed the response of local layer5-to-layer1 mPFC (electrical) stimulation-evoked activity in slices from adult *Syngap* heterozygotes was greatly increased. Results from these two studies suggest disruption of information processing in two different areas of the brain due to local circuit hyperexcitability.

Due to increased incidence of childhood epilepsy of patients with *SYNGAP1* haploinsufficiency, EEG activity is another aspect of circuit function that has been assessed. *Syngap* HET mice showed altered EEG activity of temporal and parietal cortices, recorded daily for up to two weeks during prolonged overnight and random 2-hour sample recordings. Ozkan *et al* (2014) reported the presence of intermittent (brief or prolonged), sharp epileptiform discharges that ranged in frequency from 1 to 681/hour and did not coincide with any motor events. However, they did report the presence occasional prolonged seizures (>10 sec) with a myoclonic jerk, but due to the lack of quantification of observations and the small n number (2 WT, 3 HET mice) it is difficult to correlate behavioural accompaniment to EEG activity.

Moreover, in a study where *Syngap* haploinsufficiency was induced specifically to GABAergic neurons, using a driver mouse expressing Nkx2.1 to target cells the MGE, Berryer *et al* (2016) reported reduced cortical and hippocampal gamma oscillations, as monitored through EEG during an active exploration task, suggesting that SynGAP also may play an important role in modulating inhibitory output. To further confirm deficits in inhibitory connectivity, authors assessed the synaptic output of MGE-derived interneurons that have reduced levels of SynGAP by measuring Channelrhodopsin2 (ChR2)-mediated inhibitory synaptic responses (light-evoked IPSCs) onto layer 5 pyramidal cells *in vitro* and found a dramatic decrease in the amplitude of responses, suggesting impaired GABAergic synapse function.

Finally in a study assessing connectivity, Aceti *et al* (2015) reported that the relative proportion of rabies virus (RV)-mediated long-range ipsilateral inputs into the mPFC were comparable between WT and HET mice. Furthermore, there was no observed genotype difference between the relative contralateral and ipsilateral projections to mPFC, indicating that the basic anatomical connectivity of the cortex remains unaffected. They did report some slight changes in individual areas after a brain-wide map analysis; however, individual unpaired t-test were performed for comparison of over 30 areas which makes these results more difficult to interpret.

1.2.13 Behavioural pathophysiology associated with heterozygous loss of SynGAP in mice

1.2.13.1 Neurological and sensory phenotypes in the *Syngap* HET mouse

Seizures

SYNGAP1 haploinsufficiency has been causally linked to generalised seizures as well as epileptic encephalopathy in human patients (Hamdan *et al*., 2011a, 2011b; Berryer *et al*., 2013, Carvil *et al*., 2013). While *Syngap* HET mice have not been reported to display spontaneous seizures, they present with reduced flurothyl-induced seizure threshold in the clonus (first event) and tonic-clonic (second event) phase (Clement *et al*., 2012; Ozkan *et al*., 2014). Clement *et al* (2012) also reported increased audiogenic seizure incidence at P21-25 *Syngap* heterozygotes. After exposing 6 pairs of WT-HET mice to a 126 dB alarm, they reported 6/6 HET mice to exhibit wild running and 4/6 to seize (lethal for 3 mice). Conversely, seizure incidence in WT mice was at 0%, with only 3/6 mice exhibiting wild running.

Sensorimotor gating

'Prepulse inhibition' (PPI) test has been widely used to evaluate sensorimotor gating in humans and rodents, which presents as the ability to filter and prioritize incoming information from the surrounding environment (Swerdlow *et al*., 2000, 2001; Braff *et al*., 2001). It is based on the principle that PPI occurs when a weak pre-stimulus (prepulse sound) weakens the response to an immediate following (within 150 ms) strong stimulus (startle sound). When *Syngap* HET mice were tested in the acoustically isolated test chamber, they exhibited reduced PPI to acoustic startle responses (Guo *et al*., 2009). In addition, the same study also showed increased startle reactivity, which was more evident during the highest (loudest) amplitudes. Both of the above phenotypes have been suggested to be mediated by deficits in forebrain circuit function in humans (Braff *et al*., 2001).

Other neurological aspects of behaviour have not been extensively characterised in *Syngap* HET mice. Pain sensitivity to acute thermal stimulation has been found to be unaffected (Muhia *et al*., 2010), as tested through a 'thermal nociception' test originally described by Galbraith *et al* (1993). Circadian rhythmicity has not yet been investigated, however sleep disturbances are a feature associated with pathology in individuals with *SYNGAP1* haploinsufficiency.

1.2.13.2 Behavioural abnormalities in the *Syngap* HET mouse

Anxiety and hyperactivity

Perhaps one of the most consistent findings published on *Syngap* HET mice is the increased hyperactivity followed by decreased anxiety-like behaviours. *Syngap* HET mice exhibit a strong hyperactivity phenotype as shown by distance travelled and moving speed when exposed to an open field environment (Guo *et al*., 2009; Muhia *et al*., 2010; Ozkan *et al*., 2014; Berryer *et al*., 2016). Guo *et al* (2009) also reported elevated stereotyped behaviours, which represents counts of repetitive and 'purposeless' movements, which has been found to be a prominent feature in patients with autism and schizophrenia (Randrup & Munkvad, 1974).

Anxiety-related behaviour testing has also presented with consistent results. The elevated plus maze is a task that measures anxiety-like behaviour in rodents, by utilising the rodent's natural instinctive behaviour to stay in enclosed shady places (safe arm) compared to exposed and unsafe environments (open arm) of an elevated plus maze (Lister, 1987; Peier *et al*., 2000). *Syngap* HET mice have been reported to spend significantly more time in the open arms of the maze for the duration of the task, compared to closed arms (Muhia *et al*., 2010; Ozkan *et al*., 2014; Berryer *et al*., 2016), suggesting reduced anxiety. Furthermore, in the open field test, anxiety-like behaviours can be also measured through thigmotaxis, which is the tendency of mice to prefer to stay at the perimeter of an open field environment versus the exposed (arbitrarily defined) centre. *Syngap* HET mice have been shown to spend a greater percentage of time in the centre of the arena by entering and leaving more than double

the amount of times WT controls did (Guo *et al*., 2009; Muhia *et al*., 2010). Taken together, these reports raise the possibility that elevated locomotion of HET mice directly affect their behaviour during assessment of anxiety, especially since both anxiety-related tasks use to some degree the rodents' movement as a measure.

Social interaction and communication

Disturbances in social behaviour have long been considered a characteristic trait of neurodevelopmental disorders, especially for autism. According to the Diagnostic and Statistical Manual of Mental Disorders, ASD is defined by characteristics in two main domains that emerge usually in early phases of development: repetitive and restrictive behaviours, and social interaction and communication dysfunctions (American Psychiatric Association, 2013). Designing rodent behavioural tasks that are relevant to human social behaviours can be challenging as social symptoms may be uniquely human and are usually inherently variable, therefore not all readouts of rodent social behaviour can present with face validity (Silverman *et al*., 2010; Provenzano *et al*., 2017). However, there are some tasks that have been routinely used to assess social behaviour relying on the readout for social communication, social interaction, social avoidance and social memory. The most common quantitative tasks used are the reciprocal social interaction and the three chamber apparatus tasks (Nadler *et al*., 2004; Bolivar *et al*., 2007). More specifically, the three-chamber task gives the opportunity for testing three different aspects of rodent social behaviour; social isolation, interaction, and social recognition. Both Guo *et al* (2009) and Berryer *et al* (2015) tested *Syngap* HET mice in a three-chamber task and reported lack of social recognition, with a 2min delay for short-term memory. Guo *et al* (2009) also reported unaffected social interaction and enhanced social isolation. At the same time, olfaction of *Syngap* HET mice was reported to be comparable to WT levels (Guo *et al*., 2009).

1.2.13.3 Cognitive deficits in the *Syngap* HET mouse

Spatial and working memory

It was mentioned earlier that NMDAR-dependent LTP and $mGluR_5$–dependent LTD in the hippocampus of *Syngap* HET mice were found to be strongly impaired (Komiyama *et al*., 2002; Barnes *et al*., 2015). The hippocampus is important for allocentric spatial cognition (O'Keefe and Nadal, 1978). The Morris watermaze (MWM) apparatus is commonly used to evaluate allocentric spatial learning and memory in rodents, using a variety of task versions (Morris *et al*., 1984). In the spatial reference memory task (SRM), the latency of the animal to find a submerged platform that occupies the same location on each trial, is used as a robust readout for spatial learning and memory. Komiyama *et al* (2002) and Muhia *et al* (2010) both tested *Syngap* HET mice on SRM-in the MWM and reported only mild deficits. In the first study, mice were tested with two probe trials starting 10 min after final training trial. In the first probe trial, 11/21 HET mice reached criterion and time in training quadrant was comparable between mutants and WT controls (Komiyama *et al*., 2002). They also calculated the proportion of time spent in a smaller circular zone centred on the target, and HET mice displayed decreased memory by that measure. Finally, in the second probe trial no impairment was observed by any measurement. In addition, the second study only reported a mild deficit at the first 15 seconds of the test (24h following acquisition), and not the entire 60s testing period (Muhia *et al*., 2010). These studies point to a weak, if any, memory retrieval deficit and unaffected memory acquisition and retention.

To further understand the role of dysregulated SynGAP-mediated signalling in cognition, the performance of *Syngap* HET mice has also been assessed in dry-land mazes. The radial arm maze has been considered to be a sensitive assay of spatial learning, providing the opportunity for differentiation between reference memory (RM) and working memory (WM) (Olton *et al*., 1982). Mice were trained in the four baited – four unbaited version, in which four alternate arms were baited through the experiment, leaving unbaited arms adjacent to baited. The sequences are randomly alternating, and the first assessment of behaviour is the RM, where the RM errors are

defined as the first entry to an unbaited arm. The study showed deficits in both the retrieval but also the acquisition of the RM component, as HET mice failed to show reduction of RM errors over the course of training (Muhia *et al*., 2010). The second behaviour that was tested was WM, for which re-entries into baited arms when the reward was already consumed and re-entries into never-baited arms were considered WM errors. *Syngap* HET mice displayed a significantly higher number of re-entry WM, suggesting overall lack of improvement which also agrees with the RM deficit in radial arm maze.

Furthermore, potentially one of the most reproducible results across studies is the WM impairments that *Syngap* HET mice display in a spontaneous T-maze alteration task which engages prefrontal-hippocampus networks. The task is based on the natural tendency of rodents to explore novel elements of their environment (Dember & Fowler, 1958). All studies have used an unforced spontaneous alteration task and *Syngap* HET mice were shown to fail to alternate their response (visiting the novel un-visited arm on the second trial) above chance levels (Guo *et al*., 2009; Muhia *et al*., 2010; Berryer *et al*., 2015). As the task relies on the identification of novelty over familiarity, Muhia *et al* (2010) also assessed novel object recognition memory, which was found to be unaffected in mutant mice.

Associative memory

Fear conditioning studies have been used to further assess associative cognitive performance in rodent models of neurodevelopmental disorders. Depending on the distinct subtypes of fear conditioning, there are several brain regions that are required including the hippocampus, prefrontal cortex and parts of the amygdala. Contextual fear conditioning, where the animals are exposed to context A (linked with an aversive unconditioned stimulus - footshock) and a context B (no aversive stimulus), has been shown to be hippocampus-dependent, and more specifically of the dorsal hippocampus and dentate gyrus (Sahay *et al*., 2011). In a study from Clement *et al* (2012), it was suggested that *Syngap* HET mice were unable to discriminate between the two

contexts over the same period of time. In the dataset, HET mice are presenting with lower % of time freezing to contexts A and B, however the WT discrimination is not strong. After 10 sessions of training with A+footshock, and 4 sessions of discrimination of either A+ or B-, WT mice barely reduce their % time freezing, suggesting potentially generalised effect of fear on the WT. Another study by Guo *et al* (2009) reported no difference in fear memory recall of *Syngap* HET mice in a contextual fear conditioning paradigm. Conversely, in a contextual plus cued fear conditioning paradigm, which is mediated by interactions between mPFC and amygdala (Orsini & Marren, 2012), HET mice were found to present with significantly reduced % time freezing in response to an auditory conditioning tone (CS), indicating associative memory deficits.

1.2.14 Cellular specificity underlying behavioural phenotypes

Recent studies also aimed to investigate the contribution of distinct cellular populations with reduced SynGAP expression to behavioural abnormalities observed in *Syngap* HET mice, using conditional knock-out mouse models. One such study crossed the conditional *Syngap*$^{+/fl}$ line with a mouse driver line expressing Emx1 (Emx1-*ires*-Cre; Gorski *et al*., 2002), specifically inducing cre-mediated recombination of *Syngap* in forebrain glutamatergic cells (Ozkan *et al*., 2014). Emx1-Cre; *Syngap*$^{+/fl}$ mice express reduced levels of SynGAP in glutamatergic neurons of the forebrain and hippocampus, but not striatum (Ozkan *et al*., 2014). Disruption of SynGAP in that mouse model resulted in behavioural phenotypes similar to what has been reported before for *Syngap* HET mice with the germline mutation, such as increased time spent in elevated plus maze, hyperactivity in open field, decreased seizure threshold, and inability to reach criterion at the spontaneous alteration working memory task.

Authors also induced haploinsufficiency in GABAergic neurons of the entire CNS by crossing the conditional *Syngap*$^{+/fl}$ line with a mouse driver line expressing Gad2 (Gad2-*ires*-Cre; Taniguchi *et al*., 2011), but found no behavioural abnormalities in

Gad2-Cre; *Syngap*$^{+/fl}$ mice, suggesting that the primary driver for phenotypes associated with reduced SynGAP is forebrain glutamatergic and not GABAergic neurons. Conversely, a different study (Berryer *et al*., 2016) induced haploinsufficiency to GABAergic interneurons originating from the MGE expressing Nkx2.1, which includes MGE precursor cells that give rise to most PV and SST cortical interneurons (Xu *et al*., 2008). Tg(*Nkx2.1-Cre*);*Syngap*$^{+/fl}$ mice only showed deficits in a spontaneous alteration working memory task in the T-maze, but no hyperactivity, altered levels of anxiety or deficits in social recognition memory (Berryer *et al*., 2016).

Finally, age specific induction of *Syngap* haploinsufficiency has been reported before by crossing the conditional *Syngap*$^{+/fl}$ line with a transgene mouse carrying tamoxifen inducible Cre recombinase (CAG-Cre/ERT) and introducing global haploinsufficiency at adulthood (8 weeks of age). Despite the conditional reduction of SynGAP in adulthood, mice did not present with any behavioural abnormalities, apart from reduced fluorothyl-induced seizure threshold (Ozkan *et al*., 2014), reinforcing the developmental aspect of this disorder.

1.2.15 Genetic reversal of *Syngap* haploinsufficiency in mice

Effort has also been taken to reverse behavioural impairments associated with loss of SynGAP in mice. As enhanced excitatory synaptic transmission of mPFC Layer 2/3 neurons and behavioural abnormalities have been reported in both *Syngap* HET and Emx1-Cre; *Syngap*$^{+/fl}$ mouse lines, Ozkan *et al* (2014) crossed the Emx1-Cre driver mouse to the Syngap conditional rescue line (*Syngap*$^{+/lx\text{-}st}$), to reverse pathogenic levels of SynGAP expression in glutamatergic forebrain neurons. Excitatory synaptic transmission (mEPSC amplitude and frequency) and some behavioural deficits (elevated plus maze and spontaneous alteration performance, but not hyperactivity or reduced seizure threshold) were rescued by introducing *Syngap* just to Emx1-expressing neurons. On the other hand, crossing the conditional rescue line with the

Gad2-Cre transgene line did not have any effect on core pathophysiology associated with reduction of SynGAP.

Synaptic transmission and behavioural abnormalities were also insensitive to adult genetic reversal of SynGAP levels (CAG-Cre/ERT; *Syngap*$^{+/lx\text{-}st}$; Clement *et al*., 2012; Ozkan *et al*., 2014). However, NMDAR-dependent LTP deficits in the hippocampus were rescued, followed by returned pERK1/2 response levels to LTP-inducing theta bursts in slices (Ozkan *et al*., 2014). Together, these findings suggest that cortical neurophysiological disruptions arise from developmental neuronal damage, whereas the hippocampus is more plastic to alterations of SynGAP levels in adult neurons.

Finally, it is relevant to mention that both the conditional *Syngap* knockout and the conditional rescue mouse lines were constructed with a deletion of SynGAP C-α1, (based on Kim *et al*., 2003). However, the regulation of the expression of N-terminal SynGAP isoforms is not only activity-dependent but also development-dependent. McMahon *et al* (2012) reported that SynGAP C mRNA is expressed at low levels up to P7, is then upregulated at the end of the second postnatal week (P14) and remains upregulated at stable levels at adulthood. On the contrary, both SynGAP A and B variants showed that their mRNA expression peaked at P14 and was significantly reduced by P21 (and remained reduced at adulthood). Since a lot of the behavioural phenotypes arise during development, perhaps genetic reversal by re-introducing a SynGAP isoform that is upregulated during earlier ages (juvenile), such as SynGAP B, would have resulted in successful reversal of phenotypes in adulthood.

1.2.16 Pharmacological approaches

Collectively, the above demonstrate how the *Syngap* heterozygous mouse model has provided immense insight into the role of SynGAP protein at the synapse and some mechanisms into underlying learning and behavioural deficits in the presence of dysregulated SynGAP-mediated signalling. So far, there has been less effort into identifying and developing potential therapeutic targets, but due to the accumulating

evidence of convergence of pathophysiological axis of ID disorders, this will be sure to change in the future.

One of the first attempts to reverse some of the behavioural phenotypes associated with *Syngap* haploinsufficiency in mice was at the study conducted from Guo *et al* (2009) where they tested the antipsychotic drug clozapine to reverse hyperactivity and abnormal sensorimotor gating. They found that persistent hyperactivity of HET mice was ameliorated using clozapine, however the drug had no effect in PPI in either genotype.

A more recent study used inhibitors that target and downregulate the $mGluR_5$ receptors and downstream Ras-ERK1/2 pathway in slices. Barnes *et al* (2015) used acute application of CTEP (inhibits $mGluR_5$), lovastatin (inhibits Ras through mevalonate) and U0126 (inhibits ERK1/2) in hippocampal slices of *Syngap* HET mice, to reverse elevated basal protein synthesis rates (Figure 1.4). This provided the first evidence that the same pharmacological interventions used to ameliorate phenotypes in *Fmr1* KO mice can restore translation rates of *Syngap* HET mice back to wild type levels, at least *in vitro*.

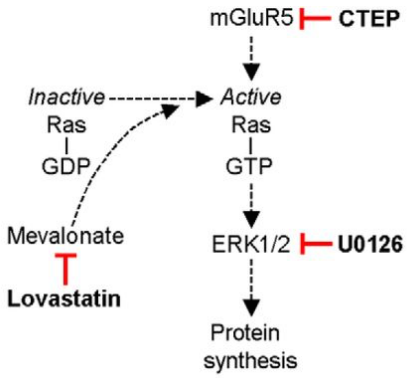

Figure 1.6 Schematic of the drug targets tested in Barnes *et al* (2015). CTEP, lovastatin and U0126 each have been previously shown to reduce Ras and ERK1/2 activation. Image adjusted by Barnes *et al.,* (2015).

1.2.17 Other animal models for neurodevelopmental disorders

1.2.17.1 Rats

Interrogating behavioural features relevant to human brain disorders, especially ID and ASD, in mice presents with some limitations. In some ways they are inflexible and present with high variability of responses due to their innate hyperactive nature. Rats are cognitively more flexible and display some social behaviours that are absent in mice, such as juvenile rough-and-tumble play (Siviy & Panksepp, 2011; more extensively discussed in Chapter1). However, the development of genetically modified rats for study of ID and ASD has been lacking in the past decades. Perhaps the most widely used rat model of autism has been that of prenatal (Schneider & Preworłocki, 2005; Schneider *et al*., 2008) or postnatal (during critical period; Kim *et al*., 2011) exposure to valproic acid (VPA), where exposed rats have shown elevated stereotypic behaviour and decreased interest in social interaction. Advances in techniques for genome manipulation, such as zinc-finger nuclease (Cui *et al*., 2011) and CRISPR-Cas9 technology (Li *et al*., 2013) have recently allowed for the generation of rat KO models of ID/ASD-related genes, including *Fmr1*, *MeCP2*, *Nlgn3*, *Nrxn1*, *GRM5*, *Pten*, and *CNTNAP2* (HorizonDiscovery). Genetically modified rat models of neurodevelopmental disorders have been shown to complement mouse studies and to expand current knowledge on the human disorder, therefore increasing translatability of potential pharmacological interventions for clinical trials in humans (Engineer *et al*., 2015; Till *et al*., 2015; Esclassan *et al*., 2015).

1.2.17.1 Non-human primates

One of the first efforts to investigate behavioural impairments of neurodevelopmental disorders in species more closely related to humans, had focused on the prenatal exposure of rhesus monkeys to IgG collected from mothers of children with ASD, the authors reported that subjects displayed behavioural deficits such as hyperactivity, increased stereotypic behaviour, and enlarged brain volume (Martin *et al*., 2008;

Bauman *et al*., 2013). However, more recent advances in genome modification tools have also paved the way to investigate the effect of monogenic mutations in non-human primates (Jennings *et al*., 2016; Chen *et al*., 2016; Bauman & Schumann, 2017). In the first study utilising transcription activator-like effector nucleases (TALENs)-mediated gene editing, Liu *et al* (2014) generated a newborn cynomoglus monkey with a frameshift mutation in the *MeCP2* gene that resulted in depletion of the encoded protein and failure to survive after birth. Subsequent studies have focused on generating and testing transgenic long-tailed macaques overexpressing the *MeCP2* gene, to study MeCP2-duplication syndrome (Ramocki *et al*., 2009; Liu *et al*., 2016). Although monkeys did not mimic the entire spectrum of MeCP2-dublication syndrome, they presented with reduced social interaction, increased repetitive circular locomotion, and weak evidence of cognitive deficits (Liu *et al*., 2016).

1.3 Aims of the thesis

The *Syngap* mouse model, carrying a heterozygous deletion of the *Syngap* gene and its encoded protein, SynGAP, has been extensively used to characterise some of the core synaptic and behavioural deficits associated with cognitive and social impairments in animal models of intellectual disability. However, there is still very little known about neuronal and circuit activity underlying deficits in behaviour and sensory processing in *Syngap* mice. In addition, there has been so far no other animal model of *Syngap* haploinsufficiency to complement existing literature and to ensure cross-species validation of phenotypes.

In **Chapter 3** of this thesis we therefore focused on addressing whether two different rodent models of *Syngap* haploinsufficiency, mice and rats, exhibit direct cross-species convergence of cognitive and behavioural endophenotypes. We took advantage of the generation of a new rat model of the disorder that is designed with a heterozygous deletion of the C2 and enzymatic GAP domain of the SynGAP protein. We aimed to characterise its behaviour by focusing on three main modalities affected in individuals with neurodevelopmental disorders; hyperactivity, cognition, and social interactions. This is crucial for further assessment of face validity and follows the recently augmented need of more animal models in the field of neurodevelopmental disorders. Furthermore, recent studies have identified new *de novo* point mutations in the C2 and GAP domains of *SYNGAP1* gene in patients with moderate-to-severe intellectual disability (Mignot *et al*., 2016). This suggests that current findings will complement existing work in *Syngap* mice and aim to provide valuable insights into the diverse phenotypic spectrum associated with patients carrying mutations in *SYNGAP1*.

In **Chapter 4** we aimed to examine *in vivo* neuronal ensemble activity and dynamics in different cortical areas of *Syngap* heterozygous mice. Individuals with intellectual disability and autism, including patients with *SYNGAP1* haploinsufficiency, have been found to exhibit sensory processing abnormalities (Joosten and Bundy, 2010; Prchalova *et al*., 2017). In addition, *Syngap* heterozygous mice exhibit behavioural abnormalities that could be explained by a dysregulation of sensorimotor processing, such as increased startle reactivity, reduced pre-pulse inhibition, hyperarousal and

hyperactivity, as well as increased incidence of seizures. These findings are accompanied by synaptic deficits and stimulus-evoked circuit hyperexcitability *in vitro* (Guo *et al*., 2009, Ozkan *et al*., 2014). We therefore aimed to address neuronal activity alterations in basal conditions and during sensory stimulation, at a single-cell level and in awake mice. Monitoring sensory network properties can help elucidate the mechanisms behind established behavioural abnormalities in mice, but can also give great insight into the varying degrees of behavioural and processing deficits seen in affected individuals.

Chapter 2

Materials and Methods

2.1 Common Methods

2.1.1 Housing and breeding

All animals were group housed and maintained on a 12:12 hour light:dark cycle and treated in accordance with the UK Animals Scientific Procedures Act (1986) guidelines and the three principles of Reduction, Refinement and Replacement. Colonies were maintained in either individually ventilated (IVC) or conventional cages in the University of Edinburgh. Food and water were provided *ad libitum*. Mutant animals were generated with wild type (WT) littermates, and experiments were carried out blind to genotype. All experimental procedures were approved by the animal welfare committee of the University of Edinburgh, and were performed under an approved UK Home Office project license.

2.1.2 Generation of the *Syngap* heterozygous mouse

The *Syngap* mouse model was generated by Komiyama *et al* (2002). Deletion of the *Syngap* gene resulted by in frame insertion of a targeting vector that consisted of a coding sequence for hemagglutinin (HA) epitope tag, followed by stop codons and an internal ribosomal entry site (IRES)-lacZ-polyA - MC1neo-polyA cassette. The resultant vector deletes exons encoding the C2 and GAP domains and allows a *β-galactosidase* reporter gene to be expressed under the control of SynGAP. Heterozygous mutants were generated by injecting targeted ES cells into C57Bl/6J blastocysts and then bred onto an MFI background (Sanger Institute), before being backcrossed to a C57Bl/6J-OlaHsd background (Harlan). Reduction of SynGAP expression by 50% was reported through immunoblotting of hippocampal extracts (Komiyama *et al*., 2002).

2.1.3 Generation of the PVcretdTom mice

Pvalb<tm1(cre)Arbr> knockin mice (PV-cre) [RRID:IMSR_JAX:008069] were generated by Hippenmeyer *et al* (2005) and obtained from Jackson Laboratory, USA. This line was designed with a PV-cre knockin allele by inserting an IRES-cre-pA cassette into the 3' UTR of exon 5, using the endogenous parvalbumin (PV) promoter to direct Cre-recombinase expression to PV-expressing cells. Mice were then crossbred with Rosa-CAG-LSL-tdTomato-WPRE::deltaNeo mice [RRID: IMSR_JAX:007914] (Madisen *et al*., 2010) (Jackson Labs, USA), which have a *loxP*-flanked STOP cassette preventing transcription of the downstream red-fluorescent protein tdTomato (tdTom). When bred with the PV-Cre mice, the resulting offspring expresses tdTom in more than 90% of neurons that express PV ($Pvalb^{+/cre}$, $Rosa26^{+/tdtom}$ *or* $Pvalb^{cre/cre}$, $Rosa26^{tdtom/tdtom}$). In this laboratory, the mice were further backcrossed onto a C57Bl/6J-OlaHsd background (Harlan).

2.1.4 Generation of the *Syngap* heterozygote and PVcretdTom double mutant mice

Syngap heterozygous and PVcretdTom heterozygous ($Pvalb^{+/cre}$, $Rosa26^{+/tdtom}$) or homozygous ($Pvalb^{cre/cre}$, $Rosa26^{tdtom/tdtom}$) mice were generated by crossing a Syngap heterozygote mouse with a PVcretdTom heterozygote or homozygote that was fully backcrossed to the C57Bl/6J-OlaHsd background. From these crosses, $Syngap^{+/+}$, $Pvalb^{+/cre}$, $Rosa26^{+/tdtom}$ *and* $Syngap^{+/-}$, $Pvalb^{+/cre}$, $Rosa26^{+/tdtom}$ were used for experimental purposes.

2.1.5 Generation of the SynGAP_GAP domain deletion heterozygous rat

The Syngap_GAP deletion rat model was designed by Peter Kind and Sally Till in consultation with Horizon Discovery and custom-generated by Horizon Discovery for

the Patrick Wild Centre, Edinburgh and Centre for Brain Development and Repair, Bangalore. Generation was employed using Sigma's CompoZr^{TM} Zinc-finger nuclease (ZFN) technology and SAGEspeed^{TM} animal knockout production processes. ZFNs were designed to target the Syngap gene sequence above and below the GAP domain to create a 3584bp deletion in the *Syngap* gene (Figure 2.1, 2.2). They were then incorporated into a plasmid with the nuclease of the Fok-1 restriction enzyme (Figure 2.2B) which provides DNA cleavage activity. ZFNs designed to target the Syngap gene were microinjected into the pronucleus of fertilized, one-cell embryos, and then bred onto a Long-Evans background. Reduction of SynGAP expression was verified through western blots of hippocampal homogenates and synaptosomes (Figure 2.2C; Dr. Sarfaraz Nawaz, unpublished data).

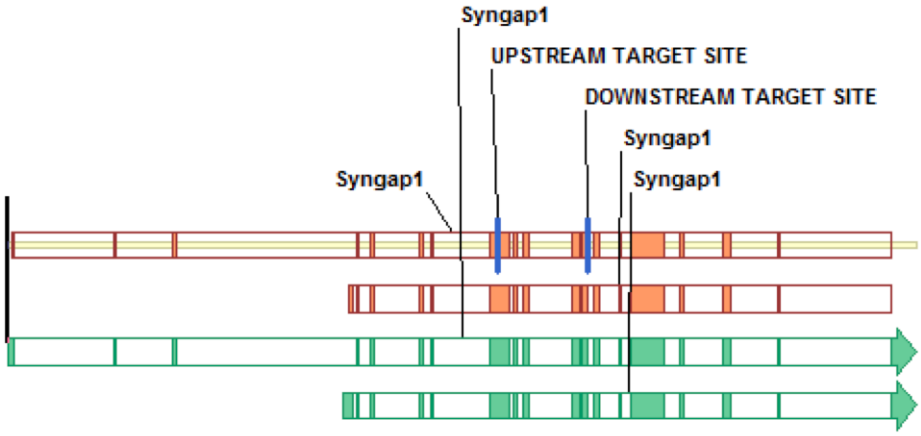

Figure 2.1 Schematic of strategy to delete the GAP domain of the *Syngap* gene for different isoforms. (SAGE laboratories, 2012). Upstream and downstream sites indicate where ZFN1,ZFN 2 targeted the *Syngap* gene to create the GAP domain deletion .

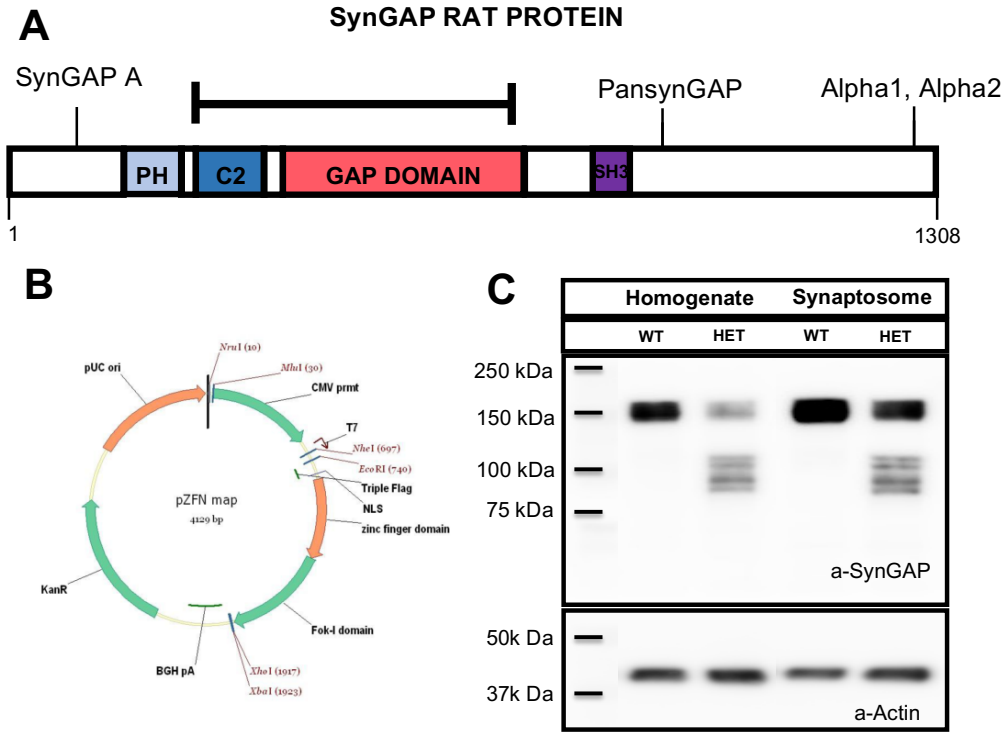

Figure 2.2 SynGAP GAP domain deletion design in Long Evans rats. (A) The Syngap knockout rat was designed with a deletion of the C2 protein domain and the GAP domain, using zinc-finger nuclease technology (Horizon). (B) The pZFN plasmid map. (C) Western blotting of SynGAP GAP domain deletion heterozygous rats shows reduction of SynGAP expression in hippocampal homogenates and synaptosomes (Experiments by Dr. Sarfaraz Nawaz). See also Appendix 1, Suppl.Figure1.4.

2.1.6 Genotyping

DNA digestion

Tissue from ear and tail clips was collected at weaning or at the end of the experimental procedures. For DNA digestion tissue samples were digested in 500µl of tail lysis solution (100mM Tris pH8.5, 200 mM NaCl, 0.2% SDS, 5 mM EDTA) with 5 µl of Proteinase K (20 mg/ml). Samples were vigorously mixed and incubated overnight (>12 hours) at 55°C in a water bath.

DNA purification

For DNA isolation and purification, samples were spun at 13000 x g for 10 minutes, and 400µl of the resulting supernatant was transferred in a new Eppendorf tube with equal volume of isopropanol. Samples were then spun again at previous conditions and supernatant was discarded. As a final wash, 70% ethanol was added to each sample, supernatant was discarded again, and DNA was resuspended and stored in ddH_2O at 4°C until use.

***Syngap* PCR reaction for mice**

For the PCR reaction, 1U HotStart Taq Polymerase (Promega), 0.3 mM dNTPs, 1x HotStart PCR buffer, 0.6 µM primers and 1 µl of DNA was used. A common reverse primer, Syn12R (20µM, Sigma-Aldrich); 5' – CAT ACA AGA ATT GCT GCA TAG AAC – 3', was used in conjunction with either a forward primer complementary to the wild type sequence, Syn11<, 5' – TTC ATG GAG CGG GAA CAC CTC ATA T – 3' (Sigma-Aldrich); or a forward primer complementary to the transgenic cassette, FCass1A, 5' - CTT CCT CGT GCT TTA CGG TAT C – 3' (Sigma-Aldrich). PCR products were determined according to the size of the PCR product. The wild type reaction product is approximately 2.5 kb and for the transgenic reaction, resulting product is approximately 1 kb. PCR products were detected on a 0.6% agarose gel for 35 minutes at 50 mV. The thermocycling conditions are listed in Table 2.1. Most of the genotyping was performed by Mark Patrizio.

PVcretdTom PCR reaction for mice

For this mouse strain, four PCR reactions were performed with probes for Cre, Pvalb-1 WT, tdRFP, and ROSA WT. Briefly, to detect the presence of Cre a forward primer (5' – TTA ATC CAR ATT GGC AGA ACG AAA ACG – 3') and a reverse primer (5' – CAG GCT AAG TGC CTT CTC TAC A – 3') were used. For the wild type allele of Pvalb-1 the primers that were used were: forward – 5' TCT CCA CTC TGG TGG

CTG AA – 5' and reverse 5' – CCG CGA AGA AGG ACT GAG ATG – 3'. Another set of primers (forward: 5' – AGA TCC ACC AGG CCC TGA A – 3'; reverse: 5' – GTC TTG AAC TCC ACC AGG TAG TG -3') was used for detection of tdRFP (tdTom). Finally, to get PCR products for ROSA WT, the forward primer 5' – TTC CCT CGT GAT CTG CAA CTC – 3' and 5' – CTT TAA GCC TGC CCA GAA GAC T -3' reverse primer was used. The genotyping for this mouse line was performed by Transnetyx Inc, Cordova, TN, USA using a real-time PCR method.

Syngap PCR reaction for rats

To genotype for the SynGAP GAP domain deletion rats, two sets of PCR assays were performed. To detect the absence of the deletion (i.e. identify the wild type allele-assay1), the first set of primers used was a forward primer targeting upstream of the deletion site (Sigma-Aldrich; 5' – GGC ACC TTC CCC AAG TAA GT – 3') and a reverse primer targeting downstream of the deletion (Sigma-Aldrich; 5' – TCA CTT GGT GAG TGA GTG CC – 3'). Then assay 2 was performed to detect sequences within the deletion site using a forward primer 5' – ACT GCG AGT TAT GCC TGG AC – 3' (Sigma-Aldrich) and a reverse primer 5' – CTC ATT GTC TGG TAA CGG GC – 3' (Sigma-Aldrich), as shown in Figure 2.3. The PCR reaction mix for both assays consisted of 16.4 µl of ddH_20, 2 µl of 10x Coral buffer from TAQ DNA Polymerase kit (Promega), 0.4 µl of dNTP Mix (Qiagen) and 0.5 µM final concentration of forward and reverse primers. 0.5-1 µl of purified DNA was added to the reaction mix and PCR products were detected by running on a 1% agarose gel at 50 mV for 30 minutes. The thermocycling conditions are listed in Table 2.1. Genotyping was initially designed and performed by Lindsay Mizen, and then was outsourced to Transnetyx Inc, Cordova, TN, USA, which uses a real-time PCR method.

	Genotyping thermocycling conditions			
	***Syngap* mouse**		***Syngap* rat**	
Step	Temperature (°C)	Duration	Temperature (°C)	Duration
1	95	15min	95	5min
2	95	30sec	95	30sec
3	94	10sec	60	30sec
4	55	30sec	68	1min
5	68	3min	Go to step2-35x	
6	Go to step3-10x		68	5min
7	94	10sec	10	1hr
8	55	30sec	4	1hr
9	68	3min		
10	Add 20sec/cycle			
11	Go to step7-28x			
12	68	7min		
13	4	1hr		

Table 2.1 Thermocycling conditions for genotyping of the *Syngap* mouse and rat colony.

2.2 Methods for Histology

2.2.1 Preparation of Slices

Aldehyde fixation by perfusion

Following anaesthesia by intraperitoneal (IP) injection of 50 mg/ml sodium pentobarbital, the chest of the experimental animals was opened, the heart was exposed, and the right atrium was lesioned with scissors. Animals was then perfused transcardially through the left ventricle, with 4% paraformaldehyde (PFA) in 0.1 M PB, following clearing of the cardiovascular system with 1 x PBS. The skull was then removed and the brain was retrieved, post-fixed in 4% PFA in 0.1 M PB overnight and stored in 1 x PBS at 4°C until use. In experiments in which animals were culled to quantify cFos expression post-behaviour, transcardial perfusions were performed within 1 hr after the end of the probe trial.

Preparation of slices for histology

Coronal or sagittal sections (40 μm) were cut on a Leica VT1000S vibratome in cold dissection buffer (1 x PBS). Sections were collected and washed in 1 x PBS twice. Cortical areas were identified using a standard adult mouse brain atlas (Paxinos and Franklin, 2004). For intracellular filling, 200 μm coronal slices were used.

2.2.2 Immunohistochemistry

Free-floating sections were rinsed in 1 x PBS and then transferred in blocking solution containing 10% Normal Goat Serum (NGS) and 0.1% Triton-X in 1 x PBS for 1 hour at room temperature (RT). Subsequently, sections were incubated in primary antibody solution consisting of 5% NGS, 0.1% Triton X, and the primary antibody/ies used in each experiment [polyclonal rabbit anti-FOS (Oncogene Research Productions; 1:250

dilution), monoclonal mouse anti-PV (SWANT; 1:5000 dilution), polyclonal rabbit anti-NeuN (Millipore; 1:1000 dilution), monoclonal rabbit anti-CaMKII (Abcam; 1:500 dilution)]. Sections in primary antibody solution were incubated for up to 48 hours at 4°C, then washed in 1 x PBS for 3 times, and transferred in secondary antibody solution containing 3% NGS, 0.1 M Triton-X and fluorescent immunoglobin G (1:1000 dilution) for 12 hours at 4°C. Finally, immunolabelled sections were washed 3 times in 1 x PBS, followed by washing in 0.1 M PB, mounted using hard-set Vectashield (Vector), coverslipped, and stored at 4°C protected from light until imaging. For some experiments DAPI (Thermofisher; 1:5000 dilution), To-Pro3 (Thermofisher; 1:1000 dilution) or NeuroTrace 435/455 (Thermofisher; 1:800 dilution) was used as a nuclear marker. This was performed after the sections were incubated in secondary antibody solution and washed in 1 x PBS twice.

2.2.3 Confocal Imaging and Analysis

Confocal imaging for c-FOS quantification

Immunolabelled slices were imaged on a Nikon A1R inverted confocal microscope. Image stacks of a minimum 15 μm were collected at x20 (Plan Apo VC; N.A 0.8) at x1 time zoom and with a Z section interval of 1 μm. Each plane was 8 times frame averaged. A minimum of two sections (bilaterally) per animal were imaged and analysed for each region of the brain. Cortical areas were identified using a standard adult mouse brain atlas (Paxinos and Franklin, 2004).

Confocal imaging for PV quantification

Immunolabelled slices (40 μm) were imaged on a Zeiss LSM510 Axiovert confocal microscope. Image stacks were acquired at x20 (Plan Neofluar; N.A 0.5) or x40 (Plan Neofluar; N.A 1.3 OIL) at x1 time zoom and with a Z section interval of 1 μm. A minimum of three slices per animal were imaged and analysed. The bilateral region of

the Visual cortex (V1) was identified using a standard adult mouse brain atlas (Paxinos and Franklin, 2004).

Analysis of c-Fos quantification

Quantitave analysis of c-Fos+ nuclei was performed manually using the computerized image analysis system Imaris 8 (Bitplane). A rectangular region of interest was randomly placed over the area of interest (i.e. mPFC) and c-Fos+ nuclei and NeuN+ neurons were counted. The size of the region of interest remained consistent between all images and animals for each given area.

2.3 Methods for Behaviour

2.3.1 Experimental Design

Mice

Mice were housed in polyethylene conventional cages (3-6 mice per cage, mixed genotype) with sawdust bedding and environmental enrichment (a tube per 2 mice, 3 wooden gnawing blocks, nesting material). Food and water were provided *ad libitum*. The light cycle in the colony was 7:00 am to 7:00 pm and experiments were performed during the light-on phase.

Three different cohorts of mice were used for experiments. Cohort 1 (10 WT and 6 *Syngap* HET) was tested in Open Field (OF) test, short-term and long-term task for Object-Location (OL). Cohort 2 (10 WT and 10 *Syngap* HET) was used in the 3-chamber social interaction task. In this experiment, the mice that were used as conspecifics (strangers) were littermates raised together and separated to a different cage. Results from this cohort of mice can be found in Appendix1 Figure 1.2. Cohort 3 (18 WT and 11 *Syngap* HET) was used in a 3-chamber social interaction task. Additional 20 C57Bl/6J-OlaHsd OLA WT (non-littermate) mice were used as

strangers to experimental animals when social interaction of cohort 1, 2 and 3 was tested. Both males and females were used in this study.

Rats

Rats were housed in polyethylene conventional cages (2-4 rats per cage, mixed genotype) with sawdust bedding and limited environmental enrichment (a tube per 2 rats and wooden gnawing blocks). Food and water were provided *ad libitum*. The light cycle in the colony was 7:00 am to 7:00 pm and experiments were performed during the light-on phase, unless otherwise stated.

Four different cohorts of rats were used for experiments. Cohort 1 (5 WT and 7 *Syngap* HET) and cohort 2 (8 WT and 8 *Syngap* HET) were tested in Open Field (OF) test, short-term and long-term memory tasks for Novel Object Recognition (NOR) and Object Location (OL) and in a 3 Chamber task (3CT) for social interaction. Olfaction (Odour Habituation-Dishabituation task) was also assessed. Originally, cohort 1 consisted of 8 WT and 8 *Syngap* HET rats but 4 rats were excluded due to failure to thrive resulting in decreased bodyweight relative to littermates. One *Syngap* HET rat from cohort 1 was also excluded due to fighting which resulted in injury. One WT rat from cohort 2 was excluded from analysis because it presented with very strong fleeing behaviour in all contexts/mazes. Cohort 3 (8 WT and 8 *Syngap* HET) was used to test Open Field (OF) and a set of spontaneous exploration tasks (object-recognition, object-place, object-context, object-place-context) in adulthood. One rat (WT) from cohort 3 was again excluded from analysis because decreased bodyweight relative to littermates. Cohort 4 (6 WT and 6 *Syngap* HET) was tested in 3CT for social interaction. Additional 24 Long-Evans WT rats were used as strangers to experimental animals when social interaction of cohort 1, 2 and 4 was tested. Both males and females were used in this study.

2.3.2 Behavioural Assays

Daily handling

Animals were familiarised with the experimenter daily, for at least two weeks prior to the start of experiments.

Handling for mice included an additional step, where animals were placed in a black box (W 40 cm x L 60 cm x H 40 cm), in which the floor was covered with sawdust bedding. The box contained three black plastic tubes, wooden gnawing blocks of different sizes and blue nitrile gloves, as environmental enrichment. Mice were put in groups (entire cage), and they stayed in the box exploring for 20 minutes each day. The experimenter would pick up each mouse multiple times during those 20 minutes, placing the animal briefly on their open hand and/or lap and then putting it back into the box. That was done to simulate the type of handling used in the actual experiment.

Habituation

An open field (for mice: 40 cm x 40 cm x 40 cm - for rats: 60 cm x 60 cm x 60 cm) was made of white laminated plywood. The open field was placed on a metal frame-platform and was covered with clean sawdust bedding (same type used in the housing cages). There were four equidistant holes in the four corners of the open field (used to secure the objects during the exploration tasks). A camera was suspended over the apparatus and connected to a video acquisition software. The room light was kept consistent for all experiments at 20 Lux in the centre of the field. For habituation, the animals were transported to the testing room, or a holding room adjacent to the testing room, 1 hour before the sessions would begin. Animals were habituated to the open field for three consecutive days (H_1-H_3), for 10 minutes each day, during which each single animal was allowed to explore the empty open field. Animals were placed into the field with their snout facing the centre of the south wall. After each animal session, the field was cleaned from droppings and the sawdust covering the floor was swirled

around to dispense any odour traces. Where different contexts were required as part of a task, the animals were habituated to all contextual configurations.

Mice also received an additional habituation session (H_0) where all the mice of the cage were put in the field together for 10 minutes. This initial habituation step was also followed when young pup rats (P<35) were used as experimental animals.

Open field test

The data that was analysed for open field (OF) was acquired in the three or four habituation sessions. Anymaze software was used to analyse the animals' behaviour post-recording. For mice (C57Bl/6J-OlaHsd, black background), Anymaze was set to track the head of the animal (snout), but since Long-Evans rats have patterned fur, tracking the centre of the body (below the neck) was more reliable. To test for anxiety, an inner zone (for mice: 15 cm x 15 cm – for rats: 30 cm x 30 cm) was drawn on Anymaze in the centre of the field, and its' size and location were kept consistent between animal sessions and cohorts. Immobility was set when the animal was tracked at the same position for more than 2 seconds.

Novel object recognition and object location recognition memory tasks

For the following two tasks, the field used was the same that was used in the OF testing (for mice: 40 cm x 40 cm x 40 cm - for rats: 60 cm x 60 cm x 60 cm). For object recognition, white walls, with one cue card (15 cm x 30 cm picture of black and white 2-3 cm wide stripes) at the north wall was used, whereas for object location the walls were changed to transparent and multiple more high contrast cues were presented outside of the north, west, and east walls.

Objects were glued on the outside base of glass Mason jars. Holes were drilled in the centre of their jar lids, and were then secured through the holes to the open field floor,

at the desired position, with screws and wing nuts. Previous pilot studies from Dr. Oliver Hardt determined which objects (different for mice and rats) would elicit adequate exploratory activity in wild type animals to provide sufficient sampling of objects. Briefly, for object location recognition testing, larger objects with multiple holes were used, like ceramic incense oil burners for rats, and cube extension plug adaptors for mice. Multiple copies of each object were stored at a place the animals could neither see nor reach.

For novel object recognition testing (NOR; Figure 2.3A), one sample trial of 5 minutes was performed, in which two copies of the same object were placed in the open field at NW-NE or SW-SE positions. Rats were then taken out of the field and placed either in a holding bucket for 2 minutes (short term memory – 2 minutes ITI) or back in their home cage for 24 hours (long term memory – 24 hours ITI). After each session objects were thoroughly cleaned with baby wipes sprayed with 70% ethanol and the sawdust bedding was swirled around to dispense odour traces. During the probe trial, one of the objects used during the sampling was removed and replaced with a new object. Only rats were tested for NOR.

For object location recognition testing (OL; Figure 2.3B), animals were presented with two copies of the same object in the sampling trials, placed at opposing positions (for eg. NE-SW, NW-SE). For the probe trial, one of the objects was moved to a new location for probing short term and long term memory. In each cohort of animals, multiple combinations of familiar and novel locations were tested. Mice received a total of nine sampling trials, 3 per day, for 5 min each, with a 2 mi ITI in a holding cage. Rats received one or three sample trials of 5 min each, and memory was tested either 2 minutes later or 24h later. When rats received three sampling trials, they were placed in a holding bucket during the 2 min ITI.

During both behavioural tests, animals were placed into the open field facing the wall or a corner from the side opposite to any object.

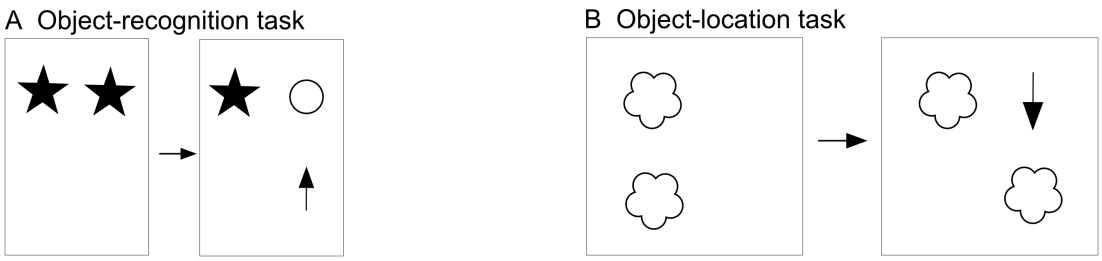

Figure 2.3 **Schematic illustration of** novel object recognition and object location tasks (A, B) Different shapes indicate different objects. Arrow notes which object or location is novel during the probe phase

Object-place, object-context and object-place-context associative recognition tasks

For these three tasks, the field used was a rectangular box (L 60 cm x W 40 cm x H 50 cm) that could be configured as either of two contexts, by changing the wall inserts and the floor. The sets of walls used were considerably different from one another in colour and texture (context 1 - white with rough paper; context 2 - blue wood laminate). Similarly, the floor could be changed from laminate (context1) to a black rubber mat (context 2). The field was resting within a black metal frame, and was surrounded in three of its four sides (north, west, east) by black cotton curtains of 200 cm height. On the north curtain, a large 3D visual cue was hung. Only rats were tested in these tasks.

The choice of objects stemmed from previous studies performed by Dr. Antonios Asiminas and adapted from Langston & Wood (2010) for testing spontaneous exploration of the *Fmr1* KO rat model during development. Objects varied more than in the previous two tasks, but sets of objects were 'paired' based on pilot data that determined which ones elicited comparable exploratory activity with wild type rats. Objects were attached to the floor of the field through a Velcro strap, and only NW-NE locations were used throughout the study.

For the object-place (OP; Figure 2.4A) task, animals are initially presented with two different objects in the rectangular field. Then during the probe phase, which occurred in the same context as the sampling phase, a further two copies of one of the two

objects presented in the sample phase were presented. In this situation, the locations remain familiar, both objects remain familiar, but for one object, the object-location configuration is novel.

The object-context (OC; Figure 2.4B) task consisted of two sample phases followed by a probe phase. During the first sampling phase (sampling 1) two identical objects were presented to the rat in context 1. Then the field was reconfigured in a different context (context 2, for sampling 2) and two identical, but novel, objects are presented. During the probe trial, the rats could explore one copy of the object in sampling 1 and one copy of the object from sampling 2 in one of the two contexts. In this situation, the objects, the contexts, and the absolute locations of the objects were familiar to the testing rat, but for one object the object-context configuration is novel in the probe phase.

For the object-place-context (OPC; Figure 2.4C) task, rats are placed in the field in either context 1 or context 2, and two different objects are present (eg. Object A in NW, and object B in NE). During sample 2 sessions, the context is changed, and the two objects that were used in sampling 1 are in the field, but in opposite locations (eg. Object B in NW, and object A in NE). Finally, during the probe phase, two identical copies of one object (either object A or object B) are presented. In this situation, one of the object copies was novel in one location in a given context, therefore the object-place-context configuration is novel.

Rats were additionally tested on a standard non-associative NOR task (as described above, but in the rectangular field), which acted as a way to establish whether the basic process of object discrimination is affected in the mutant animals.

For all the described above tasks, the sampling sessions lasted for 3 minutes (per context) and the probe test that followed was 2 minutes. The retention interval between sample phase and test phase was two minutes, in which the testing rat was put in a holding bucket.

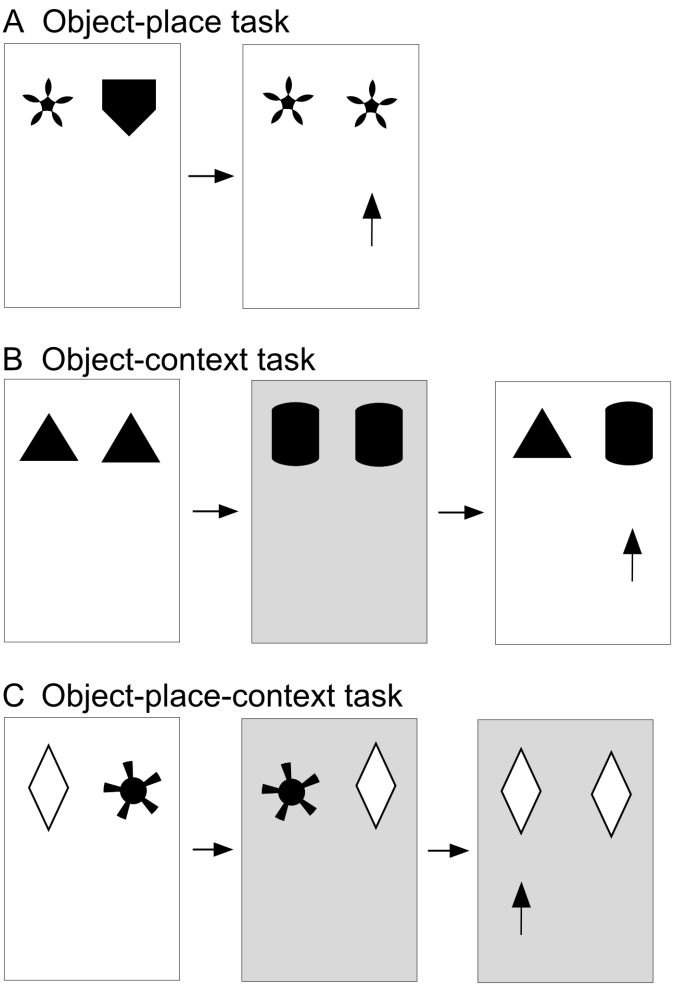

Figure 2.4 **Schematic illustration of** object-place, object-context and object-place-context tasks (A, B, C) Rentagle boxes illustrate the task apparatus, which can have two different context configurations (white or grey). Different shapes represent different objects. Arrow notes which object is at the novel configuration during the probe phase

Social interaction task

This task was designed differently for mice and rats, based on Crawley's sociability and preference for social novelty test (Moy *et al*., 2004). The apparatus for mice was a rectangular field (L 60 cm x W 40 cm x H 22 cm) divided into three equally sized chambers and made mostly of transparent Plexiglas. The floor of the field was dark grey metal and it was placed on the same metal frame-platform that was used in the open field. The camera was above the apparatus and connected to a video acquisition software. The three chambers were separated by transparent Plexiglas doors. Left and right chamber contained two identical, wire containers with removable lids that were large enough to hold a single mouse (inner diameter 7 cm, H 15 cm). These were placed one in each side of the chamber, centred. For habituation, the wire containers were removed from the field, the doors were left open and a single mouse could freely explore the entire field for 10 minutes, by being placed in the centre chamber with its snout facing the wall. Mice were habituated for three consecutive days (H_1-H_3). On the day of the experiment, the mouse was initially put in the middle chamber as before, but this time the chambers of the field are separated from each other through the Plexiglas doors. The wire cage containers are present in the left and right chamber, and the mouse is able to see them, but not explore them yet. This step was considered as a habituation4 (H_4) and lasted 5 minutes. After that, the mouse was removed from the field and placed in a holding cage for 5 minutes. On phase 1 of the experiment (sociability stage), a wild type control mouse ("stranger 1" or "conspecific 1") is placed inside one of the wire containment cages that is located in one of the side chambers. Then the test mouse is placed in the middle chamber, the doors are manually lifted by the experimenter, and the test mouse is left to explore the entire field for 10 minutes. In this situation, the stranger mouse acts as a novel social stimulus, whereas the empty wire chamber acts as a non-social (inanimate) novelty. At a second phase (social novelty stage), the procedure is repeated, but another wild type control mouse ("stranger 2" or "conspecific 2") is placed where the wire chamber was previously empty. The duration of this phase is again 10 minutes.

For sociability and social novelty testing in rats, a protocol described previously by McKibben, Reynolds, & Jenkins (2014) was adapted. The field used was a rectangular

box (L 150 cm x W 50 cm x H 30 cm), divided into three chambers and made mostly of transparent Plexiglas. The left and right chambers were of equal size (L 60 cm x W 50 cm) and the centre chamber was smaller (L 30 cm x W 50 cm). The floor was white laminated wood, and it was placed on the floor of the room, with a camera attached to the ceiling and connected to a video acquisition software. The three chambers were separated by transparent Plexiglas doors. The left and right chamber contained two identical, wire containers that were large enough to hold a single adult rat. These were placed vertically one in each side of the chamber, 30 cm from the side walls. Rats were habituated for three consecutive days, 10 minutes each day, by simulating the experiment procedure. Briefly, the test rat was placed in the central chamber of the field for 2 minutes with the doors in place. After that time, the experimenter would manually lift the doors, and the test rat is left to explore the entire arena for 10 minutes. For the first habituation session (H_1), the wire containments were absent, whereas for H_2-H_4 the cages were in place, therefore the wire containments themselves were not novel to the rats. For phase 1 (sociability) and phase 2 (social novelty) the procedure was comparable to the mouse task, but with the addition of the 2-minute hold in the centre chamber. In between phases, the testing rat was placed in a holding bucket for 5 minutes.

All experiments were counterbalanced for locations and strangers. Strangers are always adult wild type animals of the same background strain and sex to the test animals. They have been habituated to being restrained in the wire cage containments for at least 3 days prior to the start of the experiment, by simulating the entire procedure with other wild type animals (not used as testing animals). In phase 2, stranger 1 and stranger 2 are non-littermates, unless otherwise stated. After each animal session, the field and the wire cage containers were thoroughly cleaned from droppings/pee with baby wipes sprayed with 70% ethanol.

Assessment of olfaction

This task relies on the rodent's tendency to investigate, detect and differentiate smells, and is adapted from Yang and Crawley (2009) to use for rats. The test rat is transferred to a cage, similar to its' home cage, with 5-10 cm of clean sawdust bedding. Male and

female rats had separate testing cages. First, on day 1, the rat is acclimatised to the environment, the procedure and to the cotton bud, which at this stage is only infused with ddH_20 (Macknin *et al*., 2004). On the day of the experiment (day 2), the rat is transferred to the test cage, and a series of odour-infused cotton swabs are presented for 2 min each, with a min ITI during which the rat remains in the cage. The order is as follows:

ddH_20, ddH_20, non-social odour 1.1, non-social odour 1.2, non-social odour 1.3, non-social odour 2.1, non-social odour 2.2, non-social odour 2.3, social odour 1.1, social odour 1.2, social odour 1.3, social odour 2.1, social odour 2.2, social odour 2.3, ddH_20

For non-social odours, I used banana extract (1:1000 diluted in ddH_20; Foodie Flavors™) and almond extract (1:1000 diluted in ddH_20; Foodie Flavors™), as two known attractive natural odours that are unfamiliar to the rodents (Munger, 2009; Yang & Crawley, 2009; Huckins *et al*., 2013). For social odours, I used four cages of 4 group-housed adult rats (two for each sex) that have not been changed for at least 5 days. Odour cages were kept outside in a different room and swabs were taken from the bottom of the cages in a diagonal manner. Odours were counterbalanced for order of exposure, but non-social odours always come first, followed by social odours. Rats were not food restricted prior to experiment.

2.3.3 Analysis of behavioural data

Scoring and analysis of data

An experimenter blind to genotype manually scored recorded videos using established evaluation standards (Moy *et al*., 2004; Winters *et al*., 2007; Hardt *et al*., 2010). For exploratory tasks with objects, an animal was considered to be exploring an object when its' snout was within 2 cm of the object. For stranger animals, exploratory activity was considered the time spent sniffing the wire cages, or time sniffing directly the animals' snout or tail. Climbing and resting on the objects or wire cages was not considered exploratory activity. For the olfactory task, time spent directly sniffing,

licking, or gnawing the odour infused cotton bud was considered as exploratory activity. Where a novelty preference index *d* was used, that was calculated using the time spent exploring the novelty (new object, location, or configuration; t_{new}) and the time spent exploring the familiarity (old object, location, or configuration; t_{old}) as follows:

$$d = (t_{new} - t_{old}) / (t_{new} + t_{old})$$

The ratio *d* can take values between -1.0 and 1.0. To determine whether animals prefer the novelty, the observed *d* was compared against chance performance (score of $d = 0.0$) using a two-tailed one sample t-test. Values significantly above $d = 0.0$ indicate preference of the animal for novelty. Mean of $d \pm$ SE is presented for behaviour results.

For the OR, OP, OC and OPC task, rats were tested twice, with a week interval in between. *d* was calculated for each trial, and for each animal an average *d* across the two trials was presented in results.

Unpaired t-tests or one-way and two-way Analysis of Variance ($_{ANOVA}$) were used to detect group differences. Values were then Bonferroni corrected.

Exclusion criteria for behavioural data

Animals have to explore the objects during the sample phase in order to form a memory of the objects. Therefore, exploration time in sample and test phase of the tasks was carefully controlled by the use of criteria imposed on the animals amount of exploratory activity. Animals had to reach 15 seconds of total object/stranger exploration and at least 5 seconds of exploration for each object in the sample and the test phase. If these criteria were not reached during the sample or test phases, the data for the relevant animal for the entire trial was excluded from further analysis. Their locomotion activity was still relevant for further analysis, so all animals were included when data for general behaviour in the testing field is presented.

2.4 Methods for Two-photon Imaging

2.4.1 Surgical procedures

Head-plate and imaging window installation with virus injection

Adult 8- to 12-week old mice were anaesthetised with isoflurane (4% for induction and 1.5-2.5% for maintenance during surgery). The fur of the head was shaved and mice were mounted on a stereotaxic frame (David Kopf Instruments, CA) over a heating pad. Non-transparent eye cream was applied to protect the eyes (Bepanthen, Bayer, Germany) and the exposed scalp was disinfected with povidone-iodine antiseptic solution (Videne, Ecolab, UK). The following analgesics and anti-inflammatory drugs were injected subcutaneously: Veteregesic, buprenorphine, 0.1 mg/kg of body weight; Dexamethasone, 2 μg; Carpofen, 0.15 mg. An additional injection of 0.5ml Ringer's solution (VWR, USA) was injected subcutaneously to prevent dehydration. A section of the scalp was removed and the underlying bone was cleared from tissue and blood. Horizontal and vertical markings were created with a scalpel on the surface of the scull to ensure stability of the head-plate. A single craniotomy (~ 2 x 2 mm) was made over the cortical region of interest on the left hemisphere; for binocular V1 window was centered at 2.5 mm lateral to midline and 1 mm anterior to lamda, for PPC window was centered at 2 mm caudal to bregma and 1.7 mm lateral to midline. For animals smaller in size, a correction factor for determining target coordinates was used by dividing the bregma-to-lamda distance of the skull of the animal by the bregma-to-lamda distance of the stereotaxic atlas (4.2 mm, Paxinos and Franklin), and multiplying the above coordinates by this correction factor. After the craniotomy, adeno-associated (AAVs) viruses expressing the genetically encoded calcium indicator GCaMP (AAV1.Syn.GCaMP6s.WPRE.SV40 or AAV1.Syn.GCaMP6f.WPRE.SV40; 10^{10}-10^{12} IU/μL; 1:10 and 1:5 in aCSF respectively; UNC, Vector Core, Chapel Hill, NC) were injected using a micromanipulator and a pipette with a 20 μm tip diameter (Nanoject, Drummond Scientific, PA) at a speed of 9.2 nl/min, at three different depths (500, 400, and 300 μm from pia; 50 nl per site). Injections were performed at an angle to minimise compression of the brain and to avoid vasculature; for V1,the injection pipette was

inserted 45° from midline and 45° from vertical; for PPC, the injection pipette was inserted 30° from midline and 60° from vertical. After each injection, the pipette was left *in situ* for an additional 5 min to prevent backflow. The craniotomy was then sealed with a custom-shaped glass coverslip and fixed with cyano-acrylic glue. A custom-built round head-post was then implanted on the exposed skull with glue and secured in place with opaque dental acrylic (Paladur, Heraeus Kulzer, Germany). Mice were placed in a clean holding cage positioned over a heating pad and monitored until they recovered from anaesthesia, before returning to their home cage. Imaging experiments started at least 2-3 weeks following virus injection.

2.4.2 Two-photon calcium imaging

Mice were head-fixed onto a cylindrical polystyrene treadmill (20 cm diameter, on a ball bearing mounting axis) and were allowed to run freely. Habituation and imaging started at least 2-3 weeks following virus injection (bright and stable GCaMP6f expression was observed around 4 weeks following injection). Mice were always habituated to head-fixation in the dark for 2 sessions of 10-30 min. In some cases, mice were habituated for up to 4 consecutive days. Imaging was performed using a custom-built resonant scanning two-photon microscope as described previously (Pakan *et al*., 2016). In brief, two-photon imaging was performed with a Ti:Sapphire excitation laser (Charmeleon Vision-S, Coherent, CA) operated 920 nm (< 50 mW power at the sample surface). GCaMP expression was isolated using a bandpass filter (455/545; ThorLABS) and detected using two GaAsP photomultiplier tubes. Images were acquired at 40 Hz with a custom-programmed LabView based software (v8.2; National Instruments, UK) and a Olympus XL PlanN 25X (1.05 NA, Olympus; field of view 384 x 384 μm) or Nikon NIR Apo 40X water-immersion objective (0.8 NA, Nikon; 600 x 600 pixel; field of view 240 x 240 μm). I acquired time-series images of 1-4 focal planes or fields of view (FOV) per mouse, depending on the GCaMP expression spread. Different fields of view in the same mouse were imaged on the same or different sessions depending on the overall behaviour of the mouse. For L2-3 neurons I imaged at cortical depths between 160 and 260 μm from pia.

For each field of view, ~10 trials in total darkness and 10-20 trials during visual stimulation were imaged, with dark and visual stimulation trials interleaved. Major out of plane drift (x, y, or z) was not observed over each imaging session, but on occasion, the position of the microscope was adjusted. Visual stimulation protocols were generated and synchronised to the resonant scanner using the Psychophysics Toolbox package (Brainard, 1997) for MATLAB (Mathworks, MA). Visual stimuli consisted of stationary full-field square-wave gratings for 2-5 s and then a corresponding drifting phase for 2-5 s (0.05 cpd, 1-1.5 Hz temporal frequency, contrast 80%, mean luminance 37 cd/m^2). In the first set of experiments I presented 8 equally spaced directions in fixed order, which was then changed for subsequent experiments to randomised order, interleaved with a 5 s presentation of grey screen (isoluminance) preceding the presentation of each oriented grating. Each trial started and ended with a black screen followed by a grey screen for 2-5 s. In a particular set of experiments in wild type mice, I used sine-wave drifting gratings (sinusoidal, 0.05 cpd, 1 Hz temporal frequency) for 3 s at phase-reversal with a corresponding grey phase for 5 s. Visual gratings were displayed on an LCD monitor (51 x 29 cm, Dell, UK) placed 20 cm from the eye level of the animal. For imaging of neurons in the PPC the monitor was positioned in front of the animal, vertical to the snout. For imaging of neurons in the V1 the monitor was placed in front of the right eye, at an angle that elicited visual responses from the neurons in each field of view.

Locomotion on the treadmill was continuously monitored using an optical encoder (250 cpr; E7P, Pewatron, Switzerland) connected to a data acquisition device (National Instruments, UK) with LabView (National Instruments, UK), sampled at 12000 Hz and analysed post-acquisition in MATLAB (Mathworks, MA). Overall behaviour of the mice on the treadmill was monitored through an infrared camera. For some experiments, I also acquired time-series images (15fps) of the left pupil of the mouse for the duration of the imaging session. At the end of each session, I acquired a z-stack through the entire cortical column of the imaged field of view at 0.5-1 μm increments.

2.4.3 Analysis of two-photon calcium imaging data

Image analysis

Brain motion was corrected after image acquisition using 2D plane translation-based sequential image alignment (SIMA 1.2.0, Kaifosh *et al*., 2014) with a maximum displacement factor set at 50 μm. Image series where the dislocation on x, y or z was too extensive were entirely excluded from analysis. Regions-of-interest (ROIs) corresponding to putative cell bodies were selected and drawn manually on ImageJ by observing down-sampled frames (2 Hz) from the GCaMP channel, as well as the average intensity projection of each imaging stack. All recorded trials were inspected and ROIs that were overlapping partly were manually decontaminated. ROIs that had extensive overlap at some trials were excluded from the entire analysis. ROIs that changed in size (usually enlarging) over the session were excluded. For the experiments where tdTom-expressing cells were also recorded, the ROIs that expressed GCaMP and tdTom were separated again by observing down-sampled frames and the merged channel maximal projection. In those experiments, ROIs that had very bright continuous GCaMP signal which leaked to the tdTom channel were also excluded.

The intensity of all pixels inside the ROI was averaged to obtain a raw time-series fluorescence trace F(t) for each ROI. Baseline fluorescence F_0 was computed for each ROI by taking the fifth percentile of the 1 Hz lowpass smoothed F(t) (zero-phase, 60^{th}-order FIR filter) over each trial ($F_0(t)$), averages across all trials (in darkness and during visual stimulation). The change in fluorescence relative to baseline ($\Delta f/f_0$) was computed by taking the difference between F and $F_0(t)$ and dividing it by F_0:

$$\Delta f/f_0 = (F - F_0(t)) / F_0$$

Neuropil contamination signal was removed by using nonnegative matrix factorization (NMF), which is a low rank matrix decomposition method most often used for de-mixing spatially overlapping signal sources (Langville *et* al., 2014), as executed in NIMFA 1.2.1 (Zitnik and Zupan, 2012). Motion correction and neuropil

decontamination were run as Python toolboxes with WinPython 2.7.10.3. Further analysis was performed using custom-written scripts in MATLAB and R.

Analysis of locomotion responses

Movement on the cylindrical treadmill was monitored using an optical encoder (Pewatron, Switzerland) and sampled at 12000 Hz. Collected position data was then interpolated onto a downsampled rate of 40 Hz to match the sampling rate of the acquired imaging data. Stationary periods were defined as periods where instantaneous speed was less than 0.1 cm/sec. Stationary periods less than 3 s after or 0.2 sec before a period of locomotion were excluded. Locomotion corresponded to periods meeting the following criteria: instantaneous speed ≥ 0.2 cm/sec, 0.25 Hz low-pass filtered speed ≥ 0.1 cm/sec, and an average speed ≥ 0.1 cm/sec over a 2 s window centered at this point in time. Inter-locomotion intervals ≤ 500 ms were also classified as locomotion. Periods that did not fit the criteria for stationary and locomotion were separated into a group called 'positioning data'. This represented the sum of time when the mouse initiates movement, is grooming or struggling on the treadmill.

Locomotion modulation index (LMI) was defined as the difference of the mean $\Delta F/F_0$ during locomotion (R_L) and stationary (R_S), normalised by the sum of both:

$$LMI = (R_L - R_s) / (R_L + R_s)$$

Analysis of visual stimulation responses

Raw time series fluorescence traces were time aligned to the fixed duration segments of individual stimuli. Therefore, the average F(t) was calculated for each stimulus, separated for grey and for each orientation. Where static and drift gratings were presented, those were also separated. To classify neuros as visually responsive, a *1-way ANOVA* was performed between the different stimulus groups. Cells that had

significantly higher F(t) (for alpha=0.05) during any stimulus condition over darkness were classified as visually responsive.

Silent neuron elimination criteria

Neurons with a low signal to noise ratio (SNR) were classified as silent and removed from further analysis. The 'pass' criterion was defined by calculating the skewness per cell per trial and then using a cut-off skew of 0.2 in at least one trial (previously used in Pakan *et al*., 2016).

Correlation coefficients of $\Delta f/f_0$

The pairwise correlation coefficients were calculated from Pearson's correlations using the unaveraged $\Delta f/f_0$ traces. r^{signal} for response R between two neurons (*i, j*):

$$r_{i,j}^{\ signal} = corr\ (R_i, R_j)$$

Coupling of $\Delta f/f_0$

For calculating coupling of each cell to its population we computed the correlation coefficient between the response of the cell and the summed activity of the entire population using unaveraged $\Delta f/f_0$ traces.

Chapter 3

Behavioural characterisation of a new rat model of *SYNGAP1* haploinsufficiency

3.1 Introduction

The mouse model has been widely used to understand the pathophysiology underlying abnormal SynGAP-mediated signalling, much like in all genetic mutations that cause intellectual disability and autism. This results from the fact that targeted gene mutation technology was largely specific for the mouse and therefore mice are currently used throughout biomedical research as the primary model organism for generating transgenic knockout models. However, recent advances in techniques for genome manipulation, such as using zinc-finger nucleases (Cui *et al*., 2011) and CRISPR-Cas9 technology (Li *et al*., 2013), allow for the generation of rat models of neurodevelopmental disorders; enabling phenotypes to be validated across species and more effectively addressing cognitive and social dysfunction, using paradigms that are difficult to assess in mice.

The evolutionary distance between mice and rats is in fact bigger than one might imagine, the two species having separated in evolution over 12 million years ago (Kumar and Hedges, 1998; Gibbs *et al*., 2004). One of the key differences in natural behaviour is that rats are opportunistic; they can be herbivores and carnivores depending on their natural sources, in comparison to mice that are primarily herbivore scavengers (Hedrich, 2000; Barnett, 2001; Renaud *et al*., 2005). This means that rats are bolder when exploring new and potentially unfriendly environments (Renaud *et al*., 2005; Boutin and Lane, 2014), which is an important trait during assessment of anxiety, fear, cognitive function and flexibility.

A wide range of cognitive tasks has been developed, validated and optimised in rats, such as tasks related to reward-based learning (De Vries *et al*., 1998), decision making (Steiner & Redish, 2014), working memory (Deacon & Rawlins, 2006) and spatial memory (Morris, 1984). Possibly one of the main reasons why these tasks are more difficult to be optimised in mice is their impulsivity and hyperactivity, which is noticeable not only during handling, training and performance in a task, but also within the home-cage environment. Instudies that compare the two species, rats outperform mice in retention memory in a Morris watermaze task (Frick *et al*., 2000; Cressant *et*

al., 2007; Stranahan, 2011). While both rats and mice succeed in locating the hidden platform, they use different strategies; rats demonstrate a robust spatial strategy which provides greater consistency to their accuracy. In a non- spatial cognitive task, such as the spontaneous object exploration task, rats appear to perform as well as (Stranahan, 2011) or better than mice, especially when the retention interval is longer (Bevins & Besheer, 2006). During the task, rats present with significantly higher exploratory interest directed to the objects compared to tested mice (Stranahan, 2011), an important factor for that type of exploration task which can account for their faster learning curve and higher performance index.

Rat models can possibly have greater impact on understanding neurological disease by addressing more sophisticated social behaviour. Rats and mice have different social structures in the wild; rats are organised in big highly social colonies with a more fluid and dynamic hierarchy. In comparison, mice are strongly territorial and usually live in small groups with one aggressive alpha male (Barnet, 1976). Rats display a greater repertoire of juvenile play than mice (Siviy & Panksepp, 2011), accompanied by a higher number of high- frequency ultrasonic vocalisations (USVs; 50 kHz type vocalisations) that are brief calls voiced in various social appetitive, non- aversive encounters (Burgdof *et al*., 2013). These high- frequency USVs are emitted by rats not only during, but also in anticipation of play. Rats have also been found to present with more complicated empathy responses than mice. Both mice (Langford *et al*., 2006) and rats (Atsak *et al*., 2011) show increased pain sensitivity (freezing) if they have witnessed cagemate's distress caused by pain (foot shock), but rats show an additional sign of reciprocal social communication. When exposed to foot shock again, the test rat's freezing response was then in turn modulated by the witness's levels of freezing; i.e. The test rat froze more if its witness froze more, suggesting that rats exhibit empathy responses in forms of a social loop. Additional studies have confirmed rat's empathic behaviours, as displayed by preference to free caged or distressed rats over food and sharing rewards (Bartal *et al*., 2011; Sato *et al*., 2015).

Finally, rats have larger brains and hence are more amenable to whole brain, functional imaging techniques. This feature explains why rats have been the most reported rodent model for non-invasive longitudinal, whole brain imaging techniques, predominantly

resting-state (rsfMRI), stimulus-evoked (st-fMRI) and pharmacological (phMRI) functional resonance imaging. Despite the existence of a wide array of mouse models of neurological disorders, most existing rsfMRI and st-fMRI literature has focused on rats as the preferred species, as it has been reported to be very challenging to acquire reproducible brain activation data upon stimulation in mice (Jonckers *et al*., 2015). Even after the development of more advanced coil technology for mice (cryo-coils; Ratering *et al*., 2008), imaging resolution is still higher for rats (Van der Linden *et al*., 2007; Jonckers *et al*., 2011), but the overall signal-to-noise ratio is now comparable between species. Spatial resolution has also been found to be 10-fold greater in rats in positron emission tomography (PET) scanning (Zheng *et al*., 2015). An interesting finding that was reported in one of the studies mentioned above (Jonckers *et al*., 2015), was that by using independent component analysis (ICA) rsfMRI for the same networks compared between species, analysis revealed unilateral components in mice compared to bilateral components in rats. Since linked resting-state networks are considered to reflect the underlying structural connectivity (Van Den Heuvel *et al*., 2009), this might reflect a higher interhemispheric connectivity in rats.

Therefore, while the mouse has been, and continues to be an invaluable model for neurodevelopmental disorders, the advances in engineering genetically modified rats allow extended study and modelling of several key behavioural aspects of the disorders. Previous work by Till *et al* (2015) and Dr. Antonis Asiminas (thesis: Asiminas, 2016) characterised novel rat models of FXS and reported that behavioural deficits do not directly translate from mouse to rat, regardless of convergence on a molecular and synaptic level. We therefore hypothesised that in rodent models of *Syngap* haploinsufficiency similar species-specific differences in behavioural endophenotypes will be apparent.

3.2 Results

3.2.1 The mouse model of *SYNGAP1* haploinsufficiency

As *SYNGAP1* is one of the most heavily studied genes from genome sequencing studies on developmental brain disorders, the synaptic and behavioural pathophysiology of the *Syngap* mouse model has been widely studied. However, results reported by various investigating groups have used independently generated mutant lines. It is widely known that genetic background can have a profound impact on behavioural responses among inbred strains of mice (Crawley *et al*., 1997; Montagutelli, 2000; Specht & Schoepfer, 2001; Wolfer *et al*., 2002). For example, a study in the mouse model of FXS by Spencer *et al* (2011), found that multiple behavioural responses resulting from the loss of the *Fmr1* gene are dependent on genetic background.

Interestingly, the Syngap heterozygous mouse model does not breed on a pure C57Bl6/J background. The colony we have available (Komiyama *et* al., 2002) is bred on a different C57 background strain (C57Bl/6J-OlaHsd; originally from Harlan), while other groups breed Syngap heterozygotes on a mixed genetic background, such as C57Bl6/J x 129sv/ev (Guo *et al*., 2009). Considering the above, and how variable behavioural assessment can be, we first decided to replicate some of the findings in the mouse literature by examining anxiety/hyperactivity, cognition, and social interaction. All the tasks that were assessed in mice were then subsequently adjusted and repeated in the new *Syngap* rat model.

3.2.1.1 *Syngap* heterozygous mice display hyperactivity

Open field test

I used the open field as a widely-utilised task to determine whether *Syngap* HET mice experience elevated activity and anxiety levels, as previously described in the literature (Guo *et al*., 2009; Muhia *et al*., 2010; Clement *et al*., 2012; Ozkan *et al*., 2014). I first quantified the distance travelled over the course of one 10 min period (Figure 3.1B) and over 10 min exposures in the open field for three consecutive days. Consistent with what has already been published, *Syngap* HET mice exhibited significantly increased distance travelled, and don't habituate to the open field across days (2-way *ANOVA* effect of genotype $F_{(1,14)}$=11.64, p = 0.0042; day $F_{(2,28)}$=0.2546, p=0.7770; interaction genotype x day $F_{(2,28)}$=5.712, p=0.0083; Figure 3.1C). Another measure for assessing locomotion is mean speed travelled, which I also found to be significantly increased on day 2 and day 3 in *Syngap* HET mice (2-way *ANOVA* effect of genotype $F_{(1,14)}$=11.65, p=0.0042; day $F_{(2,28)}$=0.2669, P = 0.7677; interaction genotype x day $F_{(2,28)}$=5.963, P = 0.0070; Figure 3.1D). On day 3, HET mice show decreased time immobile, as considered by the summed duration of each immobile episode detected that lasted a minimum of 2 seconds (2-way *ANOVA* effect of genotype $F_{(1,14)}$=7.635, p=0.0152; day $F_{(2,28)}$=0.1822, p=0.8344; interaction genotype x day $F_{(2,28)}$=0.7300, p=0.4909; Figure 3.1E). These results suggest that *Syngap* mutant mice have abnormal activity levels in an open field. To further assess hyperactivity and anxiety, I analysed movement of animals into different area zones (Bailey and Crawley, 2009). Two variables specific to the inner zone of the open field were calculated: time spent and number of entries. *Syngap* HET mice were more likely to spend more time in the centre of the field (2-way *ANOVA* effect of genotype $F_{(1,14)}$=16.40, p=0.0012; day $F_{(2,28)}$=3.307, p=0.0513; interaction genotype x day $F_{(2,28)}$=2.912, p=0.0710; Figure 3.1G) by entering and exiting a higher number of times all three days tested (2-way *ANOVA* effect of genotype $F_{(1,14)}$=17.09, p=0.0010; day $F_{(2,28)}$=0.7632, p=0.4756; interaction genotype x day $F_{(2,28)}$=1.669, p=0.2066; Figure 3.1H).

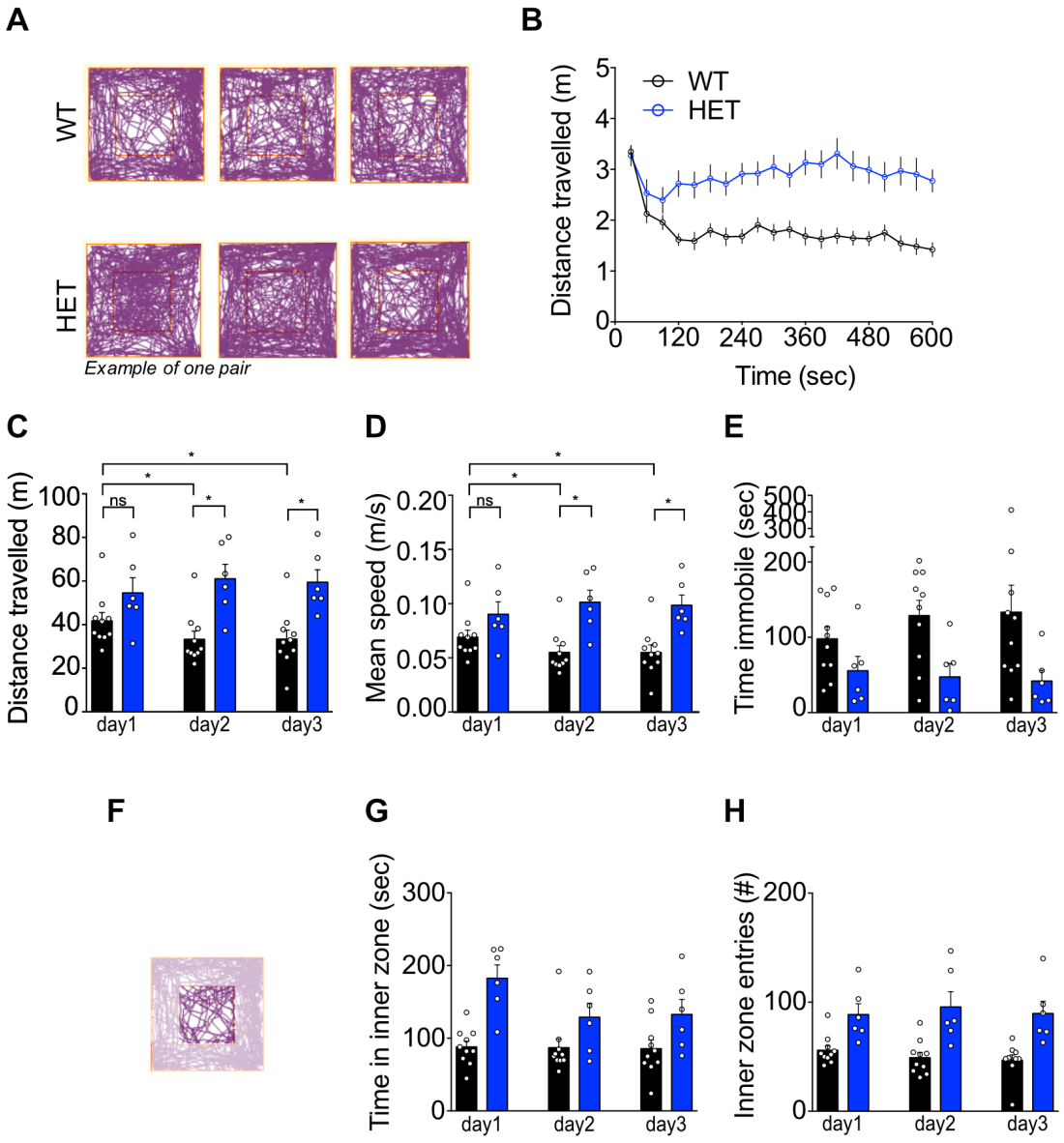

Figure 3.1 **SynGAP HET mice display enhanced horizontal locomotion.** (A) Representative trackplots of a SynGAP WT – HET pair over the course of 3 days. WT (n=10) and SynGAP HET (n=6) mice were exposed to an open field environment for 10 min for 3 consecutive days. (B) Ambulatory distance of mice on day 1 in 30 s bins. (C) Total distance travelled (2-way *ANOVA* $F_{(2,28)}$=5.712, p=0.0083; day $F_{(2,28)}$=0.2546, p=0.7770; genotype $F_{(1,14)}$=11.64, P = 0.0042) and mean speed (2-way *ANOVA* $F_{(2,28)}$=5.963, P = 0.0070; day $F_{(2,28)}$=0.2669, P = 0.7677; genotype $F_{(1,14)}$=11.65, p=0.0042) of mice over the three consecutive days show hyperactivity of SynGAP HET mice. (E) On day 3 SynGAP HET mice also show decreased time immobile (2-way *ANOVA* $F_{(2,28)}$=0.7300, p=0.4909; day $F_{(2,28)}$=0.1822, p=0.8344; genotype $F_{(1,14)}$=7.635, p=0.0152) (F,G,H) Hyperactivity was further assessed by analysis of the time spent (2-way *ANOVA* $F_{(2,28)}$=2.912, p=0.0710; day $F_{(2,28)}$=3.307, p=0.0513; genotype $F_{(1,14)}$=16.40, p=0.0012) and number of entries (2-way *ANOVA* $F_{(2,28)}$=1.669, p=0.2066; day $F_{(2,28)}$=0.7632, p=0.4756; genotype $F_{(1,14)}$=17.09, p=0.0010) in the inner zone of the open field arena across days.

3.2.1.2 *Syngap* heterozygous mice display deficits in long-term spatial memory

Spontaneous exploration task for novel object location

I assessed novel object location memory with a long-term inter-interval delay of 24 h. Mice were trained by exposing them for 3 sessions of 5 min per day for 3 consecutive days to two copies of the same object located at constant positions in a square open field. After a 24 h delay period, mice were exposed again to the same field in which one of the original objects had been moved to a new location (Figure 3.2A). Rodents are more likely to explore the moved object than the one at the familiar location, since they are attracted to novelty (Ennaceur and Delacour, 1988). Absence of exploratory preference (calculated as discrimination index, *d*) suggests absence of memory for the original location (Mumby *et al*., 2002; Winters *et al*., 2007). Only WT animals performed above chance when calculating *d* from the time the mouse spent in close interaction (sniffing) with the objects during the probe phase (one sample *t-test* d_{WT}: 0.2029±0.0762, t_7=2.660, p=0.0325; d_{HET}: 0.0649±0.1288, t_5=0.504, p=0.6359; Figure 3.2B). I also calculated *d* from the time the mice spent in the 'zone' of the object. This information was extracted from the position tracking data in Anymaze software when the animal was on and in the vicinity (<5 cm) of the object. I found that by assessing the preference of the mice through the 'zone' data, neither genotype discriminated above chance (one sample *t-tests* d_{WT}: 0.1923±0.1030, t_7=1.867, p=0.104; d_{HET}: -0.1888±0.1966, t_5=0.9605, p=0.3809; Figure 3.2B). There were no differences between the groups in overall exploration of objects (WT: 20.06±1.382; HET: 22.48±3.112; two-tailed unpaired *t-test* p= 0.4511; Figure 3.2C) suggesting differences in novelty preference were unlikely due to impaired encoding from decreased motivation or motility. While total exploratory activity was not altered in *Syngap* HET mice, the maximum time the mice spent with the new location was non-significantly decreased (WT: 5.513±1.326; HET: 2.4±0.694; two-tailed unpaired *t-test* p= 0.0848; Figure 3.2D). This finding, along with the increased distance travelled by HET mice during the probe phase of the task (WT: 10.57±1.192; HET: 16.30±1.032; two-tailed unpaired *t-test* p= 0.0046; Figure 3.2E) indicated that the hyperactivity of HET mice affects the way they interact with the objects. Finally, to examine whether the mutants exhibited impaired behavioural flexibility, I calculated their preference

index of time spent in the new location zone over the original sampling location, which I called 'phantom zone'. While WT mice appeared to have a strong preference for the new over the original zone, the *Syngap* HET mice displayed a large variability (one sample *t-tests* d_{WT}: 0.6851±0.1484, t_7=11.55, p<0.0001; d_{HET}: 0.0593±0.3382, t_5=0.4390, p=0.6790; Figure 3.2F).

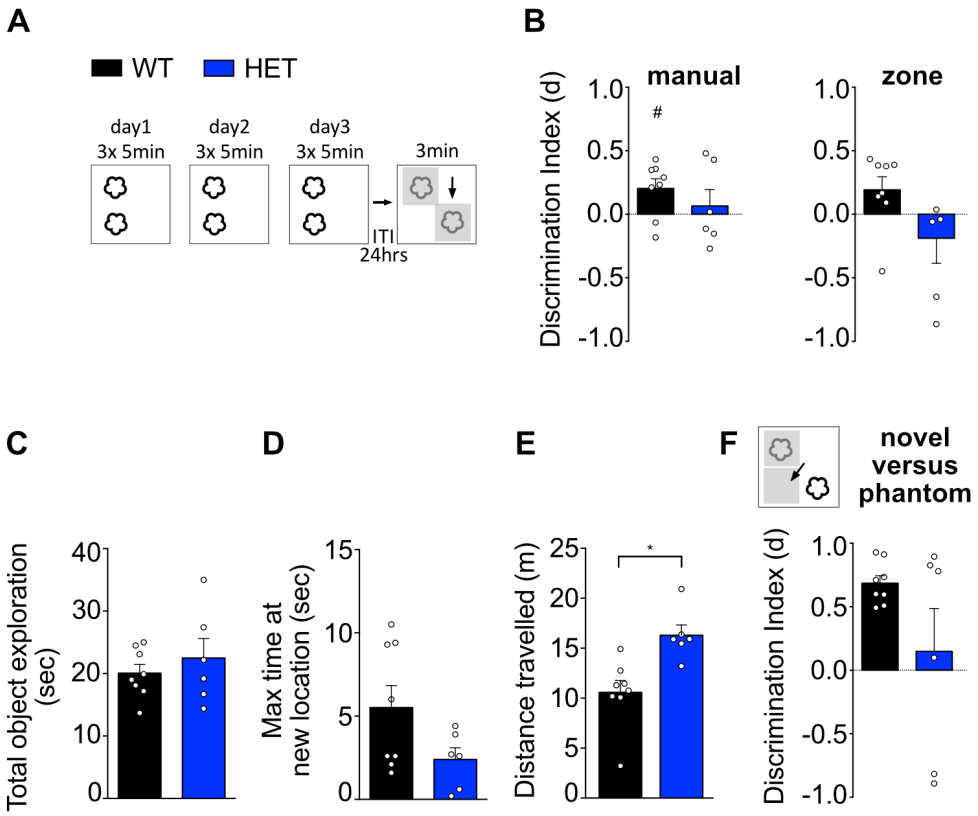

Figure 3.2 ***Syngap* HET mice show impaired performance in a hippocampus-dependent memory task.** (A) Schematic of the spontaneous exploration task for hippocampus- dependent object location memory with a long (24 h) delay. (B) Only WT mice exhibit long-term memory for OL, as measured by above chance performance (n_{WT} =8, p_{WT}= 0.0325; n_{HET}=6, p_{HET}= 0.6359). When scoring the amount of time mice spent in new (arrow) and old zone (as illustrated in grey in A), discrimination index was not significant for either genotype (n_{WT} =8, p_{WT}= 0.1041; n_{HET}=6, p_{HET}= 0.3809). (C) Total exploratory behaviour directed at the two objects was comparable between genotypes (two-tailed unpaired *t-test* p=0.4511) (D, E) The maximum amount of time SynGAP HET mice spent with the object at the new location was slightly descreased compared to WT controls (two-tailed unpaired *t-test* p=0.0848), and exhibit enhanced ambulatory distance travelled (two-tailed unpaired *t-test* p=0.0046). When scoring the amount of time mice spent in the old sampling position ('phantom' zone, arrow), the SynGAP HET mice showed increased variability (F). d ± SE is noted.

3.2.1.3 *Syngap* heterozygous mice display social isolation and lack social short-term memory

Three-chamber social interaction task

The last behavioural trait examined in mice was sociability and social novelty through a three-chamber social interaction task that is well established in the literature. Following habituation, I placed an unfamiliar stranger mouse in a wire cage in one of the three compartments of the arena. I exposed the test mouse to that field configuration (phase 1) and tested sociability by monitoring time spent exploring each chamber and time in close interaction with the stranger mouse (Figure 3.3A). After a short delay, the test mouse was exposed to a new unfamiliar stranger and tested social novelty (phase 2). When monitoring the time spent in each compartment of the 3-chamber field (Figure 3.3B), I noticed that WT animals spent less time in the non-social centre compartment in both phases of the task, compared to HET littermates. Rodents are inherently social animals, but previous work by Guo *et al* (2009) showed that *Syngap* HET mice exhibit reduced social behaviour due to their social isolation. I therefore measured social isolation by quantifying the time spent in the middle chamber during the last stage of habituation, and at phase 1 and phase 2. WT animals rapidly decreased the time they spent in the middle chamber when one or two conspecifics were introduced. On the contrary, *Syngap* HET mice preferred to stay in the centre significantly more (2-way *ANOVA* effect of genotype $F_{(1,27)}$=53.19, p<0.0001; session $F_{(2,54)}$=8.561, p=0.0006; interaction genotype x session $F_{(2,54)}$=4.849, p=0.0116; Figure 3.3E). Because the middle chamber represents a space that is separated from the other two compartments through transparent Plexiglas doors that are lifted in the start of phase 1 and phase 2, I wanted to establish whether this manual movement affected the behaviour of the mutant mice and was the reason they therefore stayed in the centre compartment more. Analysis of the latency for first entry to any of the two other chambers revealed that *Syngap* HET mice showed increased latency at the first habituation session and at phase 1, when the doors are lifted for the first time (2-way *ANOVA* effect of genotype $F_{(1,27)}$=13.70, p=0.0010; session $F_{(5,135)}$=18.18, p<0.0001; interaction genotype x session $F_{(5,135)}$=3.301, p=0.0076; Figure 3.3F). However, in phase 2 the latency between the two genotypes was

indistinguishable, suggesting that this parameter did not affect the social isolation behaviour that HET mice exhibited.

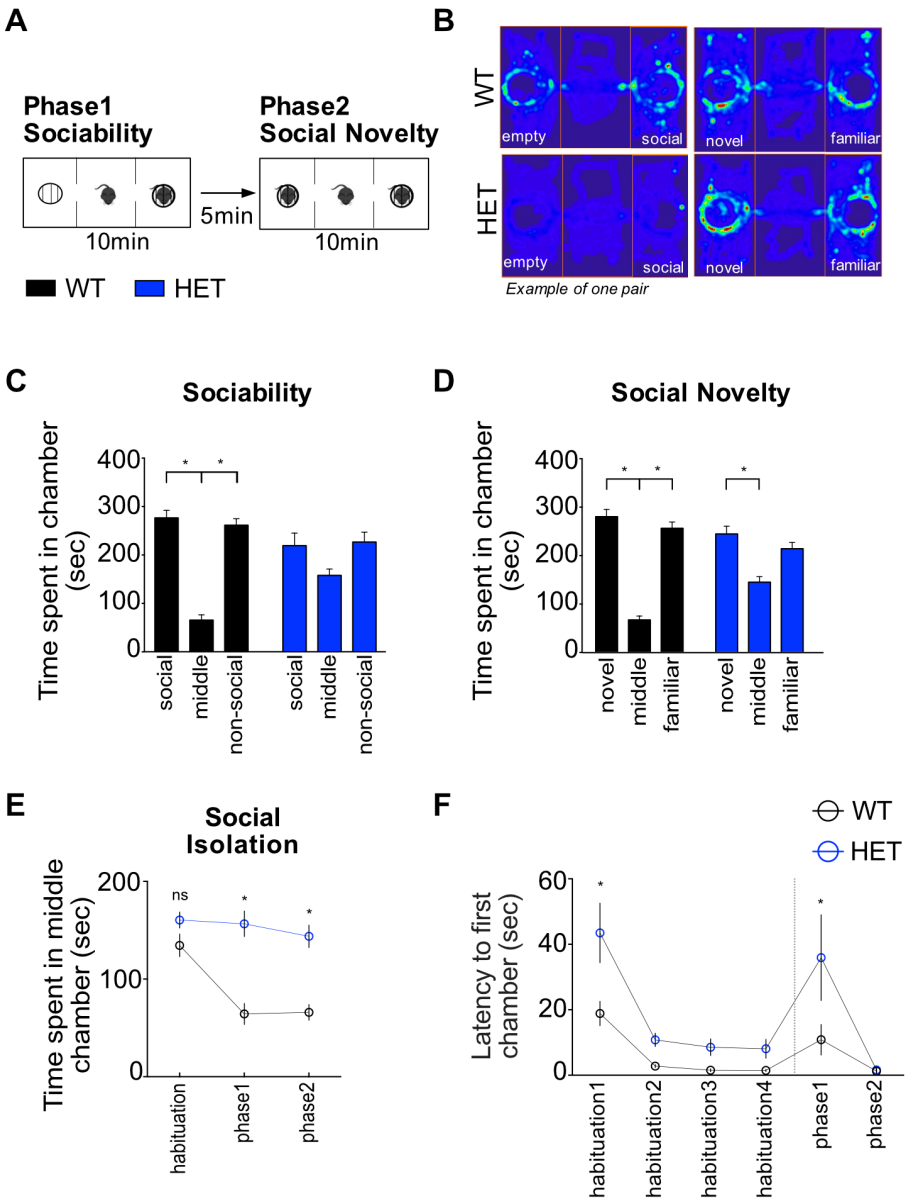

Figure 3.3 ***Syngap* HET mice show social isolation in a 3- chamber environment.** (A) Schematic of the 3- chamber task for sociability and social novelty with a short- term (5 m) delay. (B) Heat maps of mouse location in the 3- chamber field from a WT and SynGAP HET pair. (C, D) Both WT (n=18) and HET (n=11) mice spent more time in the social and non– social chamber during both phases of the task, but for HETs this preference was weaker (for sociability: 2-way *ANOVA* $F_{(2,54)}$=7.965, p=0.0009; chamber $F_{(2,54)}$=29.44, p<0.0001; genotype $F_{(1,27)}$=0.0162, p=0.899; for social novelty: 2-way *ANOVA* $F_{(2,54)}$=8.341, p=0.0007; chamber $F_{(2,54)}$=51.12, p<0.0001; genotype $F_{(1,27)}$=0.675, p=0.418). (E) Social isolation was measured as time spent in the middle compartment of the field during the last habituation session (habituation3) and the two phases of the 3- chamber task (2-way *ANOVA* $F_{(2,54)}$=4.849, p=0.0116; session $F_{(2,54)}$=8.561, p=0.0006; genotype $F_{(1,27)}$=53.19, p<0.0001). (F) When calculating the latency to entry to either side chamber during each session, SynGAP HET mice showed increased latency at the first habituation session and at phase 1 when the inter-compartment doors were lifted for the first time (2-way *ANOVA* $F_{(5,135)}$=3.301, p=0.0076; session $F_{(5,135)}$=18.18, p<0.0001; genotype $F_{(1,27)}$=13.70, p=0.0010). *ANOVAs* Bonferroni corrected.

I next assessed sociability by measuring time the mice spent in close interaction with a novel mouse (nose to nose, allogenital, tail sniffing) or the wire cage. Previous work, again by Guo *et al* (2009) showed that *Syngap* HET mice had strong preference for an unfamiliar mouse over the empty, previously seen wire cage, and therefore unaffected sociability relative to WT littermate controls. In my experiment, I wanted to additionally test whether the preference for social novelty was stronger that the preference for object novelty. For that reason, I did not expose the mice to the empty wire cages during the habituation sessions. Since their first encounter was during phase 1, the empty wire cage itself acted as object novelty. I found that WT mice showed preference for the social chamber containing the unfamiliar stranger mouse placed in the wire cage, over the non-social chamber containing only an identical wire cage (2-way *ANOVA* effect of genotype $F_{(1,27)}$=27.63, p<0.0001; chamber $F_{(1,27)}$=4.079, p=0.0534; interaction genotype x chamber $F_{(1,27)}$=0.8412, p=0.3672; Figure 3.4A).

To test for additional social interaction deficits in the HET mice, I measured their preference for a new unfamiliar (novel) stranger, over the older (familiar) one. Rodents prefer social interactions with novel conspecifics, and this is a choice dependent on a memory of previous social interactions (Crawley, 1997). WT mice spent significantly more time interacting with the novel stranger, indicating that they can form short- term social memory recognition. In contrast, *Syngap* HET mice did not distinguish between familiar and novel conspecifics (2-way *ANOVA* effect of genotype $F_{(1,27)}$=25.10, p<0.0001; chamber $F_{(1,27)}$=9.020, p=0.0057; interaction genotype x chamber $F_{(1,27)}$=3.668, p=0.0661; Figure 3.4B). However, there was a genotype difference between groups for the total exploratory activity in both phase 1 and phase 2. *Syngap* HET mice showed decreased exploratory activity directed towards object+conspecific or novel+familiar conspecific (2-way *ANOVA* effect of genotype $F_{(1,27)}$=35.63, p<0.0001; phase $F_{(1,27)}$=11.41, p=0.0022; interaction genotype x phase $F_{(1,27)}$=0.05735, p=0.8125; Figure 3.4C). This was accompanied by an increase in distance travelled (2-way *ANOVA* effect of genotype $F_{(1,27)}$=20.30, p=0.0001; phase $F_{(1,27)}$=1803, p=0.6745; interaction genotype x phase $F_{(1,27)}$=4.010, p=0.0554; Figure 3.4D) and mean speed of the mutant animals (2-way *ANOVA* effect of genotype

$F_{(1,27)}$=20.27, p=0.0001; phase $F_{(1,27)}$=0.1196, p=0.7322; interaction genotype x phase $F_{(1,27)}$=3.879, p=0.0592; Figure 3.4E), much like during the previous tasks I tested.

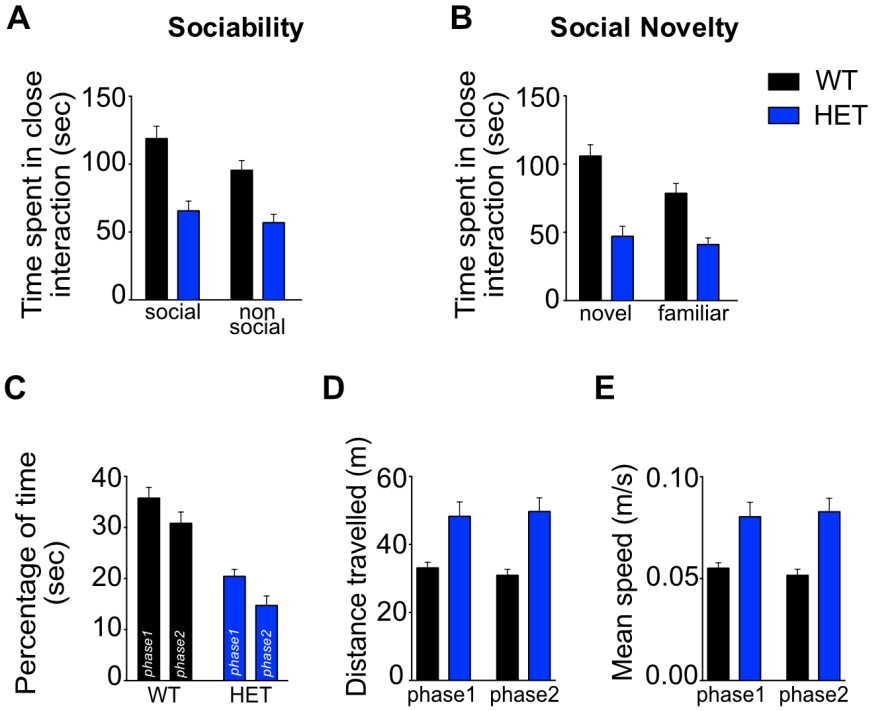

Figure 3.4 SynGAP HET mice don't show preference for sociability or social novelty in a 3-chamber environment. (A) Only WT mice (n=18) showed preference for the social chamber, containing a stranger mouse (stranger1) placed in a wire cage versus the non- social chamber that contained an empty, but identical, wire cage that acted as a novel object (2-way *ANOVA* $F_{(1,27)}$=0.8412, p=0.3672; chamber $F_{(1,27)}$=4.079, p=0.0534; genotype $F_{(1,27)}$=27.63, p<0.0001). (B) During the second phase of the task, again WT mice showed a preference for the novel stranger mouse (stranger2) whereas the *Syngap* HET mice (n=11), didn't (2-way *ANOVA* $F_{(1,27)}$=3.668, p=0.0661; chamber $F_{(1,27)}$=9.020, p=0.0057; genotype $F_{(1,27)}$=25.10, p<0.0001). (C) SynGAP HET mice showed decreased exploratory activity during the 600 seconds of phase 1 and phase 2 of the task (2-way *ANOVA* $F_{(1,27)}$=0.05735, p=0.8125; phase $F_{(1,27)}$=11.41, p=0.0022; genotype $F_{(1,27)}$=35.63, p<0.0001). (D, E) Increased ambulatory distance travelled (2-way *ANOVA* $F_{(1,27)}$=4.010, p=0.0554; phase $F_{(1,27)}$=1803, p=0.6745; genotype $F_{(1,27)}$=20.30, p=0.0001) and increased mean speed (2-way *ANOVA* $F_{(1,27)}$=3.879, p=0.0592; phase $F_{(1,27)}$=0.1196, p=0.7322; genotype $F_{(1,27)}$=20.27, p=0.0001) for HET mice.

3.2.1.4 Decreased cFos activity in the cNAc of *Syngap* heterozygous mice following assessment of social behaviour

To examine immediate early gene expression following the social interaction and novelty test, test mice were returned to their home cage for 60 minutes before sacrifice (Figure 3.5A). I measured the number of neurons ($NeuN^+$ cells) that expressed cFos, a marker of prolonged neural activity elevation in different areas of the brain (Figure 3.5B). I focused on the medial prefrontal cortex (mPFC; Figure 3.5C), the basolateral amygdala (BLA; Figure 3.5D), the nucleus accumbens (NAc; Figure 3.5E, F), and two distinct regions of the hippocampus, the ventral (Figure 3.5G) and the medial horn (Figure 3.5E), based on previous published studies about projections to and from areas that are implicated (Yizhar *et al*., 2011; Vialou *et al*., 2014; Felix-Ortiz *et al*., 2014) or favour (Gunaydin *et al*., 2014) social behaviour in mice. From these areas, I found a significant decrease in the mean number of relative $cFos^+$ neurons of HET mice only in the core of the NAc (two-tailed unpaired *t-test*; n_{WT} =5, n_{HET}=5, p=0.0081, corrected for false discovery rate through B-H procedure; see Appendix1 Table2).

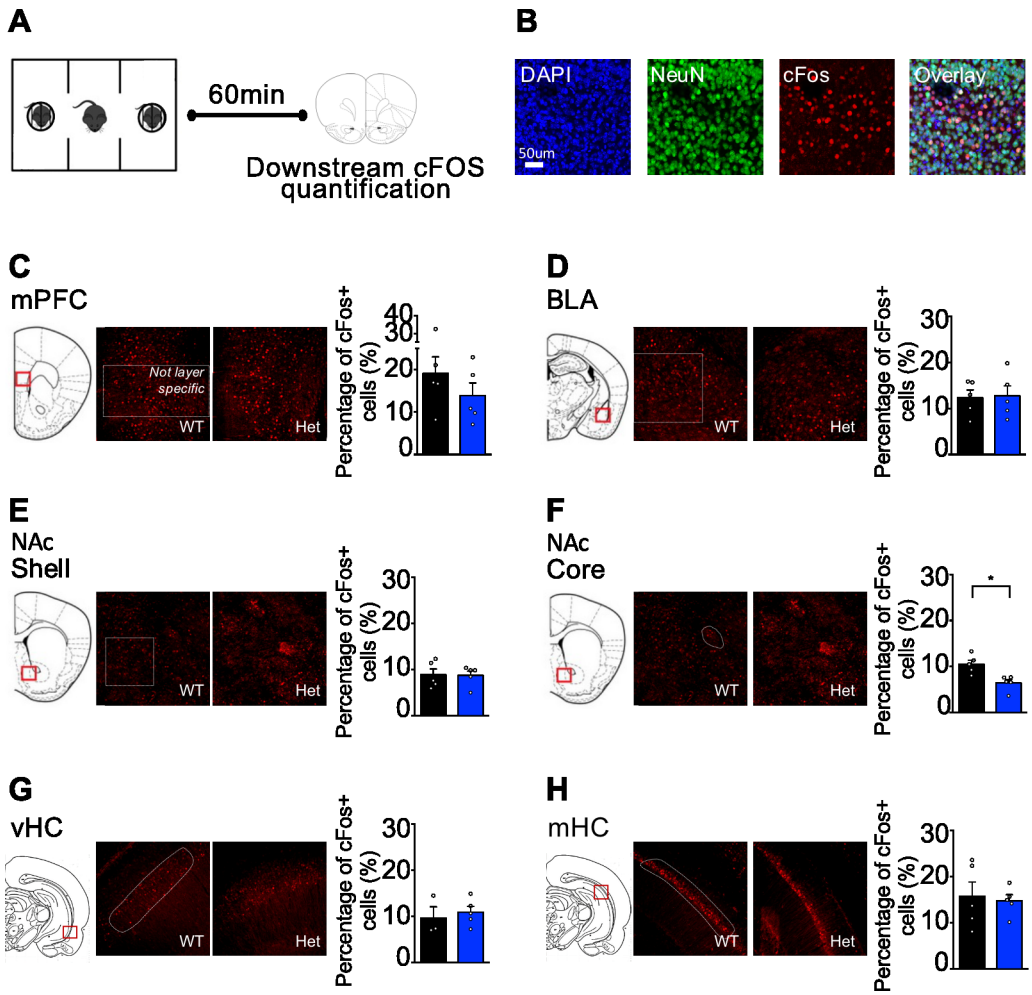

Figure 3.5 ***Syngap*** **HET mice show slight decrease in immediate early gene activity in the core of Nucleus Accumbens (cNAc) after performing a social novelty task.** (A) Schematic of the experimental set- up. After the second phase of the 3- chamber task (social novelty) mice were returned to their home cage for 1 hour and then transcardially perfused with 0.4% PFA in 0.1M PB. (B) Representative images of one prefrontal cortex slice stained with DAPI, NeuN, and cFOS, as well as the overlay. Quantification of relative $cFos^{+}$ neurons in the PL of mPFC (C), BLA (D), NAc shell and core (E, F), and the ventral (G) and medial (H) hippocampus showed a significant decrease of cFos expression only in the core of the NAc (two-tailed unpaired *t-test*; n_{WT} =5, n_{HET}=5, p=0.0081). Individual points represent animals. In each animal, counting from 2 - 3 slices per region of the brain were averaged. P-values controlled for false discovery rate using the Benjamini-Hochberg procedure with the false discovery rate set to 0.25 (also see Appendix1 Table2).

3.2.2 The rat model of *SYNGAP1* haploinsufficiency

In this study, I examined the behavioural pathophysiology associated with a new rat model of *SYNGAP1* haploinsufficiency. This rat model was designed by Peter Kind and Sally Till in consulation with Horizon Discovery and custom- generated by Horizon Discovery for the Patrick Wild Centre, Edinburgh and Centre for Brain Development and Repair, India using zinc-finger technology. The approach induced a 3584 bp deletion of the C2 protein domain and the catalytic GAP domain of the SynGAP protein, as described in the Materials and Methods section.

3.2.2.1 *Syngap* heterozygous rats are not hyperactive

Open field test

I used open field to determine whether *Syngap* HET rats demonstrated the same levels of hyperactivity that we, and other groups, found in *Syngap* HET mice. I first quantified the distance travelled over 10-minute exposures to a rectangular open field for four consecutive days. Both WT and *Syngap* HET rats habituate to the open field environment over consecutive exposures (2-way *ANOVA* effect of day $F_{(3,33)}$=10.50, p<0.0001; genotype $F_{(1,11)}$=2.665, p=0.1309; interaction day x genotype $F_{(3,33)}$=0.5267, p=0.6670; Figure 3.6A) and there was no difference between genotypes for any day analysed. I also tracked the mean speed of the rats in the arena and found the same (2-way *ANOVA* effect of day $F_{(3,33)}$=10.55, p<0.0001; genotype $F_{(1,11)}$=2.558, p=0.1381; interaction day x genotype$F_{(3,33)}$=0.5071, p=0.6801; Figure 3.6B). However, contrary to what I reported in mice, *Syngap* WT and HET rats show a similar behaviour pattern of time spent immobile during the open field testing, with HET rats overall displaying increased time immobile (2-way *ANOVA* effect of genotype $F_{(1,11)}$=5.223, p=0.0431; day $F_{(3,33)}$=3.061, p=0.0416; interaction genotype x day $F_{(3,33)}$=1.227, p=0.3155; Figure 3.6C), while the overall number of immobile episodes is comparable between genotypes (2-way *ANOVA* effect of genotype $F_{(1,44)}$=0.6730, p=0.4164; day $F_{(3,44)}$=0.5064, p=0.6799; interaction genotype x day $F_{(3,44)}$=0.4293, p=0.733; Figure 3.6D). To further assess anxiety-related phenotypes, I also calculated

time spent in inner zone and inner zone entries and found that there was an overall decreased time mutant rats spent in the inner zone of the rectangular open field arena (2-way *ANOVA* effect of genotype $F_{(1,11)}$=13.16, p=0.0040; day $F_{(3,33)}$=0.5744, p=0.6359; interaction genotype x day $F_{(3,33)}$=0.5190, p=0.6721; Figure 3.6E). This was accompanied by an overall decrease in the number of times the *Syngap* HET rats entered the inner zone (2-way *ANOVA* effect of genotype $F_{(1,11)}$=15.71, p=0.0022; day $F_{(3,33)}$=0.3802, p=0.7679; interaction genotye x day $F_{(3,33)}$=0.5428, p=0.6564; Figure 3.6F), suggesting overall preference to the outer perimeter of the field.

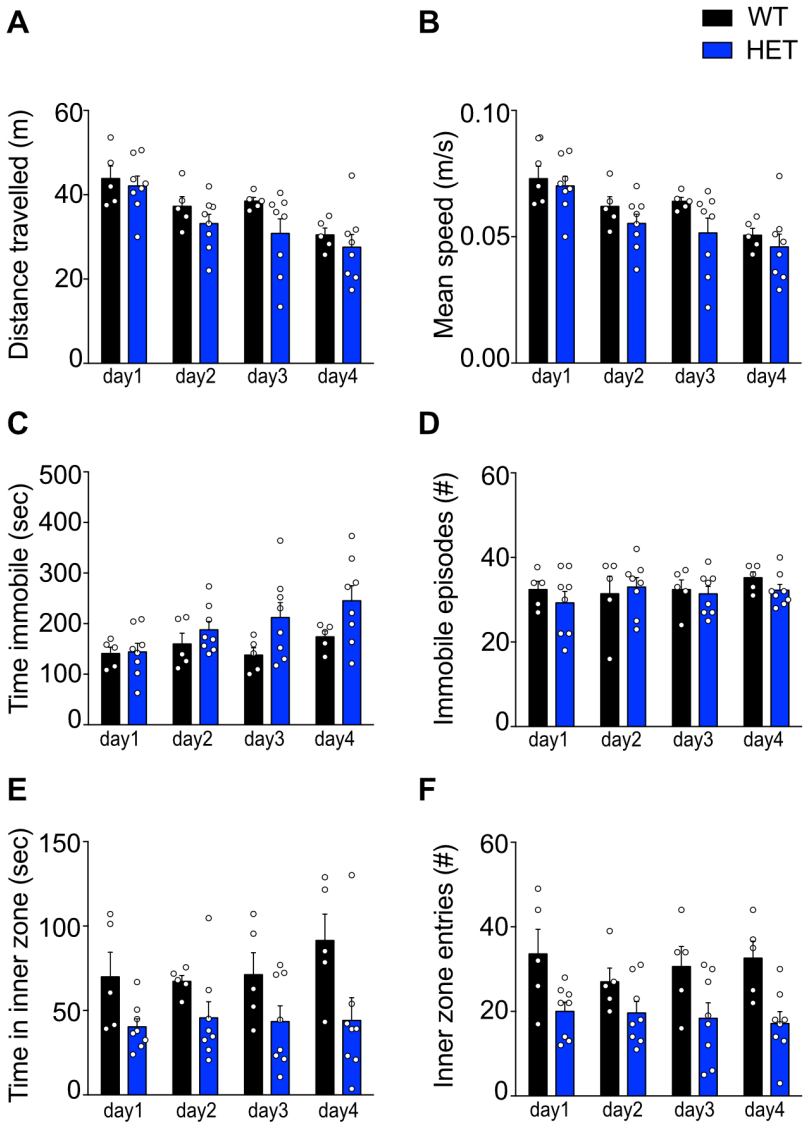

Figure 3.6 SynGAP HET rats display increased immobility during habituation to the open field. (A, B) Total distance travelled (2-way *ANOVA* $F_{(3,33)}$=0.5267, p=0.6670; day $F_{(3,33)}$=10.50, p<0.0001; genotype $F_{(1,11)}$=2.665, p=0.1309) and mean speed (2-way *ANOVA* $F_{(3,33)}$=0.5071, p=0.6801; day $F_{(3,33)}$=10.55, p<0.0001; genotype $F_{(1,11)}$=2.558, p=0.1381) of rats over four consecutive days show habituation of both genotypes to the open field arena. (C) From day 1 to day 4 SynGAP HET rats present with mildly increased immobility which results from increased time immobile (2-way *ANOVA* $F_{(3,33)}$=1.227, p=0.3155; day $F_{(3,33)}$=3.061, p=0.0416; genotype $F_{(1,11)}$=5.223, p=0.0431) while immobile episodes between WT (n=5) and HET (n=8) rats remain comparable (D). (E, F) SynGAP HET rats also exhibited decreased time in the inner zone of the open field (2-way *ANOVA* $F_{(3,33)}$=0.5190, p=0.6721; day $F_{(3,33)}$=0.5744, p=0.6359; genotype $F_{(1,11)}$=13.16, p=0.0040), and decreased inner zone entries (2-way *ANOVA* $F_{(3,33)}$=0.5428, p=0.6564; day $F_{(3,33)}$=0.3802, p=0.7679; genotype $F_{(1,11)}$=15.71, p=0.0022), consistent with previously found immobility.

3.2.2.2 *Syngap* heterozygous rats have intact short term spatial and episodic-like memory

Short-term non-associative and associative spontaneous exploration tasks

To investigate the effect of partial loss of the GAP domain of SynGAP on cognitive function, adult rats were tested on a battery of spontaneous recognition short-term memory tasks to assess non-associative memory in novel object recognition (OR), and associative memory in object-context (OC), object-place (OP) and object-place-context (OPC). These four tasks have been previously described (Eacott & Norman 2004; Langston & Wood, 2010) and used in other rat models of neurodevelopmental disorders (Till *et al*., 2015). Rats were tested twice (trial 1- week 1 and trial 2- week 2) and the mean exploratory preference (discrimination index- *d*) of these two trials was considered. Both groups showed significant memory in all four short-term memory tasks (one sample *t-tests*; for OR: d_{WT}: 0.2268±0.0792, t_4=2.865, p=0.0457; d_{HET}: 0.4198±0.0407, t_7=10.32, p<0.0001; for OC: d_{WT}: 0.3330±0.0426, t_4=7.818, p=0.0014; d_{HET}: 0.3158±0.0895, t_7=3.527, p=0.0096; for OP: d_{WT}: 0.2226±0.0478, t_4=4.666, p=0.0095; d_{HET}: 0.2719±0.0786, t_7=3.459, p=0.0106; for OPC: d_{WT}: 0.2552±0.0651, t_4=3.920, p=0.0172; d_{HET}: 0.2253±0.0637, t_6=3.538, p=0.0122; Figure 3.7A-D).

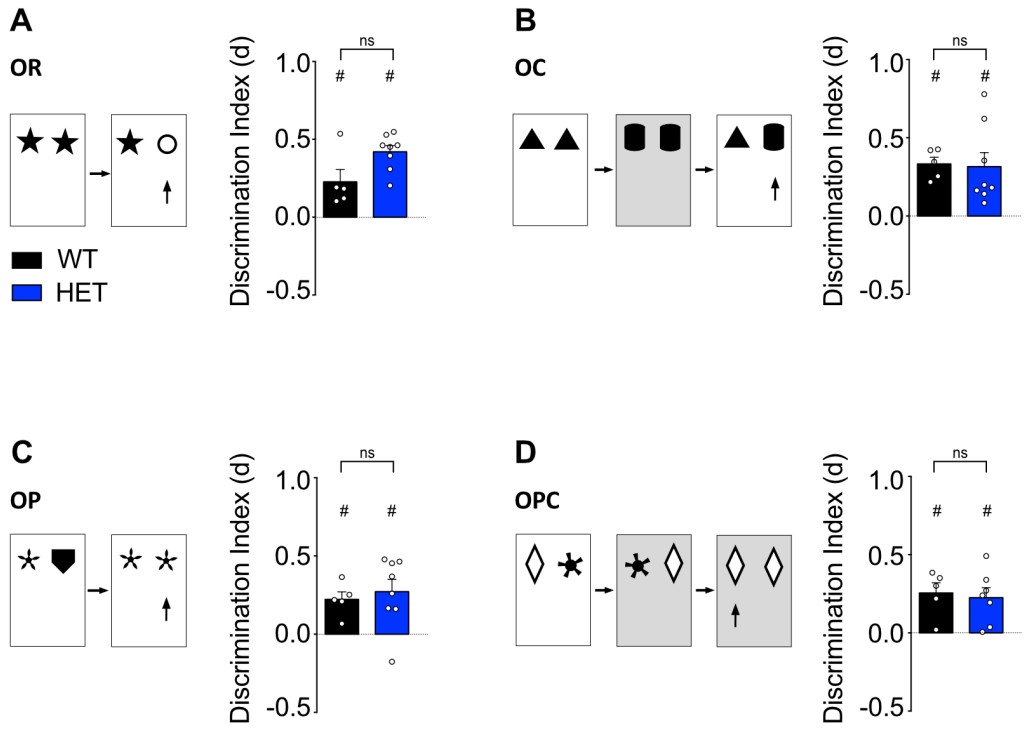

Figure 3.7 Partial loss of GAP domain in SynGAP in rats does not affect performance on spontaneous exploration tasks assessing episodic-like memory. (A, B, C, D) Both WT and SynGAP HET rats exhibit memory for all four tasks as measured by above chance performance, including OR (n_{WT} =5, p_{WT}= 0.0457; n_{HET}=8, p_{HET}<0.0001; two-tailed unpaired *t-test* p=0.0722), OC (n_{WT}=5, p_{WT}= 0.0014; n_{HET}=8, p_{HET}=0.0096; two-tailed unpaired *t-test* p=0.8655), OP (n_{WT} =5, p_{WT}= 0.0095; n_{HET}=8, p_{HET}=0.0106; two-tailed unpaired *t-test* p=0.6031), and OPC (n_{WT}=5, p_{WT}= 0.0172; n_{HET}=7, p_{HET}=0.0122; two-tailed unpaired *t-test* p=0.7459). *d* ± SE is noted.

3.2.2.3 *Syngap* heterozygous rats display deficits in long-term spatial memory

Spontaneous exploration task for novel object location

To complement our mouse data, I then assessed short- (2min) and long- term (24hour) spatial memory, by using the object location (OL) task. First, rats were tested on a standard non-associative novel object recognition task (OR), which was used to establish whether the basic process of object recognition was affected in WT and mutant animals after a long 24 h delay period. Both genotypes presented with intact short- and long- term memory for OR (one sample *t-tests*; for 2min ITI: d_{WT}: 0.4244±0.0951, t_{11}=4.461, p=0.0010; d_{HET}: 0.1814±0.0695, t_{11}=2.609, p=0.0243; for

24hour ITI: d_{WT}: 0.2172±0.0911, t_{11}=2.385, p=0.0362; d_{HET}: 0.1674±0.0668, t_7=2.507, p=0.0406; Figure 3.8A, B).

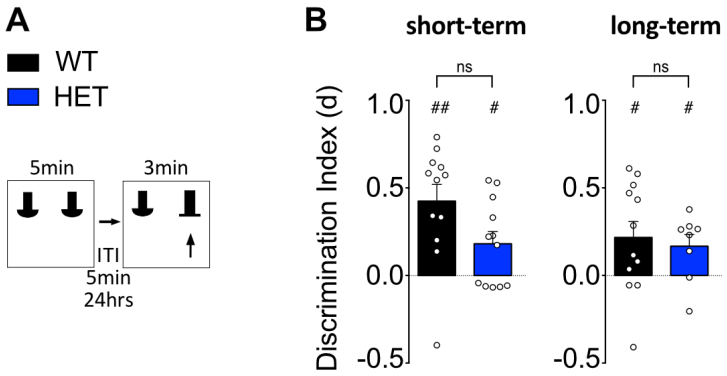

Figure 3.8 SynGAP HET rats show unaffected performance on a hippocampus- independent spontaneous exploration task. (A) Schematic of the spontaneous exploration task for novel object recognition. (B) Both WT and SynGAP HET rats exhibit memory for short- term (n_{WT}=12, p_{WT}= 0.0010; n_{HET}=12, p_{HET}=0.0243; two-tailed unpaired *t-test* p=0.0523) and long- term (n_{WT}=12, p_{WT}=0.0362; n_{HET}=9, p_{HET}=0.0406; two-tailed unpaired *t-test* p=0.6645) object memory, as measured by above chance performance. d ± SE is noted.

I tried two different paradigms to assess short- term memory for OL (Figure 3.9A). I first used a protocol with a 5min sampling session followed by a 5min ITI, but found that neither of the two genotypes could discriminate above chance during the testing phase (d_{WT}: 0.2288±0.1317, t_7=1.737, p=0.1260; d_{HET}: 0.1120±0.1130, t_{10}=0.991, p=0.3451; Figure 3.9B). Subsequently, I then increased the number of sampling sessions (3x 5min sampling sessions) and tested for short-term memory again, but found the same result (d_{WT}: 0.2590±0.1103, t_5=2.349, p=0.0656; d_{HET}: -0.0432±0.1205, t_4=0.3585, p=0.7381; Figure 3.9C). Although trends are clear, the inability to establish performance above chance was because rats were not exploring the objects (especially in the testing phase), and therefore did not pass our exploratory exclusion criteria.

I then proceeded to test long-term spatial memory. I exposed the rats to 3 x 5min sampling sessions and then waited 24 hours before assessing memory to OL (Figure 3.9D). I found that only WT rats discriminated above chance, suggesting that *Syngap* HET rats lack hippocampus-dependent long-term spatial memory (d_{WT}: 0.1763±0.0673, t_{11}=2.520, p=0.0238; d_{HET}: -0.04783±0.1109, t_5=0.4315, p=0.6841; Figure 3.9E). It was clear again that a large number of Syngap HET rats did not reach our exploratory exclusion criteria (0/12 WT rats excluded, 7/13 HET rats excluded). I therefore calculated the exploratory activity during the probe/testing phase and found that exploratory activity of mutant rats was significantly decreased in the 3 min test phase (WT: 29.41±2.958; HET: 14.27±1.859; two-tailed unpaired *t-test* p= 0.0004; Figure 3.9F), but also across most of the 3 min period when examined through 20 s binned time epochs (Figure 3.9G). To understand why the exploratory activity of *Syngap* HET rats was so low compared to WT littermates, I manually scored the behaviour of the rats during the testing/probe memory phase. I scored for time rearing (assisted rearing on walls of the arena or unassisted rearing; rearing on objects was not calculated here), time grooming and time immobile. Since the camera was over the arena, I could separate immobile sniffing time (whiskers protracting and retracting) and total immobility, which is referred to as freezing-like immobility. I found that *Syngap* HET rats spent significantly more time being immobile, in a freezing-like manner (2-way *ANOVA* effect of genotype $F_{(1,24)}$=8.799, p=0.0067; scored behaviour $F_{(3,72)}$=1.604, p=0.1958; interaction genotype x type of behaviour $F_{(3,72)}$=9.468, p<0.0001; Figure 3.9H). This observation can account for the decreased interest in actively exploring the objects during the task.

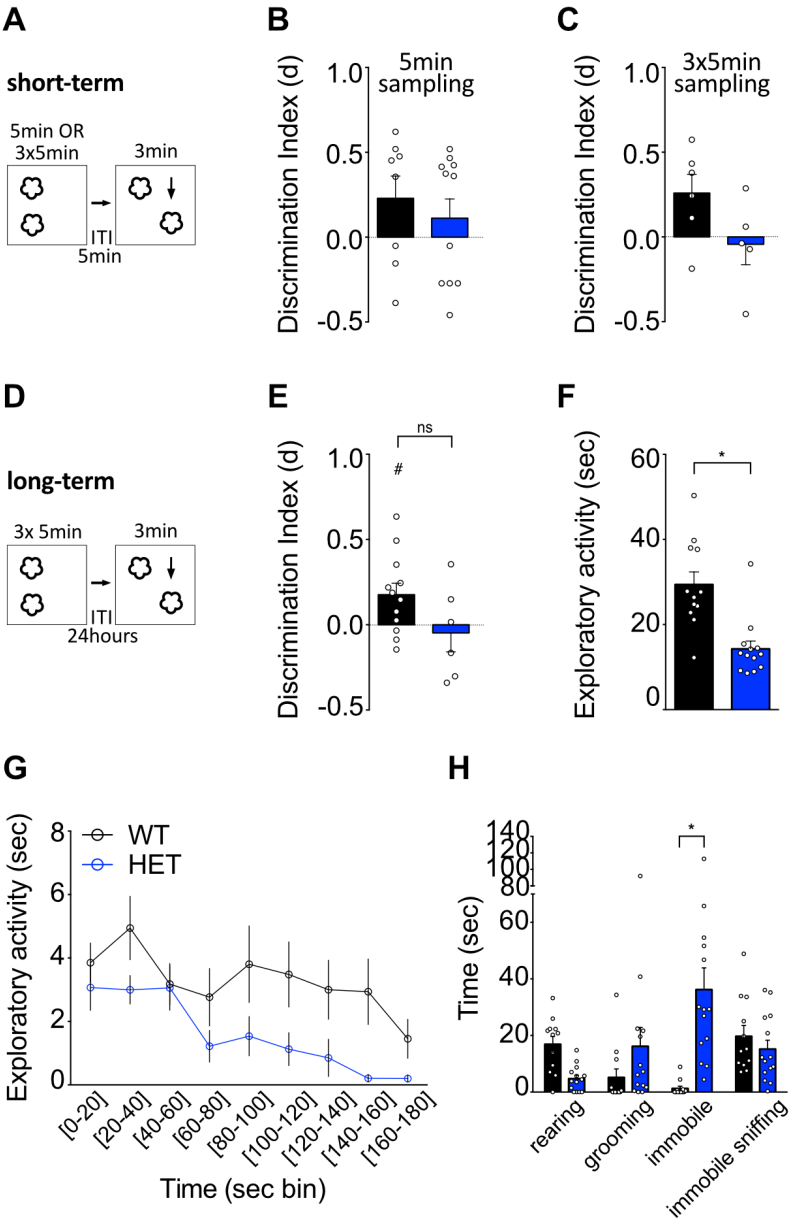

Figure 3.9 Partial loss of GAP domain in SynGAP results in impaired performance in a hippocampus-dependent long- term memory associative memory task. (A) Schematic of the spontaneous exploration task for novel object location with a short delay. (B) Both WT and SynGAP HET rats do not exhibit memory for short- term location memory when assessed after one sampling session (n_{WT} =8, p_{WT}=0.1260; n_{HET}=11, p_{HET}=0.3451) or three sampling sessions (n_{WT}=6, p_{WT}=0.0656; n_{HET}=5, p_{HET}=0.7381) (C). (D) Schematic of the spontaneous exploration task for novel object location with a long (24 hour) delay. (E) Only SynGAP HET rats do not perform above chance levels in the same OL task with a long- term memory component (d_{WT}: 0.1763±0.0673, t_{11}=2.520, p=0.0238; d_{HET}: -0.04783±0.1109, t_5=0.4315, p=0.6841; two-tailed unpaired *t-test* p=0.0869). (F, G) Object exploratory activity for HET rats during the probe phase of the OL (24hr) remained significantly decreased in total (two-tailed unpaired *t-test*; n_{WT} =12, n_{HET}=13, p=0.0004), as well as across most of the 3 min period when examined through 20 second epochs, which resulted from immobility (2-way *ANOVA* $F_{(3,72)}$=9.468, p<0.0001; scored behaviour $F_{(3,72)}$=1.604, p=0.1958; genotype $F_{(1,24)}$=8.799, p=0.0067) (H). d ± SE is noted. *ANOVA* Bonferroni corrected.

3.2.2.4 *Syngap* heterozygous rats lack social short-term memory

Three-chamber social interaction task

I used the three-chamber social interaction task to assess social interactions and social novelty preference in *Syngap* HET rats. Based on my previous findings on social isolation in mice, we decided to build a custom-made arena with two equally sized bigger side compartments, and a smaller centre compartment. In this way, we expected the rats to be motivated to explore the two side chambers more than staying in the centre. Following habituation to the entire arena and empty wire cages, test rats were exposed to an unfamiliar conspecific in a wire cage in one of the two chambers (phase 1). After a 5 minute ITI, test rats were returned to the arena, but now were exposed to an unfamiliar and a familiar conspecific (phase 2; Figure 3.10A). By tracking the position of the testing rat in the arena (Figure 3.10B) and time spent in each chamber, I found that during phase 1, both genotypes preferred the compartment where the stranger rat was placed over the compartment with the identical empty wire cage (2-way *ANOVA* effect of chamber $F_{(2,48)}=14.09$, $p<0.0001$; genotype $F_{(1,24)}=0.0057$, $p=0.94$; interaction chamber x genotype $F_{(2,48)}=4.149$, $p=0.0218$; Figure 3.10C), however the two genotype groups showed different patterns of behaviour. While WT rats spent significantly more time in the social compartment over the middle and the non-social, the *Syngap* HET rats did not show preference for the social over the middle. I therefore proceeded to test for social isolation, by separating time spent only in the middle chamber during the last stage of habituation, and phases 1 and 2. Both WT and HET rats slightly decreased the time they spent in the centre compartment when one or two conspecifics were introduced (2-way *ANOVA* effect of session $F_{(2,48)}=4.598$, $p=0.0149$; genotype $F_{(1,24)}=3.773$, $p=0.0639$; interaction session x genotype $F_{(2,48)}=0.3816$, $p=0.6838$; Figure 3.10E).

I then manually measured the time the rats spent in close interaction with conspecifics or the wire cage in the first three minutes of the task, as previously described. Both WT and *Syngap* HET rats had a strong preference for the unfamiliar rat over the empty wire cage (2-way *ANOVA* effect of chamber $F_{(1,24)}=178.4$, $p<0.0001$; genotype $F_{(1,24)}=25.03$, $p<0.0001$; interaction chamber x genotype $F_{(1,24)}=21.89$, $p<0.0001$;

Figure 3.10F), suggesting no deficits in sociability in phase 1. However, during the second phase of the task, only WT rats spent significantly more time interacting with the novel stranger rat, suggesting intact short-term social memory (2-way *ANOVA* effect of chamber $F_{(1, 24)}$=7.523, p=0.0113133; genotype $F_{(1, 24)}$=7.840, p=0.0099; interaction chamber x genotype $F_{(1,24)}$=4.476, p=0.0449; Figure 3.10G). In comparison, *Syngap* HET rats did not distinguish between novel and familiar conspecifics.

Consistent with our previous results in mice, the total exploratory activity of HET rats was decreased in both phases (2-way *ANOVA* effect of genotype $F_{(1,24)}$=19.21, p=0.0002; session $F_{(1,24)}$=3.139, p=0.0891; interaction genotype x session $F_{(1,24)}$=0.06199, p=0.8055; Figure 3.10H), but distance travelled was comparable between genotypes (Figure 3.11A). I therefore again scored for innate behaviours in the 3-chamber arena during the second phase of the task. I found that HET rats spent more time rearing and being immobile (2-way *ANOVA* effect of genotype $F_{(1,24)}$=12.67, p=0.0016; scored behaviour $F_{(2,48)}$=3.761, p=0.00304; interaction genotype x type of behaviour $F_{(2,48)}$=6.596, p=0.0029; Figure 3.11B). Due to the position of the camera during this experiment (ceiling), I was not able to dissociate between time immobile sniffing and freezing-like immobility consistently, so they are reported together.

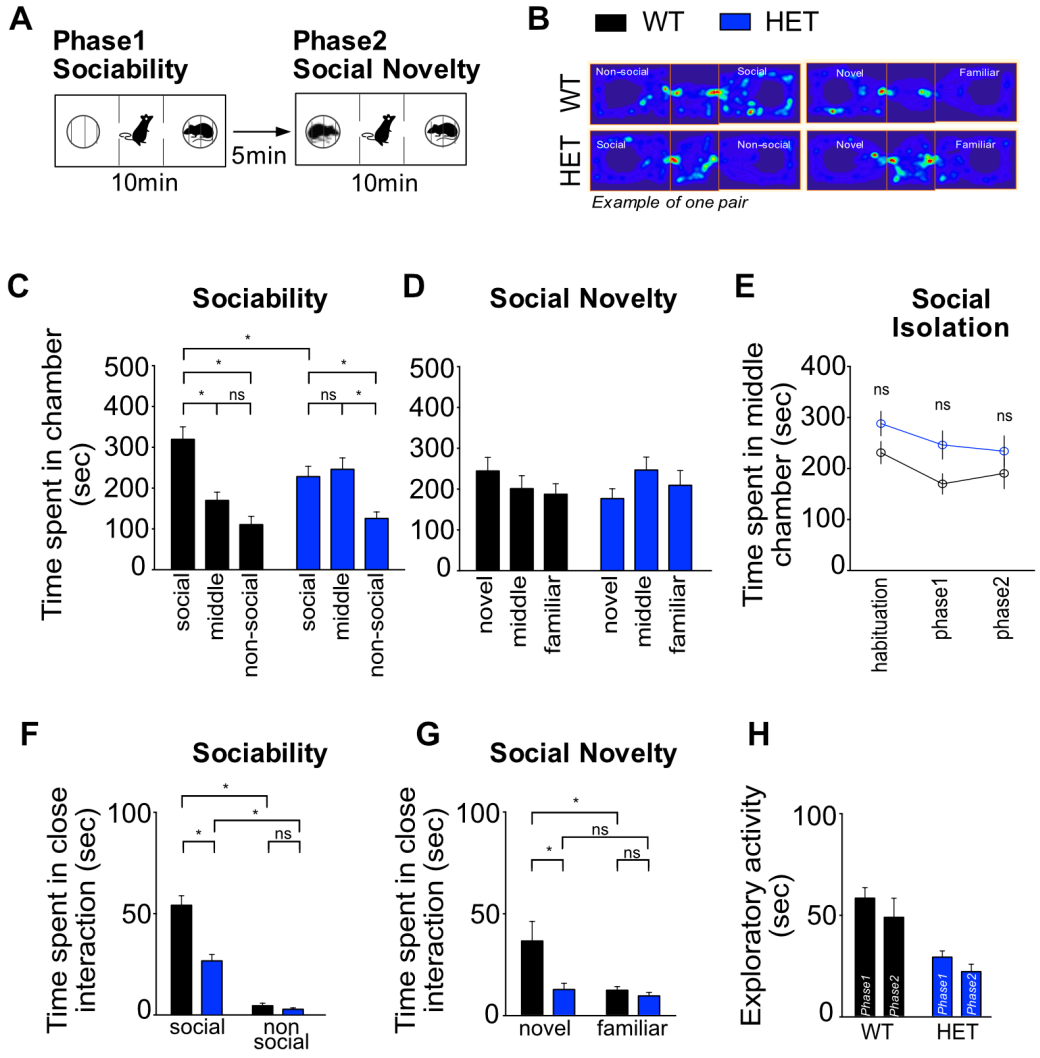

Figure 3.10 SynGAP HET rats don't show preference for social novelty when tested in a 3-chamber environment. (A) Schematic of the designed 3- chamber task for sociability and social novelty with a short- term (5min) delay. (B) Heat maps of rat location in the 3- chamber field from a WT and SynGAP HET pair. (C, D) When examining the time spent in chamber, I found a similar pattern of chamber preference for both WT (n=12) and SynGAP HET (n=14) rats in both phases of the task. (E) Social isolation was measured as time spent in the middle compartment of the field during the last habituation session (habituation3) and the two phases of the 3- chamber task (2-way *ANOVA* $F_{(2,48)}$=0.3816, p=0.6838; session $F_{(2,48)}$=4.598, p=0.0149; genotype $F_{(1,24)}$=3.773, p=0.0639). (F) When examining the time in close interaction (sniffing), both WT and HET rats showed preference for the social chamber, containing a stranger rat (stranger1) placed in a wire cage versus the non-social chamber that contained an empty, identical wire cage (2-way *ANOVA* $F_{(1,24)}$=21.89, p<0.0001; chamber $F_{(1,24)}$=178.4, p<0.0001; genotype $F_{(1,24)}$=25.03, p<0.0001). (G) During the second phase of the task, only WT rats showed preference for the novel rat (stranger2), but *Syngap* HET rats didn't (2-way *ANOVA* $F_{(1,24)}$=4.476, p=0.0449; chamber $F_{(1,\ 24)}$=7.523, p=0.0113133; genotype $F_{(1,\ 24)}$=7.840, p=0.0099). (H) When calculating the time spent in close interaction, HET rats presented with decreased exploratory activity during both phases of the task (2-way *ANOVA* $F_{(1,24)}$=0.06199, p=0.8055; session $F_{(1,24)}$=3.139, p=0.0891; genotype $F_{(1,24)}$=19.21, p=0.0002). *ANOVAs* Bonferroni corrected.

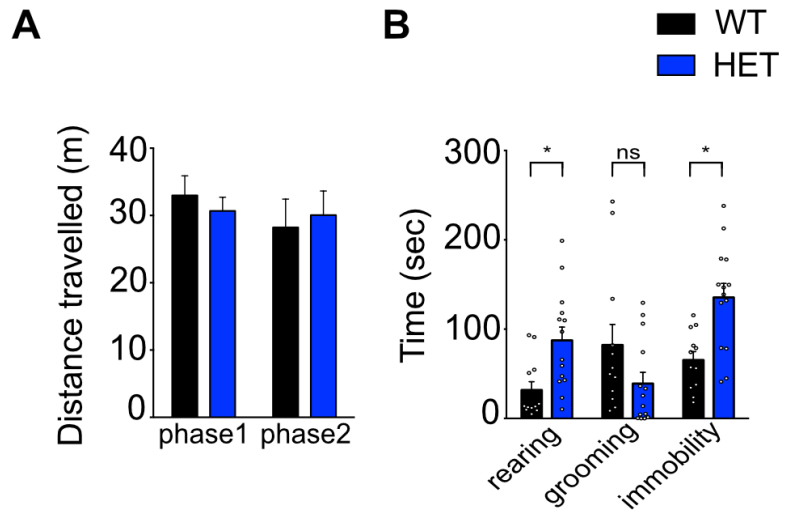

Figure 3.11 SynGAP HET rats display increased rearing and immobility during testing for social novelty in a 3-chamber environment (A) Distance travelled during both phases of the 3- chamber social interaction task was comparable between WT and SynGAP HET rats. (B) When scoring rearing, grooming, and locomotion behaviour, HET rats showed increased time rearing and increased immobility during the second phase of the task (social novelty phase) (2-way *ANOVA* $F_{(2,48)}$=6.596, p=0.0029; behaviour $F_{(2,48)}$=3.761, p=0.00304; genotype $F_{(1,24)}$=12.67, p=0.0016). All *ANOVAs* Bonferroni corrected.

3.2.2.5 *Syngap* heterozygous rats are not anosmic

Odour habituation-dishabituation task

Since olfactory cues are essential for a wide range of behaviours, including social interaction tasks, I tested WT and *Syngap* HET rats for their ability to detect and differentiate different odours. Following pre-test acclimation to ddH_20 infused cotton buds, rats were exposed to sequential presentations of both non-social odours (banana extract, almond extract; conc 1:1000) and social odours (swabs from home cages) as olfactory stimuli in a clean holding cage, similar to their home cage (Figure 3.12A). Both WT and HET rats show reduced exploratory activity when an odour is re-introduced for second and third time (habituation) and a reinstatement of exploration when a novel odour is presented (Figure 3.12B).

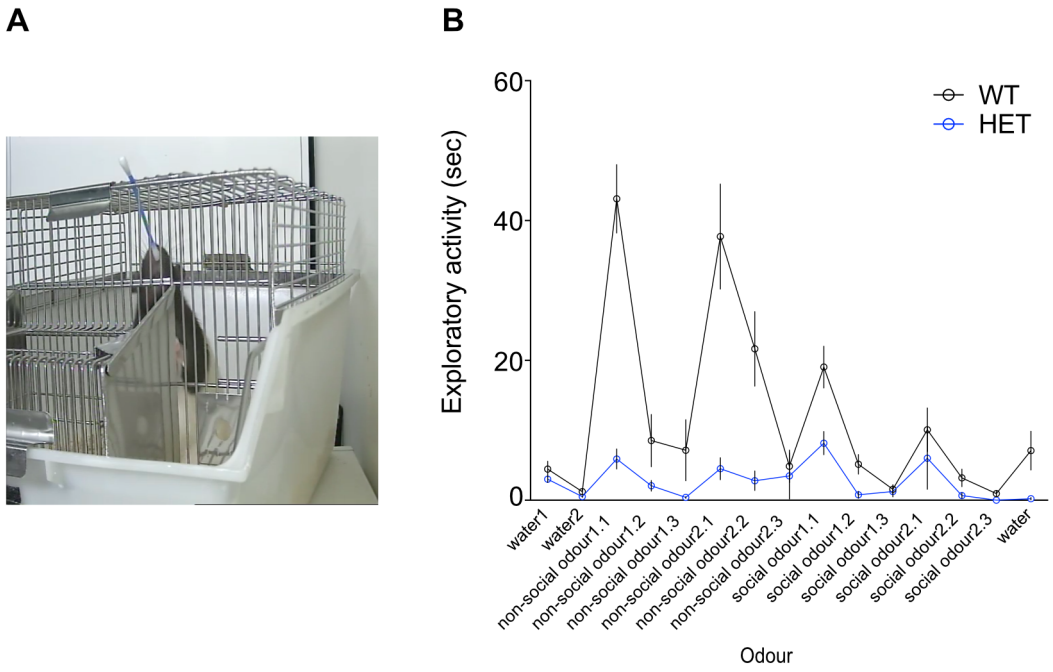

Figure 3.12 Partial loss of the GAP domain in SynGAP rats does not affect olfaction. (A) The testing environment, an empty, clean rat cage containing a layer of bedding and a cotton- tipped plastic swab secured at the cage door. (B) Both WT (n=11) and HET (n=10) rats showed habituation and dishabituation to consecutive presentations of social and non- social odours, as illustrated by the shapes of the curves of time spent sniffing the odour- saturated cotton swabs. The exploratory activity and time spent sniffing the non- social odours was higher than the time spent sniffing social odours for WT rats, but not for HETs.

Although habituation and dishabituation was reported for both genotypes, I noticed a clear genotypic difference in the level of exploratory activity (Figure 3.13A, B). As the primary purpose for conducting this task was to simply assess whether heterozygous rats have intact sense of smell, I ignored the exploration variable by normalizing to each first exposure of every odour, i.e. $(t_{odour1.2} / t_{odour1.1}) * 100$, for t equal time spent exploring. Both genotypes show habituation to the stimulus, irrespective of time exploring (Figure 3.13C). In addition, when exploratory activity was plotted by odour, both genotypes showed a slight preference to banana extract, rather than almond (Figure 3.12D, E).

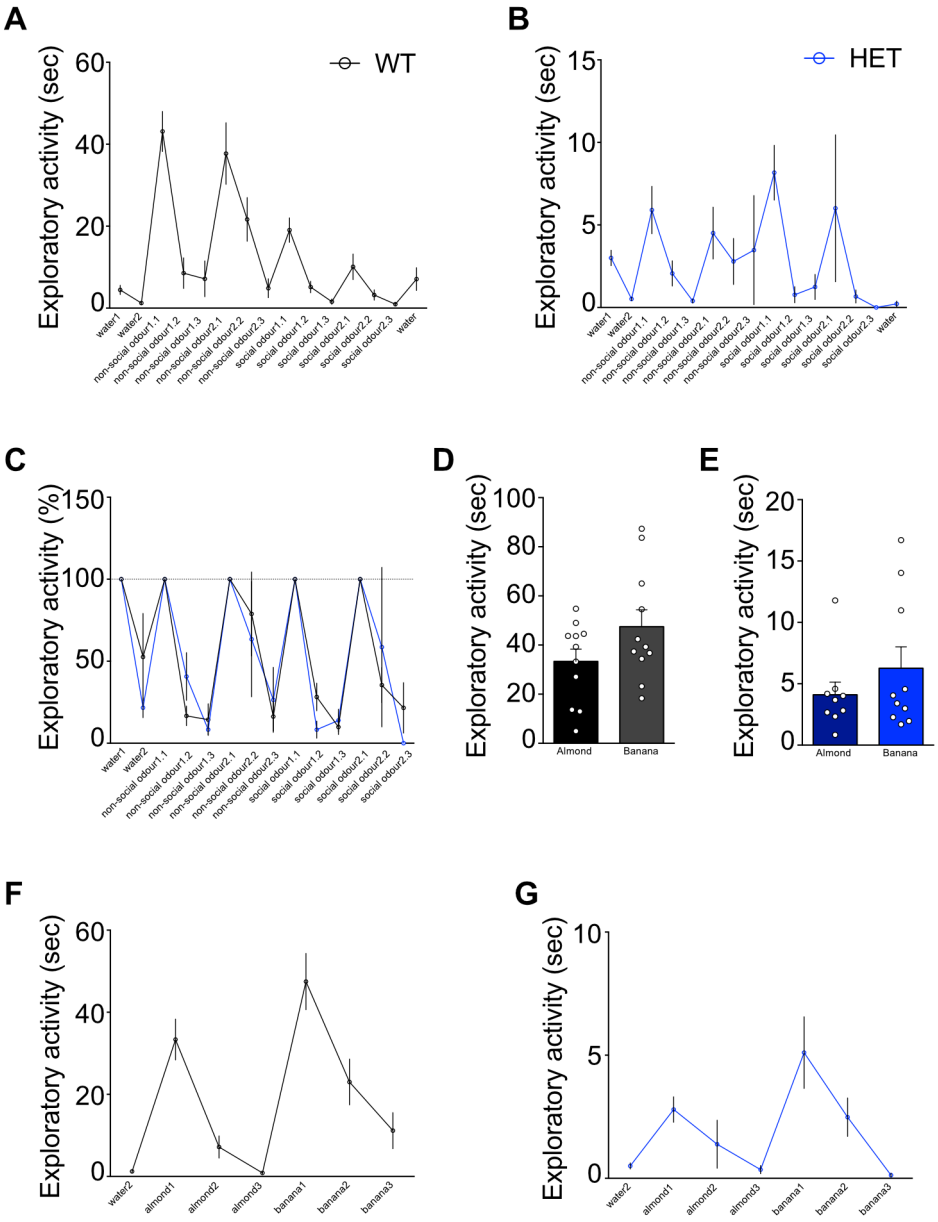

Figure 3.13 SynGAP HET rat olfaction is comparable to WT. (A, B) Separated graphs for olfactory habituation and dishabituation for WT (n=11) and SynGAP HET (n=10) rats. WT rats have a stronger preference to non- social odours and they explore the odours more than HET rats. (C) When normalised to each first odour exposure, both WT and HET rats show the same pattern of habituation to respective odour. (D, E) Non- social odours presented separated for: imitation banana flavouring (1:1000) and imitation almond flavouring (1:1000). Both genotypes show a slight preference for banana flavouring. (F, G) Graphs for olfactory habituation and dishabituation for non-social odours show again slightly increased exploratory behaviour of rats of both genotypes to the first exposure of banana (banana1) over the almond (almond1).

3.3 Discussion

3.3.1 Summary of key findings

The aim of this part of the thesis was to directly compare behavioural pathophysiology in SynGAP deficient mice and rats. As such, I first reproduced and extended current knowledge on deficits associated with heterozygous loss of SynGAP in mice:

- *Syngap* heterozygous mice display hyperactivity in all tested environments, which is consistent with previous findings of other groups.
- Heterozygous loss of SynGAP in mice causes impairments in spatial long-term memory, as examined in a hippocampus-dependent OL task with a 24hour delay.
- During social interaction assessment, *Syngap* HET mice do not display preference for social stimulus over object novelty. In addition and consistent with previous reports, *Syngap* HET mice display social isolation and lack social short-term memory.
- Following assessment of social novelty, *Syngap* HET mice display decreased activation of the core of nucleus accumbens.

I then aimed to determine whether there is cross-species convergence of behavioural pathophysiology in other rodent models of *Syngap* haploinsufficiency.

- In contrast with heterozygous mice, *Syngap* heterozygous rats do not present with hyperactivity and can be habituated to an open field environment.
- *Syngap* HET rats present with unaffected short-term associative recognition memory, as tested through an array of spontaneous exploration tasks. However, as in mice, we report impairments in spatial long-term memory.
- *Syngap* HET rats have unaffected sociability but lack social short-term memory.
- Both *Syngap* heterozygous mice and rats display decreased exploratory activity during the tasks. However, opposite to our findings in mice, in rats this is due to immobility in the arenas.

3.3.2 Extended discussion

As already mentioned in the introduction, several groups have independently reported *de novo* mutations in the *SYNGAP1* gene in patients with moderate to severe ID, often co-morbid with ASD and epilepsy. Because *SYNGAP1* appears to be high on the priority list for ID and ASD (sfari.org-gene list), the mouse model has been extensively used to understand behavioural disturbances that rise from abnormal SynGAP-mediated signalling. In this chapter of the thesis, I first focused on ensuring that I could replicate and extend some of the key findings in the literature to examine three basic modalities: anxiety/hyperactivity, cognition/memory, and social interaction. I then completed a cross-species comparison on the same behavioural traits using a new rat model of *SYNGAP1* haploinsufficiency, custom-designed by the Kind lab and generated by Horizon discovery using Zinc-finger nuclease technology.

3.3.2.1 Heterozygous loss of SynGAP in mice causes aberrant hyperactivity

I found that constitutive heterozygous SynGAP knockout mice exhibit a strong hyperactivity phenotype that does not habituate over time in the open field environment during a single session or after repeated exposure for three consecutive days. This has been the most robust finding in past literature, consistent in different *Syngap* mouse background strains and ages (Guo *et al*., 2009; Muhia *et al*., 2010; Ozkan *et al*., 2014; Berryer *et al*., 2016). I tried to dissociate hyperactivity from anxiety by examining the time the mice spent in the centre of the arena, which was increased for the mutants. Although locomotor activity and anxiety are potential confounds of each other during any given task, my data lean towards a hyperactivity deficit. This view is strengthened by results of other groups in the elevated plus maze. Guo *et al*, Muhia *et al* and Berryer *et al* reported that *Syngap* HET mice prefer to stay in the open arm during the duration of the task, rather than rest at the closed arm, indicating reduced anxiety.

Interestingly, increased locomotion and reduced anxiety are both features commonly found in, but not specific to, studies where hippocampal lesions were induced (Deacon *et al*., 2002; Balst and Feldon, 2003; Bannerman *et al*., 2003). In addition, older studies in the depression field report that acute or chronic pharmacological NMDA receptor blockade induces hyperactivity but has also concurrent anxiolytic effects (Mariusz *et al*., 1994; Wiley *et al*., 1995; Silvestre *et al*., 1997). As SynGAP is directly coupled to NMDARs through PSD-95 and other MAGUK proteins (Kim *et al*., 1998; Li *et al*., 2001), my findings are consistent with the impact of SynGAP dysregulation on NMDAR-mediated downstream signalling dysfunction.

3.3.2.2 Do *Syngap* heterozygous mice display spatial memory impairments?

Komiyama *et al* (2002) first reported that, following high-frequency stimulation, NMDAR-dependent LTP induction in the CA1 of SynGAP HET mice was strongly reduced. In addition, SynGAP has been found to regulate another distinct form of glutamate receptor-dependent plasticity in the hippocampus. *Syngap* HET mice show increased $mGluR_5$–dependent LTD, that is independent of local protein synthesis, in contrast to WT controls (Barnes *et al*., 2015). In line with the above observations, I decided to examine whether *Syngap* haploinsufficiency affects allocentric spatial memory, which is a hippocampus-dependent cognitive process (O'Keefe and Nadal, 1978). There have been two reports of spatial learning deficits in *Syngap* HET mice, however both show mild transient results. In the first report, Komiyama *et al* (2002) tested the mice in a MWM task with two transfer tests (platform removed) starting 10 min after the final acquisition trial. In the first transfer test, *Syngap* HET mice showed decreased performance when calculating the proportion of time spent in a zone centred around the target (with 11/21 mice reaching performance criterion), but no significant difference from WT on the conventional measure of time in training quadrant. In the second transfer test no impairment was detected, suggesting a potential mild deficit on the rate of spatial learning. A similar transient result was reported by Muhia *et al* (2010), when a mild deficit was only observed in the early phase of the first 15 seconds of the transfer test, while the preference for target quadrant during the entire 60sec

testing period was comparable to WT. Since one of the tests was designed with a short-term (10 min following acquisition; Komiyama *et al*., 2002) and the other long-term ITI (24 hr following acquisition; Muhia *et al*., 2010), it suggests that this difference is a possible weak memory retrieval deficit rather than memory retention. Finally, in both cases the acquisition was clearly unaffected.

Following these two reports, I decided to use a different paradigm. We know that *Syngap* HET mice exhibit normal object recognition performance (Muhia *et al*., 2010), therefore I used a spontaneous exploration task for novel object location, which is a task that has been widely used in rats to test allocentric spatial memory, and depends on the dorsal hippocampus (Mumby *et al*., 2002; Vogel-Ciernia & Wood, 2004; Lee *et al*., 2005). Mice were tested for long-term memory 24 hours after the last sampling session and I found that only WT mice showed significant preference for the novel location over the old one, indicating that *Syngap* HET mice did not express memory for this task. However, I noticed that the maximum time mutant mice spent in the zone of the object (at novel position) was significantly decreased compared to WT controls. This was accompanied by increased locomotion, indicating that hyperactivity of HET mice could influence the way they interact with the objects; i.e. even though their summed exploratory activity towards the objects is comparable to WT, it consists of many short visits between running. This could potentially influence memory encoding and be a confounding factor in my task. Indeed, work from Muhia *et al* (2010) also failed to show locomotor habituation of HET mice during the radial arm maze and the elevated plus maze. Therefore, it is difficult to determine whether my finding is a true cognitive deficit resulting from reduction in SynGAP expression or is a manifestation of impaired spatial habituation due to hyperactivity.

On the other hand, if we do accept that *Syngap* HET mice exhibit true cognitive impairments, this indicates that OL and MWM tasks assess allocentric spatial memory differently. Since spontaneous exploration tasks do not involve any reward-based or punishment-based training, they represent a more naturalistic approach. Mice, unlike rats, are not naturally born swimmers therefore tasks like the MWM, where finding the platform is potentially critical for survival, may push them to perform more efficiently. Finally, even though both tasks require the hippocampus to be intact, it is

highly unlikely that any phenotype we find can be attributed to functional perturbation of a single isolated brain structure. Taken together, my data suggests that SynGAP selectively affects a subset of hippocampus-dependent processes that arise from associations of different circuits.

3.3.2.3 Heterozygous loss of SynGAP affects social behaviour in mice

In the next set of experiments, I assessed social interactions and social memory. Mice are highly social species (Grant and McIntosh, 1963; Laviola and Terranova, 1998) and the 3-chamber task has been widely used to quantitatively investigate social behaviours and social deficits in mice (Nadler *et al*., 2004). I first quantified levels of sociability, as a measurement of tendency to initiate social contact. *Syngap* HET mice have previously been found to have unaffected sociability by preferring to spend more time in the compartment where a mouse is present, over the compartment with an empty wirecage (Guo *et al*., 2009). In this protocol, the mice have been originally habituated to the entire arena, including the wirecages, therefore they didn't act as a novelty. I decided to alter this protocol slightly, by refraining from habituating test mice to the wirecages, to investigate whether HET mice had stronger preference for social company over preference for object novelty. While WT mice explored the stranger mouse more than the empty cage as expected, HET mice expressed equal levels of exploration. Preference for social novelty was then quantified, as the tendency to initiate contact with new individuals compared to familiar ones, based on memory of past social experiences. I used non-littermate strangers during the task, as I previously found that if mice are exposed to a novel and a familiar conspecific that originated from the same litter, both WT and HET mice cannot discriminate between the two (See Appendix1 Figure 1.2). Consistent with previous reports (Guo *et al*., 2009; Berryer *et al*., 2016), I found that *Syngap* HET mice lack social short-term memory. I also observed a display of social isolation in mutant mice, replicating previous work (Guo *et al*., 2009). Overall, findings from previous groups combined with my data suggest social impairments in *Syngap* HET mice.

To ensure that my results are not confounded by other aspects of mouse behaviour, I calculated the sum exploratory activity during close interaction (sum time sniffing). This has not been previously explored as groups focus on calculating the time test mice spend in chamber, rather than manually calculating time sniffing (Guo *et al*., 2009; Berryer *et al*., 2016). I found that *Syngap* HET mice display decreased exploratory activity, which likely stems from their hyperactivity behaviour in the arena. This again could influence performance during the task or memory encoding.

Following the 3-chamber social task, I decided to investigate immediate early gene expression in brain regions that have been associated with social processing and behaviour in rodents. Focusing on behaviours that do not include mating or fostering, such as social recognition, social affiliation and social dominance, I first decided to assess cFos expression in mPFC, and projecting areas that control emotional behaviour, BLA and NAc (Heidbreder and Groenewegen, 2003; Vialou *et al*., 2014). I found a slight, but not significant, decrease of $cFOS^{+}$ neurons in the mPFC (infralimbic area) of *Syngap* HET mice compared to WT littermates following the social novelty task. I also found significantly decreased number of $cFOS^{+}$ neurons in the core of NAc, while there was no difference between genotypes in the BLA.

Many recent papers highlight the important role of the mPFC and NAc circuitry in social behaviour modulation. E/I imbalance, through selective ChR2- mediated activation of excitatory neurons in the infralimbic area of the mPFC has been found to significantly impair social behaviour and conditioning in a 3-chamber task, without affecting anxiety (Yizhar *et al*., 2011). In addition, increased mPFC activity induced by ChR2 high-frequency stimulation in mice that have undergone social defeat stress, has been found to restore normal levels of social interaction in a social approach test (Covington *et al*., 2010). A later study by Vialou *et al* (2014), found that selectively stimulating mPFC projections to NAc (mPFC-to-NAc) reversed social avoidance in mice with social defeat-induced depression, but stimulation of corticoamygdala projections (mPFC-to-BLA) only reversed elevated anxiety, with no effect in social dysfunction. Activation of VTA-to-NAc, but not VTA-to-mPFC, projections has also been involved in encoding and predicting social interactions in a home cage social assay and in a 3-chamber task (Gunaydin *et al*., 2014).

Moreover, the hippocampus is shown to have an important role in social discrimination. Incisions of the fimbria, the band of white matter along the medial edge of the hippocampus, has been found to disrupt social recognition in rats (Maaswinkel *et al*., 1996; Kogan *et al*., 2000). In addition, more olfaction-dependent tasks are known to be mediated by the hippocampus, such as odor-paired stimulus-stimulus associations, social transmission of food preferences, and odor-guided non-matching to sample (Winocur, 1990; Bunsey and Eichenbaum, 1995; Wood *et al*., 1999). More recently, the ventral horn of the hippocampus, but not the dorsal, has been selectively found to be required for social interaction during a resident/intruder test for social aggression (McHugh *et al*., 2004). However, because of the nature of the lesions performed (large cytotoxic lesions) it is unclear if the medial part of the hippocampus was inactivated as well. Furthermore, Felix-Ortiz and Tye (2014) demonstrated that Chr2-mediated activation of BLA-to-vHC resulted in a decrease in social interaction in both the resident/intruder test and the 3-chamber task. Interestingly, this was accompanied by an increase in anxiety-like behaviours, as tested through elevated plus maze and open field. Conversely, inactivating projections from BLA-to-vHC, resulted in the opposite phenotype, suggesting that the BLA-vHC circuit can simultaneously modulate anxiety and social interactions. I therefore decided to also quantify cFOS expression in the hippocampus; WT and *Syngap* HET mice showed comparable levels of $cFOS^{+}$ neurons in the vHC and the mHC following the social novelty task, suggesting that the mPFC-to-NAc pathway is more likely to be affected in HET mice and correlate with the social interaction and social novelty deficits I observed.

Nevertheless, there is one main limitation in my study that needs to be noted. This set of experiments is lacking a control condition where mice encountered novel objects, rather than novel conspecifics, to analyse levels of cFOS expression due to anxiety or general (object) novelty during the task. In addition, it would be interesting to investigate whether naïve (non-behaved) WT and HET mice have different levels of basal cFOS expression, to verify if there are differences within genotypes in constitutive FOS expression in the absence of any behavioural paradigm. That could again reflect their anxiety/hyperactivity level in their home-cage, and would provide additional control information for the data I acquired.

3.3.2.4 Characterisation of a new rat model of *SYNGAP1* haploinsufficiency

Over the past two decades there has been a combined effort by the research community that focuses on disorders of brain development to understand the pathophysiology associated with syndromic and non-syndromic causes of ID and autism, and therefore several preclinical mouse models, like the *Syngap* mouse model, have been generated and show construct validity with the in-question disorders. While using mouse models has been the most robust approach to understand the basic neurobiology, as well as to perform pharmacological interventions, the development of rat models provides another level of valuable information that can strengthen the validity of genetic models of neurodevelopmental disorders.

In this study, I examined the pathophysiology associated with a new rat model of *SYNGAP1* haploinsufficiency bred onto the Long-Evans background. This rat model was designed with a heterozygous deletion of the C2 and catalytic GAP domain of the protein SynGAP (HET rats), using zinc-finger nuclease technology (Horizon). Agreeing with previous findings in the mouse literature (Komiyama *et al*., 2002; Kim *et al*., 2003; Vazquez *et al*., 2004), rats with a homozygous deletion of the GAP domain are much smaller in size, show no gross anatomical abnormalities but all die perinatally, not surviving past postnatal day 10 (See Appendix1 Figure 1.3). However, and in contrast with the *Syngap* HET mouse model, there are smaller forms of SynGAP that are produced in HET rats and localise to the synapses at the same levels as wild-type SynGAP (See Appendix1 Figure 1.4). Since the GAP domain has been found to be the catalytic domain of the protein (Kim *et al*., 1998), these forms of GAP-deleted SynGAP will not be enzymatically active, but may still have important biological function by regulating PSD-95 function (Walkup *et al*., 2015; see discussion below).

The residual presence of small GAP-deleted forms of SynGAP was an interesting observation considering the spectrum of *de novo* mutations in *SYNGAP1* gene that cause ID in humans, with or without comorbid ASD and epilepsy. Several pathogenic *de novo* point mutations (affecting one or few nucleotides) have been described in *SYNGAP1* patients with moderate-to-severe NSID, most of which are nonsense and frameshift mutations predicted to truncate the protein (See Appendix1 Table 1).

However, recent published studies have identified at least 7 pathogenic *de novo* missense mutations in the *SYNGAP1* gene (Berryer *et al*., 2013; O'Roak *et al*., 2014; Parker *et al*., 2015; Mignot *et al*., 2016; DECIPHER), including at least 3 point mutations in the active GAP domain and at least 2 point mutations in the C2 domain. While the mechanisms by which most of these mutations disrupt *SYNGAP1* function in humans have not yet been explored, Berryer *et al* (2013) reported that introducing either of the two *de novo* missense mutations they identified (p.W362R in C2 domain, p.P562L in GAP domain) in cortical organotypic cultures completely suppresses the ability of SYNGAP1 to inhibit ERK activation. The above suggest that studying this new rat model will provide with valuable insight into the phenotypic spectrum associated with mutations in the *SYNGAP1* gene in human patients of ID and further reinforces the need of more animal models in the field of neurodevelopmental disorders.

At the same time, recent evidence suggests that the role of SynGAP at the PSD extends further than regulation of Ras-ERK1/2 pathway. It has been highlighted that SynGAP-α1 directly affects protein and receptor composition at the PSD, by restricting binding to the PDZ domains of PSD-95 (Walkup *et al*., 2015; Walkup *et al*., 2016). This reduced binding ability could lead to more PDZ domains binding to protein receptors (like AMPARs) and holding them at the synaptic membrane. Walkup *et al* (2016) further reported that in SynGAP heterozygous mice, reduced SynGAP expression at the PSD was accompanied by increased expression of Transmembrane AMPAR Regulatory Protein (TARP2,3,4,γ8) and Leucine Rich Repeat Transmembrane Neuronal Protein (LRRMTM2), which are protein families that contribute to clustering of AMPA receptors to the membrane of glutamatergic synapses (Siddiqui *et al*., 2010). The above challenge the current theory that SynGAP predominately regulates synaptic plasticity through downregulating downstream signalling pathways due to its GTPase activity (through its catalytic GAP domain) on Ras. We therefore believe that this new rat model, designed with a heterozygous deletion of C2 and GAP domain, can also help elucidate the importance of GAP activity in synaptic and behavioural pathophysiology.

3.3.2.5 Cognitive phenotypes of *Syngap* heterozygous rats

One of the strongest and most robust phenotypes that *Syngap* HET mice express, is hyperactivity in every arena that I have exposed them to. As discussed above, this makes it difficult to determine whether some of the cognitive phenotypes the mutants exhibit are due to impaired spatial habituation to the arenas which can cause memory encoding dysfunction. I found that in contrast with *Syngap* HET mice, HET rats do not present with hyperactivity and can be habituated to the open field as well as WT littermates. Of note, *Syngap* HET rats display unaffected motor learning on the rotarod (See Appendix1 Figure 1.5). Further analysis of their locomotor activity during the open field revealed that they become more and more immobile, following exposure to the apparatus over consecutive days. It would be beneficial to assess anxiety-related behaviours with a different task to compliment the OF findings. The use of the light/dark box could be one potential task; however, it has been proven quite challenging to get consistent results in rats, due to rat's bolder innate behaviour when exploring novel environments relative to mice (Hascoet & Bourin, 2009; Holter *et al*., 2015).

I then assessed cognition, by testing episodic-like and spatial memory in *Syngap* HET rats. While adult HET rats do not present with memory impairments, as tested through preference for novelty at four spontaneous exploration tasks, OR (short and long-term), OC, OP and OPC, I found that they do exhibit spatial memory impairments in an OL task, but only when a long 24hour delay was introduced following sampling phase. When exploratory activity was examined, I found that *Syngap* HET rats explored significantly less than WT; but instead of being due to hyperactivity, as in HET mice, in rats this decrease in exploratory activity is due to "freezing-like" immobility.

While this spatial memory deficit agrees with my findings in the *Syngap* mouse, the decrease of exploration is an important factor that needs to be addressed. First of all, OPC is the most complex of the spontaneous exploration associative tasks I performed and requires the hippocampus (Langston & Wood, 2010) as well as the prefrontal and lateral entorhinal cortices (Chao *et al*., 2016). During this task, I did not find a memory

deficit in the *Syngap* HET rats and I also did not find any differences in exploratory activity, possibly because rats were more 'compelled' to explore the objects in a much smaller arena. In addition, when examining hippocampal pathophysiology, Dr. Adam Jackson found that, in contrast to HET mice (Barnes *et al*., 2015), the magnitude of DHPG-induced $mGluR_5$-dependent LTD is not increased in HET rats, suggesting that at least this form of hippocampal synaptic plasticity remains unaffected (See Appendix1 Figure 1.6). Together the above could suggest that the deficit I observed in spatial long-term memory stems from the hypoactivity of *Syngap* HET rats influencing their performance or memory encoding during the task. It is plausible that repeating the experiment with extending the time in testing phase until the HETs can accumulate a certain amount of exploratory activity (equal to the mean exploration of WT) can yield more informative data. Alternatively, assessing spatial memory in other tasks, such as the delayed matching-to-place water maze task (da Silva *et al*., 2014) could also provide valuable information about whether or not spatial memory is intact.

On the other hand, it is possible that this data suggests that loss of the GAP domain of SynGAP in rats selectively affects a subset of hippocampus-dependent process that require memory. This could be due to recruitment of different circuits during these two distinct tasks, OPC and OL. Understanding the underlying circuit activity and connectivity, and how they are affected in *Syngap* haploinsufficiency would be key to assess the arising behavioural phenotype in spatial memory. Finally, another possibility is that the OL task revealed differences between genotypes because it included a long-term 24hour delay, in which case adjusting the OPC task for a longer ITI could yield positive results and complement findings in hippocampus-dependent cognitive impairments.

3.3.2.6 *Syngap* heterozygous rats exhibit social impairments

Conspecific discrimination, using the innate tendency of rodents to investigate novel stimuli more persistently than familiar ones, is essential for development of social bonds and social hierarchy in a group of rodents (Crawley, 2004; Perna & Engelmann,

2015). Similar to *Syngap* HET mice, I found that *Syngap* HET rats also lack the ability to discriminate novel conspecifics in a social interaction and social novelty task. Furthermore, and again contrary to mice, *Syngap* HET rats showed no signs of social isolation. My findings indicate that deletion of the GAP domain of the SynGAP protein results in a significant memory impairment in social novelty in both mice and rats, but sociability in rats remains unaffected. It has been proposed that social isolation behaviour is mediated by the same cortico-limbic circuits that control specific social context behaviours, such as aggression and anxiety (Agis-Balboa *et al*., 2007; Nelson & Trainor, 2007). It is therefore possible that social isolation and social recognition deficits, even if tightly linked in the tasks used in the literature, arise from distinct underlying neural mechanisms.

Consistent with my findings in mice, the exploratory activity of Syngap HET rats was again significantly reduced in both phases of the 3-chamber task. This could be a confounding factor for my results, however, even decreased relative to WT littermates, the mean sum exploration of HET rats was over 40sec, which is considerably higher than the mean sum exploration towards objects (14.29±1.859 sec). Scoring the innate behaviours of the rats during the second phase of the task revealed increased immobility but also increased rearing in the *Syngap* HETs. Since I didn't include stimulus-oriented (social or object) rearing in my analysis and the rats have been habituated to the environment, I don't expect rearing to be due to environmental, spatial, or stimulus novelty (Lever *et al*., 2006). This could suggest either classical risk assessment behaviours, such as elevated anxiety or fear as an attempt to escape (Blanchard *et al*., 1990; Blanchard *et al*., 1991; Griebel *et al*., 1996), or increased vigilance (Inglis *et al*., 2001; Dielenberg *et al*., 2001; Merali *et al*., 2004). Interestingly, hippocampal lesions in wild type rats have been shown to increase rearing frequency, while decreasing each events' duration resembling more stereotypic behaviours (Mitchell *et al*., 1993; Liu *et al*., 2001). Therefore, re-evaluating rearing by separating events based on the animal behaviour, i.e. wall-assisted rearing, rearing followed by jumps, exploratory rearing, could reveal some informative results.

Finally, this cohort of rats used has been assessed in multiple behavioural paradigms, including OF experiments, spontaneous exploration tasks (OR, OP, OC and OPC) and spatial OL tasks. I therefore wanted to verify that repeated testing was not factor for the reduction in exploratory activity during social behaviour assessment. The 3-chamber experiment was repeated with naïve 8-10week old rats that had not undergone any other behavioural tasks, and I confirmed the social recognition phenotype as above (See Appendix1 Figure 1.7). Consequently, this replicated the social interaction deficits in two independent cohorts of *Syngap* HET rats. In addition, since my original data was acquired when the rats were ~ 6 months old, it also confirms the same deficit in a younger age (8-10week young adults).

Olfaction abilities are considered to play a key role in social recognition in rodents (Cheal & Sprott, 1971; Wrenn *et al*., 2003). Chemical induced anosmia, and removal of the olfactory bulbs or the vomeronasal organ blocks novel conspecific discrimination (Matochik, 1988; Bluthe & Dantzer, 1993) and can induce extreme aggression between males (Liebenauer & Slotnick, 1996). Previous studies have shown that *Syngap* HET mice have intact olfaction, as assessed through their ability to find buried food in a test cage (Guo *et al*., 2009). However, Yang and Crawley (2009) noted that in some cases mice can fail to find the food in time, due to immobility, vigorous digging or burrowing under bedding, and other novelty-induced responses. Since *Syngap* HET rats already display increased immobility and low levels of exploratory activity, I decided to assess olfaction through an odour habituation/dishabituation task that relies on the rat's tendency to detect and differentiate novel smells. I found that both WT and *Syngap* HET rats showed habituation to consecutive presentations of the same non-social or social odour and recovery of high exploration (dishabituation) when a novel odour was introduced. Odour-directed exploratory activity of HET rats was decreased relative to WT, in agreement with exploration data in previous tasks.

A point I noticed when analysing the data was that the exploratory activity of the WT rats towards the non-social odours was much higher than for social ones, in contrast to previous studies in mice where the opposite phenotype has been reported (Baum & Keverne, 2002; Yang & Crawley, 2009). However, those experiments were performed

with swabs infused with fresh urine samples, rather than swabs from cages and therefore that could induce the difference between studies.

3.3.2.7 Hyperactivity and hypoactivity; same cause but different manifestation?

As mentioned above, assessing cognitive and social behaviours in both species revealed that *Syngap* HETs had consistently decreased exploration towards objects, conspecifics, or odours. However, while in mutant mice this appeared to be due to hyperactivity, in mutant rats I discovered the opposite phenotype, hypoactivity. One possibility is that the underlying core phenotype is the same, but it manifests in different ways in different rodent species due to their ethological differences, as it has been proposed for multiple behaviours (Gerlai & Clayton, 1999).

To understand why the HET rats stayed more immobile in the arena during the task, which then consequently leads to a decrease in sum exploration compared to WT levels, I scored their innate behaviours, including grooming, rearing and immobility. Differentiating immobility is quite challenging since I only acquired data through one camera that was suspended vertically over the arena. However, when I could resolve different types of immobility, i.e. immobility when the rat is still whisking, sniffing the bedding or the environment, and immobility where the rat is in alert mode with no whisker movement (this was possible during the OL task, but not the 3-chamber), I found that *Syngap* HET rats tended to spend more time in freezing-like immobility. Subsequent experiments performed by Dr. Sally Till showed that *Syngap* HET rats display increased percentage of time freezing during pre-CS (pre-'neutral conditioned stimulus'), CS, and rest periods in a cued-fear conditioning paradigm, suggesting that they present with generalised fear. In addition, while the protocol used included only three CS presentations, WT rats were already extinguishing fear association by CS3, whereas the level of freezing for HET rats remained unaffected (See Appendix1 Figure 1.8).

The prelimbic (PL) and infralimbic (IL) regions of the mPFC and the basolateral amygdala (BLA) have been found to be important structures for fear memory processing. Projections of PL to the BLA are known to preferentially mediate fear expression before and after extinction (Orsini *et al*., 2011; Orsini & Marren, 2012; Knapska *et al*., 2012). Furthermore, in a more recent study, Senn *et al* (2014) showed that projections from BLA to PL (L5) are activated during fear conditioning, while projections from BLA to IL (L5) are mainly activated during fear extinction, suggesting that fear conditioning induces pathway-specific intrinsic plasticity for the circuits involved. While the above studies have focused mainly in contextual fear conditioning, we also know that the lateral nucleus of the amygdala (LA), and its connectivity to mPFC and hippocampus, is a key structure of plasticity underlying fear learning (Blair *et al*., 2001; Maren and Quirk, 2004; Schafe *et al*., 2005). Cortical modulation, mainly through IL, of associative LTP in neurons of the LA has been shown to be important for 'neutral conditioned stimulus'-to-'aversive unconditioned stimulus' (CS-US) association.

Notably, physiology experiments performed in the *Syngap* HET rat by lab members Dr. Adam Jackson and Anna Toft, show that deletion of the GAP domain of SynGAP impairs maintenance of stimulation-induced LTP in pyramidal neurons in L5 of PL and in excitatory neurons in the LA, without affecting their basal properties (See Appendix1 Figure 1.9, Figure 1.10). These findings suggest that deficits found in synaptic plasticity of regions of the mPFC and the amygdala can give rise to impaired recall of fear associations in *Syngap* HET rats. This then in turn could be the core reason driving freezing-like immobility, and subsequent decreased task-directed exploratory activity in the various testing apparatus.

Conversely, *Syngap* HET mice have been found to display significantly reduced freezing in response to an auditory conditioning tone (CS) in a contextual plus cued fear conditioning paradigm (Guo *et al*., 2009). When the authors examined whether the presentation of the CS induced hyperactivity in the mutants, they found that during training and before any US, the CS alone did not induce increased locomotor activity in either genotype. However, during fear recall (testing phase) HET mice responded to the CS with a dramatic elevation in locomotion, illustrating that a strong

hyperactivity response is linked in the expression of cued fear in *Syngap* HET mice. I therefore suggest that both *Syngap* HET mice and rats show decreased exploratory behaviour during tasks because of elevated fear, which manifests in different ways; HET rats become more immobile in a freezing-like manner, while HET mice display exaggerated running behaviour in the arena.

Since humans with mutations in *SYNGAP1* often express co-morbid epilepsy, I can't exclude that the freezing-like immobility phenotype detected is due to absence seizures. Indeed, enhanced seizure susceptibility has been shown in many animal models of monogenic causes of ID and autism, such as *Fmr1* (Bear *et al*., 2004; Silva & Ehninger, 2009), *MeCP2* (Chahrour & Zoghbi, 2007) and *TSC1* (Uhlmann *et al*., 2002). *Syngap* HET mice have been previously shown to present with reduced flurothyl-induced seizure threshold in the clonus (first event) and tonic-clonic (second event) phase (Ozkan *et al*., 2014). In addition, EEG recordings in awake adult mice have revealed frequent generalised sharp discharges of high amplitude in the temporal and parietal cortex of HET mice, but not coinciding with any significant motor events (Ozkan *et al*., 2014). Notably, Berryer *et al* (2013) reported cortical generalised seizures with myoclonic features in human patients with *de novo* truncating mutations in the *SYNGAP1* gene (c.1735C>T, nonsense in GAP domain; c.321_324del, frameshift in PH domain). For that reason, it would be important to monitor cortical oscillatory patterns through EEG during active exploratory behaviour of *Syngap* HET rats.

3.3.2.8 Is the behaviour of the mutant rats affecting the wild types?

An observation for rats in the *Syngap* colony was their highly active/aggressive behaviour. Male rats in the cages would often become aggressive towards one another, and some rats would be 'bullied' and stay in the corners. Aggressiveness increased with age, especially after 4 months old. Since I was blind to the genotypes in the cage, I took note of their ear notches and recorded observational information. From 9 male WT rats, 4 were often actively fighting each other causing bite marks down each

other's tail. From 7 male HET rats, 4 were often quietly sitting at corners occasionally being 'bullied' by WT littermates, and 1 was heavily injured during an incident and was separated from the cage. Unable to be re-introduced after healing, it was sacrificed. HET rats also carried bite marks down their tails, in lesser degree than WTs.

Even though aggressiveness was apparent in males, both female and males were also quite active and difficult to be handled. The *Syngap* rat colony was maintained in a room with a FXS rat colony and cages of WT rats for breeders. While all mentioned colonies were on the same Long-Evans background strain, aggressive behaviour was not observed in the same degree in the other colonies. Quantifying this behaviour, through a home-cage monitoring system, rather than relying on experimenter's observations is clearly needed. Further experiments to establish social hierarchy and dominance could also be highly informative. The aggressive behaviour could potentially give additional information about the decreased interest of HETs in general exploration; if HET rats are low in social rank, it could be possible that they are less motivated to explore around and get in contact with non-social or social stimuli, even non-social odours due to fear.

In addition, I also noticed that the exploratory activity of WT rats was quite low during assessing episodic-like memory of *Syngap* HET rats through the battery of four spontaneous exploration tasks in adulthood and in development (See Appendix1 Figure 1.11- also discussed further below). I compared that with previous studies in the lab from Dr. Antonis Asiminas, where he examined episodic-like memory in FXS rats (Till *et al*., 2015). In both studies, the animals used were of the same genetic background (Long-Evans), assessed in the same room and box, with the same objects, and therefore I was expecting the discrimination indices and exploration of WT rats in the *Syngap* and FXS colonies to be comparable. However, I found that while WT rats from the FXS colony explored the objects for more than 20sec (25sec on average for all tasks, over 30sec for OR), WT rats from the *Syngap* colony consistently explored less than 15sec on average (with 20sec for OR). Finally, the variability of discrimination index of the WTs for those tasks during development was much higher than for the WT rats from the FXS colony. It is unknown whether mutant behaviour

of rodents can directly affect their wild type littermates, however it could provide a possible explanation for the level of exploratory behaviour of the wild types.

3.3.2.9 Relevance of early life phases in neurodevelopmental disorders

One of the main symptoms with individuals that have *SYNGAP1* haploinsufficiency is moderate-to-severe non-syndromic global developmental delay, usually co-occurring with hypotonia and manifesting at the end of the first year or during the early second year of life (Hamdan *et al*., 2009; Berryer *et al*., 2013; Carvill *et al*., 2013; Parker *et al*., 2015). Based on the clinical phenotypes those studies describe, affected children most frequently start to walk later in life (range 14-30 months), although, there are cases where onset of walking is at a normal age depending on the gravity of delay. In addition, language development is also impaired at varying degrees. Usually being determined by the severity of ID, some children develop language delayed but with moderate speech impairments, whereas a big percentage remains non-verbal. Interestingly, studies in individuals with FXS showed that in children where ASD is co-morbid with ID, the presence of ASD enhances the delay of cognitive, language and motor development (Bailey *et al*., 2001).

The mouse model of *SYNGAP1* haploinsufficiency has been widely used to study the effect of SynGAP dysregulation in synapse formation and synaptic transmission during potentially critical phases for development. As described in the introduction, studies have shown increased maturation of pyramidal and neocortical neurons (spine anatomy/dynamics and synaptic properties) at early stages of development, especially around the second postnatal week, when these regions undergo extensive synapse remodelling due to circuit formation (Meredith *et al*., 2012; Portera-Cailliau, 2012). In *Syngap* mice some synaptic phenotypes were transiently expressed during development (Clement *et al*., 2013; Aceti *et al*., 2015) whereas some persisted through adulthood (Carlisle *et al*., 2008; Clement *et al*., 2012), consistent with the theory for critical windows of synaptic dysfunctions in cognitive disorders. Interestingly, *Syngap* haploinsufficiency in glutamatergic mPFC neurons, also induced robust cortical

hyperexcitability persisting to adulthood (Clement *et al*., 2012). In studies in conditional mutants, restoration of SynGAP in adult SynGAP HET mice had minimal impact on behaviour and cognition, as tested through open field, elevated plus maze, and a spontaneous alteration task (Clement *et al*., 2012). In addition, global induction of *Syngap* haploinsufficiency during adulthood had the same effect (Ozkan *et al*., 2014), illustrating normal SynGAP function as a critical determinant in processes that promote the development of cognition and other behaviours.

Focusing on a developmental profile of rodent behaviours with mutations in genes affected in neurodevelopmental disorders can expand our knowledge for the underlying neuronal circuits involved, based on known phases of circuit formation, plasticity, and maturation in wild type animals. It can also identify early-life critical windows when physiological and behavioural phenotypes arise, which will then set grounds for more effective intervention strategies. Therapeutic treatments, such as pharmacological interventions, focused at different ages, pre-symptomatic, during manifestation of phenotypes, or late-stage during adulthood can be an approach with more potential translational advantages. Intervention strategies need not be only limited to pharmacological rescue; several studies have shown beneficial effects of environmental enrichment in FXS mice (Restivo *et al*., 2005), but more recently a study showed that only early-life social enrichment, through enhanced maternal stimulation, can have long-lasting effects in anxiety-related, cognitive and social behaviours manifested in adulthood and associated with the loss of FMRP (Oddi *et al*., 2014).

Therefore, longitudinal studies focusing on how behaviours emerge through rodent behaviour, ie the developmental trajectory of the behaviour, within the same group of subjects, can be very advantageous. Longitudinal social behaviour studies have been performed to assess the development of dominance and aggression (Blanchard *et al*., 1988; Hood & Cairns, 1989), juvenile play (Laviola & Terranova, 1998; Ricceri *et al*., 2007) and USVs (Knutson et al., 2002; Ricceri *et al*., 2007). But only one study examining the effect of paediatric traumatic brain injury on behaviour in mice assessed social novelty through a 3-chamber task during adolescence (P35-42) and adulthood (P60-70) in the same subjects (Semple *et al*., 2012). However, in the case of the mouse

models of gene mutations that cause ASD literature is less focused on the age-related development of the novelty for conspecifics. *Syngap* HET mice have been shown to lack social short-term memory in adulthood (Guo *et al*., 2009) and in younger ages (P36- Berryer *et al*., 2016). My data shows that heterozygous loss of SynGAP in both adult mice and rats also causes social novelty deficits, and it would therefore be advantageous to assess this deficit in rats in different developmental time-points, from early weaning to late adulthood.

Furthermore, longitudinal studies on cognitive development have been also lacking in the literature, very likely due to the learning effect of multiple exposures to the same training/conditioning-based task, for example during watermaze or radial maze. However, spontaneous exploration tasks for episodic-like memory (OR, OP, OC, OPC) do not require any training and rely on the animal's innate tendency for novelty, therefore the only parameter that could affect performance over time is over-habituation to the testing arena. Recently, two studies examined the distinct developmental trajectory of episodic-like memory; one in Lister-Hooded rats (Lyon & Langston, 2014) and one in a Sprague-Dawley and Long-Evans rat model of FXS (Till *et al*., 2015; Asiminas, 2016). When I used the same optimised assay to determine the age that novelty for different types of episodic-like memory arises in *Syngap* rats, my results were a lot more variable than the previous studies (See Appendix1 Figure 1.11). With the exception of the OR task, I failed to establish above chance performance in WT or *Syngap* HET rats at the predicted ages when those preferences would emerge, i.e. P34 for OC and P49 for OP and OPC. Nevertheless, when I repeated the tasks in a naïve adult cohort I found that both genotypes performed above chance for all four tasks at P70 (with a much smaller number of animals), suggesting that repeated exposure to the testing apparatus every week decreased the exploratory interest of younger rats and therefore affected their performance during the testing phase. Repeating the experiment over development could however yield interesting information as to whether *Syngap* HET rats perform as well as WT during all ages, or if they exhibit a transient developmental delay at a critical time window that improves later on. As the sequence of key milestones in brain development appears to be quite conserved between humans and rodents (Semple *et al*., 2013), developmental studies

offer a great opportunity to understand the underlying circuit mechanisms and to use this information to make early-phase interventions that could potentially be more successful to alleviate symptoms in affected individuals.

3.3.2.10 Divergence of behavioural phenotypes with other models of Intellectual Disability

Regardless of the diversity of monogenic causes of ID and ASD, studies suggest that there is a functional convergence of several cellular and biochemical pathways that are affected (Auerbach *et al*., 2011). This has lead to the idea that multiple highly penetrant mutations, such as FXS, can provide valuable insight into the pathophysiology and pharmacological rescue of other, genetically distinct forms of ID (Wijetunge *et al*., 2013). Indeed, Barnes *et al* (2015) showed that SynGAP haploinsufficiency in mice mimics the synaptic pathophysiology associated with deletion of *Fmr1* in the CA1 of the hippocampus, including decreased $mGluR_5$-dependent LTD and increases in basal protein synthesis.

I find that while the *Syngap* HET rats phenocopy some of the cellular deficits that have been found in *Fmr1* KO rats, including the synaptic plasticity deficits in mPFC and the LA nucleus of the amygdala, but not in CA1 of the hippocampus (Dr. Adam Jackson and Anna Toft, unpublished data), behavioural phenotypes remain distinct between the two rat models. *Fmr1* KO rats display no hyperactivity or anxiety phenotype in the open field and the light/dark box, and have no deficits in memory for social novelty (Asiminas, 2016). In contrast, they do present with episodic-like memory impairments in an OPC task (Till *et al*., 2015), long-term associative memory impairment in OR (Asiminas, 2016) and altered fear memory recall through reduction of freezing in a cued-fear conditioning paradigm (Dr. Sally Till, unpublished data). These represent behavioural phenotypes on the opposite spectrum of my findings in the *Syngap* rat and highlight the need to understand how conserved key cellular phenotypes manifest in such distinct behaviours in different models of monogenic causes of neurodevelopmental disorders.

3.3.2.11 Looking forward to new rat model of *SYNGAP1* haploinsufficiency

Recent advances in whole-genome sequencing studies in idiopathic and sporadic cases of ID, ASD, and epilepsy have contributed breakthrough discoveries of novel genetic mutations in neurodevelopmental disorders (Fitzgerald *et al*., 2014). Generation of robust animal models of human neurodevelopmental disorders based on these emerging genetic risk factors would greatly contribute to our understanding of the underlying pathophysiology that contributes to a wide range of symptoms in affected individuals and therefore validate theories underlying targeted approaches to therapies of those symptoms.

While a high number of genes arising from the DDD study have been relatively understudied, the role of *SYNGAP1* gene and its encoding protein, SynGAP, has been largely examined through the development of various mouse models. Recent advances in genome-manipulation techniques have allowed for the generation of transgenic animals, other than the widely used, and usually kept highly inbred, mouse. New rodent models, such as rats, can enable for comparison of key molecular, physiological, circuit and behavioural phenotypes, enabling us to investigate validity across species evolutionary separated for more than 12 million years (Gibbs *et al*., 2004). In this chapter, I focused on the behavioural characterisation of a new rat model of *SYNGAP1* haploinsufficiency in Long-Evans rats. Following the design and induction of the mutation, we found that in contrast to the mouse, targeted deletion of the C2 and GAP domain of SynGAP in rats resulted in smaller forms of GAP-deleted SynGAP protein that localise to the synapses. Since at least 5 different pathogenic *de novo* missense mutations in the C2 and GAP domain have been previously reported in humans (Berryer *et al*., 2013; O'roak *et* al., 2014; Parker *et al*., 2015; Mignot *et al*., 2016; DECIPHER), this rat model represents a great opportunity to investigate how a point mutation would affect the structure and function of SynGAP protein and its impact on brain development and function. And in addition, is it in a different way than a truncating frameshift or nonsense mutation?

Comparing the pathophysiology and behavioural deficits I reported with a rat model with a null deletion of the SynGAP protein will complement my study and will give

valuable insight into whether these smaller GAP-deleted forms of SynGAP also differentially affect the reported endophenotypes. Indeed, in the lab we now have a custom-generated rat model of heterozygous null deletion of the SynGAP protein and currently running direct-comparison experiments. Therefore, development and subsequent in-depth study of mouse and rat models of mutations in the *Syngap* gene will further accelerate understanding of the spectrum of symptoms associated with abnormal SynGAP-mediated signalling.

Chapter 4

Behavioural-state dependent neuronal activity deficits in a mouse model of *SYNGAP1* haploinsufficiency

4.1 Introduction

Ongoing neuronal activity in the cortex, both spontaneous and sensory-driven, is dependent on the local microcircuit activity and on the long-range input it receives from other regions of the brain (Arieli *et al*., 1995; Arieli *et al*., 1996). Thus, cortical neuron activity can vary greatly depending on the state of the animal; whether that is internal Up/Down brain states (Gilbert & Sigman, 2007; Poulet & Petersen, 2008) or behavioural states, such as attention, arousal, vigilance (Petersen & Crochet, 2013; Erisken *et* al., 2014; Reimer *et al*., 2014; McGinley *et al*., 2015). Top-down modulation of network activity during different behaviour states is critical for shaping sensory perception and encoding, learning and memory, and cognition, and therefore essential for normal brain function (Gilbert & Sigman, 2007; Petersen & Crochet, 2013). For example, in macaques attention synchronises visually evoked activity (Moran & Desimore, 1985; Connor *et al*., 1997; Fries *et al*., 2001) and somatosensory activity (Hsiao *et al*., 1993; Johansen-Berg & Lloyds, 2000) and expectation boosts synchrony in motor cortex (Riehle *et al*., 1997; Salinas & Sejnowski, 2001). In rodents, processing of sensory inputs in the barrel cortex is different in quiet wakefulness than in active whisking (Crochet & Petersen, 2006), while attention/arousal and locomotion modulate response properties of neurons in the primary visual cortex, with and without sensory stimulation (Niel & Stryker, 2010, Bennett *et al*., 2013; Polack *et al*., 2013; McGinley *et al*., 2015; Pakan *et al*., 2016).

Efficient neuronal network function and dynamics during development is crucial for shaping and wiring of neuronal circuits (Hensch, 2005), especially during critical periods for experience-dependent plasticity. Indeed, the many symptoms associated with neurodevelopmental disorders are believed to arise as a result of circuit disruption during critical periods.

At the level of synapses, many studies have reported subtle anatomical and functional developmental abnormalities in neurons of various mouse models of ID and autism, including the mouse model of *SYNGAP1* haploinsufficiency. Notably, Clement *et al* (2012, 2013) showed an elevated input-output (I/O) relationship in the CA1 of the

hippocampus during development, while Ozkan *et al* (2014) reported increased mEPSC amplitude and frequency accompanied by decreased mIPSC amplitude of pyramidal mPFC neurons in adult *Syngap* HET mice. In addition, these synaptic abnormalities were accompanied by photostimulation-induced hyperexcitability in DG, CA3 and CA1, as well as electrical stimulation-evoked hyperexcitability in mPFC tested in slices *in vitro*. Furthermore, *Syngap* HET mice exhibit numerous behavioural deficits that could be explained by neuronal network hyperexcitability, such as increased incidence of sharp epileptiform discharges, reduced fluorothyl-induced seizure threshold, increased startle reactivity, reduced pre-pulse inhibition (PPI), hyperarousal and hyperactivity, suggesting abnormal sensorimotor processing (Guo *et al*., 2009, Ozkan *et al*., 2014).

In contrast, despite the importance of neural microcircuits in sensory processing and cognition, little is known about alterations in network properties and function of *Syngap* HET mice. In a study from Belmonte *et al* (2004), it has been hypothesised that the phenotypic heterogeneity found in patients with autism might not be caused by a single subtle cellular deficit but rather reflect abnormalities in network properties and network connectivity that arise when neurons interact. If the same can be proposed for patients with varying degrees of ID, understanding circuit-level alterations could potentially provide greater insight in the behavioural and intellectual deficits seen in individuals with *SYNGAP1* haploinsufficiency.

This part of the thesis is therefore dedicated to investigating neuronal ensemble dynamics and neuronal circuit properties emerging from heterozygous loss of SynGAP in awake mice through two-photon calcium imaging. We hypothesised that cortical neurons of *Syngap* HET mice would display hyperactivity and increased synchrony of responses, which have been previously demonstrated in another model of ID and autism, the *Fmr1* KO mouse (Gonçalvez *et al*., 2013).

Furthermore, I decided to test whether neurons of HET mice display impaired activity in response to distinctive behavioural states, and whether that impairment is exaggerated when combined with sensory stimulation. Indeed, sensory processing of information has been shown to be impaired at varying degrees in individuals with

autism and ID (Joosten and Bundy, 2010) and recent evidence also supports sensory oversensitivity in *SYNGAP1* haploinsuficient patients (Prchalova *et al*., 2017). I therefore focused on two cortical regions; the posterior parietal cortex (PPC), as an association area important for multisensory integration (Olcese *et* al., 2013), and the primary visual cortex (V1), an area that is easily accessible and well established in the literature to present with strong responses to visual sensory input. I recorded cell type-specific and non-specific somatic calcium responses in awake head-restrained animals, in response to locomotion and presentation of visual stimuli. The results presented below are part of an ongoing project.

4.2 Results

4.2.1 Imaging calcium responses of neurons in layer 2/3 of PPC

In vivo two-photon microscopy was used with a previously described custom-built imaging system (Pakan *et al*., 2016), where animals were awake and head-fixed, but able to run freely on a cylindrical treadmill (Figure 4.1; also see Materials and Methods).

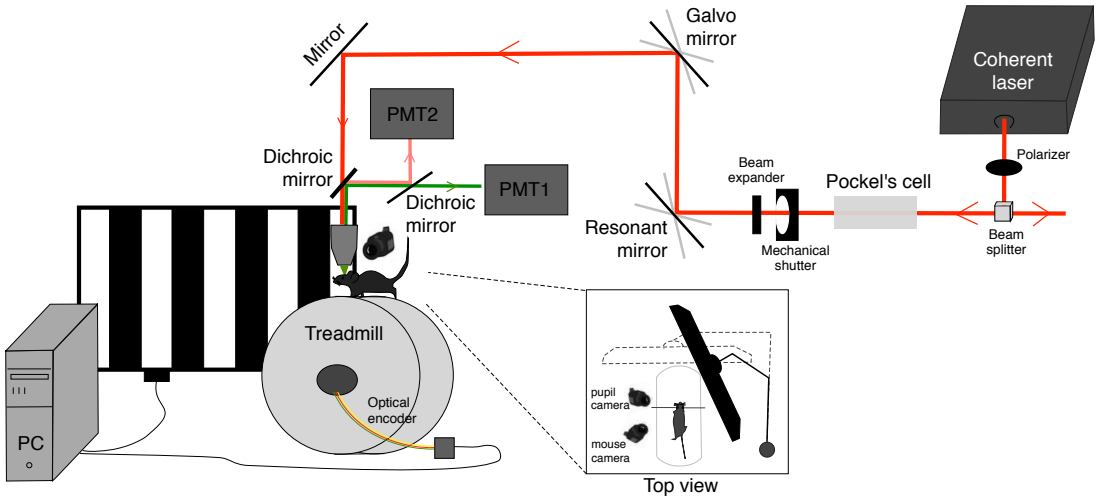

Figure 4.1 Two-photon imaging set-up for *in vivo* recordings in awake mice. Schematic illustration of experimental two-photon apparatus; a two-photon set-up is used to image through the cranial window of an awake mouse that is head-restrained but freely running on a cylindrical Styrofoam treadmill. Speed is recorded through an optical encoder on the treadmill. Ti:Sapphire pulsing laser system from Coherent was tuned to 920nm. Generated laser beam passes through a beam splitter for simultaneous imaging in two two-photon set up. Each laser beam then passes through a computer-controlled Pockel's cell attenuator (limiting the maximum laser intensity), a mechanical shutter and then a beam expander for free tuning of the laser beam diameter. Two mirrors, one galvanometer scan mirror and one resonant scan mirror, direct the laser beam to any XY position in the field of view. After brain surface illumination, the generated fluorescence light is separated from the excitation beam with a dichroic mirror, a band pass filter and then spectrally separated fluorescence light is sent on to photomultiplier tubes for simultaneous signal detection (one for each channel). Head-fixed mice face an LCD monitor which is dark or presents visual stimuli (grey screen or oriented gratings) during concurrent calcium imaging. Multiple infrared cameras record the behaviour of the mouse on the treadmill, including a camera recording the pupil dilation and a second camera recording whisking (facial vibrissae). Insert; Schematic illustration from top-view. Screen is positioned in the front for two-photon imaging in PPC and on the side (right) for V1 recordings.

To image layer 2/3 neurons of the PPC, I used the genetically encoded calcium indicator GCaMP6s or GCaMP6f (Chen *et al*., 2013), which increases fluorescence intensity in response to action potential firing, therefore widely used as a non-linear proxy for neuronal spiking activity. GCaMP6 was used under a synapsin promoter (Syn), therefore labelling all neurons. Mice underwent surgery at 2-4 months of age (>P60) for virus injection (based on coordinates from Harvey *et al*., 2009), and were then imaged 2-4 weeks later depending on GCaMP expression (Figure 4.2A, B). I confirmed targeting of medial PPC post-imaging using immunofluorescence in 40 μm slices (Figure 4.2C-F). All injections sites for the following PPC dataset can be found in the Appendix1 Figure 1.12. Animals where the injection site was too caudal or lateral were excluded from analysis.

The PPC subchapter consists of two parts; first, imaging GCaMP6s-calcium responses of layer 2/3 PPC neurons in *Syngap* heterozygous and WT controls. This was followed by imaging GCaMP6f-calcium responses of PPC neurons of *Syngap* HET mice and WT littermate controls with tdTom expression in the endogenous PV population (See Materials and Methods). With my injection protocol, I was able to image from the surface of the brain up to ~500 μm deep (Figure 4.3).

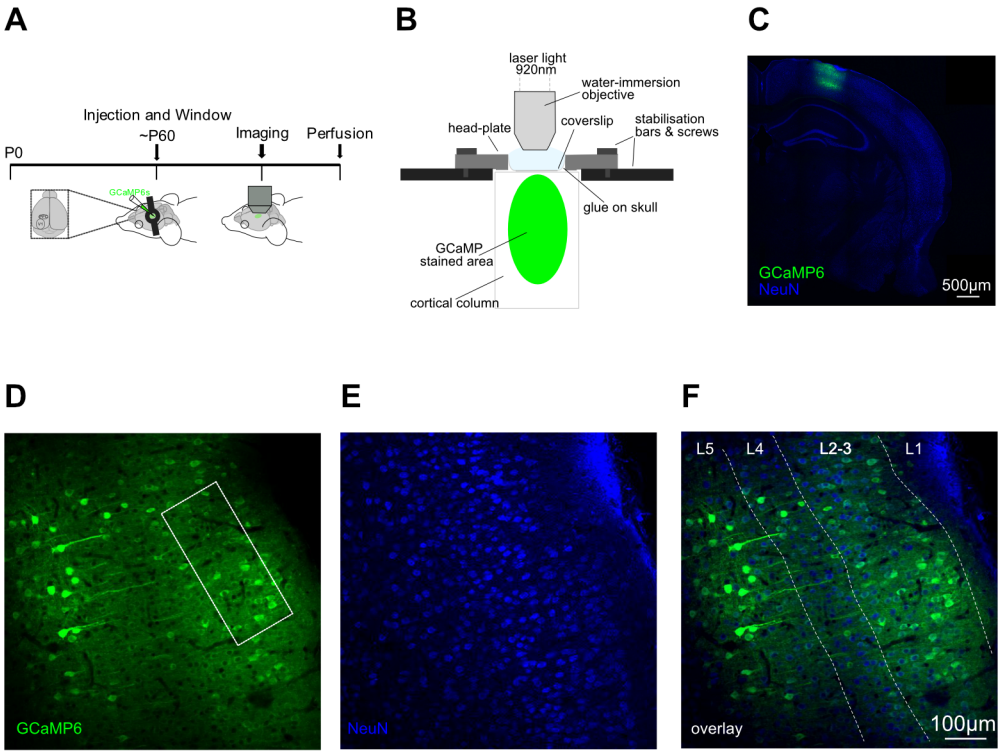

Figure 4.2 Using GCaMP6 as a calcium indicator for *in vivo* two-photon imaging of neurons. (A) Experimental timeline; AAV-mediated delivery of genetically encoded calcium indicators (GCaMP6s or GCaMP6f) and cranial window surgery was performed at a single site, V1 or PPC, of adult mice (≥ P60) two to four weeks before *in vivo* two-photon imaging. Following experiment, mice were transcardially perfused with 4% PFA in 0.1M PB. (B) Schematic drawing of the experimental arrangement; mice were head-fixed under the microscope through stabilizing the head-post, and the GCaMP6 stained area was imaged through a coverslip glued to the skull, with a water-immersion 25x or 40x objective. (C) Low magnification confocal image of a 40µm thick coronal section of a brain post-two-photon imaging with a GCaMP6s injection at the PPC; GCaMP6s in green, NeuN in blue. (D, E, F) Same GCaMP6 stained area as in (C) imaged in 20x magnification with confocal imaging; GCaMP6s in green (D), NeuN in blue (E), composite (F). We imaged upper layer 2/3 (white box in GCaMP channel in D). Layers are outlined in overlay (F). Scale bars, 500µm and 100µm respectively.

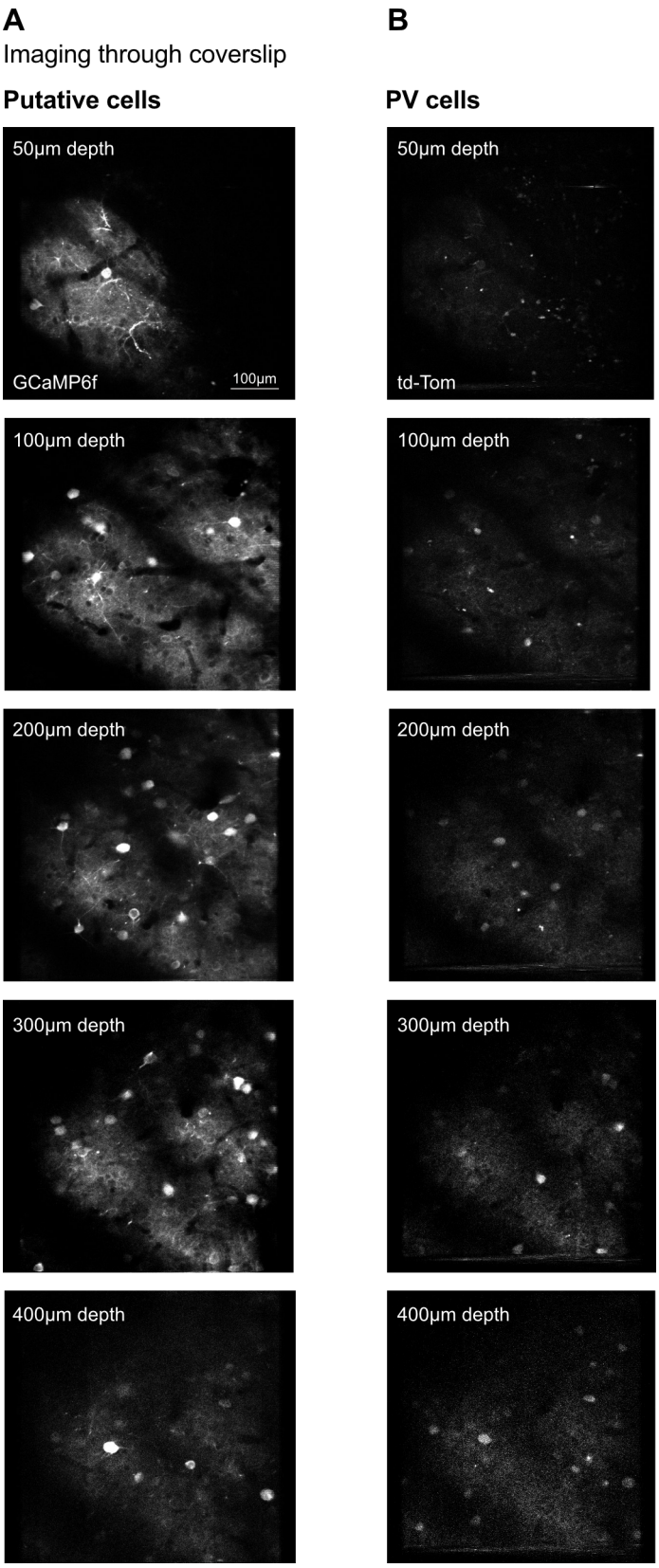

Figure 4.3 ***In vivo*** **calcium imaging of neuronal populations in different depths in the mouse cortex.** (A, B) Two-photon raw images of GCaMP6 expressing neurons (left) and PV interneurons expressing td-Tomato (right) obtained at increasing depth. Imaging depth for upper layer 2/3 experiments was 170-250 µm deep from pia surface. Scale bar, 100µm.

4.2.2 Hyperactivity of head-fixed *Syngap* HET mice during sensory stimulation

In consideration of my OF hyperactivity results in Chapter 3.2.1.1, and previously published data of other groups (Guo *et al*., 2009; Muhia *et al*., 2010; Clement *et al*., 2012; Ozkan *et al*., 2014), I first sought to establish whether *Syngap* HET mice also presented with hyperactivity of locomotor responses when head-fixed under the two-photon microscope (Figure 4.4A). For this purpose, I analysed the time mice spent being stationary, positioning, and freely running, as monitored using an optical encoder and sampled at 12.000 Hz (for classification criteria see Materials and Methods). Prior to imaging sessions, mice were habituated to the head-fixed environment, free to run on the treadmill in the darkness, for 30 minute sessions over at least 2 consecutive days. HET mice were usually habituated for a minimum of 3 consecutive days before they started voluntarily running. Mice of both groups had a strong preference for being stationary, over running. However, HET mice spent a significantly increased percentage of time running compared to WT controls during visual stimulation (2-way *ANOVA* $F_{(2,10)}$=38.95, p<0.0001; movement type $F_{(2,10)}$=2904, p<0.0001; genotype $F_{(1,5)}$=1.211, p=0.3212) but not during darkness (2-way *ANOVA* $F_{(2,10)}$=1.046, p=0.3869; movement type $F_{(2,10)}$=73.12, p<0.0001; genotype $F_{(1,5)}$=1.700, p=0.2491) (Figure 4.4B, C).

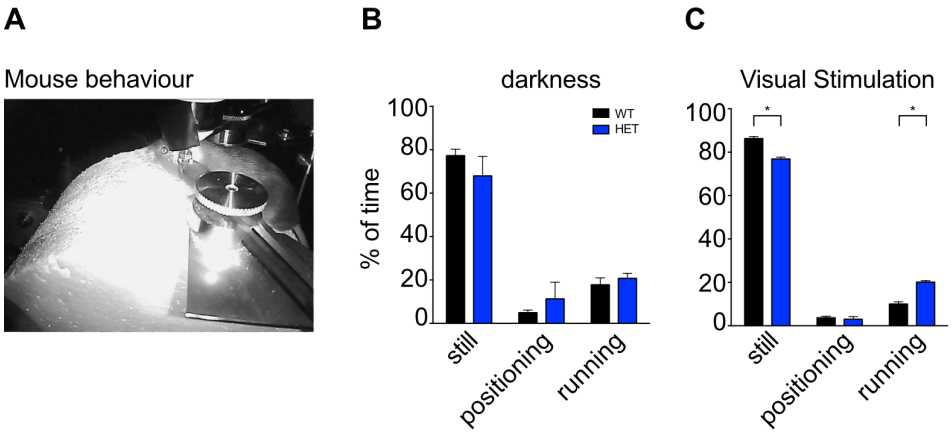

Figure 4.4 ***Syngap*** **HET mice spend more time running on the treadmill only during visual stimulation.** (A) Snapshot of a mouse running on the treadmill through the infra-red camera in the microscope set-up. (B) Percentage of time mice spend still, positioning or running (locomotion) on the treadmill in darkness (2-way *ANOVA* $F_{(2,10)}$=1.046, p=0.3869; movement type $F_{(2,10)}$=73.12, p<0.0001; genotype $F_{(1,5)}$=1.700, p=0.2491) and (C) during visual stimulation (2-way *ANOVA* $F_{(2,10)}$=38.95, p<0.0001; movement type $F_{(2,10)}$=2904, p<0.0001; genotype $F_{(1,5)}$=1.211, p=0.3212). *mean* ± SE is noted. All *ANOVAs* Bonferroni corrected.

4.2.3 Apparent hypoactivity of PPC neurons of *Syngap* heterozygous mice at stationary, but not running, conditions.

During the first set of experiments, baseline activity was initially recorded during darkness (Figure 4.5A). I imaged ~65 GCaMP6s expressing cells simultaneously (Figure 4.5B) within an area of 240 x 240 μm with a 40x objective (range 52-82 cells per animal; 244 cells from 4 WT mice, 184 cells from 3 *Syngap* HET mice). Nearly all imaged cells showed significant amplitude of calcium transients during the imaging session but neurons that didn't reach criterion were considered silent and were excluded from analysis (see Materials and Methods subsection 2.3.3). Acquired wheel positioning data (running speed) were downsampled to match the sampling rate (40 Hz) of acquired somatic $\Delta f/f_0$ transients (Figure 4.5C) and neuronal responses were separated for still (when animal stationary) and locomotion (when animal running) phases.

When animals were still, neurons in layer 2/3 of the PPC of *Syngap* HET mice showed a 34.27% lower in mean amplitude of calcium transients compared to WT controls (Figure 4.5D; mean $\Delta f/f_0$: for WT=0.2915±0.03, for HET=0.1916±0.02). Furthermore, during locomotion the mean $\Delta f/f_0$ response of neurons increased. This was true for both WT and HET cells. This was consistent with previous findings in superficial layers of the visual cortex of wild type mice (McGinley *et al*., 2015; Pakan *et al*., 2016). However, calcium transient responses were found to be slightly exaggerated in *Syngap* HET PPC neurons (Figure 4.5D, E). The above suggests that PPC neurons of *Syngap* HET mice are hypoactive during basal conditions but locomotion enhances their activity to levels comparable to WT. To further quantify the effect of locomotion, I calculated a locomotion modulation index (LMI) for each neuron of each genotype. LMI corresponded to the difference between the mean $\Delta f/f_0$ of a given neuron during locomotion and still periods, normalised by the sum of the mean $\Delta f/f_0$ during both behavioural states. Therefore, LMI values equal to 0 indicate no difference between locomotion and still periods, while LMI values equal to 0.5 illustrate an average amplitude of $\Delta f/f_0$ three times higher during locomotion than during still. Comparing the distribution of LMIs between the two genotypes, I found that modulation of

neuronal activity of HET cells by locomotion was slightly higher than in WT controls (mean of median LMI: for WT=0.17, for HET=0.20, $p>0.05$ t-test; Figure 4.5F). Finally, I calculated the variance of calcium responses per cell over trial and found that HET cells presented with lower variance of $\Delta f/f_0$ which increased during locomotion in slightly higher levels that WT cells (Figure 4.5K).

Statistical evaluation of differences

Since two photon imaging has been established the last couple of years and is still predominantly used in wild type studies, small sample sizes like ours (eg. n=3 animals) remain common in published literature. Usually authors approach such datasets by pooling all the neurons from multiple animals and using a sample size that equals number of neurons imaged. Subsequent statistical analysis employs two way *ANOVA*s, regression analyses based on scatterplots (*F-test* as in Figure 4.5E), *K-S* tests on cumulative distributions or even unpaired *t-tests*, all with n= # of cells. However, neurons imaged within a single animal are not independent replicates. Indeed, a number of variables can differ between animals and imaging sessions that effect all neurons within an animal equally but differ between animals. Such factors include the actual age of the mouse (eg. 8 weeks versus 10 weeks), stress levels due to surgery or handling, number of areas (FOVs) imaged based on spread of injection site, number of detectable GCaMP6+ cells (ROIs), possible variability in x, y, z coordinates within the targeted cortical area, and the number of imaging sessions. Furthermore, when we include a different genotype as a variable, we should also consider its relation to the WTs, i.e. littermate or non-littermate controls. Treating cells as the independent replicate results in artificially increased power of the experiment and an increased probability of Type I error (pseudoreplication).

A more conservative statistical approach is to use animal as the independent replicate by calculating the mean amplitude of all the cells per animal, avoiding assumptions regarding normality and variance, and calculate the mean of the mean using paired or unpaired rank-based *t-tests* (for multiple measurements within the same animal, eg.

$\Delta f/f_{0STILL}$ - $\Delta f/f_{0LOCO}$). However, in this stringent approach we compress a lot of information (number of cells varies greatly from 60-250 per FOV), losing the abudant, within animal variability, and increasing the probability of a Type II error, thus potentially hiding a positive result. Given the variability of responses, on a cell-by-cell and animal-by-animal basis, and considering that in the field of neurodevelopmental disorders the general effect sizes between genotypes are usually small (20-40%), that would also lead to an unnecessarily large number of animals needed to reach significance with a power over 0.80. Furthermore, the variability per genotype in these type of experiments is not equal (i.e. the standard deviation between the genotype datasets), which makes calculating sample sizes (number of animals) *a priori* even more difficult. Indeed, a brief power analysis I performed on my dataset (2-sampled 2-sided equality) with n= # of animals, suggested that to achieve 80% power with an α=0.05 we would need: n=14 using the standard deviation (σ) of the HET, n= 46 using the σ of the WT. Sample sizes as big as 46 per genotype are generally unfeasible, especially since the actual number of animals that is used is always unavoidably higher than the reported sample size due to various reasons including non-clearing cranial windows, GCaMP6 expression too weak for imaging, or location of the injection site outside of the preferred cortical boundaries/target.

To avoid these two statistical issues, we used linear mixed modelling and generalized linear mixed modelling to determine the differences of log transformed $\Delta f/f_0$ values ($\log(\Delta f/f_0)$; Figure 4.5G-J) between groups, which is basically an *ANOVA* procedure in which we can include random and fixed factors, as well as covariates (predictors), and the calculations are performed using a *least squares regression* (best fit to a particular theoretical distribution). The fit to a series of linear mixed models was performed with 'animal', 'litter' and 'ROI' as random effects, and different fixed effects. We continued with using two distributions that presented with best fits; log-normal distribution (LMM) and gamma-distribution (GLMM), (Akaike's Information Goodness-of-fit Criterion (AIC): $AIC_{log\text{-}normal}$= -592.1635; AIC_{gamma}= -317.3748; See Appendix2 Figure2.1). Looking closer into the effect sizes, we can see that the difference between WT_{still} and WT_{loco} is 0.41, and the difference between WT_{still} and HET_{still} is 0.29, which are similar at least at an order of magnitude (Also see

Appendix2). By fitting the data to the log-normal distribution we calculate a p=0.3197 for genotype and movement main effects plus the interaction between the two VERSUS just the movement as main effect, which suggests that interaction between genotype and movement does not provide a better fit than movement on its own (still→loco). Furthermore, by using a gamma-distribution the model with movement**x**genotype main effects and an interaction between the two is close to being a significantly better fit than a model with just movement main effect (p=0.06582). Again, the effect sizes are on the same order of magnitude (difference between WT_{still} and WT_{loco} is 0.36; difference between WT_{still} and HET_{still} is 0.45).

While the effect sizes of both models seem to be close for movement and for genotype, we still don't calculate a better fit with movement**x**genotype and the interaction between the two versus just the movement, which suggests that either the genotype presents with slightly higher variability, or movement is less variable because the measurements (i.e. still/loco) for each neuron are linked (matched). From the above analysis while there appears to be an effect of genotype on neuronal activity in the still condition, it is also clear that the between animal variability means a sample size of 4 WT and 3 *Syngap* mice is underpowered for this kind of study and a higher number of animals is needed to determine which model is the most accurate for further statistical analysis to complement the apparent hypoactivity finding. As a result, all subsequent datasets that include n>3 for animals, use both log normal- and gamma-distributions to fit the data to and present results for both. In Appendix2 there is a more detailed representation of the mixed model analysis, including plots for best fit.

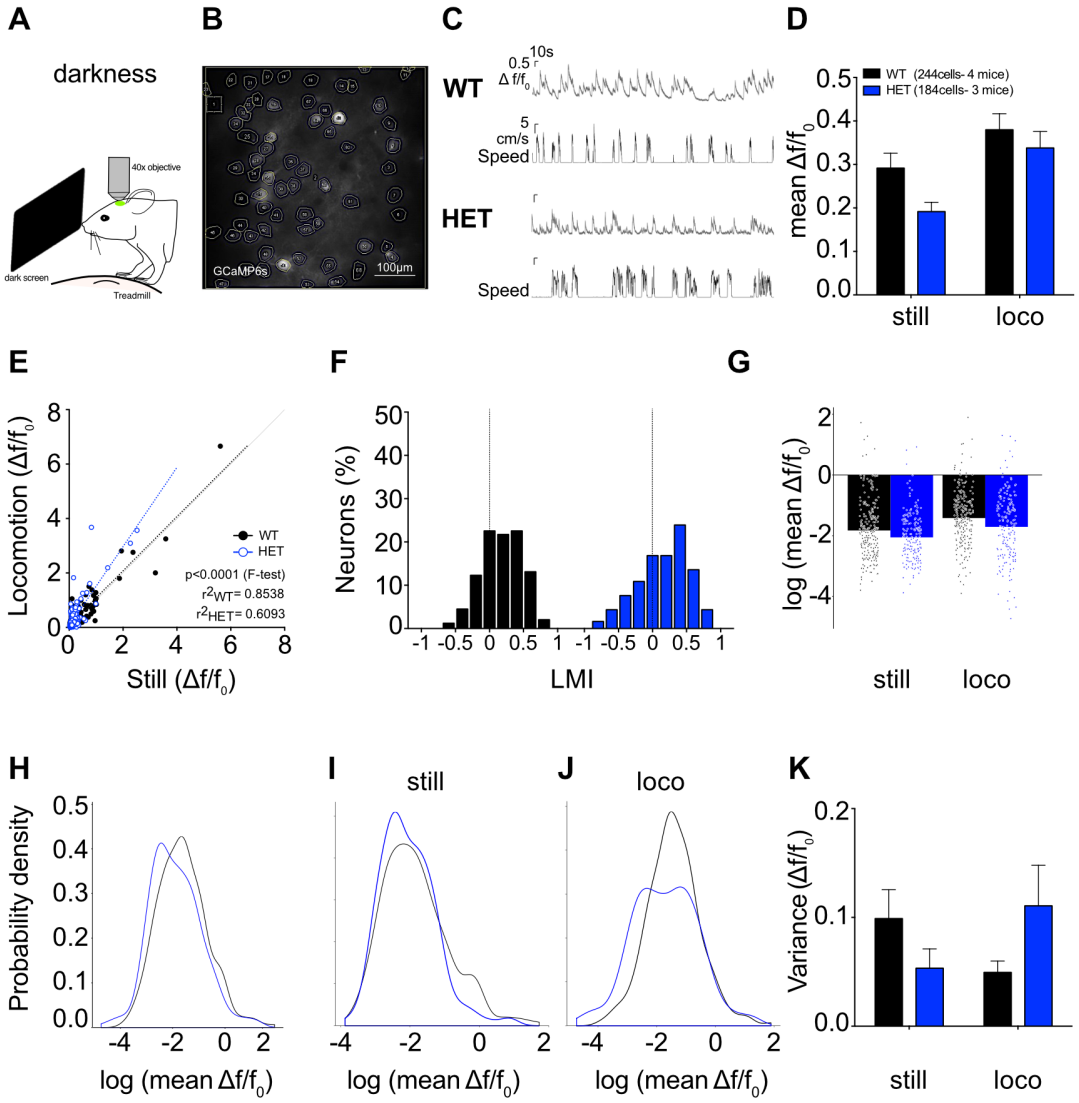

Figure 4.5 Decreased calcium responses of neurons in *Syngap* HET mice during stationary but not running conditions. (A) Experimental set-up for two-photon calcium imaging in PPC of awake-behaving mice, during presentation of a black screen (darkness). (B) *In vivo* two-photon image of a field of view with cells labelled with GCaMP6s under the synapsin (Syn) promoter (all neurons); cortical depth is ~200µm for layer 2/3 recordings in the PPC. (C) Representative examples of GCaMP6s calcium transients ($\Delta f/f_0$) of a WT and a HET neuron recorded in dark conditions (grey traces). Corresponding running speed of the mouse on the treadmill is shown below each trace (cm/s, black traces). (D) Mean amplitude of fluorescent changes (mean $\Delta f/f_0$) of neurons of each genotype for stationary periods (still) and running periods (locomotion). (E) Scatterplot of the $\Delta f/f_0$ of each neuron for locomotion periods versus still periods (*F-test* $F_{(2,424)}$=23.60, p<0.0001). (F) Histograms of the distribution of locomotion modulation indices, LMI = $(R_L-R_S)/(R_L+R_S)$, where R_L and R_S are the mean $\Delta f/f_0$ during locomotion and still periods respectively, for each genotype during darkness. An LMI equal to 0 (dotted lines) indicates no difference for the neuron's activity when the animal is running or still. (G) Mean amplitude of fluorescent changes (mean $\Delta f/f_0$) of neurons transformed on a log scale for still and locomotion (same data as in D, individual points represent cells). (H-J) Probability density plots for values shown in (G) for both conditions. (K) Mean variance of $\Delta f/f_0$ per cell over trials for WT and HET mice during both conditions. *mean* ± SE is noted. Scale bar, 100µm.

Visual stimulation results

To test whether modulation of neuronal activity by locomotion is sensory context-dependent, I decided to use a previously described visual stimulation (VisStim) paradigm (Pakan *et al*., 2016), which included a sequential presentation of unidirectional square-wave static and drifting gratings of 8 orientations (Figure 4.6A) through an LCD screen positioned in front of the mouse (20 cm distance). Pyramidal and PV^+ neurons of the PPC have been previously found to show enhanced responses to sensory input, including visual, auditory and whisker stimuli in a unimodal or multimodal fashion in rodents (Wallace *et al*., 2004; Olcese *et al*., 2013; Song *et al*., 2017). I found that a comparable proportion of both WT and *Syngap* HET neurons were visually responsive, 41.8% of WT (102/244 total) and 46.2% of HET neurons (85/184 total) (Figure 4.6B). In addition, mean amplitude of calcium transients of all PPC neurons of *Syngap* HET mice were again decreased relative to WT controls when the mice are stationary (Figure 4.6C; 44.61% decreased; mean $\Delta f/f_0$: for WT=0.3015±0.04, for HET=0.1607±0.012).

If we briefly compare the mean responses of PPC neurons in darkness (previous Figure 4.5E) with the mean responses during visual stimulation (all gratings), we see that visual stimulation did not have a strong effect on the mean $\Delta f/f_0$ (Figure 4.6C). The mean neuronal responses of WT cells during still and locomotion remain comparable regardless of the context, while HET cells show a slight decrease in their mean $\Delta f/f_0$ in stationary conditions during visual stimulation compared to darkness (for HET-$\Delta f/f_0$ during darkness: 0.1916±0.0212; $\Delta f/f_0$ during VisStim: 0.1607±0.0121). In addition, like my dark recordings, the change of mean $\Delta f/f_0$ during locomotion is higher for *Syngap* HET cells than for WT controls (Figure 4.6D). Comparing the histograms of LMIs for both genotypes, I found that modulation of neuronal activity of HET cells remains slightly higher during visual stimulation than WT controls, much like during darkness (mean of median LMI: for WT=0.20, for HET=0.27, $p>0.05$; Figure 4.6E).

While comparisons of the LMI distributions of WT and HET cells indicate how neuronal populations are modulated by locomotion during a different context, i.e.

exclusively during darkness (Figure 4.5J) or during visual stimulation (Figure 4.6E), information about context-dependent responses of single neurons is lacking. I therefore examined the LMI value in darkness versus during visual stimulation for each neuron by calculating the difference between the LMI value during VisStim and the LMI value during darkness (Figure 4.6F). Neurons near the identity (0) line (range: $-0.2<LMI_{Stim}-LMI_{Dark}<0.2$) show context-independent responses, while negative and positive values ($LMI_{Stim}-LMI_{Dark}<-0.2$ and $LMI_{Stim}-LMI_{Dark}>0.2$) indicate increased responses to locomotion in any of the two contexts over the other. I found no shift of any neuronal population towards positive or negative values, indicating that modulation of $\Delta f/f_0$ during locomotion is context-independent for neurons of the PCC for both genotypes.

In an attempt to statistically evaluate this dataset, we again used mixed models; $\Delta f/f_0$ data were transformed on a log scale (Figure 4.6 G-I) and compared to the theoretical distribution. We again found the log-normal and gamma-distribution to fit best ($AIC_{log-normal}$= -643.6909; AIC_{gamma}= -375.8312; See Appendix2 Figue2.2). By fitting the data to the log-normal distribution we calculated a p=0.4447 for genotype and movement main effects plus the interaction between the two VERSUS just the movement. However, by using a gamma-distribution we calculate that to be p=0.009031. Like previous findings, more animals are needed to accurately characterize whether that difference is significant between genotypes and which is the most appropriate statistical mixed model to fit my dataset to.

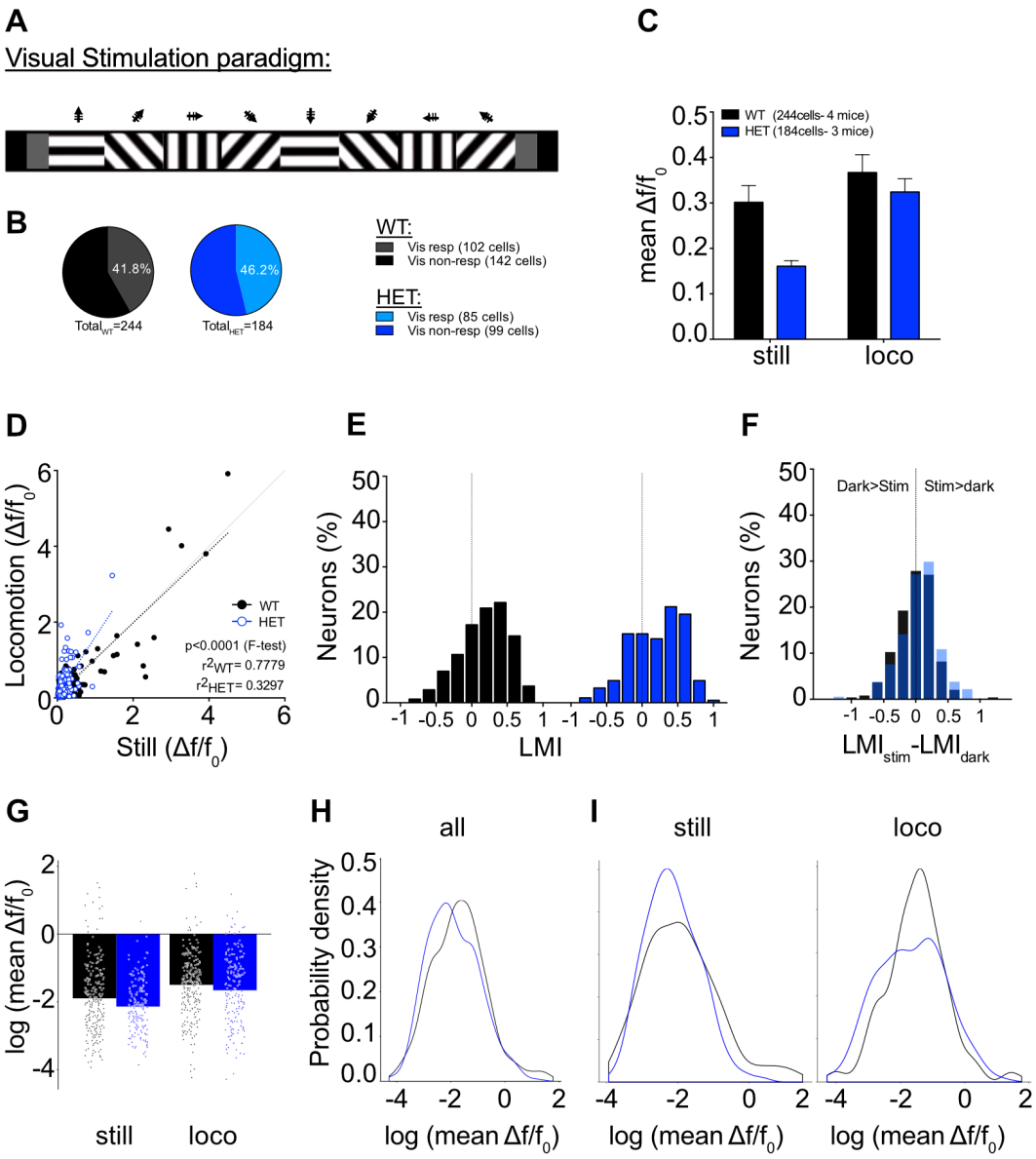

Figure 4.6 Decreased mean calcium transients of neurons in the PPC of *Syngap* HET mice during presentation of oriented gratings. (A) Schematic illustration of the visual stimulation paradigm in each visual stimulation trial (60sec total); Unidirectional square-wave drifting (2 sec) gratings with a static period of 5 sec for a sequence of 8 orientations: 0, 45, 90, 135, 180, 225, 270, 315 (0.05 cpd, 1Hz). Before and after grating exposure, there was a brief (2 sec) presentation of grey screen. (B) The absolute number of visual responsive cells was comparable between genotypes (WT: 41.8%, 102/244 cells; HET: 46.2%, 85/184 cells). (C) Mean amplitude of fluorescent changes (mean $\Delta f/f_0$) of each neuron of each genotype for stationary periods (still) and running periods (loco). (D) Scatterplot of the $\Delta f/f_0$ of each neuron for locomotion periods versus still periods during presentation of gratings (*F-test* $F_{(2,1441)}$=16.35, p<0.0001). (E) Histograms of the distribution of locomotion modulation indices, LMI = $(R_L-R_S)/(R_L+R_S)$, where R_L and R_S are the mean $\Delta f/f_0$ during locomotion and still periods respectively, for each genotype during visual stimulation. (F) Histogram of the difference between the LMI during visual stimulation and in darkness (LMI_{Stim}-LMI_{Dark}) for each genotype. Negative values indicate increased responses to locomotion in the dark compared with visual stimulation and numbers within the range -0.2<LMI_{Stim}-LMI_{Dark}<0.2 indicate context-independent responses. (G) Mean amplitude of calcium responses (mean $\Delta f/f_0$) of neurons transformed on a log scale for still and locomotion (same data as in C, individual points represent cells). (H) Probability density plots for values shown in (G) for both conditions and for (I) still and locomotion separated. *mean* ± SE is noted.

Does visual stimulation influence $\Delta f/f_0$ in a cell-by-cell manner?

By directly comparing the $\Delta f/f_0$ of individual neurons during darkness versus during visual stimulation for still and locomotion periods respectively, I found that PPC neurons present with slightly higher mean $\Delta f/f_0$ values during darkness. The difference between genotypes is stronger during still (Figure 4.7A) conditions rather than locomotion (Figure 4.7B), recapitulating my previous data on a cell by cell basis, rather than mean $\Delta f/f_0$ of the population. Finally, since PPC neurons show higher $\Delta f/f_0$ values during darkness and their LMI values is context-independent, I decided to focus further preliminary analysis on just the recordings were acquired during darkness.

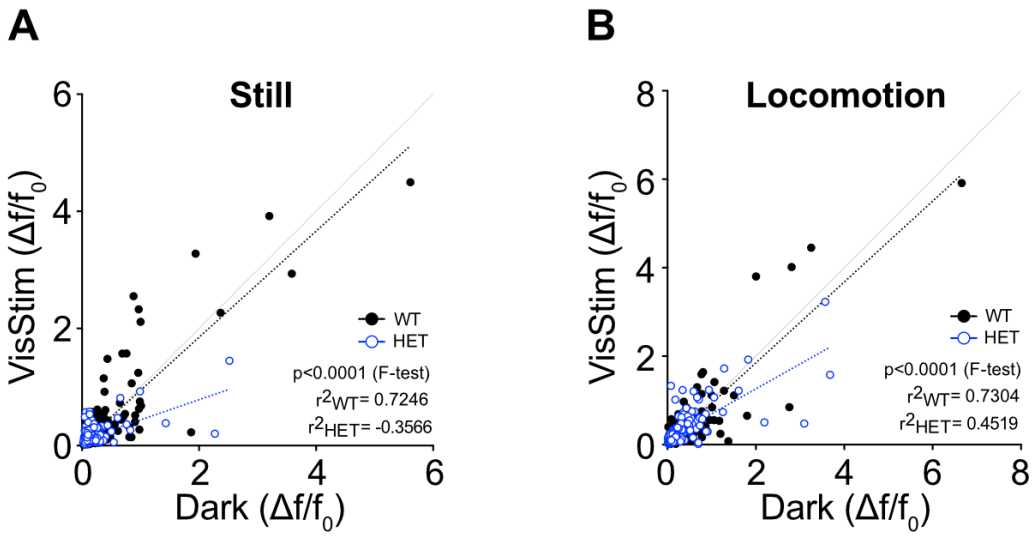

Figure 4.7 Slight preference of PPC neurons for darkness over visual stimulation in both WT and SynGAP HET mice. (A, B) Scatterplots of the mean amplitude of $\Delta f/f_0$ of individual WT and HET neurons for darkness versus patterned visual stimulation with oriented gratings during stationary conditions (still, A) and during running (locomotion, B) respectively.

4.2.4 Cell type-specific imaging of neuronal activity in the PPC

While up to 70-80% of neurons in the cortex are excitatory pyramidal cells (White & Keller, 1989; DeFelipe & Fariñas, 1992; Thomson & Deuchars, 1994) the remaining 20-30% are mostly inhibitory interneurons, with diverse morphological, physiological and synaptic features (DeFelipe, 1993; Cauli *et al*., 1997; Kawaguchi & Kubota, 1997; Gupta *et al*., 2000). Therefore, in parallel with statistical analysis being performed on the data discussed above, I explored the possibility that inhibitory neuron activity can account for the decrease in mean amplitude of response of *Syngap* HET PPC neurons during stationary conditions that increased to WT levels when mice are running. I decided to initially focus on one of the molecularly defined types of interneurons, PV+ neurons that include several subtypes of basket and chandelier cells in the cortex (Wang *et al*., 2002; Makram *et al*., 2004) and provide inhibition to the soma of excitatory pyramidal cells suppressing their postsynaptic activity (Burkhalter, 2008), drive gamma rhythms (Sohal *et al*., 2009) and promote cortical circuit performance as well as cognitive flexibility (Cardin *et al*., 2009). In addition, based on two recent studies in layers 2/3, 4 and 5 of the region of visual cortex in wild type mice, PV interneurons were shown to be locomotion responsive in a context-independent manner (Fu *et al*., 2014; Pakan *et al*., 2016).

Syngap heterozygous mice and WT littermate controls with tdTom expression in the endogenous PV population were generated by crossing a *Syngap* heterozygote with a $Pvalb^{+/cre}$, $Rosa26^{+/tdtom}$ or a $Pvalb^{cre/cre}$, $Rosa26^{tdtom/tdtom}$ (See Materials and Methods). I repeated previous experimental procedures and imaged GCaMP6f expressing neurons and tdTom expressing PV interneurons of the PPC in two different channels. I therefore separated two populations for further analysis; the putative cell population (mostly excitatory neurons, no PV, green channel) and the genetically-identified endogenous PV cell population (overlapping green and red channel) (Figure 4.8A-C). Somatic changes in fluorescence intensity were recorded and wheel positioning data (running speed), which were subsequently downsampled and matched to the imaging sampling rate (Figure 4.8D). I imaged both during darkness and during visual

stimulation, but as mentioned above, I focused further analysis on recordings acquired during darkness. Results in the two following sections of this chapter represent preliminary data.

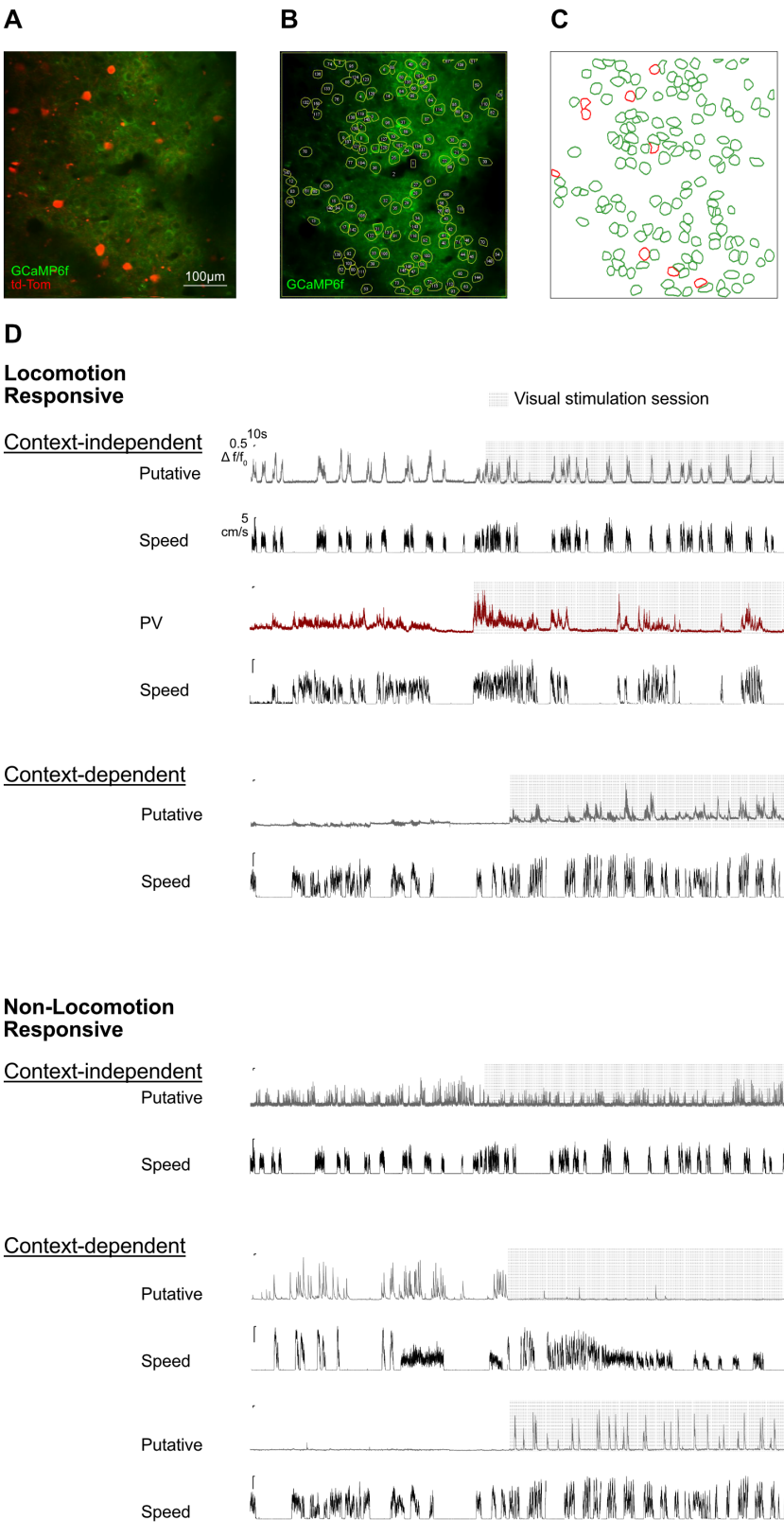
A
B
C
GCaMP6f
td-Tom
100μm
GCaMP6f
D
Locomotion Responsive
Visual stimulation session
Context-independent
0.5
Δ f/f0
10s
Putative
5
cm/s
Speed
PV
Speed
Context-dependent
Putative
Speed
Non-Locomotion Responsive
Context-independent
Putative
Speed
Context-dependent
Putative
Speed
Putative
Speed

Figure 4.8 Imaging neuronal activity of putative excitatory and inhibitory neurons in mouse PPC. (A) *In vivo* two-photon image of all neurons labelled with GCaMP6f and PV interneurons with endogenous td-Tomato expression; cortical depth is 210μm. (B) GCaMP6f channel with flattened drawn ROIs of individual neurons; ROI1 is background, ROI2 is total neuropil. (C) Same ROI locations extracted; green ROIs are putative cells, red ROIs are PV cells. (D) Representative examples of GCaMP6f calcium transients ($\Delta f/f_0$) of locomotion and non-locomotion responsive neurons, in darkness and during visual stimulation with oriented gratings (grey windows behind trace). Putative cells in grey traces and PV interneurons in red. Corresponding running speed of the mouse on the treadmill is aligned below each trace in cm/s (black trace). Scale bar, 100μm.

4.2.5 Preliminary findings of decreased activity of PV interneurons of *Syngap* heterozygous mice during locomotion

The activity of neurons in the PPC during darkness (Figure 4.9A) was recorded within an area of 384 x 384 μm with a 25x objective (Figure 4.9B). To acquire a larger number of interneurons I imaged 2-4 distinct fields of view (FOV) at slightly different depths of upper layer 2/3, or at different x, y coordinates based on injection site. As a result, for this experiment I acquired GCaMP6f fluorescence signals (Figure 4.9C) for a larger number of neurons (range 136-217 cells per FOV; 2-4 FOV per mouse; 1177 cells from 4 WT mice, 268 cells from 1 HET mouse). Nearly all imaged cells showed significant amplitude of calcium transients during the imaging and silent neurons were excluded from further analysis.

Putative excitatory neurons

Mean neuronal activity responses ($\Delta f/f_0$) were compared between WT cells (from 4 mice) with *Syngap* HET cells (from 1 mouse), and consistent with previous observations (Subchapter 4.2.3; Figure 4.5) I found that mean $\Delta f/f_0$ of HET cells was decreased relative to WT during still conditions (Figure 4.9D). Directly comparing the $\Delta f/f_0$ of individual neurons during different behavioural states, I also found that locomotion enhances the mean activity of HET cells in a greater degree than that of WT control cells (Figure 4.9E). Finally, the mean variance of calcium responses per

cell over trial was greatly reduced in *Syngap* HET cells during both still and locomotion periods (Figure 4.9F).

PV neurons

To determine how locomotion selectively activates PV interneurons in the PPC, I examined the activity of identified tdTom positive cells in my imaging data (Figure 4.9G). For each PV interneuron (68 PV neurons from 4 WT mice, 14 PV neurons from 1 HET mouse), the mean amplitude of calcium transients ($\Delta f/f_0$) was quantified during still and during locomotion in the absence of visual stimulation, in darkness. Like the locomotion responses of excitatory neurons, responses of PV cells of PPC were also heterogeneous. As seen through the LMI index of each individual cell, while some PV interneurons were negatively associated with locomotion, most PV neurons' calcium responses were enhanced, and thus the mean LMI for PV interneurons of WT animals was positive at 0.327±0.027 (AU). At the same time the mean LMI for *Syngap* HET cells was slightly decreased compared to WT, at 0.202±0.076 (AU) (Figure 4.9H). Plotting the mean $\Delta f/f_0$ of individual PV interneurons during both behavioural states I noticed that, as seen in putative excitatory cells, during stationary conditions the mean calcium response of the HET PV neurons was also decreased compared to WT PV cells (mean $\Delta f/f_0$ for WT: 0.2291±0.018; mean $\Delta f/f_0$ for HET: 0.1252±0.014). And furthermore, while WT PV cells have a strong mean enhancement of calcium response from still to locomotion (mean $\Delta f/f_{0(LOCO)}$ for WT: 0.450±0.027), HET PV interneurons present with a much lower response (mean $\Delta f/f_{0(LOCO)}$ for HET: 0.202±0.031) (Figure 4.9I). This was not due to a larger number of HET PV cells being suppressed by locomotion, but rather due to a lower mean fold change of $\Delta f/f_0$ in transition from the stationary to 'running' state (Figure 4.9J). Finally, and as seen in putative cells, the mean variance of calcium transients was reduced during both still and locomotion conditions. These preliminary results suggest a possibly distinct effect of locomotion on the responses of the PV neurons of *Syngap* HET mice in the absence of visual stimulation.

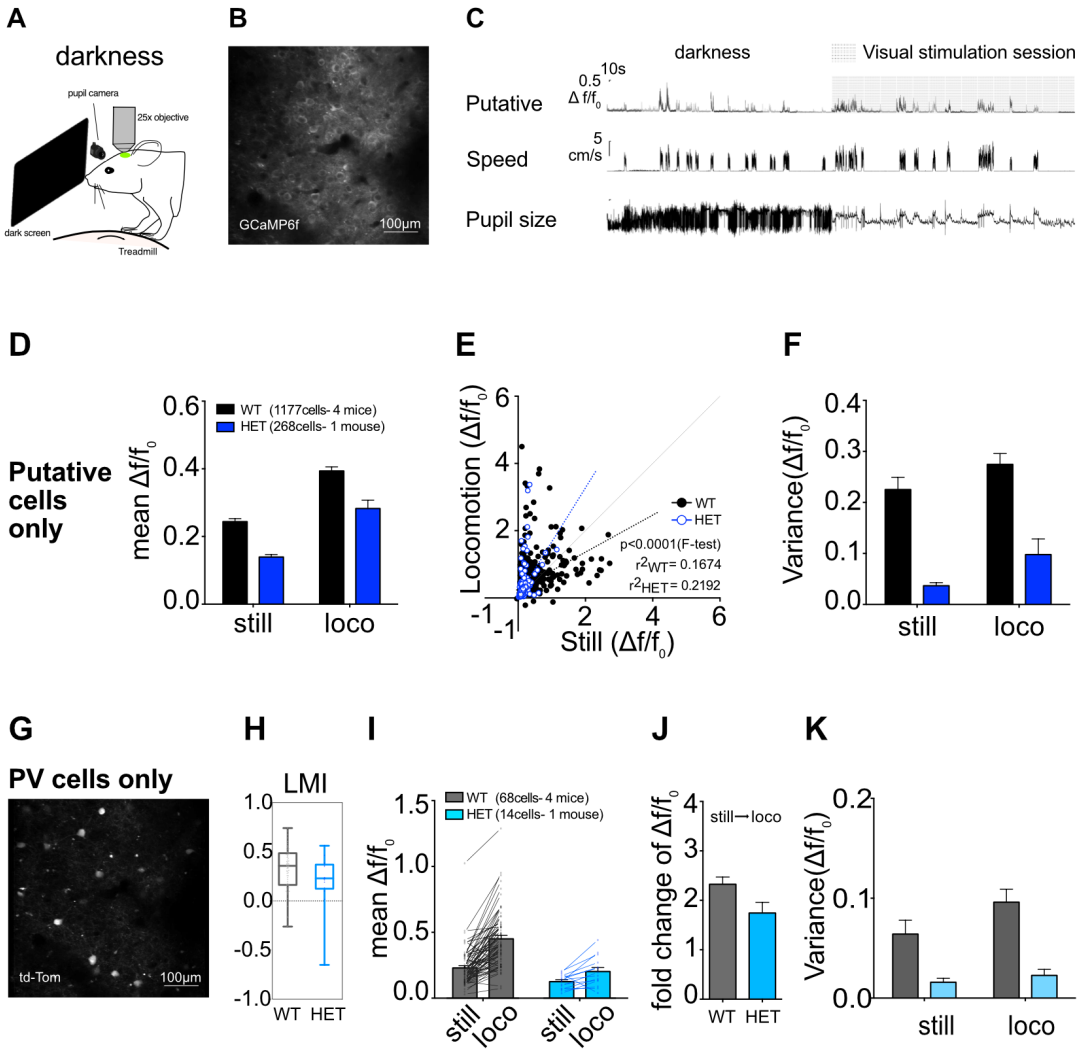

Figure 4.9 Locomotion differentially modulates *Syngap* HET PV interneurons of PPC during darkness. (A) Same experimental set-up for two-photon calcium imaging in PPC of awake-behaving mice, during presentation of a black screen (darkness). (B) *In vivo* two-photon image of a field of view with cells labelled with GCaMP6f under the synapsin (Syn) promoter (all neurons); cortical depth is ~200µm for layer2-3 recordings in the PPC. (C) Representative examples of GCaMP6f calcium transients ($\Delta f/f_0$) recorded in dark conditions and during visual stimulation with oriented gratings (grey windows behind trace). Corresponding running speed of the mouse on the treadmill is shown below each trace (cm/s). For these experiments corresponding pupil size of the left eye was recorded with an infrared camera and downsampled to match the calcium imaging rate. (D) Mean amplitude of fluorescent changes (mean $\Delta f/f_0$) of putative excitatory neurons of each genotype for stationary periods (still) and running periods (locomotion). (E) Single-cell mean amplitude of $\Delta f/f_0$ of individual WT and HET neurons for still versus locomotion during darkness (*F-test* $F_{(2,1441)}$=16.35, p<0.0001). (F) Mean variance of $\Delta f/f_0$ per cell over trials for WT and HET mice during both conditions. (G) *in vivo* two-photon images of PV neurons labelled with tdTom; same cortical depth as (B). (H) Mean LMI index for WT and HET PV neurons during darkness. (I) Mean amplitude of fluorescent changes (mean $\Delta f/f_0$) of PV interneurons of each genotype for stationary periods (still) and running periods (locomotion). Individual cells are noted, lines connect individual neurons. (J) Mean fold change of $\Delta f/f_0$ for each genotype, as R_L/R_S, where R_L and R_S are the mean $\Delta f/f_0$ during locomotion and still periods respectively. (K) Mean variance of $\Delta f/f_0$ per cell over trials for WT and HET mice during both conditions. *mean* ± SE is noted. Scale bar, 100µm.

4.2.6 Preliminary findings of increased neuronal correlations and network coupling of *Syngap* heterozygous neurons

To investigate the reasons behind the reduced variance of calcium responses of individual HET cells over the course of imaging trials (subchapter 4.2.2, Figure 4.5H; subchapter 4.2.4, Figure 4.9F), two parameters of multi-neuronal activity patterns not reducible to the response properties of individual cells were calculated; neuronal correlations and coupling to the population activity.

Pairwise correlations

Neuronal correlations (Pairwise correlations or Pearson correlations) can be a statistical description of functional connectivity and synchrony, mainly reflecting endogenous network activity, local short-range synaptic connections, but also shared long-range inputs from other regions (Yatsenko *et al*., 2015). I calculated pairwise correlations as the mean spontaneous trial-to-trial fluctuations in calcium activity shared by a pair of neurons, in lack of visual stimuli (Figure 4.10A). As my imaging experiments were recorded with a frame rate of 40 Hz (25cpms), $\Delta f/f_0$ traces were downsampled to 8 Hz prior to calculating pairwise correlations. I found preliminary evidence for higher correlation coefficients for putative HET cell pairs in the PPC during still conditions (mean correlation coefficient: WT=0.198±0.005; HET=0.2843±0.008), but not during locomotion (mean correlation coefficient: WT=0.196±0.004; HET=0.2102±0.006) (Figure 4.10B). As I currently only had 14 HET PV cells, correlation or coupling analysis for PV interneurons was not performed.

Population coupling

To characterise if putative cortical neurons of WT and *Syngap* HET mice relate to large-scale firing patters differently, I calculated the correlation of each individual putative neuron to the summed activity of all neurons in the recorded population

(population activity) at any time point in darkness during still and locomotion (Figure 4.10C). Consistent with my pairwise correlation data, putative HET cells in the PPC show increased mean coupling to the population activity in absence of visual stimuli (mean coupling: WT=0.172±0.003; HET=0.242±0.011) in still conditions, which reduces when the mouse starts running. Finally, I examined whether the mean amplitude of calcium responses is related to the mean population coupling by plotting the mean amplitude of $\Delta f/f_0$ versus the mean coupling of each individual cell. The activity of putative neurons of both genotypes did not correlate with the mean coupling during stationary conditions (Figure 4.10E), however during locomotion more cells with higher $\Delta f/f_0$ were strongly coupled to the population (Figure 4.10F).

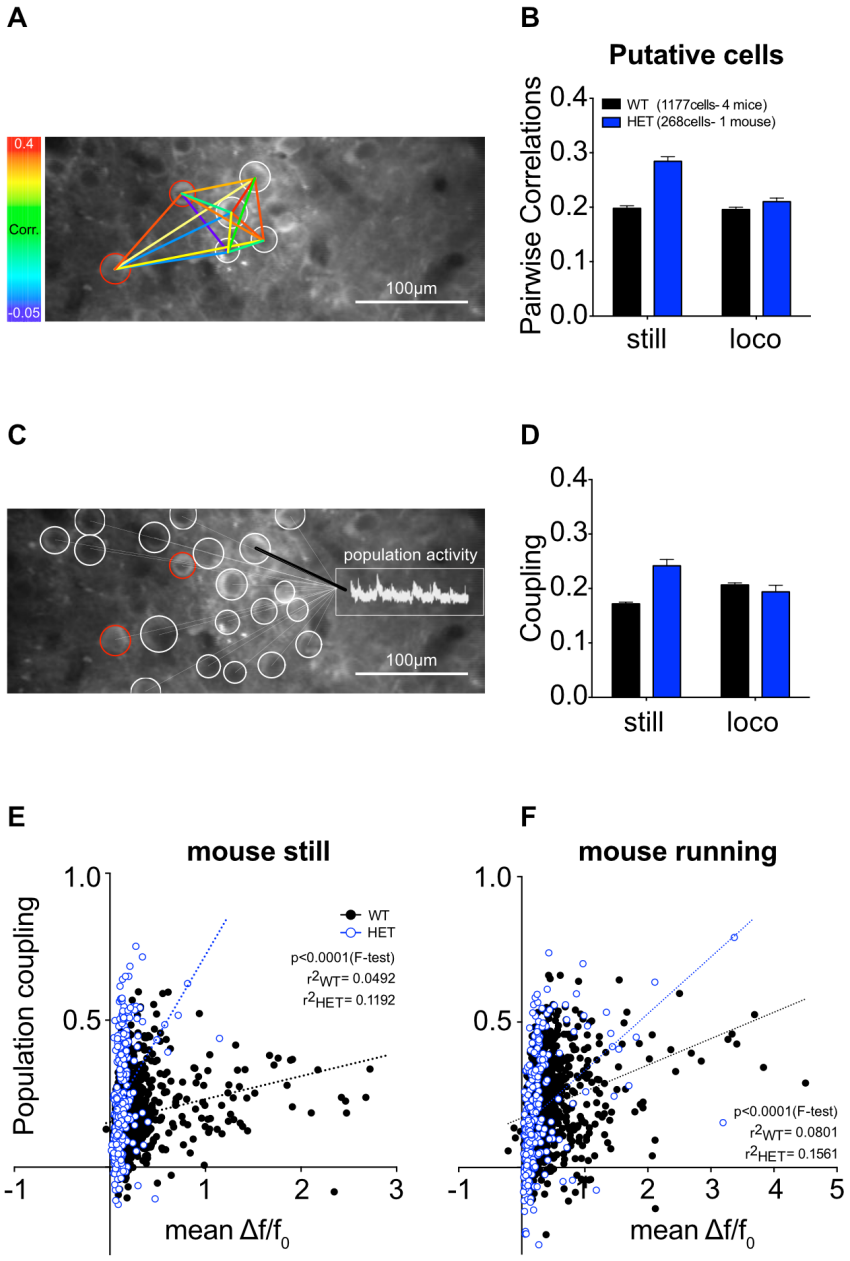

Figure 4.10 Increased pairwise correlations and population coupling *Syngap* HET cells in the PPC. (A) Pairwise correlations of downsampled calcium transients ($\Delta f/f_0$) in awake behaving mice shown as colour linkages between neurons (outlined) and corresponding colour key on the left. *Corr.* stands for correlation value. (B) Mean pairwise correlation values recorded during darkness for all cell pairs of both genotypes during still and locomotion periods. (C) Coupling of the calcium transients ($\Delta f/f_0$) of an individual cell (black line) to the population activity (white trace), which is the sum of the activity of all cells in the FOV (dashed white lines). (D) Mean coupling values of all cells of both genotypes measured during baseline activity in the darkness. (E, F) Single-cell mean mean amplitude of $\Delta f/f_0$ of individual WT and HET neurons plotted against the mean population coupling response of each cell during still and locomotion periods respectively. White outlined circles, putative excitatory neurons; red circles, PV interneurons. *mean* ± SE is noted. Scale bar, 100µm.

4.2.7 Recording cell type-specific neuronal responses in layer 2/3 of the V1

In primary sensory areas, different behavioural states, such as locomotion, arousal or attention, also modulate spontaneous neuronal activity and activity in response to sensory stimuli (Niell & Stryker, 2010; Petersen & Crochet, 2013; Erisken *et al.*, 2014; Reimer *et al*., 2014; McGinley *et al*., 2015; Pakan *et al*., 2016). To characterise whether locomotion differentially modulates the response properties of neurons in a primary sensory area and to complement my current findings in PPC, I used *in vivo* two-photon calcium imaging to monitor the activity of putative excitatory neurons and PV inhibitory interneurons in layer 2/3 of the area of visual cortex (V1) in *Syngap* HET / PVcretdTom double mutant mice and *Syngap* WT / PVcretdTom littermate controls. To image V1 neurons, I performed a 2mm craniotomy centred over V1 and injected the genetically encoded calcium indicator GCaMP6 (AAV1.Syn.GCaMP6f.WPRE.SV40; Chen *et al*., 2013) under the promoter synapsin (Syn) which labels all neurons (see Materials and Methods). Same imaging set up and routine was used as in PPC recordings, where mice were awake, head-fixed and free to run on a cylindrical treadmill with an LCD screen at a 45° angle, which was inactivated for dark imaging sessions. I recorded somatic GCaMP6f signals and wheel positioning data (running speed), which were subsequently downsampled and matched to the imaging sampling rate. Results in this section of the chapter represent preliminary data.

4.2.8 Layer 2/3 increased cell type-nonspecific responses in *Syngap* heterozygous neurons during locomotion

Baseline activity of putative excitatory cells and tdTom positive PV interneurons was recorded in V1 during darkness (Figure 4.11A) within an area of 384 x 384 μm with a 25x objective (Figure 4.11B). I imaged 2-4 distinct FOVs at slightly different x, y, and z coordinates within the limit of upper layer 2/3, to acquire a larger number of PV cells. Nearly all imaged cells showed significant amplitude of calcium transients

during the imaging session (range 87-276 GCaMP6f expressing neurons per FOV; 2-4 FOV per mouse) and silent neurons were excluded from further analysis.

Putative excitatory neurons

I compared mean calcium responses ($\Delta f/f_0$) of WT putative cells (1383 cells – from 3 mice) and *Syngap* HET cells (1196 cells – from 2 mice) and observed that contrary to my PPC recordings, HET cells in V1 had a higher $\Delta f/f_0$ relative to WT in stationary conditions (mean $\Delta f/f_0$ for WT: 0.1268±0.005; mean $\Delta f/f_0$ for HET: 0.2821±0.012) (Figure 4.11C). In agreement with previous observations (Polack *et al*., 2013; Pakan *et al*., 2016), I also found that on average, locomotion increased the amplitude of calcium transients in both WT and HET putative excitatory neurons (mean $\Delta f/f_0$ for WT: 0.2128±0.012; mean $\Delta f/f_0$ for HET: 0.4751±0.025) (Figure 4.11C, D), and the activity of HET cells remained higher in both conditions. The mean variance of *Syngap* HET cells was also increased compared to WT cells in both conditions (Figure 4.11E). I then calculated pairwise correlations, based on the trial-to-trial comparison of downsampled $\Delta f/f_0$ transients. Putative HET cell pairs presented with increased levels of correlation coefficients during still (mean correlation coefficient: WT=0.1670±0.004; HET=0.2676±0.006) and locomotion (mean correlation coefficient: WT=0.1068±0.003; HET=0.2300±0.005) (Figure 4.11F), while the mean coupling of putative cells to the population activity in absence of visual stimuli remains comparable between genotypes (Figure 4.11G). These preliminary findings in V1 suggest seemingly different computations of neurons of superficial layers of different regions of the cortex in *Syngap* haploinsufficiency.

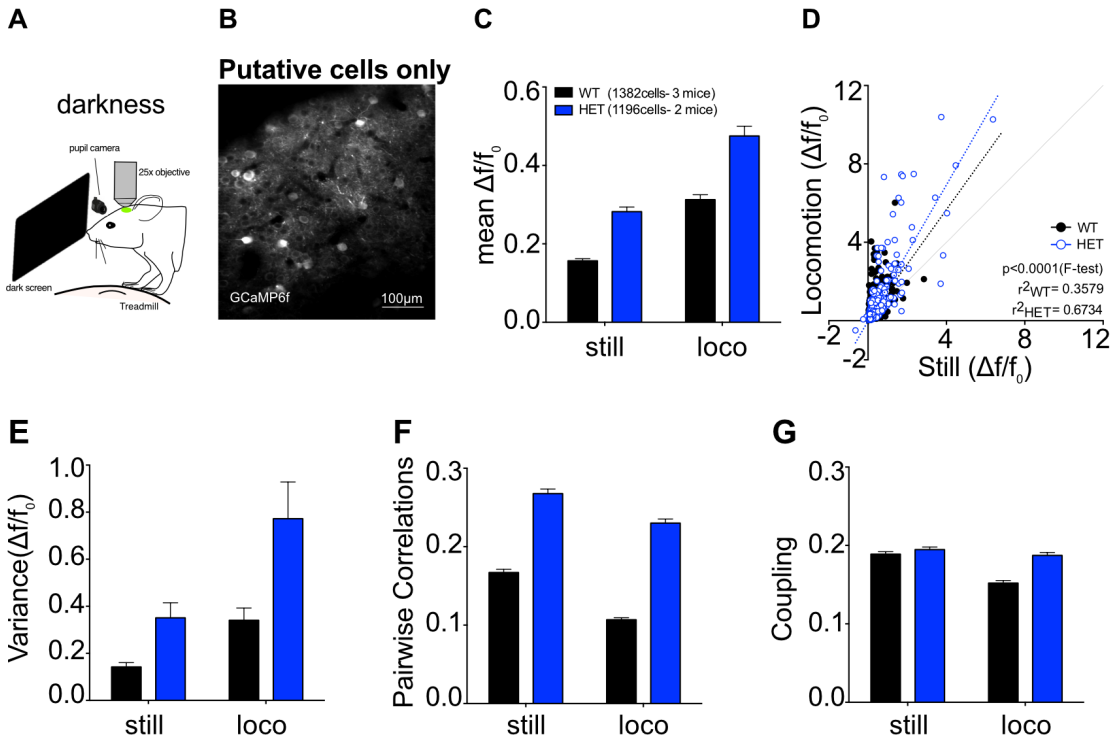

Figure 4.11 Increased modulation of putative excitatory neuronal responses by locomotion in *Syngap* mouse V1 during darkness. (A) Experimental set-up for two-photon calcium imaging in V1 of awake-behaving mice, during presentation of a black screen at 45° angle (darkness). (B) *In vivo* two-photon image of a field of view with cells labelled with GCaMP6f under the synapsin promoter (all neurons); cortical depth is ~210µm for layer2-3 recordings in the V1. (C) Mean amplitude of fluorescent changes (mean $\Delta f/f_0$) of putative excitatory neurons of each genotype for stationary periods (still) and running periods (locomotion). (D) Scatterplot of mean amplitude of $\Delta f/f_0$ of individual WT and HET neurons for still versus locomotion during darkness (*F-test* $F_{(2,2574)}$=16.95, p<0.0001). (E) Mean variance of $\Delta f/f_0$ per cell over trials for WT and HET mice during both conditions. (F) Mean pairwise correlation values recorded during darkness for all putative excitatory neuron pairs of both genotypes during still and locomotion periods. (G) Mean coupling values of all cells of both genotypes measured during activity in the darkness. *mean* ± SE is noted. Scale bar, 100µm.

PV neurons

Comparing V1 PV interneuron activity between genotypes (63 PV cells from 3 WT mice, 75 PV cells from 2 HET mice) I observed that the mean amplitude of calcium transients in darkness ($\Delta f/f_0$) was increased for *Syngap* HET cells during both behavioural states (for still: mean $\Delta f/f_{0WT}$= 0.2044±0.019, mean $\Delta f/f_{0HET}$=

0.2913±0.028; for locomotion: mean $\Delta f/f_{0WT}$= 0.2675±0.038, mean $\Delta f/f_{0HET}$= 0.4343±0.06) (Figure 4.12A, B). However, plotting the single-cell $\Delta f/f_0$ responses during still versus during locomotion, I noticed that recorded PV interneurons were less locomotion responsive than putative cells in V1 (see Figure 4.11D) and WT PV interneurons in PPC (see Figure 4.9H). Finally, the mean variance of calcium responses (Figure 4.12D) and pairwise correlations (Figure 4.12E) were increased for HET cells relative to WT controls, while the coupling of interneurons to the general population activity remained unchanged both between behavioural states, but also invariable between genotypes (Figure 4.12G).

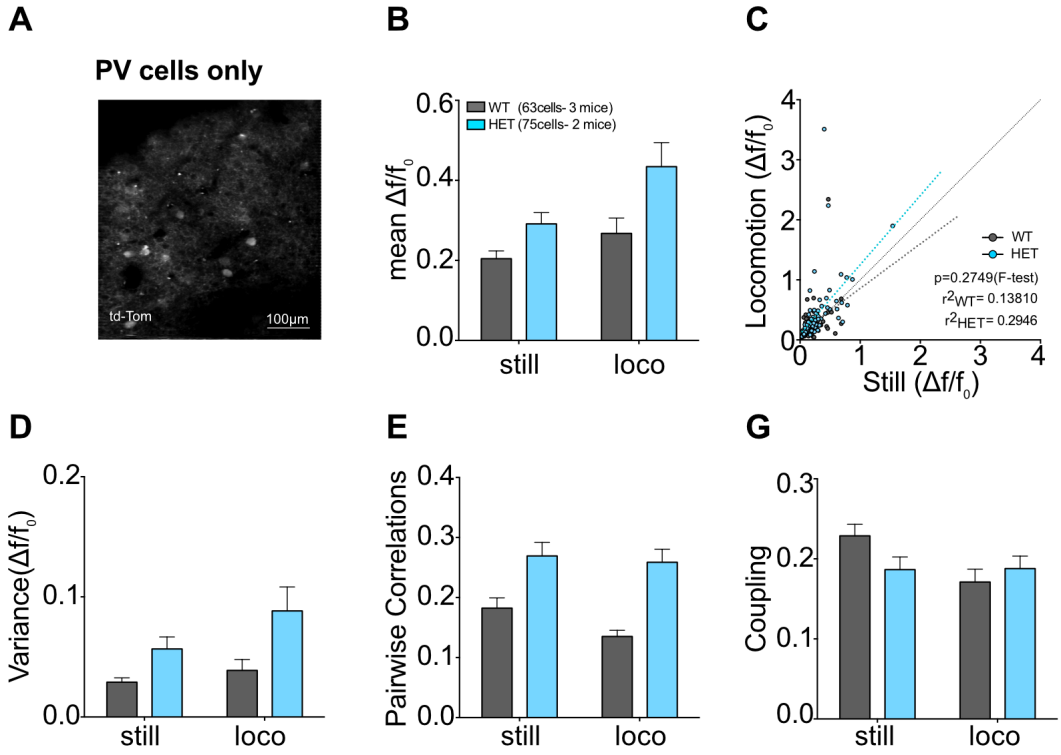

Figure 4.12 Increased calcium responses of *Syngap* HET PV interneurons of V1 during darkness. (A) *In vivo* two-photon images of PV neurons labelled with tdTom; same cortical depth as Figure 4.11B. (B) Mean amplitude of fluorescent changes (mean $\Delta f/f_0$) of PV interneurons of each genotype for stationary periods (still) and running periods (locomotion). (C) Scatterplot of mean amplitude of $\Delta f/f_0$ of individual WT and HET PV interneurons for still versus locomotion during darkness (*F-test* $F_{(2,134)}$=1.304, p=0.2749). (D) Mean variance of $\Delta f/f_0$ per cell over trials for WT and HET mice during both conditions. (E) Mean pairwise correlation values recorded during darkness for all PV neurons of both genotypes during still and locomotion periods. (G) Mean coupling values of all cells of both genotypes measured during baseline activity in the darkness. *mean* ± SE is noted. Scale bar, 100µm.

4.2.9 Similar, but not comparable, responses of V1 neurons to locomotion in wild type mice of two different background strains

While analysing mean calcium responses ($\Delta f/f_0$) recorded in layer 2/3 of V1 (seen in Figure 4.11C, D), I noticed that the effect of locomotion in activity of WT cells was not as pronounced as in previous published literature (Pakan *et al*., 2016). Notably, the background strain of my experiments is C57Bl/6J-OlaHsd (Ola), Pakan *et al* (2016) used mice that were bred on a C57Bl/6J (Jax) background. Relevant to this, analysis of RNA-sequencing data collected from visual cortex of P31 and P76 Ola and Jax mice have revealed that multiple genes are differentially expressed across the two strains, including Gamma-Aminobutyric Acid Type A Receptor Alpha 2 Subunit gene (*GABRA2*), which was found to be enriched in visual cortex of wild type Ola mice (juvenile and adult) relative to Jax (Appendix1 Figure 1.13; unpublished data; analysis Dr. Owen Dando). Following this, we decided to directly test the activity of neurons of these two background strains *in vivo*.

To directly compare the modulation of neuronal activity by locomotion in these two background strains, I used two-photon calcium imaging of the primary visual cortex, in awake head-fixed mice, initially during darkness (Figure 4.13A). I recorded the relative changes in baseline somatic fluorescence of the genetically-encoded calcium indicator GCaMP6s through AAV injections (AAV1.Syn.GCaMP6s.WPRE.SV40; Chen *et al*., 2013) in coordinates described above (Figure 4.13B, C). I quantified the mean amplitude of calcium transients for each neuron of Ola (681 cells in 5 mice) and Jax mice (554 cells in 5 mice) during locomotion periods and stationary periods in darkness. While neurons from both wild type strains increase their mean activity during locomotion, there was a higher increase in the mean activity of Jax neurons (Figure 4.13D; for still: mean $\Delta f/f_{0Ola}$= 0.1207±0.016, mean $\Delta f/f_{0Jax}$= 0.1200±0.021; for locomotion: mean $\Delta f/f_{0Ola}$= 0.2104±0.019, mean $\Delta f/f_{0Jax}$= 0.3665±0.105). Modelling the data with any of the two models and comparing between a model containing movement and genotype main effects and an interaction between the two VERSUS just movement main effect is highly significant (p<2.2e-16 for long-normal and p=5.41e-16 for gamma-distributions, See Appendx2 Figure 2.3). The effect of

locomotion was also apparent when I plotted the single-cell $\Delta f/f_0$ response of each individual neuron during in each condition (Figure 4.13E). Comparing the distribution and the mean values of locomotion modulation indices for each neuron, also confirmed that change in behavioural state affects neurons of Jax mice more than those of Ola mice (mean LMI_{dark} for Ola: 0.1047±0.014, for Jax: 0.3485±0.013) (Figure 4.13F, G). Finally, the mean variance of $\Delta f/f_0$ per cell over trial was comparable between background strains for both conditions (Figure 4.13H).

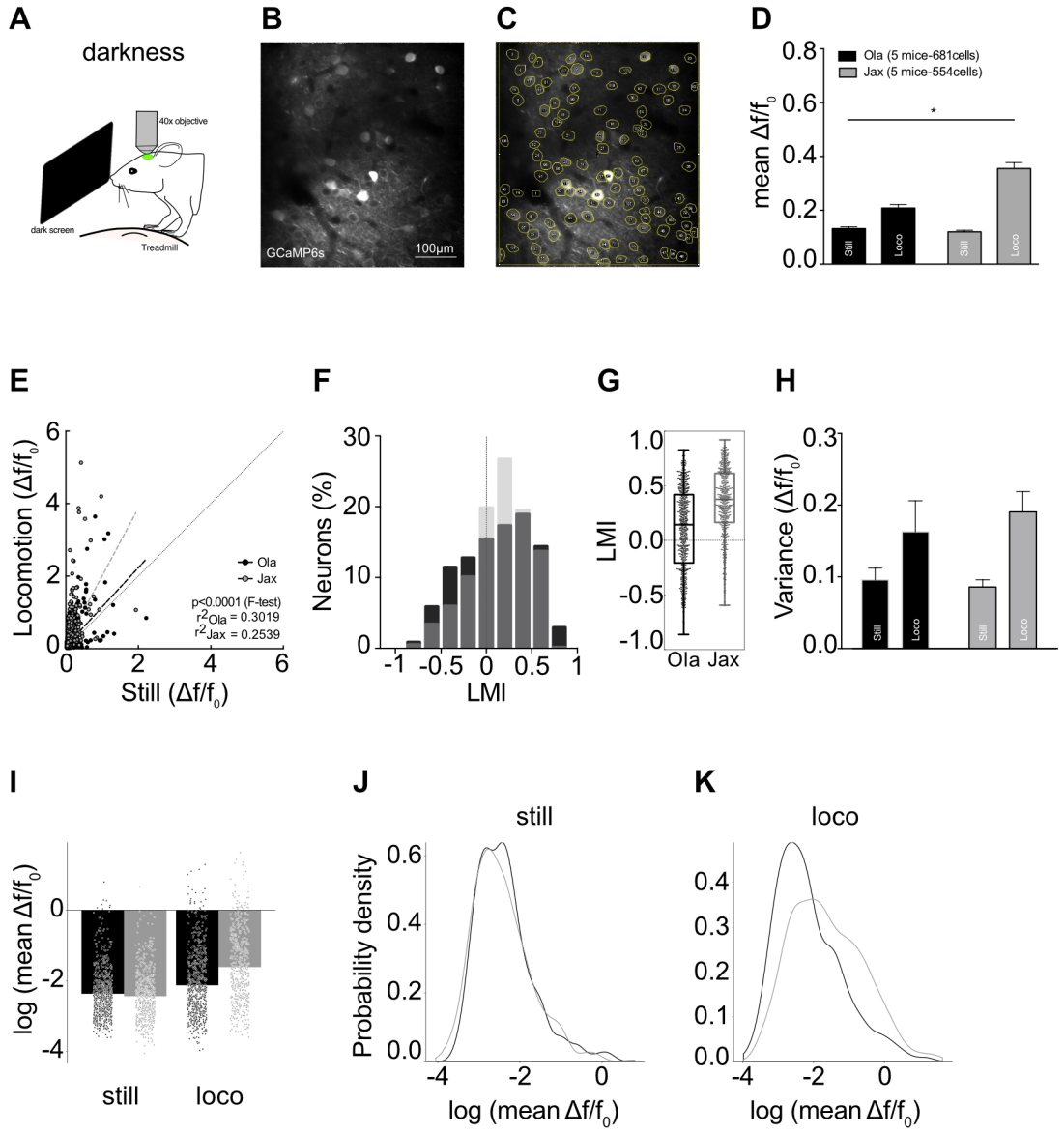

Figure 4.13 Locomotion differentially modulates neuronal responses in different wild-type mouse background strains during darkness. (A) Experimental set-up for two-photon calcium imaging in V1 of awake mice. Black screen (for dark recordings) in front of the mouse. (B) *In vivo* two-photon image of a field of view in layer 2-3 of V1 with cells labelled with GCaMP6s under the synapsin (Syn) promoter (all neurons); cortical depth is ~220µm. (C) Same field of view with flattened drawn ROIs of individual neurons; ROI1 is background, ROI2 is neuropil. (D) Mean amplitude of fluorescent changes (mean $\Delta f/f_0$) of each neuron of WT mice of the C57Bl/6J-OlaHsd (Ola) and C57Bl/6J (Jax) background strains, for stationary periods (still) and running periods (locomotion). (E) Scatterplot of the $\Delta f/f_0$ of each neuron for locomotion periods versus still periods (*F-test* $F_{(2,1231)}$=45.49, p<0.0001). (F) Histograms of the distribution of locomotion modulation indices (LMI) for each group. (G) Min-to-max plots of LMI for each individual cell (found in D). (H) Mean variance of the amplitude of neuronal responses per cell over trials for both groups. (I) Mean amplitude of fluorescent changes (mean $\Delta f/f_0$) of neurons transformed on a log scale for still and locomotion (same data as in D, individual points represent cells). (J,K) Probability density plots for values shown in (I) for both conditions. *mean* ± SE is noted. Scale bar, 100µm. * represents significant interactions, as calculated by fitting log transformed data to two different linear mixed models: data modelled with a log-normal distribution (LMM) p<2.2e-16; with a gamma distribution (GLMM) p=5.41e-13.

4.2.10 Locomotion strongly increases the gain of neuronal visual responses in Jax mice

Since locomotion affects the activity of neurons from Jax mice to a greater degree than that of Ola mice, I also tested the hypothesis that sensory stimulation would affect neurons of different wild type background strains differently. Additional findings in the lab have previously demonstrated that during visual stimulation through oriented gratings and simultaneous recording of field potentials (LFP) in the layer 4 of the binocular region of the primary V1, Ola mice present with a peak of gamma power at 60-80 Hz, which is absent in Jax mice (Appendix1 Figure 1.14; unpublished data). I thus compared the mean response of $\Delta f/f_0$ of V1 neurons of both background strains using a visual stimulation paradigm with presentation of both patterned and non-patterned gratings (Figure 4.14A). In agreement with previous electrophysiological (Niell & Stryker, 2010; Petersen & Crochet, 2013) and imaging (Pakan *et al*., 2016) findings, locomotion increased the amplitude of calcium transients of neurons in V1 during visual stimulation with oriented drifting gratings. However, this gain of response was greater for Jax neurons, compared to Ola neurons (for still: mean $\Delta f/f_{0Ola}$= 0.1095±0.016, mean $\Delta f/f_{0Jax}$= 0.1359±0.006; for locomotion: mean $\Delta f/f_{0Ola}$= 0.3012±0.011, mean $\Delta f/f_{0Jax}$=0.4824±0.002) (Figure 4.14B). $\Delta f/f_0$ values were log transformed (Figure 4.14C-E) and log-normal and gamma-distribution mixed models both gave significant results (p=2.85e-15 for log-normal and p=9.603e-07 for gamma-distribution, see Appendix 2 Figure 2.4). Since my results showed modulation of neuronal responses through locomotion during both darkness and presentation of sinusoidal drifting gratings, I tested whether this increase in $\Delta f/f_0$ amplitude was due to the presence of visual stimuli or just to the presence of light. The mean activity of neurons during isoluminant grey screen illumination was calculated, which is commonly used to record 'spontaneous visual activity' of visual cortex neurons. I found comparable effect of locomotion on neuronal $\Delta f/f_0$ during grey screen visual stimulation, as when presenting the gratings (Figure 4.14F-I; p<2.2e-16 for log-normal and p=9.642e-15 for gamma-distribution, see Appendix 2 Figure 2.5), suggesting that that both sensory stimulation and change in behavioural state has an effect in neurons of layer 2/3 of visual cortex in wild type mice, but less in Ola compared to Jax.

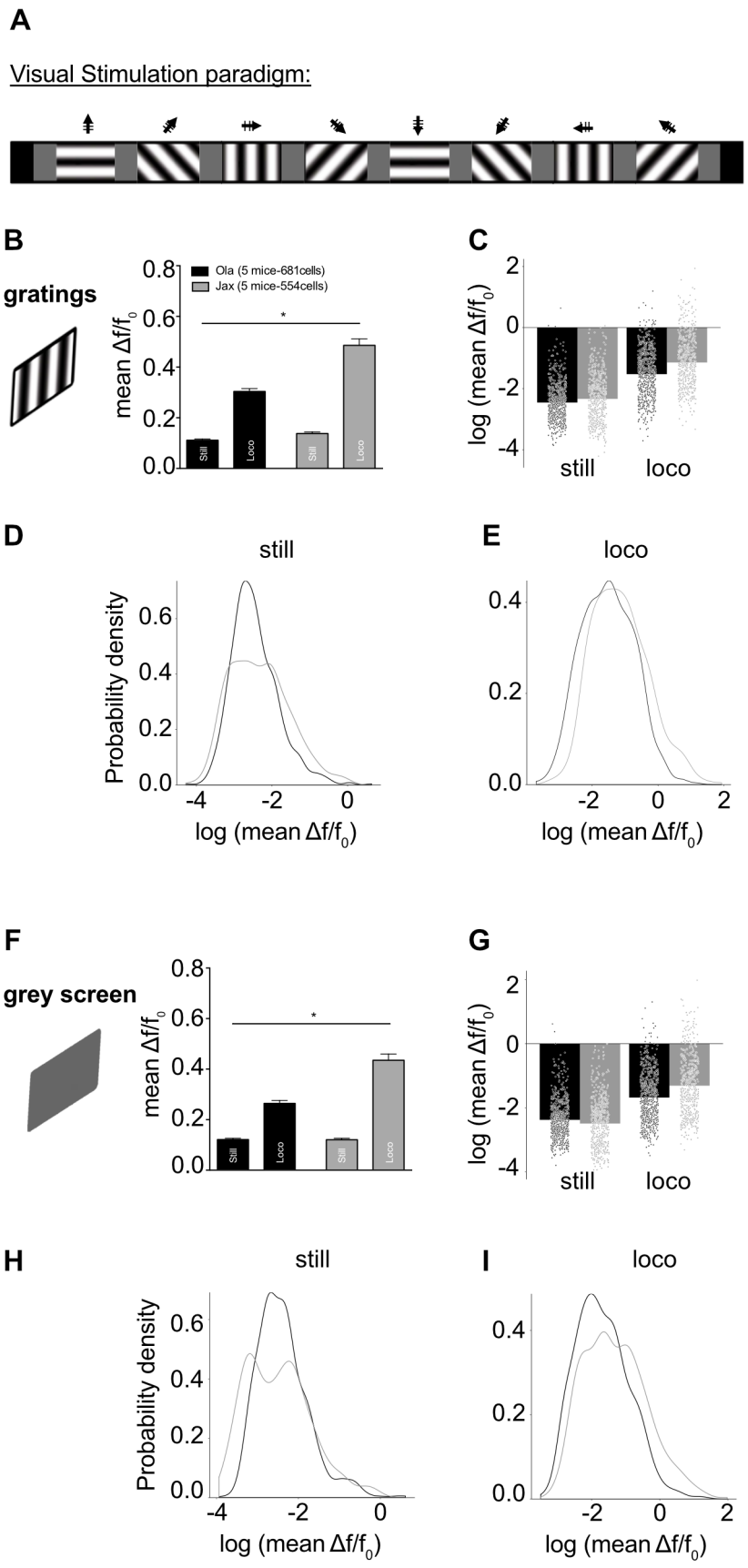
A
Visual Stimulation paradigm:
B
gratings
Ola (5 mice-681cells)
Jax (5 mice-554cells)
mean Δf/f0
Still
Loco
C
log (mean Δf/f0)
still
loco
D
still
Probability density
log (mean Δf/f0)
E
loco
log (mean Δf/f0)
F
grey screen
G
H
I

Figure 4.14 Wild type Jax mice show increased mean activity of neuron responses by locomotion during patterned (oriented gratings) and non-patterned (grey screen) visual stimuli. (A) Schematic illustration of the visual stimulation paradigm in each visual stimulation trial (72sec total); Phase-reversing sinusoidal drifting (3 sec) gratings for a randomised sequence of 4 orientations: 0, 45, 90, 180 (0.05 cpd, 1 Hz). Before and after each grating exposure, there was a brief (2 sec) presentation of grey screen. Additional 2 sec presentation of black screen in the beginning and end of visual stimulation trial. (B) Mean amplitude of fluorescent changes (mean $\Delta f/f_0$) of each neuron of WT mice of the C57Bl/6J-OlaHsd (Ola) and C57Bl/6J (Jax) background strains, for stationary periods (still) and running periods (loco) for presentation of oriented gratings. * represents significant interactions, as calculated by fitting log transformed data to two different linear mixed models: data modelled with a log-normal distribution (LMM) p=2.851e-15; with a gamma distribution (GLMM) p=9.603e-07. (C) Data presented in (B) transformed on a log scale for still and locomotion. (D, E) Probability density plots for both conditions. (F) Mean amplitude of calcium responses (mean $\Delta f/f_0$) of each neuron of WT mice of the Ola and Jax background strains, for stationary periods (still) and running periods (loco) for presentation of grey screen. * represents significant interactions, as calculated by fitting log transformed data to two different linear mixed models: data modelled with a log-normal distribution (LMM) p<2.2e-16; with a gamma distribution (GLMM) p=9.642e-15. (G) Data presented in (F) transformed on a log scale for still and locomotion. (H, I) Probability density plots for both conditions. Individual points represent cells. *mean* ± SE is noted.

4.3 Discussion

4.3.1 Summary of key findings

The aim of this part of my thesis was to investigate network-level alterations that arise from dysregulated SynGAP-mediated signalling following heterozygous loss of the protein in mice. Using two-photon imaging neuronal activity and spatiotemporal circuit dynamics were recorded in two distinct areas of the cortex, the PPC and V1. I acquired the following preliminary data:

- In PPC, the effect of locomotion appeared to be greater than the effect of visual stimulation in the amplitude of calcium responses of neurons in both WT and *Syngap* HET mice.

- Neurons in the PPC of *Syngap* HET mice show decreased mean calcium responses during animal immobility, which is accompanied by increased synchrony and coupling to the population activity.

- During locomotion both WT and Syngap HET neurons of the PPC show behavioural state-induced increase in mean calcium responses, but for HET neurons this appears to be at a slightly greater degree.

- HET PV interneurons may contribute in part to behavioural state modulation of neuronal responses in PPC.

- In contrast with PPC, in V1 *Syngap* HET neurons show increased activity during both stationary and running conditions. This is also accompanied by increased synchrony of neuronal responses.

- Wild type mice in the C67Bl/6J-OlaHsd background show slightly reduced locomotion- and sensory stimulation- induced gain of calcium responses in V1.

4.3.2 Extended discussion

Over the last two decades, various changes at the level of synaptic morphology and alterations in synaptic strength and plasticity have been reported in the mouse model of *SYNGAP1* haploinsufficiency (Jeyabalan & Clement, 2016). Most of this work, presented in detail in the introduction, includes studies that dramatically extended our knowledge on the molecular signalling cascades regulated by SynGAP protein following ion channel and neurotransmitter receptor activation. Furthermore, a growing body of work has focused on the anatomical and neurophysiological synaptic properties in the mouse model of *SYNGAP1* haploinsufficiency, such as synaptic strength and plasticity, as well as morphology and developmental regulation of cortical neurons and their dendritic spines. We also have a high level of understanding of the behavioural deficits associated with global, cell type-specific or region-specific heterozygous loss of SynGAP in mice, which now extends to behavioural characterisation in other rodent species.

However, despite these advances, we still know very little about the circuit-level abnormalities that underlie the sensory, cognitive and social deficits induced by mutations in the *Syngap* gene. Linking such behavioural impairments to specific phenotypes in involved circuits is a potential alternative avenue for targeting therapeutic interventions for affected individuals, than trying to target defects at a molecular/biochemical level. There is therefore a need to bridge the knowledge gap between molecular, cellular and behavioural levels, which will complement and accelerate our understanding on *Syngap*-related symptomatology and be a critical step towards development of successful therapies.

In the second part of the thesis, I therefore sought to test if neuronal responses to sensory stimuli and distinctive behavioural states are altered in *Syngap* HET mice. Using *in vivo* two-photon calcium imaging in awake mice, I focused on two different areas of the cortex; an association area, the medial PPC in which multiple sensory modalities are integrated, and a primary sensory area, visual cortex (V1). In both areas, I aimed to uncover cortical activity phenotypes and circuit properties of neurons in superficial layer 2/3.

4.3.2.1 Imaging network activity in an association area of the cortex

I focused on posterior parietal cortex (PPC) as an association area between M1, S1 and V1, important for many cognitive behaviours, such as decision-making and working memory. In primates, PPC plays an important role in working memory and the preparation of action (Chafee & Goldman-Rakic, 1998; Quintana & Fuster, 1999), as well as perceptual decision-making and categorisation (Shadlen *et al*., 2001; Gold & Shadlen, 2007; Curtis & Lee, 2010; Freedman & Assad, 2011); achieved through sustained and persistent reverberatory loops of firing activity with PFC (Compte *et al*., 2000) proposed to be mediated by NMDA receptors at recurrent synapses (Wang, 2001). In addition, PPC has been found to be important for movement planning (Andersen & Cui, 2009) and task-critical spatial attention (Bisley & Goldberg, 2010; Crowe *et al*., 2010).

In rodents, PPC has been shown to imprint accumulation of sensory information through ranks of increased firing rate (Hanks *et al*., 2015), encode route progression in spatial navigation experiments (McNaughton *et al*., 1994; Nitz, 2006; Whitlock *et al*., 2008; Save & Poucet, 2009; Whitlock *et al*., 2012) and to maintain firing activity patterns during (working) memory-guided sensorimotor decision tasks. More specifically, PPC neurons were shown to present with divergent trajectories of activity, from transient to sustained, during the cue (stimulus), delay (memory), and response epochs. This was true for presentation of different sensory stimulations, such as visual (Harvey *et al*., 2012; Raposo *et al*., 2014; Goard *et al*., 2016; Licata *et al*., 2017), auditory (Nakamura,1999; Erlich *et al*., 2015) and whisker (Guo *et al*., 2013). Testing the behavioural performance of the animals after PPC silencing has shown discrepancies. PPC appears to be necessary for visual sensorimotor decision tasks, as reported after inactivation of the region (Harvey *et al*., 2012; Raposo *et al*., 2014), but not in auditory and whisker (Guo *et al*., 2013; Erlich *et al*., 2015). These may be due to targeting of different stereotaxic coordinates, use of different species, sensory modality and behavioural paradigm.

Rodent PPC is located in the middle of a network of primary sensory cortices (Kolb & Walkey, 1987; Reep *et al*., 1994) receiving inputs from sensory, vestibular, thalamic

and motor areas (Mohan *et al*., 2017). Due to its location, PPC is poised to integrate multisensory inputs and present with multi-modal neurons, i.e. neurons that respond to sensory stimuli of multiple modalities (Wallace *et al*., 2014). Work from the visual field has demonstrated that several association areas around the extended visual region (Wang & Burkhalter, 2007) differ in their response properties to sensory stimuli (Andermann *et al*., 2011; Roth *et al*., 2012). One study in rostromedial PPC (referred to as visuotactile area between V1 and S1- or RL) demonstrated that both pyramidal and PV neurons in RL respond to visual, tactile or visuotactile (combined) inputs, therefore cells were either unimodal or bimodal to their 'preference' of receiving sensory input (Olcese *et al*., 2013).

As multisensory integration is critical for sensory processing by enhancing our ability to perceive our environment, imbalances in excitatory and inhibitory processes can directly affect sensory perception and subsequent behaviour, and could explain the wide array of deficits observed in autism (Green *et al*., 2013). Indeed, multisensory integration is affected in children with both ID and ASD (Joosten & Bundy, 2010; Kwakye *et al*., 2010), as well as in individuals that exhibit seizures (Besle *et al*., 2008). Therefore, the PPC is a great circuit candidate to investigate neuronal network activity in response to different behavioural states and sensory stimulation in *Syngap* HET mice.

Furthermore, cortical hyperexcitability has been proposed to lead to poor differentiation of cortical maps and to impair sensory and cross-modal processing across several brain areas (Baum *et al*., 2015). *Syngap* HET mice exhibit numerous behavioural deficits associated with sensorimotor processing, accompanied by stimulus-induced *in vitro* hyperexcitability in the hippocampus (Clement *et al*., 2012) and mPFC (Ozkan *et al*., 2014). Of note, I have found that pyramidal cells in PPC are anatomically and functionally connected with mPFC neurons (Appendix1 Figure1.15, Figure 1.16) but also project to mPFC, a cortical area that is essential for maintaining working memory (Baeg *et al*., 2003; Liu *et al*., 2014), which is a cognitive function that is also affected in *Syngap* HET mice (Guo *et al*., 2009; Ozkan *et al*., 2014; Berryer *et al*., 2016).

4.3.2.2 Apparent behavioural state - dependent hypoactivity of layer 2/3 neurons of PPC in adult *Syngap* heterozygous mice

Based on the above, I hypothesized that heterozygous loss of SynGAP in mice would lead to increased network activity of neurons in layer 2/3 of the PPC. Indeed, in the *Fmr1* KO mouse model of ID and autism, which shows a high-degree of convergence of phenotype in the hippocampus (Barnes et al., 2015), multiple studies have reported that KO neurons show abnormally increased rates of firing activity *in vivo* during development up to postnatal week 4 (Gonçalvez *et al*., 2013). Increased network activity has also been demonstrated pharmacologically *in vitro* in *Fmr1* KO mice. Using bicuculline to block GABAergic synapses led to prolonged epileptiform network activity of hippocampal KO slices (Chuang *et al*., 2015). In addition, application of picrotoxin and CGP55845 ($GABA_A$ and $GABA_B$ receptor antagonists) in thalamocortical slices of KO mice led to prolonged rhythmic bursts of activity of barrel cortex (Hays *et al*., 2011).

Two-photon calcium imaging was used to record the, initially spontaneous (during darkness), simultaneous temporal and spatial patterns of activity of large ensembles of neurons *in vivo*. Contrary to my expectations, neurons in adult HET mice showed decreased activity (by 34.27%). This decreased activity was behavioural state-dependent; when the animal was running, calcium responses of HET neurons abnormally increased to the level of WT neurons, suggesting that locomotion input differentially modulates HET neurons in layer 2/3 of the PPC. This may be particularly important for pathogenesis of *SYNGAP1* haploinsufficiency, as it suggests that input to PPC from other areas during a behavioural state change exaggerates the gain of calcium responses of neurons.

4.3.2.3 Potential cell type-specific mechanisms underlying behavioural state modulation of neuronal responses in PPC

My initial findings of hypoactivity prompted speculation about the activation of inhibitory interneurons during locomotion. Excitation in healthy cortical networks is precisely balanced by GABAergic inhibition, which regulates local network excitability and facilitates accurate encoding of incoming synaptic inputs by restricting the temporal window for integration of inputs that will generate action potentials (Pouille & Scanziani, 2001). GABAergic neurons are also implicated in generation of brain rhythms and temporal synchrony among cortical and subcortical networks, therefore presenting with a crucial role in many cognitive functions, such as memory and perception (Buzsáki & Watson, 2012; Kepecs & Fishell, 2014). Furthermore, GABAergic neurons alter dendritic integration of sensory signals (Xu *et al*., 2012; Huber *et al*., 2015) and multiple interneuron subtypes have been suggested to play mediating roles in sensory processing during attention, therefore being behavioural-state dependent (Buia & Tiesinga, 2008). In addition, inhibition plays a critical role in modulating critical-period developmental plasticity in juvenile mice (Morales *et al*., 2002; Hensch, 2005), highlighting the importance of GABAergic interneurons of cortical circuits in neurodevelopmental disorders. Indeed, alterations in glutamatergic or GABAergic transmission are prominent in rodent models of ID and autism, more often reported together as E/I imbalances (Dani *et al*., 2005; Durand *et al*., 2012; Clement *et al*., 2012; Gkogkas *et al*., 2013; Bateup *et al*., 2013; Ozkan *et al*., 2014), although separating a causal relationship from a compensatory change is lacking.

SynGAP expression is well documented in both glutamatergic (Chen *et al*., 1998; Knuessel *et al*., 2005; Guo *et al*., 2009; Muhia *et al*., 2010; Clement *et al*., 2012; Clement *et al*., 2013) and GABAergic (Zhang *et al*., 1999; Moon *et al*., 2008; Ozkan *et al*., 2014; Berryer *et al*., 2016) neurons (>60% $GAD67^+$ / $SynGAP^+$ in dissociated culture cells). However, GABAergic cells include a wide variety of different interneuron subtypes, which express different molecular markers, morphological and electrophysiological properties (Kepecs & Fishell, 2014). I decided to initially focus on one interneuron subtype; parvalbumin-expressing (PV) neurons, which have also

been demonstrated to express SynGAP in dissociated neuronal cultures (Berryer *et al*., 2016) for several reasons.

Recent work showed that *Syngap* haploinsufficiency, selectively induced in PV cells derived from the medial ganglionic eminence, is enough to reduce inhibitory synaptic activity, diminish cortical gamma oscillations in awake mice and impair performance in T-maze and induce hyperactivity (Berryer *et al*., 2016). These data suggest that heterozygous loss of SynGAP in PV cells contributes to circuit deficits and therefore likely affects behaviour. In the PPC, PV interneurons have been found to mediate feedforward inhibition of visual inputs and contribute to auditory dominance over visual cues (Song *et al*., 2017). In rostromedial PPC (or RL), another study found that while PV interneurons present with scarcer bimodal responses in visual and tactile stimuli, they robustly boost multisensory integration in neighbouring pyramidal cells (Olcese *et al*., 2013), indicating an important role of PV neurons in controlling the activity of excitatory cells in the region to incoming inputs.

PV interneurons represent the majority of the interneurons across layers (Kepecs & Fishell, 2014) in visual cortex, and present with heterogeneous responses to locomotion, but they are locomotion-responsive on an average population level (Niell & Stryker, 2010; Pakan *et al*., 2016). This is true both in darkness and during visual stimulation, suggesting that they are context-independent, unlike SST interneurons (Pakan *et al*., 2016). My preliminary data suggests that PV interneurons in layer 2/3 of the PPC in WT animals exhibit the same properties regarding locomotion. PV expressing cells in the neocortex are heterogeneous; not only basket cells express PV, but also some chandelier cells (DeFelipe *et al*., 1989). Furthermore, not all PV cells are fast-spiking (Markram *et al*., 2004). As a result, different populations of PV expressing cells could explain the variability in locomotion responses encountered and has been previously reported. Ultimately, a combined expression of markers, along with anatomical and electrophysiological identification would be required to fully identify different PV populations in my dataset.

I also found that PV calcium responses for HET cells were lower compared to WT cells, during stationary conditions, much like what I found with all neurons and

putative excitatory neurons. In addition, during locomotion, the mean change of calcium response of HET PV neurons was also reduced. Even though additional animals are required to make a conclusion from this dataset, it suggests that PV interneuron activity contributes to the exaggerated gain of calcium responses exhibited by HET putative neurons. If correct, HET cells in layer 2/3 of the PPC may be differentially modulated during locomotion due to the reduced PV locomotion responsiveness.

While this would be an interesting hypothesis, during stationary condition the activity of putative excitatory and PV neurons is both decreased, which would mean that just the contribution of the PV cells does not explain this dataset in full (or at least not the still data). It is therefore likely that inhibitory activity from a combination of interneuron subtypes mediates my results.

4.3.2.4 A role for cholinergic input in ASD and Syngap phenotypes?

Neuromodulatory input, such as nicotinic cholinergic input from the basal forebrain has the crucial function of promoting attention and wakefulness (Pinto *et al*., 2013). Fu *et al* (2014) showed that acetylcholine (local injection) reliably activated vasoactive intestinal peptide (VIP) neurons in the V1 *in vivo*, a class of inhibitory interneurons that is strongly responsive to locomotion (Fu *et al*., 2004; Reimer *et al*., 2014; Jackson *et al*., 2016). Acetylcholine activation in VIP was blocked by co-application of nAChR antagonists mecamylamine (MEC) and methylyaconitine (MLA; Fu *et al*., 2004). Interestingly, activation of β-adrenergic and cholinergic receptors has been shown to synergistically activate mitogen-activated protein kinase (MAPK) through the Ras-ERK or Ras-PI3K pathways (Watanabe *et al*., 2000) to promote AMPA receptor insertion at the PSD (Man *et al*., 2003; Saneyoshi *et al*., 2008; Araki *et al*., 2015), which are pathways that SynGAP, following phosphorylation from CAMKII, negatively regulates. Furthermore, activation of MAPK has been found to lead to reduction of A-type K currents (I_A) and increase in neuronal excitability following LTP induction (Rosenkranz *et al*., 2009). While these studies are in excitatory neurons,

we know that inhibitory neurons do not express CaMKII, but they do express the protein phosphatase calcineurin (CaN), which is the only Ca^{2+}-activated phosphatase in the brain (Heifets *et al*., 2008). CaN regulates multiple downstream signalling pathways for the trafficking of AMPARs (PKA/MAPK) at the PSD surface and mediating LTD at inhibitory synapses (Baumägrtel & Mansuy, 2012; Jensen & Edwards, 2012), but the exact signalling cascades in interneuron plasticity are still poorly understood. If CaN mediates AMPAR insertion in inhibitory neurons in a similar way as CaMKII does in excitatory neurons, then it is possible that when cholinergic input activates VIP neurons of *Syngap* HET mice, endogenous MAPK activity would be abnormally high, subsequently leading to hyperexcitability of VIP cells. Therefore, activation of VIP HET neurons could result in stronger VIP-mediated inhibition. Based on connectivity studies, VIP neurons mainly inhibit a second subtype of inhibitory interneurons that express SST (Pfeffer *et al*., 2013; Jiang *et al*., 2015; Urban-Ciecko & Bath, 2016). SST neurons in turn inhibit both excitatory cells by targeting dendrites and PV cells by directly inhibiting soma and dendrites (Urban-Ciecko & Bath, 2016). Assuming the cholinergic input is comparable between genotypes, the result would be that, in darkness, HET VIP neuron hyperexcitability during locomotion will increase activity of neighbouring excitatory cells through disinhibition (see Figure 4.15).

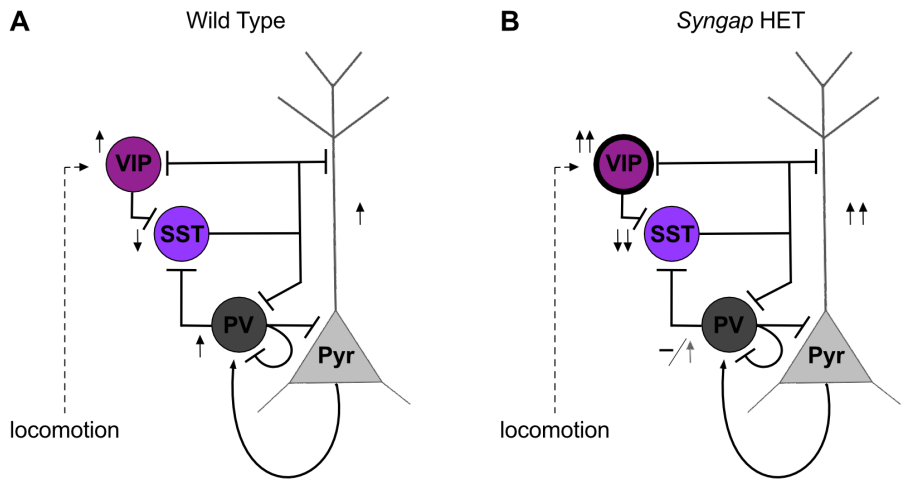

Figure 4.15 Suggested model based on preliminary results in differential modulation of responses of *Syngap* HET neurons by locomotion during darkness in the PPC. (A, B) Schematic proposed illustrations. Connectivity between pyramidal (Pyr) neurons and three different classes of inhibitory interneurons; parvalbumin (PV), somatostatin (SST) and vasoactive intestinal peptide (VIP) expressing neurons, reported from *in vitro* (Pfeffer *et al*., 2013; Jiang *et al*., 2015) and in vivo (Fu *et al*., 2014; Pakan *et al*., 2016) studies in primary visual cortex of mice. Arrow direction indicates celltype – specific proposed response to locomotion (increasing or decreasing calcium responses). Grey arrow represents moderate increase of mean response. Darker outline on schematic VIP cell represents increased excitability.

In support of a role for ascending cholinergic input in ASDs, some children present grey matter reduction in the magnocellular basal forebrain cholinergic system, one of the two major groups of cholinergic neurons in the human brain (Riva *et al*., 2011). Another study by Cheon *et al* (2011) also showed reduced anisotropy and increased diffusivity in the uncinate fasciculus, the fibre tract that connects frontal lobe-temporal lobe-amygdala carrying cholinergic fibres (Highley *et al*., 2002), suggesting reduced nAChR-mediated cholinergic modulation to fronto-temporal and amygdalar regions. Furthermore, galantamine, a cholinesterase inhibitor (preventing the breakdown of ACh), has been shown to reduce pharmacologically-induced sensory processing deficits in rats, such as PPI (Hohnadel *et al*., 2007). Finally, open label clinical trials using cholinesterase inhibitors have shown positive results in children with ASD (Niederhoffer *et al*., 2002; Chez *et al*., 2004*;* Nicolson *et al*., 2006). Reduced presynaptic input would be in interesting path to explore as it might be more accessible

for further targeted therapeutic intervention. However, it would not explain the increased locomotion-induced changes in $\Delta f/f_0$ of neurons in PPC, although it might be implicated in the general apparent hypoactivity during stationary conditions. Additional experiments to pharmacologically activate cortical ACh receptors (AChRs; application AChCl or carbachol; Metherate *et al*., 1992) could prove informative. While nicotinic AChRs (nAChRs) are primarily expressed in layer 4 and layer 5 cortical neurons, muscarinic AChRs (mAChRs) are expressed through all layers of the cortex, at least in rats. Therefore, mAChR modulation in PPC during *in vivo* anaesthetised conditions could be a new avenue for further study. Alternatively, stimulation of nucleus basalis of the basal forebrain would increase cortical ACh levels through thalamic input (Buzsáki *et al*., 1998; Rodriguez *et al*., 2004) and potentially restore mean $\Delta f/f_0$ of *Syngap* HET cells to levels comparable to WT. Notably, Goard & Dan (2009) reported that nucleus basalis stimulation caused decorrelation of multi-unit recorded neuronal activity in the rat visual cortex. As I found increased pairwise correlations of neurons in both PPC and V1 of *Syngap* HET mice, modulating Ach input through activation of nucleus basalis might be more advantageous.

4.3.2.5 Preliminary findings on increased network synchrony of *Syngap* heterozygous PPC neurons

Over the past decade, desynchronization of cortical neurons has been shown to be an essential step in the development of the regions of the neocortex, such as the somatosensory (Golshani *et al*., 2009) and the visual (Rochefort *et al*., 2009). This sparsification of neuronal firing patterns, occurring usually during maturation post - second postnatal week in rodents, is essential to give rise to more computationally efficient coding and save energy (Olshausen & Field, 2004; Averbeck *et al*., 2006). Correlations of spontaneous spiking activity have been extensively studied to understand circuit organisation through reflection of synaptic connectivity (Gerstein & Clarck, 1964), cell types (Hofer *et al*., 2011), cortical layer specificity (Smith *et al*., 2013), physical distances between neurons (Smith & Kohn, 2008; Denman & Contreras, 2013), stimulus response similarity (Cohen & Maunsell, 2009; Ecker *et al*.,

2010) and changes due to sensory stimulation or global brain states (Greenberg *et al*., 2008; Goard & Dan, 2009; Renart *et al*., 2010; Rothschild *et al*., 2010; Yatsenko *et al*., 2015). While we know a lot about SynGAP-mediated signalling on the molecular, synaptic and behavioural level, our circuit-wide knowledge is very limited. In my effort to uncover PPC network phenotypes, I found preliminary evidence of abnormally high synchrony of calcium responses in the putative excitatory *Syngap* HET cells during basal, stationary conditions in the darkness. This was also followed by a decrease in the mean variance of $\Delta f/f_0$ of HET cells over the course of each imaging trial, suggesting exaggerated synchrony of calcium activity due to a high network invariance.

Increased synchrony of neuronal responses has been reported before in *Fmr1* KO mice using *in vitro* and *in vivo* calcium imaging. Luongo *et al* (2016), reported abnormally high synchrony of calcium responses in layer 5 neurons mPFC of *Fmr1* KO mice (and the valproic acid mouse model for autism). Furthermore, application of the cholinergic agonist carbachol, which decorrelates activity in WT slices had no effect in KO slices, suggesting a persistent hypersynchrony endophenotype. Increased network synchrony has been also demonstrated in experiments performed *in vivo* through development up to P40 (Gonçalvez *et al*., 2013). Recordings were performed using OGB1-AM, which has a very fast sharp rise time of change in fluorescence intensity and can therefore resolve frequency of events. This is something my data lacks, at least without further analysis through 'deconvolution' algorithms (Vogelstein *et al*., 2010; Oñativia *et al*., 2010; Dyer *et al*., 2010) to attempt to recover spiking rate. Nonetheless, the mean pairwise correlation value of my experiments for WT putative excitatory cells under stationary conditions (0.198±0.005) is similar to their reported values of ~0.15 for WT animals P30-P40.

Interestingly, it has been demonstrated that optogenetic inhibition of PV interneurons increased synchronous calcium responses in the visual cortex (Sohal, 2012; Sippy & Yuste, 2013). Given the decreased mean activity of HET PV cells during stationary conditions, this could be a mechanism that promotes increased pairwise correlations. However, this does not fit with my data during locomotion, which suggests that when

additional input arrives to the cortex, highly locomotion responsive neurons desynchronise the overall network activity. Additional analysis of pairwise correlations for locomotion responsive and non-responsive cells would address this discrepancy. Finally, experiments in reported Sippy &Yuste (2013) were performed *in vitro*, and the mechanisms mediating excitatory neuron synchrony through PV interneuron activity is likely different in awake animals, especially during attention.

As coupling to the mean population can represent neuronal computations through the joint activity of multiple cells, I also investigated the relationship between the activity of WT and *Syngap* HET putative excitatory cell to the population sum response during each trial. A study from Okun *et al* (2015) used a computational model to predict pairwise correlations by summing the activity of multiple neurons and correlating the spike train with the result. Input parameters arose from experimental data in mouse V1 and primate visual cortex and concluded that the majority of the pairwise correlations in a population of neurons can be explained by the coupling of each neuron to the population rate, even though the variance of coupling can range between cells. The finding that *Syngap* HET neurons were more strongly coupled to the population activity could suggest that HET neurons in PPC are more coordinated to any input that increases the activity of their local network ('choristers' not 'soloists', as Okun *et al* described). As this data is during darkness, that input would include neuromodulation, long-range synaptic connectivity or spontaneous fluctuation of the network.

Deficits in maturation and plasticity of *Syngap* HET mice during development could be a likely contributor to the elevated synchrony that my preliminary results show. Some studies have shown alterations in dendritic spine shape, maturity and stability (Clement *et al*., 2012, 2013; Aceti *et al*., 2014), E/I imbalances (Ozkan *et al*., 2014), as well as cortical hyperexcitability (Clement *et al*., 2012, 2013; Ozkan *et al*., 2014). Given the widespread expression of SynGAP protein, subtle increases in network synchrony could be a generalised phenomenon widespread across all cortical regions. This would then provide insight into the abnormal EEG findings demonstrated in *Syngap* HET mice (Ozkan *et al*., 2014). Understanding local network properties and connectivity can therefore prove critical to elucidating mechanistically how

computations affect behaviour through learning, experience, or by changes in behavioural context.

It is obvious that for circuit-based analysis of synchrony and coupling it is advantageous to have large FOVs with as many cells as possible. However, the dataset presented in this thesis (and discussed above) is comprised 1177 putative excitatory cells from 4 WT mice and 268 cells from 1 heterozygous *Syngap* mouse (see Figure 4.10). I therefore repeated this analysis for my initial imaging dataset for which I recorded GCaMP6s calcium transients with a 40x objective (see Figure 4.5). I found no difference in pairwise correlations or in mean population coupling between genotypes (See Appendix1 Figure 1.17). There are multiple reasons why this difference between datasets might arise. One reason is the type of calcium indicator used. Initial experiments were performed with GCaMP6s, which has slower kinetics (Chen *et al*., 2013) making it more difficult to resolve accurate coupling data, as slower GCaMP6s transients could potentially mask differences between genotypes. The second reason would be the number of neurons; even though the initial dataset consists of 4 WT and 3 HET mice, the number of neurons per animal is much lower (average- 60 cells per animal; total- 244 cells for WT, 184 cells for HET) reducing the power of the experiment. Finally, as the imaging FOV is much smaller under a 40x objective, it is possible that *Syngap* HET neurons display larger differences in pairwise correlations in cells farther apart, than in close proximity. It would therefore be informative to perform a correlative analysis of distance versus correlation coefficient when the dataset is complete. Finally, I refrained from presenting PV interneuron data in regards to circuit-based activity as my small sample size (68 WT PV cells, 14 HET PV cells) is insufficient to demonstrate even preliminary findings.

4.3.2.6 Can increased circuit network synchrony underlie the altered EEG of *Syngap* HET mice?

As 70-80% of individuals with *SYNGAP1* haploinsufficiency present with generalised seizures with an onset during early childhood (Hamdan *et al*., 2011a, 2011b; Berryer

et al., 2013, Carvil *et al*., 2013), Clement *et al* (2012) and Ozkan *et al* (2014) both investigated seizure incidence in *Syngap* HET mice. They reported reduced threshold of flurothyl-induced seizures at the 1st clonus and the tonic/clonic (T/C) phases. Furthermore, Ozkan *et al* (2014) examined EEG activity in the temporal and parietal cortices of *Syngap* heterozygotes and reported sharp epileptiform activity (intermittent discharges) in awake state. Interestingly, this type of epileptiform activity was not coinciding with any motor events. my preliminary data suggests an increase in local network synchrony in PPC of *Syngap* HET mice, as illustrated by increase in both the pairwise correlations of the neurons, as well as the coupling of HET neurons to the mean population activity. Combining EEG with concurring two-photon imaging to investigate whether there is a temporal correlation between coupling activity and EEG would be advantageous and could provide a causal link between the two.

4.3.2.7 Context-independent neuronal responses to locomotion in layer 2/3 of PPC

Results on locomotion-induced increased calcium responses of PPC neurons of *Syngap* HET mice also prompted speculation regarding the activity of HET neurons during sensory stimulation. I hypothesized that during sensory stimulation of a single modality in stationary conditions, *Syngap* HET neurons would have abnormally high calcium responses which would increase their mean $\Delta f/f_0$ to comparable levels as WT neurons. This would then be exaggerated during running conditions, due to the additive effect of locomotion in neuronal responses. I therefore decided to use a visual stimulation paradigm with static and drifting gratings to further our analysis of orientation selectivity (OSI) and direction selectivity (DSI) of neurons of different genotypes. Similar visual stimulation protocols have been widely used before in visual cortex experiments from Pakan *et al* (2016) and others (Niell & Stryker, 2010; Fu *et al*., 2014). For recordings in the PPC, Goard *et al* (2016) used a drifting grating of two orientations (0° and 90° from vertical) as a cue stimulus in a visual discrimination memory-guided task and in the study of Olcese *et al* (2013) in the RL (rostromedial PPC), square drifting gratings (0° and 180° from vertical) were presented in anaesthetised mice. I found about 40% of neurons of both genotypes to be visually

responsive, however visual stimulation did not have a large effect on the mean $\Delta f/f_0$. HET cells were again more strongly modulated by locomotion, in a context-independent fashion, suggesting that in general, behavioural state has a stronger effect on PPC neuron calcium responses than visual stimulation.

However, there are several factors that could have affected my results; first, it would be highly informative to refine the current analysis and to filter for subpopulations of neurons of either genotype, for eg. either highly visually responsive neurons, or neurons with other visual properties such as strong orientation or direction selectivity indices (OSI, DSI >0.5). Indeed, Olcese *et al* (2013) reported that many visually responsive cells in RL present with direction selectivity to moving stimuli during anaesthesia, but percentage of visually responsive neurons was not clarified. An older study by Marshel *et al* (2011), identified visually responsive neurons in cortical areas surrounding the primary visual cortex of mice. A high percentage of visually responsive neurons were orientation selective (OSI>0.5), and the OSI was comparable between V1 and visual association areas. V1 and surrounding regions also had comparable percentage of direction selective neurons of similar DSI values. Based on my stereotaxic coordinates, some of those regions would be rostral or lateral to PPC, or including regions of PPC, and it would therefore be advantageous to separate specific neuronal populations to quantify the effect of visual stimulation to neurons of the PPC and to compare between WT and *Syngap* HET mice.

Second, it is possible that the visual stimulation paradigm used was not optimal to elicit large stimulus-locked calcium responses to neurons of PPC. I used comparable visual paradigms for PPC and V1 stimulation, with spatial frequency (SF) of 0.05 cpd and temporal frequency (TF) varying from 1 to 1.5 Hz. The study by Marshel *et al* (2011), illustrated that cells have different combinations of spatial and temporal features encoded by each surrounding area of the primary visual cortex (for V1: pref. SF 0.045 cpd, pref. TF 0.69 Hz). Surrounding regions spanned from 0.022 to 0.046 cpd for SF and 0.87 to 1.8 Hz for TF. It is therefore possible that the temporal frequency was lower than the optimal for acquiring most cells with selective responses to oriented gratings. Furthermore, full field flashing light (50ms illumination at 10 Hz) has been used before to record visual activity responses in PPC, however in addition

to the strong stimulus the screen was also positioned much closed to the contralateral eye (10 cm, compared to 20 cm that I used; Song *et al*., 2017). Song *et al* (2017) also suggested the possibility of gaining larger visual stim-locked responses by presentation of natural scene movies, rather than gratings or flashing light, based on work on visual salience representation in monkey parietal cortex (Gottlieb *et al*., 1998).

Finally, as neurons in the greater PPC region have been found to respond to both visual, tactile, auditory and combined inputs (Oclese *et al*., 2013; Song *et al*., 2017), it is possible that visual selectivity of excitatory neurons is disrupted by the arrival of a stimulus from a different modality. Indeed, Olcese *et al* (2013) established that both excitatory (pyramidal) and inhibitory (PV) neurons can be unimodal and bimodal for visual and tactile input, and that increasing the activity PV neurons optogenetically during combined stimulation results in a large reduction of spiking responses of pyramidal cells. Furthermore, another study using an auditory-visual discrimination task, found that auditory cortex (AC) and V1 send converging inputs to PPC, while co-activation of those inputs causes audition dominance over vision mediated through PV neurons in the PPC (Song *et al*., 2017). This suggests another cross-modal integration mechanism, where PV interneurons in PPC are responsible for AC-specific feedforward inhibition of V1 inputs. While I did not perform combined sensory stimulation for a different modality than vision, there are two parameters that need to be noted. One is that animals are awake, running on a treadmill. This on its own provides a large motor cortex-specific input to all cortical areas. Second, even when the animals are still, behavioural context modulation through arousal will be much larger than in anaesthetised animals. Third is that in my experiments the vibrissae system remains intact as I did not pluck/trim the whiskers. While observing the infrared videos of the animal behaviour I noticed that the longest whiskers touch the surface of the treadmill. This therefore will provide additional stimulation during random periods of the imaging sessions that I have not tried to dissociate from the data, and could account for the lack of visual-evoked increase in mean $\Delta f/f_0$.

4.3.2.8 Can we resolve useful information from neuropil responses?

Notably, cell bodies were not the only structure labelled with genetically-encoded calcium indicator GCaMP6s or GCaMP6f under the synapsin promoter. AAV injection to the cortex also stained the surrounding neuropil, which consists of presynaptic boutons and axons (>50%), dendrites (30%), and glial processes (10%) (Chklovskii *et al*., 2002; glia however are not stained with GCaMP6). While the neuropil staining pattern was diffuse, some dendrites and axons could be resolved, and in cases when I imaged with 40x objective, some dendritic structures such as dendritic spines. Since various neuronal compartments express the calcium indicator, it is important to manually decontaminate overlapping cells and processes, and then to use an additional decontamination algorithm to subtract the neuropil signal from the fluorescence time course signal of the region of interest (ROI), which in my experiments is the soma.

However, previous studies using the calcium dye OGB1-AM as an indicator to image cells in layer 2/3 of V1 have reported increased neuropil fluorescence during periods of running in awake mice head-fixed on a Styrofoam ball (Dombeck *et al*. 2007). This increased change in fluorescence was accompanied by a reduction in the baseline frequency of transients during stationary (rest) periods, much comparable to somatic calcium responses. Further analysis on correlation-coefficients revealed that fluorescence transients in neuropil regions were strongly correlated with the running speed of all mice, with a mean *Corr*=0.6 (*Corr*>0.5: 31±15%; 0.5>*Corr*>0.3: 53±28%; 0.3>*Corr*>0: 19±20%); however, the OGB1-AM neuropil $\Delta f/f_0$ transients recorded were about 8 times smaller than the typical cell $\Delta f/f_0$ (~2-5% $\Delta f/f$ for neuropil versus ~15-30% $\Delta f/f$ for cell bodies). Dombeck *et al* (2007) also reported mixed results for correlation of astrocytic fluorescence changes and locomotion, but since the AAVs used in my experiments are under a synapsin promoter, glial structures were not labelled.

Another study reported prominent (0.1-0.3 $\Delta f/f$ in the 0.5-1 Hz range) spontaneous neuropil calcium transients while imaging layer 2/3 of motor cortex using the same experimental procedures in anaesthetised rats (Kerr *et al*., 2005). In this study, Kerr *et*

al (2005) addressed the origin of neuropil calcium responses through combining *in vivo* two-photon imaging with optical encephalogram (ECoG) and whole-cell electrophysiology. Neuropil peak fluorescence responses were highly synchronised to ECoG, irrespective of the depth from pial surface, suggesting that neuropil calcium signals are linked to ongoing cortical electrical activity. As astrocytes display very broad and slow OGB1-AM calcium transients and are therefore unlikely to contribute to this ECoG activity, the remaining two calcium signals that could influence neuropil fluorescence flunctuations would be either presynaptic (i.e. axonal) or postsynaptic (i.e. dendritic). Subsequent experiments performed in the presence of AMPA receptor antagonists GyKI53655, which should only have a postsynaptic effect, had no effect on neuropil calcium transients and ECoG (Kerr *et al*., 2005), therefore suggesting that dendritic calcium responses contribute little if at all to OGB neuropil signal. Therefore, neuropil Δf/f, mainly caused by bulk signals in axonal structures, could subsequently be considered as a measure for local input activity to the examining cortical region.

Many studies have suggested that in individuals with ID and autism local intracortical connectivity is enhanced while long-range connectivity of the neocortex is reduced (Belmonte *et al*., 2004; Courchesne & Pierce 2005; Geschwind & Levitt, 2007; Rippon *et al*., 2007; Kroon *et al*., 2013; Rane *et al*., 2015). Some other studies have also suggested neocortical hyperconnectivity in young children with autism (Rudie & Dapretto, 2013). Even though these results can be confounding, long-range connectivity has been characterised as largely atypic. Differences between hyper- and hypo-connectivity may result from the heterogeneity in the mutations carried by screened individuals as well as the age of selected cohorts. Furthermore, in a recent study combining fMRI and viral tracing approaches in the mouse model of FXS, Haberl *et al* (2015) reported anatomical hyperconnectivity of primary V1, accompanied by low connectivity of V1 with other cortical regions, such as prefrontal areas.

Analysing the mean response of neuropil calcium transients could therefore be advantageous for this current project. Given the apparent behavioural-state dependent hypoactivity of HET PPC neurons, we could also hypothesise that input to layer2/3 PPC in *Syngap* HET mice is increased during locomotion. As GCaMP6-neuropil

signal would include only processes that are coming from cells that have been virally targeted, this would mean that the axonal structures labelled would be from cells located in layers 4, 5, and 6 of the cortex. Nevertheless, this could then provide interesting information as to whether HET neurons receive increased input compared to WT controls.

4.3.2.9 Preliminary findings on behavioural state - independent hyperactivity of layer 2/3 neurons of V1 in adult *Syngap* heterozygous mice

Based on findings in PPC, I decided to also examine the modulation of neuronal activity by locomotion in a primary sensory area, layer 2/3 of primary V1. In line with a lot of published work in visual cortex (Niell & Stryker, 2010; Keller *et al*., 2012; Fu *et al*., 2014; Pakan *et al*., 2016), I found enhancement of calcium responses of V1 putative excitatory and PV interneurons during locomotion in darkness. However, in contrast with previous findings in PPC, *Syngap* HET neurons in V1 showed increased mean $\Delta f/f_0$, in both behavioural states, suggesting state-independent hyperactivity. The above was true for both putative and PV cells, although the difference between genotypes was stronger in putative excitatory neurons which can be explained by the much larger sample size. It therefore seems that heterozygous loss of SynGAP in visual cortex and parietal cortex affects network computations differently during locomotion, although both datasets are preliminary.

Furthermore, and similar to results in PPC, *Syngap* HET V1 putative excitatory and PV cells showed increased pairwise correlations in calcium responses. As discussed previously, hyperactivity and hypersynchrony of neuronal activity are two features that have been previously reported *in vitro* (La Fata *et al*., 2014; Chuang *et al*., 2015) and *in vivo* (Gonçalvez *et al*., 2013) in a different mouse model of ID and autism, the *Fmr1* KO mouse. My visual cortex results fit well with previous findings of cortical hyperexcitability (Clement *et al*., 2013; Ozkan *et al*., 2014) and hyperactive EEG spike discharges (Ozkan *et al*., 2014) in the *Syngap* HET mice, as well as with published literature in *Fmr1* KO mice. Finally, coupling to the general population mean was

comparable between genotypes and did not follow the pairwise correlation data. This could be potentially explained by the increased variance of responses *Syngap* HET neurons exhibit (as well as large variability of that variance, illustrated by the large standard error), which could make it more difficult to interpret whether the increased synchrony of responses is a real demonstration of connectivity or just arises by many variant calcium transient fluctuations during the recordings.

4.3.2.10 C57Bl/6J-OlaHsd background strain shows decreased locomotion-induced modulation of calcium responses

One robust finding across labs that work with *Syngap* HET mice is that they do not survive on a pure C57Bl/6J (Jax; Jackson labs) background. However, a lot of published work in the visual cortex field that I compare a lot of my findings to, including Pakan *et al* (20016), is on wild type mice acquired from Jackson labs.

In our lab, the *Syngap* HET mouse was developed on a C67Bl/6J-OlaHsd (Ola; Harlan; Komiyama *et al*., 2002) background strain. To create the SyngapPV line, I first backcrossed the interneuron line to the Ola background and mated offsprings with *Syngap* heterozygotes. When I noticed that the effect of locomotion on activity of putative excitatory cells of WT mice in V1 was not as pronounced as it has been previously reported, I hypothesized that the background strain might have contributed to that observation. Prior to initiating this project, Dr. Chih-Yuan Chiang in the Kind laboratory, found differences in visually evoked potentials (VEP) from layer 4 visual cortex in awake adult mice of different backgrounds (Chiang, 2016). More specifically, he tested two different wild type strains, Ola and Jax mice, and found that Ola mice failed to exhibit stimulus-specific response potentiation (SRP) of VEP over the course of 7 days, that is characteristic of Jax mice (Sawtell *et al*., 2003). This finding was accompanied by a sharp peak of field potential activity at the gamma frequency band in Ola mice, which was lacking in the Jax animals. Subsequent experiments performed in the lab to investigate differential gene expression of these two wild type strains, revealed that Gamma-Aminobutyric Acid Type A Receptor

Alpha 2 Subunit gene (*GABRA2*) gene was enriched in the visual cortex of Ola mice relative to Jax.

Following these observations, I compared the activity of neurons of these different wild type background strains to locomotion and to visual stimulation to directly test whether background strain is a contributor to the lack of strong locomotion mediated modulation of activity enhancement of WT cells. Neurons from Jax mice presented with a much higher increase of calcium responses during locomotion than Ola mice in darkness, while their variance of fluorescence change remained comparable. In addition, locomotion during visual stimulation further increased their mean calcium responses to a greater level than that of Ola neurons. The lack of gamma peak activity in layer 4 does not represent a causal explanation to my findings, however the global downregulation of *GABRA2* in visual cortex of Jax mice could contribute to a lack of inhibitory drive and subsequent 'abnormally' high increase of responses of neurons when locomotion or thalamic inputs arrive to the cortex following sensory stimulation or behavioural state change.

4.3.2.11 Relationship between relative fluorescence changes and spiking activity

In this part of the thesis I used the relative changes of somatic fluorescence transients of neurons labelled with genetically-encoded calcium indicators GCaMP6s or GCaMP6f (Chen *et al*., 2013) as a proxy for neuronal activity. Genotype aside, the relationship between fluorescence changes and spiking activity can be affected by several factors; such as the balance between calcium influx and efflux, internal calcium release and the concentration of calcium buffers in the somas (Grienberger *et al*., 2012). Care must be taken when extrapolating calcium imaging data collected from awake recordings after sensory or behavioural perturbations as it is possible that for the same number of spikes we get a higher increase of cytosolic free calcium concentration during locomotion versus stationary periods, or dark versus visual stimulation. Considering that neuromodulators such as acetylcholine can regulate calcium influx through voltage gated calcium channels (Fucile, 2004; Shen & Yakel,

2009) it is possible that context and/or behavioural state modifies the level of neuromodulators and increases the amount of calcium entering the neuron in response to each spike. This is important, as it would mean that for a given spike, the increase in fluorescence would be higher during certain conditions (i.e. locomotion or/and sensory stimulation).

A second confounding factor for current and future interneuron experiments is the possibility of different intracellular dynamics between the different types of neurons, such as excitatory and interneurons, or between subtypes of excitatory or inhibitory neurons. I cannot exclude the possibility that both different neuron types and contexts/behavioural states affect the relationship between recorded fluorescence responses and number of spikes without an independent readout of spiking activity, for eg. simultaneous electrophysiological recordings. I can, however, compare with published literature. Polack *et al* (2013) recorded changes in firing rate between different neuronal populations of layer 2/3 in V1 during locomotion and stationary conditions, in darkness and during visual stimulation (drifting gratings). Authors reported frequency of spikes in darkness (for $excitatory_{still}$: 0.8±1.0 spike/sec, for $excitatory_{loco}$: 1.1±2.2 spikes/sec; for PV_{still}: 14.3±12.7 spikes/sec, for PV_{loco}: 22.5±16.1 spikes/sec), which enhances during visual stimulation (approximate doubling of firing rate) for both excitatory wild type neurons, and PV interneurons, while spontaneous membrane resistance (Rm) and time constant (τ) remain unaffected (Polack *et al*., 2013- Suppl. Tables1, 2 and 3). I find comparable relative change in mean $\Delta f/f_0$ from still to locomotion, suggesting that $\Delta f/f_0$ responses reflect changes in spiking activity, in transition between behavioural states and during presentation of visual stimulation, at least in the visual cortex.

The above do not only refer to WT neurons, but also neurons from SynGAP heterozygous mice. However, as SynGAP negatively regulates Ras and ERK there are some additional points to be considered. Partial loss of SynGAP would not likely directly affect the calcium influx in the neuron, although there is the possibility that channel density (such as VGCCs) can have a major effect. Furthermore, SynGAP is downstream of calcium/calmodulin-dependent kinase (CaMKII), a major target of

calcium influx through the NMDA receptor (Leonard *et al*., 1999; Sheng & Kim, 2002). Following CaMKII activation, SynGAP is phosphorylated increasing its Ras GAP activity by ~70% and therefore negatively regulating Ras and ERK (Chen *et al*, 1998; Oh *et al*., 2004). Abnormal regulation of Ras/ERK pathway due to partial loss of SynGAP could therefore trigger homeostatic mechanisms involving upregulation of other signaling Ras/ERK pathways (Grewal *et al*., 1999), such as the phospholipase C (PLC) and protein kinase C (PKC) pathway (Cullen & Lockyer, 2002), forming inositol trisphosphate (IP3) and releasing Ca^{2+} from the endoplasmic reticulum to the cytoplasm (Mikoshiba, 2006). Therefore, loss of SynGAP can provide alternative mechanisms through which Ras-mediated calcium dynamics regulate neuronal activity.

4.3.2.12 Further technical considerations for future experiments

Location of PPC recordings

In my study, a smaller proportion of cells of the PPC were found to be visually responsive than reported before. Olcese *et al* (2013) demonstrated that in RL during presentation of either a visual stimulus (one full field flash), a tactile stimulus (whisker pad deflection) or bimodal stimulation, 19% cells were unimodal-tactile, 16% were unimodal-visual, 63% were bimodal and only 2% of cells were not modulated by sensory stimulation. However, these recordings were multi-unit recordings in urethane-anaesthetised mice, which quite possibly explains the small percentage of non-modulated unit responses. Multi-unit recordings were followed by two-photon imaging experiments in anaesthetised mice using OGB-1AM as a calcium indicator, and cells that did not present with calcium responses during stimulation conditions were not included in the dataset. Furthermore, the aim of the study was to characterize the cytoarchitecture and physiological properties of different cells responding to uni- or bi-modal stimuli. For that reason, after identification of V1/V2 and S1, targeted regions of interest for subsequent imaging were as proximal to those cortical regions as possible. From the figures, it is easy to see that recording sites imaged are 3-3.5mm

on the mediolateral axis, whereas my injections were targeted at 1.7mm lateral to midline and performed at a 30° angle, based on coordinates from Harvey *et al* (2012) (same as Guo *et al*., 2014; Goard *et al*., 2016). There are therefore quite a few differences between the location of imaging and the experimental protocol that make it difficult to draw direct comparisons.

As PPC is relatively extended in the medial-lateral direction, from Paxinos and Watson (2004) we can argue that it spreads ~ 4mm in that direction, the antero-posterior length is much more limited (~1mm). It would be advantageous for future experiments to confirm, prior to imaging, that my imaging field of view (FOV) does not coincide with extended visual association areas (secondary V2 areas), as there is a possibility that the spread on the antero-posterior axis could be broader than this. Finally, even though the precise location of the border between mouse PPC and V2 areas still remains somewhat debated, as all my injections in mutant and wild type animals are targeted at the same stereotaxic coordinates, the only inconsistency should arise from inter-animal variability, which is a consideration for every study.

Layer 4 visual cortex experiments

After initiating this project, Dr. Sam Booker in the Kind laboratory found an increased number of SST neurons in layer 4 of the V1 of *Syngap* HET mice (see Appendix1 Figure 1.18). In addition, as layer 4 receives direct and indirect input from the thalamus following visual stimulation (Sherman & Guillery, 2002), it would be potentially advantageous to perform recordings in layer 4 rather than layer 2/3. However, based on general findings in the two-photon literature, layer 4 data are difficult to directly compare to layer 2/3. Main reason is that targetting layer 4 usually results in a weaker and sparser expression of GCaMP6, often due to its inherently resistant nature to transfection using AAVs that have standard promoters, for eg. eF-1a, CamKII or (h)Syn. While in layer 2/3 and layer 5 the transfection efficiency is high and uniform, it is possible that AAVs in layer 4 preferentially target cells that are of a specific subtype or have specific properties. It would be therefore ideal to target layer 4 with a

specific marker/promoter incorporated in our expression system, rather than using the current viruses used in this thesis.

Astrocytic activity during locomotion

Astrocytic contribution to development and function of neurons is now becoming more and more appreciated as studies focus on the control of formation, maturation and elimination of synapses during critical periods of development through astrocyte-neuron contact-mediated signaling (Stevens, 2008; Clarke & Barres, 2013). In addition, emerging evidence has linked astrocyte-dysregulated function to an array of neurodevelopmental conditions such as schizophrenia, epilepsy and Rett syndrome, as well as neurodegenerative disorders, such as amyotrophic lateral sclerosis and Parkinson's disease (Parpura *et al*., 2012; Yamamuro *et al*., 2015). Pacey & Doering (2007) showed the importance of astrocytic function on FXS, being the first to report the expression of FMRP in astrocytes, as well as dysregulated dendritic arborization when culturing WT neurons with *Fmr1* KO astrocytes (Jacobs *et al*., 2010).

More specifically for my work, while astrocytes are incapable of generating action potentials (Haydon, 2000), locomotion has been found to trigger simultaneous responses of astrocyte networks (>50% of recorded astrocytes showed *Corr*>0.3) in multiple brain circuits through norepinephrine-induced calcium elevations (Dombeck *et al*., 2007; Paukert *et al*., 2014). Astrocyte calcium fluctuations have been found to be induced not only by locomotion, but also by startling movements in wild type mice (Srinivasan *et al*., 2015). While there are no studies to date to suggest expression of SynGAP protein in astrocytes, it would be advantageous to consider their contribution to dysregulated circuit activity of neurons of *Syngap* HET mice.

Chapter 5

Afterthoughts

Mutations in genes that encode for synaptic function have long been associated with phenotypic manifestation that includes ID and other comorbid disorders, such as autism, epilepsy, and schizophrenia. Some of the most common single-gene mutations that cause syndromic ID and autism give rise to Tuberous Sclerosis (*TSC1*, *TSC2*), Fragile X (*FMR1* gene), Rett (*MeCP2*), Phelan-McDermid (*SHANK3*) and Angelman (*UBE3A*) Syndromes. Due to advancement of whole genome and exome sequencing techniques, more and more rare *de novo* dominant mutations that lead to nonsyndromic forms of ID are being discovered. As such, genetic screening of patient cohorts with ID have revealed several pathogenic *de novo* mutations in *SYNGAP1*, which are predicted to lead to functional loss of one copy of the gene (haploinsufficiency). *SYNGAP1* has been identified as one of the top 5 recurrently mutated genes in individuals with developmental brain disorders (Fitzgerald *et al*., 2014), while the prevalence of *SYNGAP1* haploinsufficiency has been reported to be as high as 2-4%, which would make it one of the most common dominant autosomal causes of nonsyndromic ID and autism (O'roak *et al*., 2014; Parker *et al*., 2015; Mignot *et al*., 2016, sfari.org).

At present, current therapeutic strategies for neurodevelopmental disorders are either intended to treat patient symptomatology (hyperactivity, aggressive behaviour, anxiety) or aimed towards the identification and targeting of specific 'core deficits' that underlie each disorder, such as targeting the Ras-ERK1/2 pathway in FXS (Berry-Kravis, 2014). Notably, regardless of the heterogeneity of single-gene mutations that cause ID and autism, numerous studies aim to establish whether there is convergence of cellular and molecular phenotypes that underlie affected behaviour (Auerbach *et al*., 2011, Barnes *et al*., 2015, Till *et al*., 2015). As the ultimate goal is the identification of effective treatments to alleviate patient symptoms, this could lead to the ideal outcome where pharmacological rescue of one disorder can also provide rescue of other, genetically distinct disorders. However, while recent studies report cellular and molecular phenotypic similarity across mouse models of ID/ASD (from *Fmr1* to *Syngap* mouse; Barnes *et al*., 2015) and across rodent species (from mouse to rat; Till *et al*., 2015), behavioural phenotypes appear more complicated. Till *et al* (2015) first reported that behavioural deficits across rodent species of FXS remain distinct,

regardless of convergence on a molecular and synaptic level. In my efforts to directly compare behavioural phenotypes in *Syngap* deficient mice and rats, we also observed that while some deficits were shared by both species, others were manifested in different ways. Furthermore, by comparing my findings with those in the *Fmr1* KO rat (Till *et al*., 2015; Asiminas, 2016), we also found that behavioural phenotypes are not shared across rat models of ID. And interestingly, even some forms of the synaptic plasticity deficits reported in *Fmr1* KO rats, such as mGluR-dependent hippocampal LTD, remain unaffected in *Syngap* HET rats (Dr. Adam Jackson, unpublished data). These findings challenge the idea of convergence of phenotypes across neurodevelopmental disorders, even on a cellular level, and highlight the importance of more animal models of disease to draw conclusions regarding behaviour and applicability of future therapeutic approaches.

One of the ways to bridge the gap between molecular, cellular and behavioural deficits would be to extensively examine local network and circuit activity. Undoubtedly, circuitry underlying behaviour remains the least studied aspect of phenotypic characterisation in *Syngap* heterozygous mice, despite its importance. As patients with ID and autism, including individuals with *SYNGAP1* haploinsufficiency, display seizures, hyperactivity and sensory hypersensivity, the idea of neuronal and circuit hyperexcitability can possibly provide an explanation for reported symptomatology. In accordance to that, previous studies have reported disruption of information processing in the *Syngap* HET mouse, induced by increased evoked hyperexcitability of local circuits *in vitro* (Clement *et al*., 2012; Ozkan *et al*., 2014). Furthermore, studies from the *Fmr1* KO mouse also report increased neuronal hyperactivity and network synchrony at different cortical areas (Hays *et al*., 2011; Gonçalvez *et al*., 2013). Certainly, the concept of neuronal and circuit hyperactivity/hyperexcitability fits well with the current unifying theory of autism by Markram & Markram (2010), which suggests that the core behavioural and cognitive features of autistic individuals, including hypersensitivity, hyperattention, and hyperemotionality, arise from local circuit hyperfunctioning. However, my preliminary results challenge this theory as I do not report neuronal hyperactivity in all the regions we examined. In the PPC, my findings lean towards a hypoactivity phenotype of neurons, which is differentially

modulated by sensorimotor input during locomotion. On the other hand, my findings in V1 show enhanced responses of cells during both behavioural contexts. It would be tempting to hypothesize that while all sensory areas of *Syngap* heterozygous mice present with hyperactivity, such as the visual or barrel cortex, this does not follow for association areas of the cortex, such as the PPC. That could imply that long-range inputs to other brain regions from local primary sensory areas are decreased or not as efficient. Indeed, many fMRI studies have suggested that individuals with ID and autism present with long-range cortico-cortical underconnectivity (Belmonte *et al*., 2004; Just *et al*., 2012; Kroon *et al*., 2013; Rane *et al*., 2015). This hypothesis could provide a new avenue to follow up my study in the *Syngap* mouse model, by interrogating the spread of activity using voltage-sensitive dye (VSD) imaging. This would in turn provide valuable insights into the temporal and spatial patterns of sensory-evoked spread of neuronal activity within a certain cortical area but also to other brain regions.

Assessing perceptual decision-making and working memory (WM) is also certainly of interest. Neurons in layer2/3 of the PPC have been shown to present with sustained activity during different epochs of visually-guided working memory decision tasks, such as the delay epoch (memory retention) and response epoch (lick or turn; Harvey *et al*., 2012; Raposo *et al*., 2014; Goard *et al*., 2016; Licata *et al*., 2017). In addition, Harvey *et al* (2012) reported that bilateral inactivation of PPC impaired the performance of mice during the task. In their experimental set up, mice were head-fixed under the two-photon microscope in a tube and oriented gratings were presented (0°/90°) as a visual stimulus. My present results demonstrate decreased calcium responses of layer 2/3 HET PPC neurons during visual stimulation when mice are stationary, which would directly relate to the cue epoch of the experiments Harvey *et al* (2012) conducted. In addition, as their data is all collected when mice are in a tube, my stationary results are comparable (but not identical) to that condition. Of note, *Syngap* heterozygous mice display working memory impairments in an unforced spontaneous alteration task (in a T-maze) as well as during the WM-component of a spatial memory task, assessed using the radial arm maze (Guo *et al*., 2009; Muhia *et al*., 2010; Ozkan *et al*., 2014; Berryer *et al*., 2016). It would therefore be interesting to

further assess the activity of cells of *Syngap* HET animals during the delay and response epochs and directly correlate it to the animal's behavioural output.

At the same time, one of the main brain regions implicated in working memory is mPFC. Previous studies have shown that WM-related activity during the delay period is encoded in neurons of mPFC in rodents and that perturbation of mPFC activity results in impairment of WM (Baeg *et al*., 2003; Fujisawa *et al*., 2008; Erlich *et al*., 2011; Meyers *et al*., 2012; Liu *et al*., 2014). *Syngap* heterozygous mice exhibit not only behavioural deficits associated with mPFC function, but also develop alterations in neuronal synaptic transmission in adulthood (Ozkan *et al*., 2014). This is also accompanied by increased stimulus-evoked spread of activity within layers of the mPFC (Ozkan *et al*., 2014). It would certainly be worth testing the activity of mPFC neurons of *Syngap* HET mice *in vivo* during a visually-guided working memory decision task, as described above. While mPFC is more difficult to access due to depth, a recent study utilising optogenetic inhibition showed that frontal motor cortex/anterior cingulate cortex is also critical and required for performing in the same visually-guided WM decision task (Goard *et al*., 2016). Alternatively, recent technological advancements allow for the use of endoscopes to monitor calcium activity in deeper cortical and subcortical areas of the brain, during head-restrained but also freely-moving animals (Resendez *et al*., 2016).

Finally, it is important to consider how multisensory integration of sensorimotor stimuli is important for behaviours other than cognition. A recent fMRI study examined the brain activity of high-functioning ASD patients while they were performing a social interaction task (interpretation of speaker's communicative intent) with and without the introduction of a mildly aversive sensory distracter (Green *et al*., 2017). They reported that ASD patients processed social information in a more 'effortful' way relative to control subjects in the presence of the distracter, as reflected through a pattern of abnormally increased activation of medial prefrontal and temporal areas of the cortex. This study demonstrated for the first time how sensory stimuli can directly disrupt social behaviour in ASD individuals with sensory hypersensitivity. This would then suggest that sensorimotor processing and multisensory integration abnormalities in cortical networks can also contribute to social cognition deficits in

patients with neurodevelopmental disorders. Notably, *Syngap* heterozygous mice exhibit sensorimotor gating abnormalities (reduced PPI and increased startle reactivity) and social behaviour abnormalities, such as social interaction and social novelty deficits, and social isolation. Furthermore, social novelty impairments were reproduced at the *Syngap* heterozygous rat model. Investigating altered sensory processing of neuronal network and circuit activity can therefore not only be critical for understanding underlying deficits in cognition, but also in aberrant social behaviour.

In conclusion, my findings encourage additional experiments not only to solidify my current preliminary findings but also to elucidate neuronal activity and circuitry abnormalities that underlie atypical behavioural phenotypes in animal models of ID and ASD. This would then provide additional insight into how we can connect genetic changes to circuit-level and behavioural phenotypes, in order to pave the way for targeted pharmacological interventions which will alleviate symptoms associated with such debilitating disorders.

Appendix 1

Additional figures and data

Supplementary Materials and Methods for Appendix figure 1.15, 1.16

Injections were performed on male C57Bl/6J-OlaHsd mice between postnatal week 8 and 12. Preparation for surgery, drug administration and recovery procedure was repeated as described in detail in the main Materials and Methods subsection 2.4.1.

Retrograde and anterograde tracing experiments

Tracing experiments were performed using stereotaxic coordinates (Paxinos and Franklin) through a small craniotomy (~1.2mm) on the left hemisphere. Viruses or dyes were injected using a Nanoject system (Nanokect II autonanoliter injector, Drummond Scientific), through a glass pipette with a broken tip, backfilled with mineral oil. For injection in the infralimbic area of mPFC the coordinates were as follow: 1.9 mm posterior to bregma, 0.35 mm lateral, 1.9 mm below the pia surface, with a 0° angle. For injection in the PPC: 2 mm anterior to bregma, 1.7 mm lateral, 300 µm below the pia surface at a 0° or 30° angle. For retrograde tracing 96.6 nL of Fast Blue (~0.5-1% in ddH_20; Polysciences) were delivered at a rate of 30 nL/min. For anterograde tracing AAV2-hSyn-hChR2(H134R)-mCherry (~10^{12} IU/µL; UNC, Vector Core, Chapel Hill, NC) or AAV1/2-CAG-GFP (~10^{7}-10^{10} IU/µL; plasmid from UNC; virus constructed by Edinburgh Vector Core, Edinburgh, UK) were injected. Viral injections were typically 202.4 nL but in some cases varied ± 50 nL. Skin was sutured and sealed, and mice were placed in a clean holding cage positioned over a heating pad and monitored until they recovered from anaesthesia, before returning to their home cage. Further experiments started at 1-5 weeks following injections.

Electrophysiology

Four to five weeks following virus injection 400 µm coronal brain slices were prepared and whole cell patch-clamp recordings were performed from neurons in layers 2/3 of the PPC. Slices were cut at ice cold cutting aCSF (c-aCSF) solution with the following composition (in mM): NaCl 86, NaH_2PO_4 1.2, KCl 2.5, $NaHCO_3$ 25, glucose 25, sucrose 75, $CaCl_2$ 0.5, $MgCl_2$ 7. For recording extracellular aCSF (n-aCSF) was made of (in mM): NaCl 124, NaH_2PO_4 1.2, KCl 2.5, $NaHCO_3$ 25, glucose 20, $CaCl_2$ 2, $MgCl_2$ 1. Maintenance solution substituted of 50% c-aCSF and 50% n-aCSF.

Intracellular solution had the following composition in mM: K gluconate 130; NaCl 8.5, HEPES 5, EGTA 0.5, Na_2GTP 0.3, MgATP 4, biocytin 3 mg/ml. All recordings took place at 37 ± 2°C.

Recordings used Multiclamp or AxoClamp amplifiers (Molecular Devices) and data were sampled at 20 kHz and digitized using a Digidata 1320A (Molecular Devices). ChR2 was activated by 470nm light (irradiance ~140mW/mm^2) through an LED (ThorLABS) attached to the epifluorescence port of the microscope as previously described by Golzalez-Sulser *et al* (2014). In the presented figures, light stimuli had a duration of 10 ms, and repeated at 5, 10, 20 and 50 Hz for ten sweeps each in voltage clamp and 10 sweeps at current clamp. Series resistance compensation was applied in voltage-clamp and was ≤30 MΩ. Where CNQX (20 μM; Abcam) was used, it was applied to the standard extracellular solution for 5 min before repeating ChR2 activation, subsequently washed off for 15 min and repeating ChR2 activation in n-aCSF. Cells were initially separated in pyramidal and fast-spiking based on afterhyperpolarization (AHP) of ≥10 mV, then confirmed anatomically following streptavidin conjugation and PV immunohistochemistry.

Table1

Nucleotide change	Protein change	Mutation type	Inheritance	Domain	Diagnosis	References
c.283dup	p.His95Profs*5	FRAMESHIFT	mosaic in father	PH	Moderate ID, epilepsy	Berryer et al. (2013)
c.321_324del	p.Lys108Valfs*25	FRAMESHIFT	*de novo*	PH	Moderate to severe ID, microcephaly, epilepsy	Hamdan el al. (2011), Carvill et al. (2013)
c.333del	p.Lys114Serfs*20	FRAMESHIFT	*de novo*	PH	Epileptic encephalopathy, moderate ID	O'Roak et al. (2014)
c.348C>A	p.Tyr116*	NONSENSE	*de novo*	PH	Severe ID, ASD, epilepsy	von Stülpnagel (2015), Mignot et al. (2016)
c.387+1G>C		SPLICE_SITE	*de novo*	PH	Severe ID, epilepsy	DECIPHER (ID290491)
c.389–2A>T		SPLICE SITE	*de novo*	PH	Epileptic encephalopathy, severe ID, ASD	Carvill et al. (2013)
c.403C>T	p.Arg135*	NONSENSE	*de novo*	PH	Mild ID, ASD	Mignot et al. (2016)
c.412A>T	p.Lys138*	NONSENSE	*de novo*	PH	Moderate to severe ID, mild epilepsy	Hamdan et al. (2009)
c.427C>T	p.Arg143*	NONSENSE	*de novo*	PH	Epileptic encephalopathy, severe ID, ASD	Carvill et al. (2013), Mignot et al. (2016)
c.431_434del	p.Thr144Serfs*29	FRAMESHIFT	*de novo*	PH	Moderate ID, ASD	Parker et al. (2015), DECIPHER (ID259214)
c.439C>T	p.Gln147*	NONSENSE	*de novo*	PH	Moderate ID, ataxia	DECIPHER (ID319514)
c.455_459del	p.Arg152Glnfs*14	FRAMESHIFT	*de novo*	PH	Severe ID, ASD	Mignot et al. (2016)
c.490C>T	p.Arg164*	NONSENSE	*de novo*	PH	Severe ID, ASD	Mignot et al. (2016)
c.509G>A	p.Arg170Gln	MISSENSE	*de novo*	PH	Moderate ID, ASD	Parker et al. (2015), DECIPHER (ID259840)
c.509+1 G>T		SPLICE_SITE	*de novo*	PH	Severe ID, ASD	Mignot et al. (2016)
c.510–1G>A		SPLICE_SITE	*de novo*	PH	Moderate to severe ID, epilepsy	de Ligt et al. (2012)
c.698G>A	p.Cys233Tyr	MISSENSE	*de novo*	PH		O'Roak et al.(2014)
c.800G>A	p.Trp267*	NONSENSE	*de novo*	C2	Epileptic encephalopathy, severe ID, ASD	Carvill et al. (2013)
c.828dup	p.Lys277Glnfs*7	FRAMESHIFT	Parents not tested	C2	Mild to moderate ID, ASD	Mignot (2016)
c.980T>C	p.Leu327Pro	MISSENSE	*de novo*	C2	Severe ID, ASD, ataxia	Parker et al. (2015)
c.1043_1044del	p.Val348Alafs*70	FRAMESHIFT	*de novo*	C2	Moderate to severe ID	Vissers et al. (2010)
c.1057del	p.Leu353Trpfs*13	FRAMESHIFT	Parents not tested	C2	Moderate ID, ataxia	Mignot et al. (2016)

c.1084T>A	p.Trp362Arg	MISSENSE	*de novo*	C2	Moderate ID, epilepsy, ASD	Berryer et al. (2013)
c.1253_1254del	Lys418Argfs*54	FRAMESHIFT	*de novo*	GAP	Severe ID	Rauch et al. (2012), Mignot et al. (2016)
c.1552_1555del	p.Tyr518Asnfs*8	FRAMESHIFT	*de novo*	GAP	Moderate ID	Parker et al. (2015), DECIPHER (ID259041)
c.1630C>T	p.Arg544*	NONSENSE	*de novo*	GAP	Severe ID, no other tests due to age	Mignot et al. (2016)
c.1648G>C	p.Ala550Pro	MISSENSE	*de novo*	GAP		DECIPHER (ID328457)
c.1652T>C	p.Leu551Pro	MISSENSE	*de novo*	GAP	Severe ID	DECIPHER (ID282601)
c.1685C>T	p.Pro562Leu	MISSENSE	*de novo*	GAP	Moderate ID, ASD	Berryer et al. (2013), Mignot (2016)
c.1735C>T	p.Arg579*	NONSENSE	*de novo*	GAP	Moderate to severe ID, mild epilepsy	Hamdan et al. (2009)
c.1782del	p.Leu595Cysfs*55	FRAMESHIFT	*de novo*	GAP	Moderate ID, ASD, epilepsy	O'Roak et al. (2014), DECIPHER (ID263788)
c.1823_1824del	p.Phe608Trpfs*9	FRAMESHIFT	*de novo*	GAP		O'Roak et al. (2014)
c.1922C>A	p.Ser641*	NONSENSE	*de novo*	GAP	Severe ID	DECIPHER (ID285402)
c.1995T>A	p.Tyr665*	NONSENSE	Parents not tested	GAP	Severe ID	Mignot et al. (2016)
c.2104C>T	p.Gln702*	NONSENSE	*de novo*	GAP	Epileptic encephalopathy, moderate ID	Carvill et al. (2013)
c.2184del	p.Asn729Thrfs*31	FRAMESHIFT	*de novo*	GAP	Moderate to severe ID, epilepsy, ASD	Berryer et al. (2013), Dyment et al. (2014)
c.2212_2213del	p.Ser738*	NONSENSE	*de novo*		Moderate ID	Berryer et al. (2013)
c.2214_2217del	p.Glu739Glyfs*20	FRAMESHIFT	*de novo*		Mild ID, ASD	Mignot et al. (2016)
c.2294+1G>A		SPLICE_SITE	*de novo*		Moderate to severe ID, ASD	Hamdan et al. (2011)
	p.Tyr805	NONSENSE	*de novo*		Severe ID, Lennox-Gestaut syndrome	Carvill et al. (2013)
c.2438del	p.Leu813Argfs*23	FRAMESHIFT	*de novo*		Moderate to severe ID	Hamdan et al. (2009)
c.2630dup	Thr878Aspfs*60	FRAMESHIFT	*de novo*		Severe ID	Rauch et al. (2012)
c.2677del	p.Gln893Argfs*184	FRAMESHIFT	*de novo*		Moderate to severe ID, microcephaly, epilepsy	Hamdan et al. (2011)
c.2764C>T	p.Arg922*	NONSENSE	*de novo*		Moderate ID, ASD	Parker et al. (2015), DECIPHER (264135)
c.2774del	p.Leu925Profs*152	FRAMESHIFT	*de novo*		Moderate ID, ASD	Parker et al. (2015)

c.2782C>T	p.Gln928*	NONSENSE	*de novo*		Moderate ID	Parker et al. (2015), DECIPHER (ID258913)
c.2933del	p.Pro978Hisfs*99	FRAMESHIFT	*de novo*		Moderate ID, ataxia	Mignot et al. (2016)
ACAGT>A	p.Val1078Alafs*51	FRAMESHIFT	*de novo*		Moderate ID, ASD	DECIPHER (ID273439)
C>T	p.Gln1082*	NONSENSE	*de novo*		Moderate ID, ASD, epilepsy	DECIPHER (ID300389)
AC>A	p.Arg1085Glyfs*45	FRAMESHIFT	*de novo*		Severe ID, ataxia	DECIPHER (ID271605)
c.3277C>T	p.Q1079*/p.Gln1093*(?)	NONSENSE	*de novo*		Moderate ID	Parker et al. (2015), DECIPHER (ID258536)
c.3406dup	p.Gln1136Profs*17	FRAMESHIFT	Parents not tested		Severe ID, ASD	Mignot et al. (2016)
c.3408+1G>A		SPLICE_SITE	*de novo*		Severe ID, ASD	Mignot et al. (2016)
A>AA	p.Ile1168Asnfs*22	FRAMESHIFT	Unknown het			DECIPHER (ID339981)
c.3583-1		SPLICE_SITE	unknown			Xu et al. (2012)
c.3583-6G>A		SPLICE SITE	*de novo*			Redin et al. (2014)

Table 1. Summarizes published pathogenic mutations found in individuals with presumed causative mutations in *SYNGAP1*. Domains mentioned: Pleckstrin homology (PH), Protein kinase C conserved (C2), RasGAP (GAP). Positions of domains were defined through Ensembl genome browser (Yates *et al*., 2015; Aken *et al*., 2016). Table does not include (*de novo* or inherited) copy number variation (CNV) deletions or translocation in this gene. *ID,* Intellectual Disability; *ASD*, Autism Spectrum Disorders.

Nucleotide change	P-values (t-test)	Benjamini-Hochberg significance	Benjamini-Hochberg p-value
NAc Core	0.0081	significant	0.0486
mPFC (ILA)	0.3243	not significant	0.9362
vHC	0.6281	not significant	0.9362
mHC	0.7699	not significant	0.9362
BLA	0.8936	not significant	0.9362
NAc Shell	0.9362	not significant	0.9362

Table 2. B-H statistical overview for cFos experiments. Acquired p-values were then analysed to control for false discovery rate (FDR) with the Benjamini-Hochberg procedure. FDR was set to 0.25. Column 3 indicates that the p-value is significant at the FDR chosen. B-H p-value can also be calculated, as seen in column 4. *NAc*, nucleus accumbens; *mPFC* (*ILA)*, infralimbic region of the medial prefrontal cortex; *vHC*, ventral hippocampus; *mHC*, medial hippocampus; *BLA*, basolateral amygdala

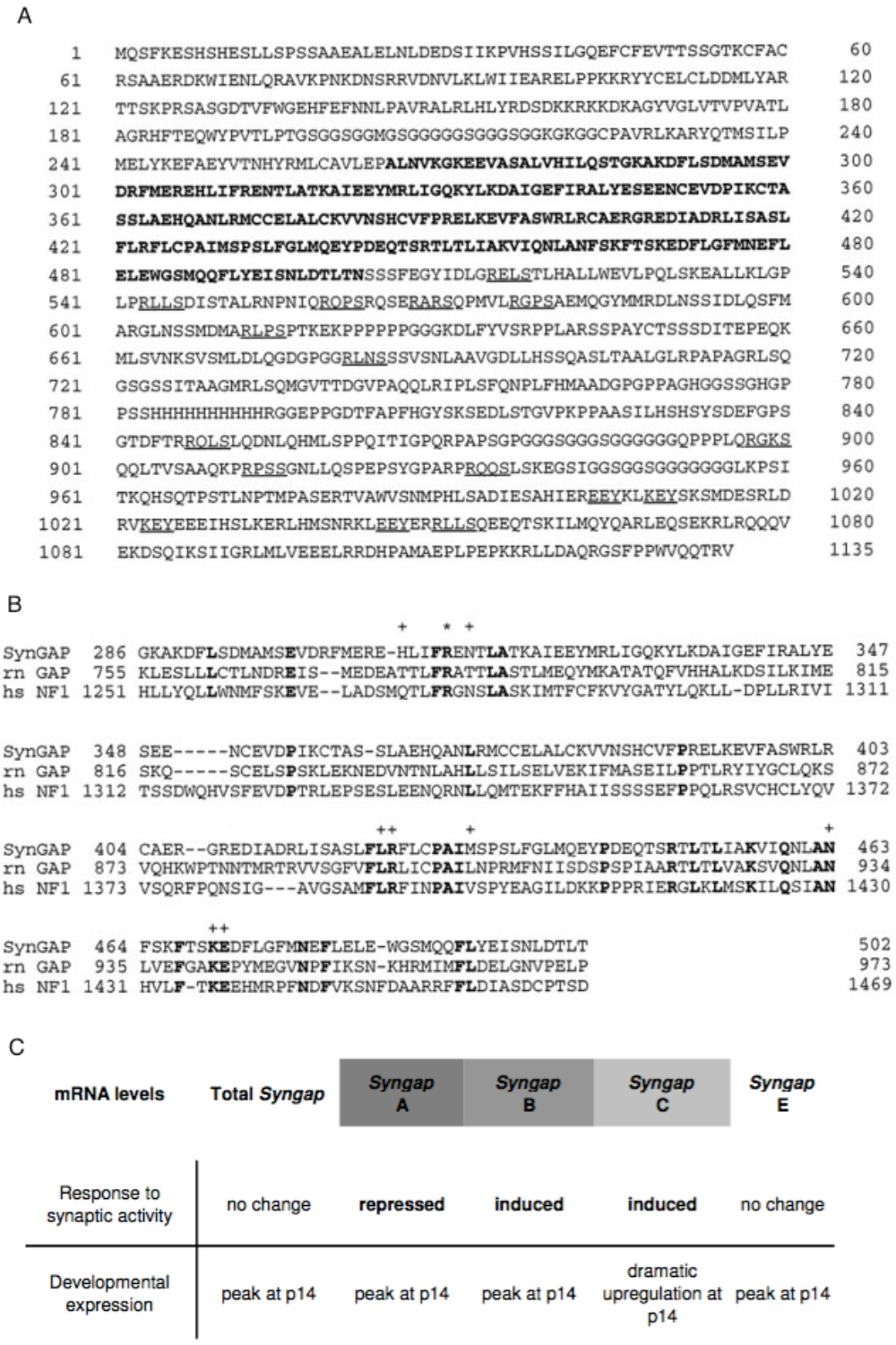

Figure 1.1 Structure of SynGAP and isoforms. (A) Amino acid sequence; SynGAP is a 1135 amino acid protein with a RasGAP (bold) and serine and tyrosine phosphorylation sites (underlined). (B) Alignment of the RasGAP domain with *Rattus norvegicus* (rn GAP) and *Homo sapiens* (hs NF1). Identical residues in bold. Residues in interactions with Ras (+). (C) Overview of SynGAP variants differentially regulated in response to synaptic activity and during development. Figure adjusted: (A, B) from Kim *et al*., 1998; (C) from McMahon *et al*., 2012.

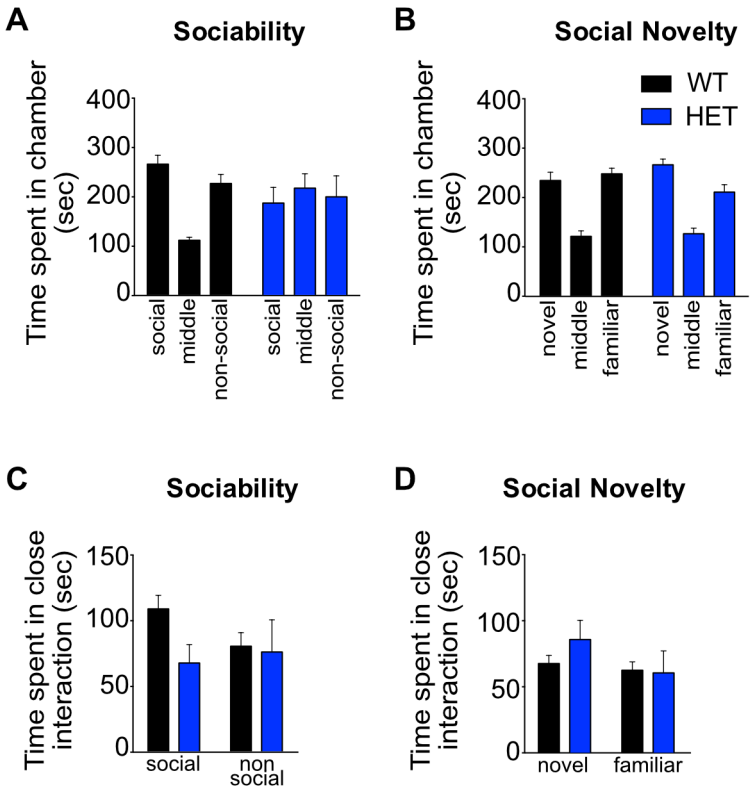

Figure 1.2 Both WT and SynGAP HET mice don't show preference for social novelty when using littermate strangers for the task. (A) WT mice (n=10) spent more time in the social and non-social chamber, whereas SynGAP HET mice (n=10) spent equal time in all three chambers. (B) During the second phase of the task, both WT and HET mice spend more time in the social chambers. (C) WT mice show a slight preference for the social (with stranger1) over the non-social chamber, when scoring the time in close interaction (sniffing). However, in phase two, neither the WT nor the HET mice discriminate the novel stranger mouse (stranger2), which was a littermate of the stranger mouse used in phase 1 (D).

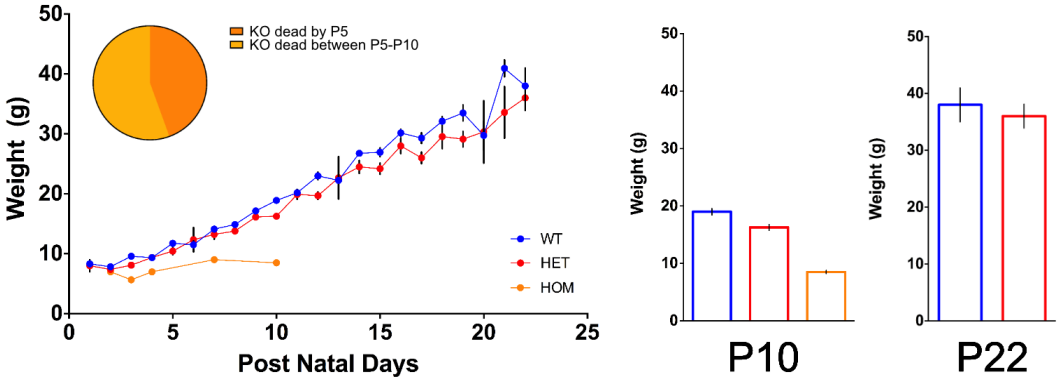

Figure 1.3 Rats homozygous (KO) for GAP deletion in SynGAP die by postnatal day10. *Syngap* KO pups, are much smaller in size, show no gross anatomical abnormalities but all die by P10, indicating that the full GAP domain of SynGAP in essential for postnatal viability. Bodyweight of *Syngap* HET rats is reduced at P10, but comparable to WT littermates by P22. Data collected by Dr. Lindsay Mizen.

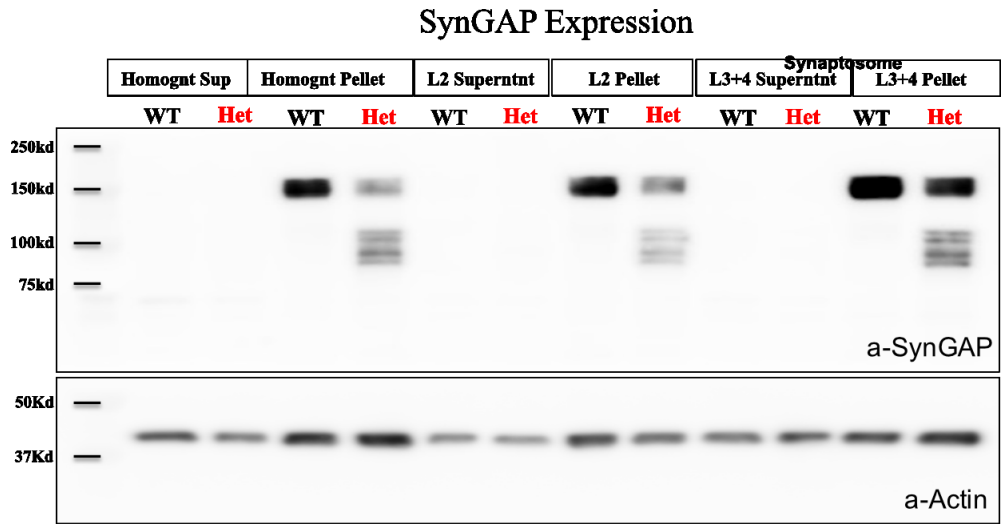

Figure 1.4 Reduction of SynGAP expression in hippocampal homogenates and synaptosomes in *Syngap* HET rats. Western blot analysis of extracts from rat hippocampal brain homogenates. Only a single band of SynGAP protein is detected at the epected size (~150kDa) in both homogenates and synaptosomes (L3+4 pellet) from WT animals. Syngap HET rats a corresponding SynGAP band was detected along with several other bands of lower molecular weight. Synaptosomes were isolated through Percoll gradient centrifugation. Experiments performed by Dr. Sarfaraz Nawaz.

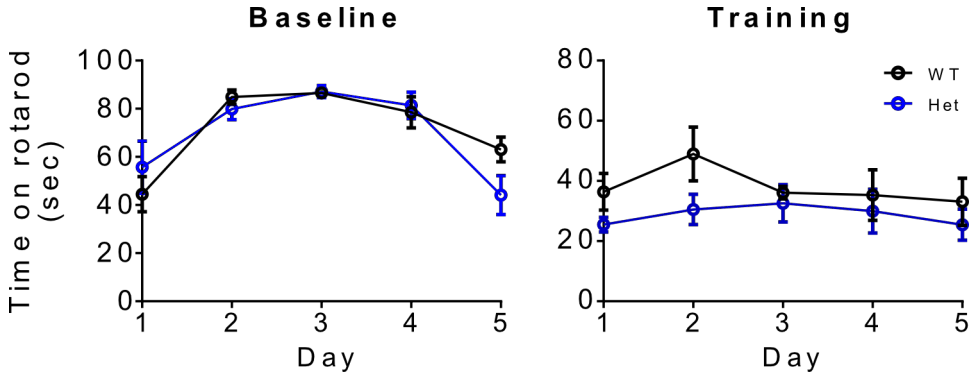

Figure 1.5 ***Syngap*** **HET rats display unaffected motor learning.** Unaffected motor learning on the rotarod apparatus, as measured by latency to fall during baseline conditions and during training over 5 consecutive days. Experiments performed by Natasha Anstey.

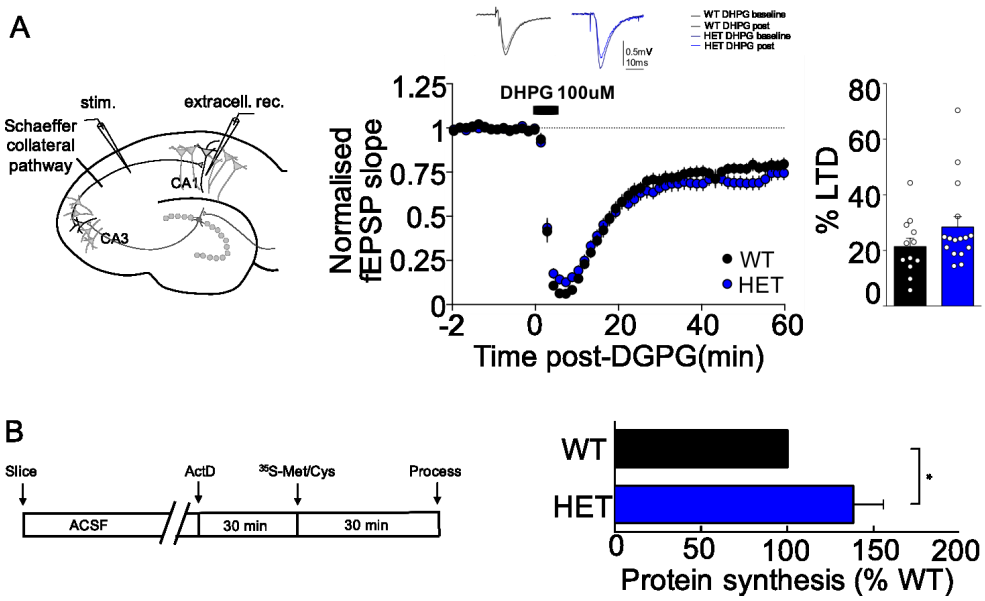

Figure 1.6 Partial deletion of the GAP domain of SynGAP in rats does not fully recapitulate findings in *Syngap* HET mice. (A) On left, diagram of experimental setup. On right, Average fEPSP plots for WT and *Syngap* HET slices normalised to pre-DHPG baseline reveal that the magnitude of DHPG-induced LTD was not different between genotypes. Experiments performed by Dr. Adam Jackson. (B) On left, schematic of experimental timeline for ^{35}[S]-Met/Cys metabolic labeling. On right, excessive levels of basal protein synthesis in dorsal hippocampal slices from *Syngap* HET rats compared to WT. Experiments performed by Shinjini Basu.

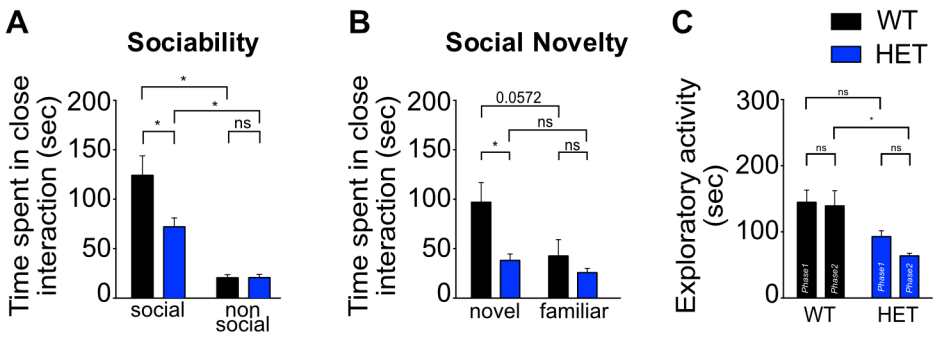

Figure 1.7 Naïve adult SynGAP HET rats don't show preference for social novelty when tested in a 3- chamber task. (A) Both WT (n=6) and HET (n=6) rats showed preference for the social chamber, containing a stranger rat (stranger1) versus the non-social chamber (2-way *ANOVA* $F_{(1,10)}$=4.860, p=0.0520; chamber $F_{(1,10)}$=42.87, p<0.0001; genotype $F_{(1,10)}$=6.443, p=0.0294). (B) But only WT rats showed preference for the novel rat (stranger2) during the second phase of the task (2-way *ANOVA* $F_{(1,10)}$=1.951, p=0.1927; chamber $F_{(1,10)}$=4.912, p=0.0510; genotype $F_{(1,24)}$=10.42, p=0.0091). (C) Again, adult naïve HET rats presented with decreased sum exploratory activity during the 3- chamber task (2-way *ANOVA* $F_{(1,10)}$=0.8241, p=0.3853; session $F_{(1,10)}$=1.748, p=0.2155; genotype $F_{(1,10)}$=13.01, p=0.0048). All *ANOVAs* Bonferroni corrected. Data collected with the help of Natasha Anstey.

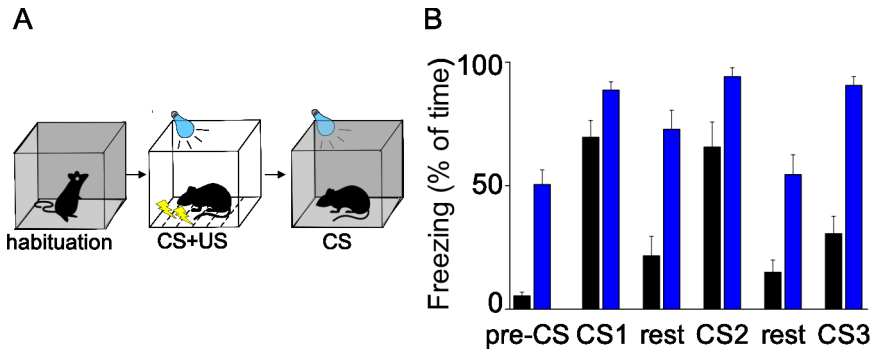

Figure 1.8 ***Syngap*** **HET rats display impaired recall of fear association.** (A) Cued-fear conditioning paradigm in Long-Evans rats. (B) HET rats display generalised fear in pre-CS, increased freezing responses during CS presentations (CS1-CS3) and rest periods (rest1-rest2). Experiments performed by Dr. Sally Till.

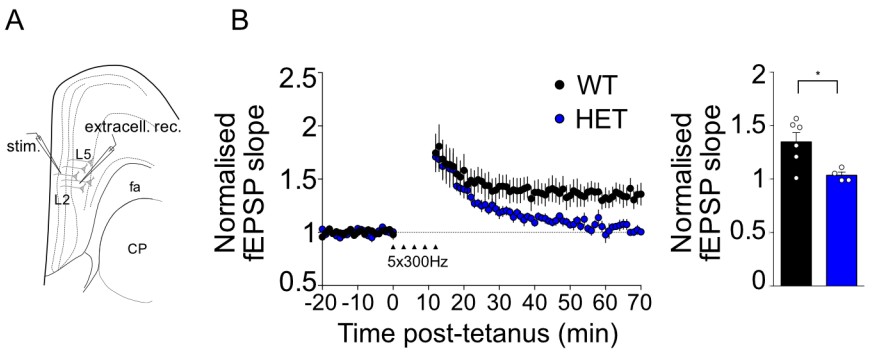

Figure 1.9 ***Syngap*** **HET rats show reduced mPFC long-term potentiation (LTP).** (A) Diagram of experimental setup. (B) Average fEPSP plots for WT and *Syngap* HET rats normalised to pre-tetanus baseline reveal that high- frequency stimulation did not induce LTP in HET rats. Experiments performed by Dr. Adam Jackson.

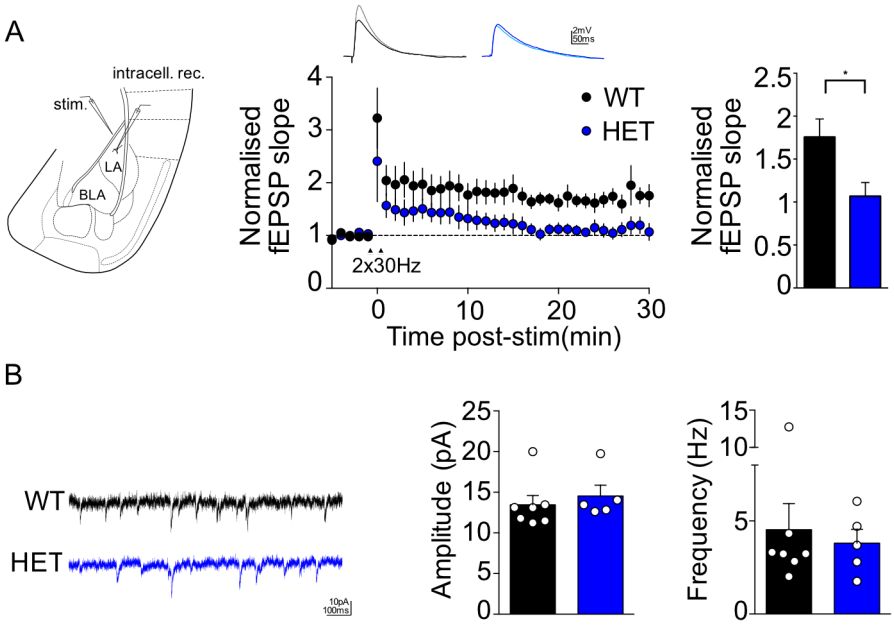

Figure 1.10 Partial loss of the GAP domain in SynGAP impairs synaptic plasticity, in the lateral amygdala of rats. (A) On left, diagram of experimental setup. On right, average fEPSP plots for WT and *Syngap* HET rats normalised to pre-stim baseline reveal that low-frequency stimulation did not induce LTP in HET rats. (B) mEPSC amplitude and frequency remains unchanged in *Syngap* HET rats. Experiments performed by Anna Toft.

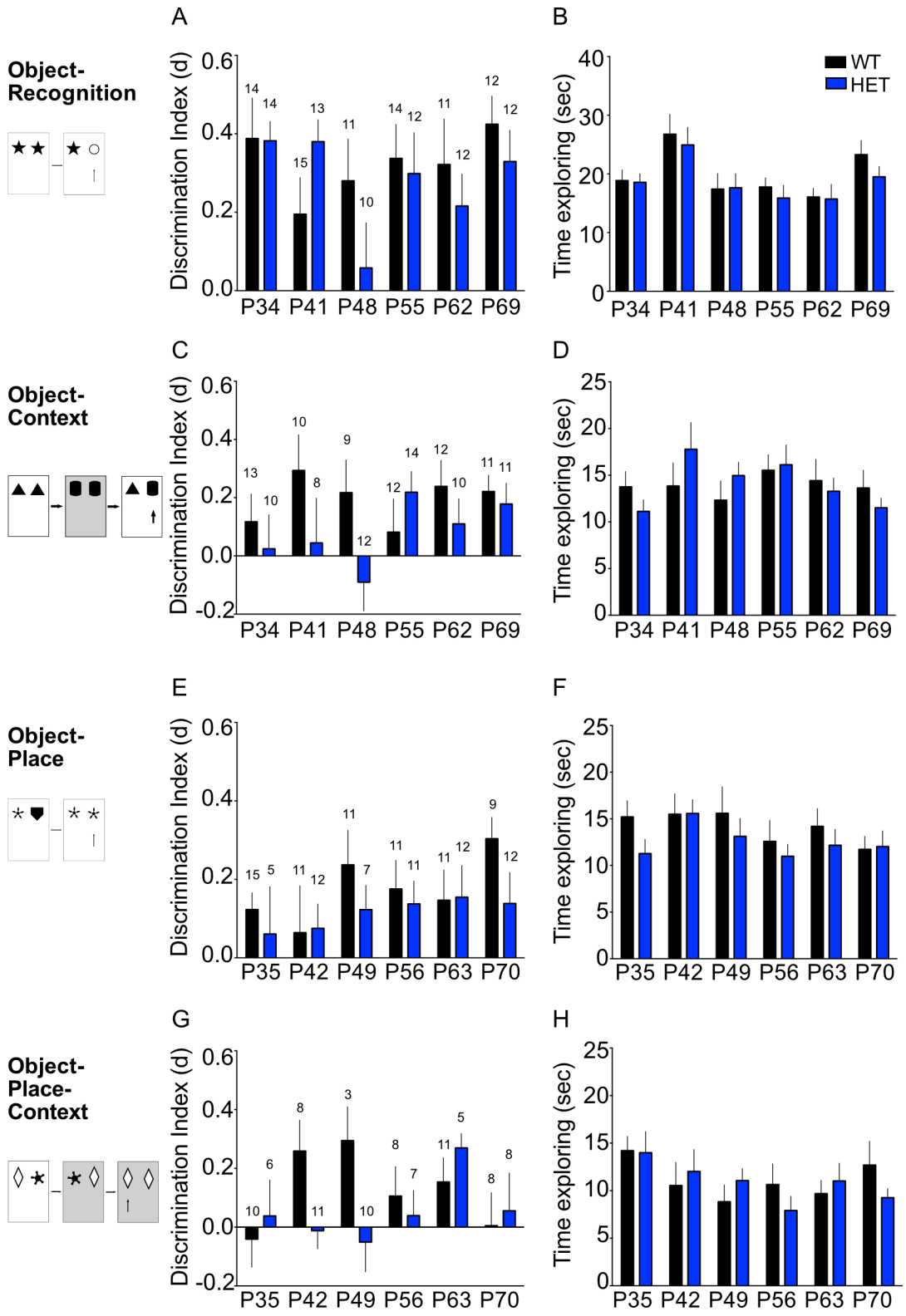

Figure 1.11 Developmental trajectory of spontaneous exploration tasks in *Syngap* HET rats. (A) Development of novel object recognition preference from P34 to adulthood and corresponding sum of exploratory activity of all rats during the test phase the task (B). (C, D) Same for object-context recognition, (E, F) object-place recognition and (G, H) object-place-context recognition. Some rats have been excluded based on criterion set for exploration. Number over each graph indicates the number of animals plotted.

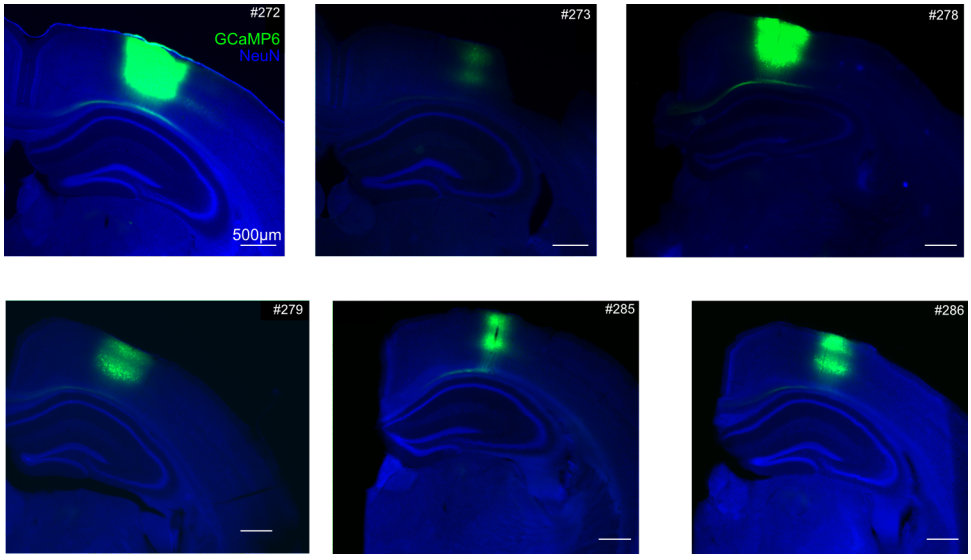

Figure 1.12 GCaMP6s injections in PPC. Injection sites in *Syngap* HET and WT control animals that were used for the dataset presented in subchapter 4.2.1, 4.2.2 and 4.2.3. Low magnification epifluorescence image of 40µm thick coronal sections of brains post-two-photon imaging with a GCaMP6s injection at the PPC; GCaMP6s in green, NeuN in blue, overlaid. Scale bar, 500µm. Number (#) indicates animal identification number.

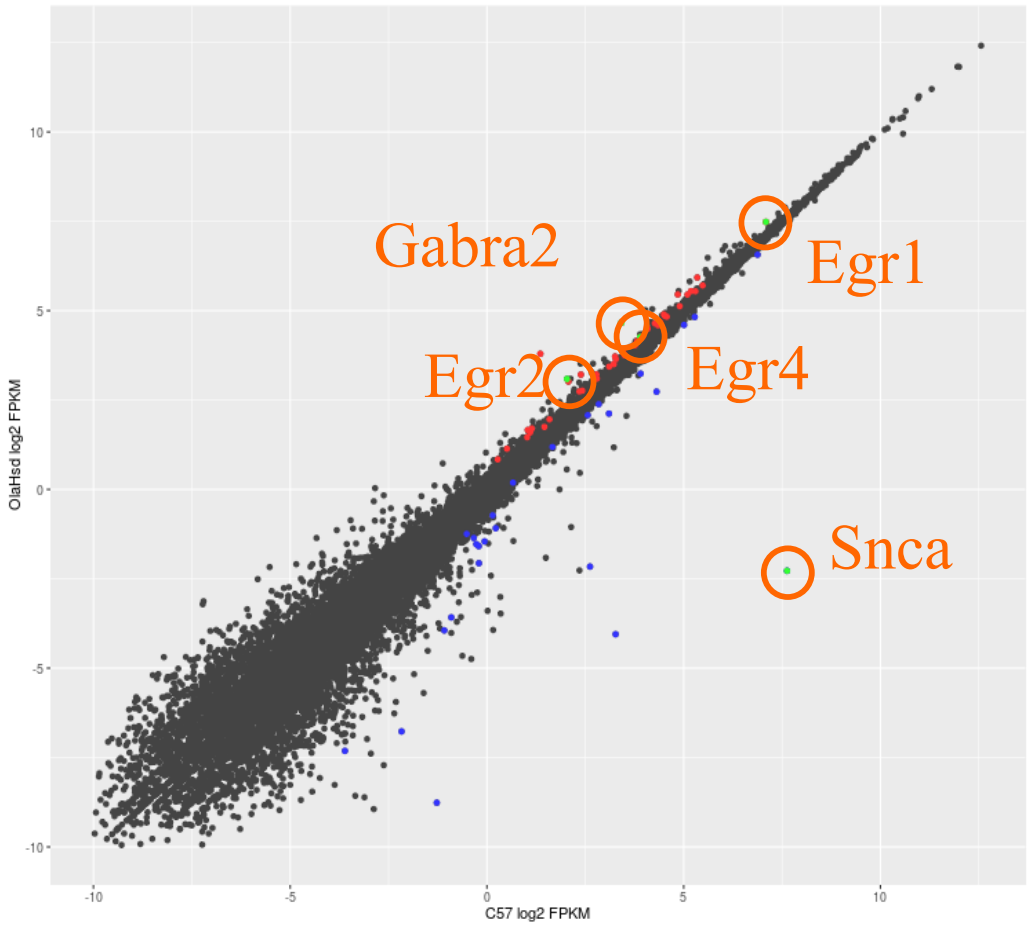

Figure 1.13 **Differential gene expression using RNA-seq.** Correlation beween RNA abundancies from visual cortex dissections of two different wild type background strains of adult mice (P76). Differential gene expression was analysed using the "DESeq" R package. Average log2 normalised counts. Blue, green and red points represent significant changes. *Gabra2*, Gamma-aminobutyric acid receptor subunit alpha-2, *Egr family*, Early growth response protein family, *Snca*, Alpha-synuclein. Dissections by Dr. Janelle Pakan and Danai Katsanevaki, processing by Shinjini Basu, Analysis performed by Dr. Owen Dando. *C57*, is C57Bl/6J (Jax) (Jax); *OlaHsd*, C57Bl/6J-OlaHsd (Ola).

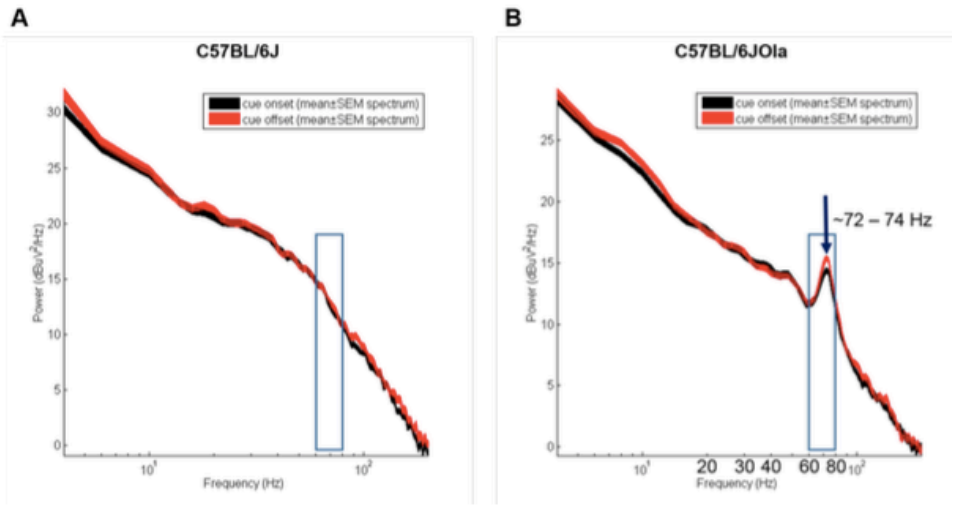

Figure 1.14 Example of mean gamma power distributions between substrains C57Bl/6J-OlaHsd (Ola) **and C57Bl/6J.** C57Bl/6J-OlaHsd (Ola) (Ola) mice presented with increased LFP with a noticeable frequency peak at 72-74 Hz, within the gamma range. VEP responses during the cue on-set and off-set phase are indicated in box. *C57Bl/6JOla*, Ola; *C57Bl/6J*, Jax. Adjusted from Dr. Chih-Yuan Chiang (thesis).

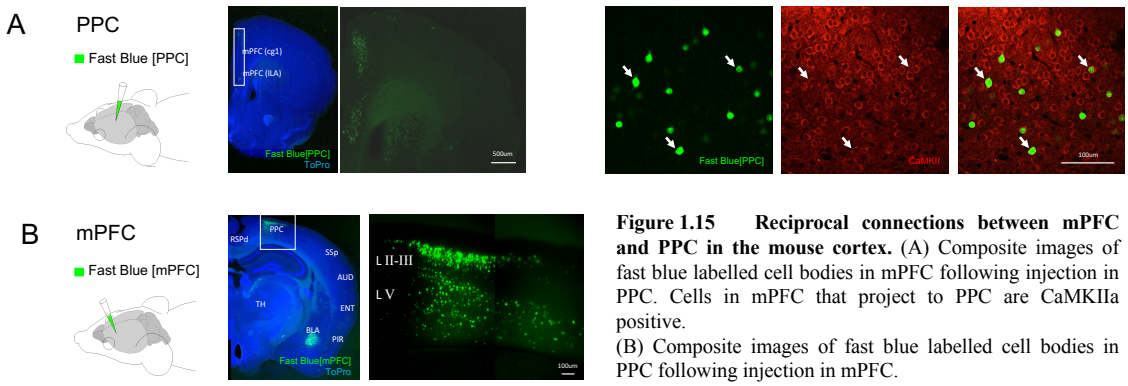

Figure 1.15 Reciprocal connections between mPFC and PPC in the mouse cortex. (A) Composite images of fast blue labelled cell bodies in mPFC following injection in PPC. Cells in mPFC that project to PPC are CaMKIIa positive.
(B) Composite images of fast blue labelled cell bodies in PPC following injection in mPFC.

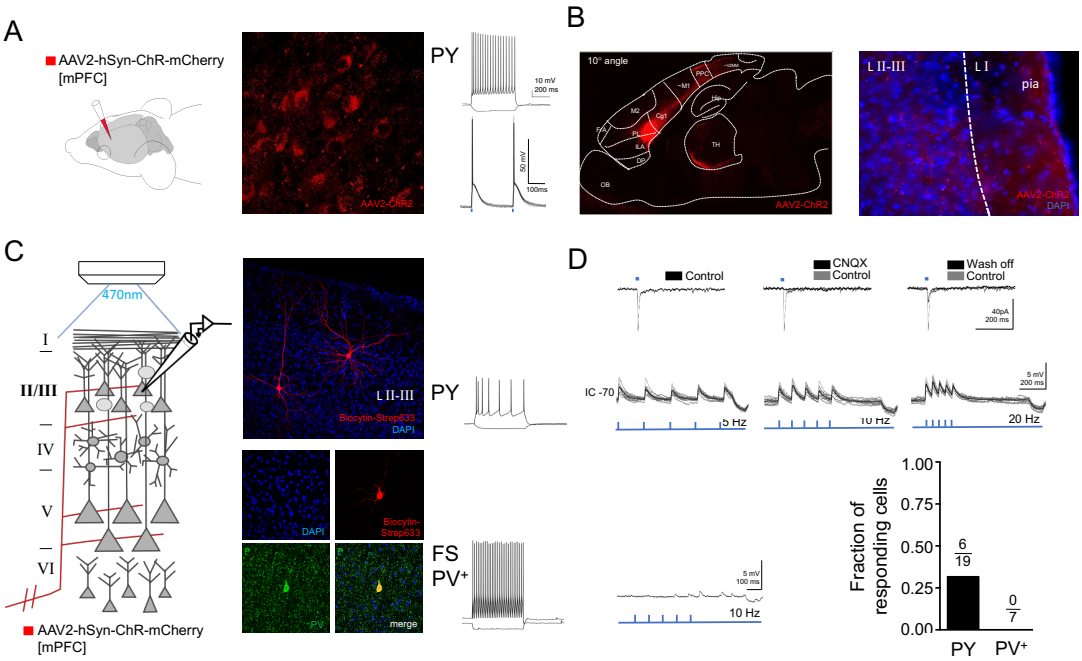

Figure 1.16 Axonal projections from mPFC target PY neurons in layer 2/3 PPC. (A) AAV-ChR2 expression in mPFC 4 weeks post-injection and example Aps elicited by photostimulation. (B) Composite images of ChR2+ axonal labelling in PPC following injection to mPFC. (C, D) Responses to activation of mPFC fibers in neurons of PPC. (D) Examples of light-induced EPSCs with and without CNQX. Example of EPSPs in pyramidal and FS interneurons (PV+). Connectivity probability was calculated at 31.6% (6/19 cells) for PY neurons.

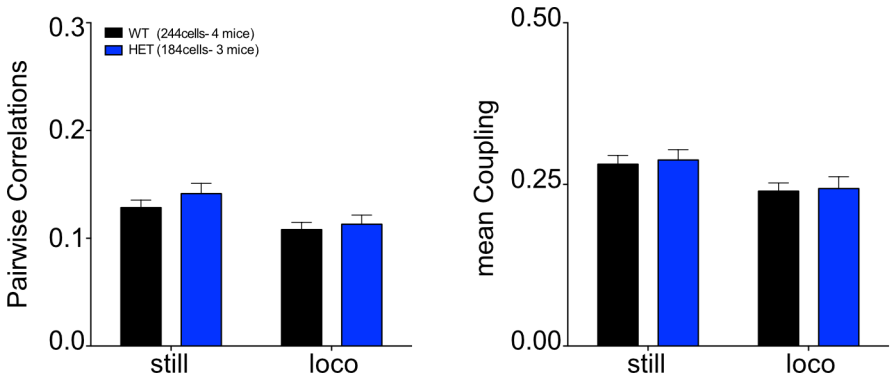

Figure 1.17 Pairwise correlations and coupling of *Syngap* HET mice. Left; Mean pairwise correlation values of downsampled calcium transients ($\Delta f/f_0$) recorded in awake behaving mice during darkness for all cell pairs of both genotypes during still and locomotion periods. Right; Mean coupling values of all cells of WT and HET neurons measured during baseline activity in the darkness. Corresponds to data from subchapter 4.2.1, 4.2.2 and 4.2.3. *mean* ± SE is noted.

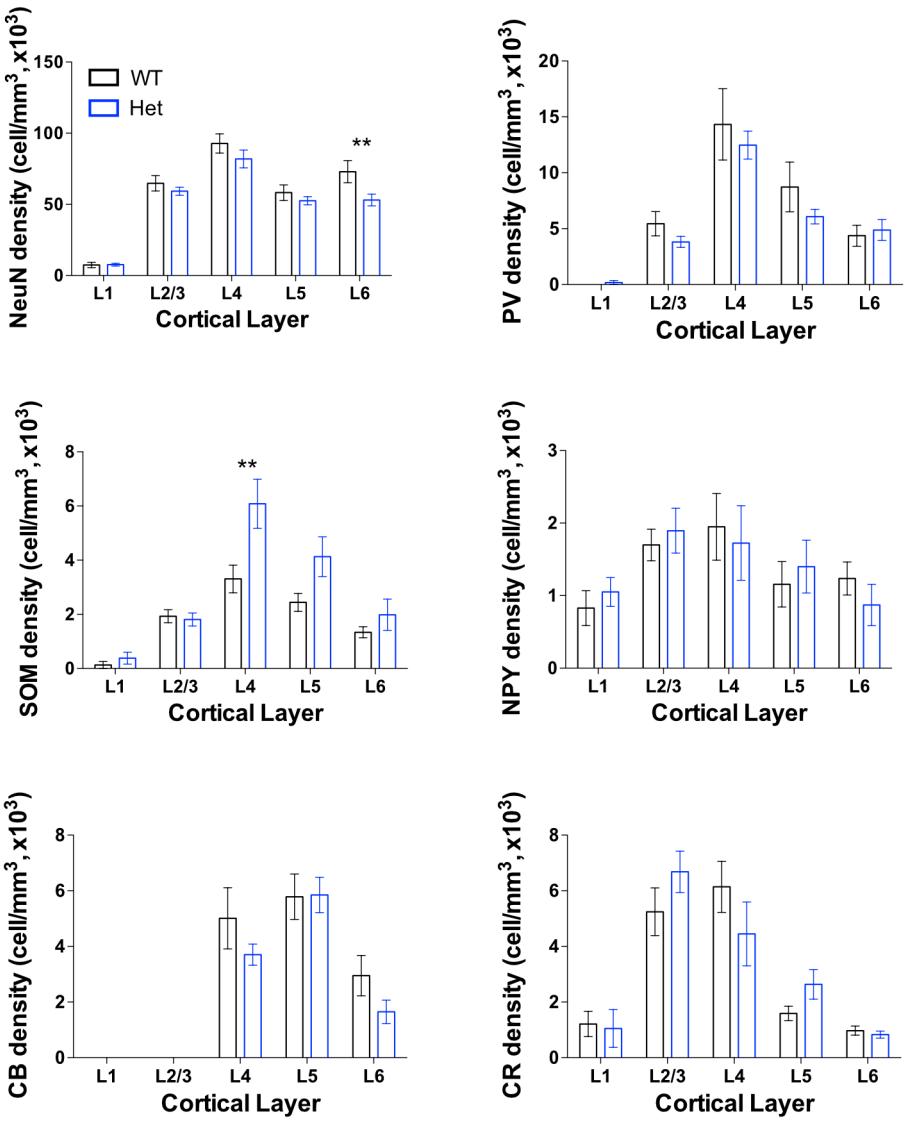

Figure 1.18 Interneuron quantification for cortical layer of binocular V1. Density of NeuN, and density of PV, SOM, NPY, CB, CR interneuron markers normalised to NeuN density. *PV*, Parvalbumin; *SOM*, Somatostatin, *NPY*, Neuropeptide Y; *CB*, Calbindin; *CR*, Calretinin. Experiments performed by Dr. Sam Booker. $p<0.05$; 2-way *ANOVA*.

Appendix 2

Statistical approach

Appendix2 refers to the statistical approach towards analyzing two-photon calcium imaging data (directly related to Subchapters 4.2.3-4.2.9).

No statistical test was used to prospectively calculate sample sizes before experiments began. Calculation of power at the start of the project would have been ideal, however in two-photon imaging experiments with variables including animals, fields of view, number of cells, and experimental conditions (i.e. if animal is running on wheel and for how long to acquire usable locomotion data), expected effect sizes are difficult to estimate *a priori*. My data is undoubtedly underpowered at the current stage of this study; based on previous work from Pakan *et al* (2016) or Goncalvez *et al* (2013), my sample size has not reached adequate number. However, as results in Chapter 4 are part of an ongoing project, my effort was to analyze and comprehensively report them while acknowledging the limitations of current work.

As such, comparisons between genotypes were attempted with the use of mixed model analyses implemented using custom-written R code by our bioinformatician Dr. Owen Dando. Outlier analysis, most commonly used in two-photon imaging published studies, were not performed in my dataset; we strongly believe that given the nature of the variability of the experiments, anomaly detection on the basis of thresholding 3σ from the mean is arbitrary unless there is a biological reason for exclusion of cell/animal activity.

For analyzing mean fluorescence changes ($\Delta f/f_0$) we first fitted log-transformed data to probability-probability plots (p-p) to investigate which distribution best fits the data by examining how close the cumulative distribution of my data is to the particular theoretical cumulative distribution function, i.e. how close the points are to the straight line. Next, we calculated 'goodness-of-fit' statistics for my data fitted to the various distributions using Akaike's Information Criterion (AIC) and Bayesian Information Criterion (BIC), where lower numbers generally indicate a better fit. Following this analysis, we proceeded by fitting models using the two distributions my data best fits to.

We fitted a series of linear mixed models using the log-transformed data with three random effects: animal, ROI (i.e. cell), and litter. To get p-values we compare models, calculating if sequentially adding fixed effects gives a better fit (given the additional explanatory variables):

- No fixed effects
- Movement (i.e. still→locomotion) main effect
- Genotype main effect
- Movement and genotype main effect
- Movement and genotype main effects plus the interaction between the two

2.1 Calcium responses in PPC during darkness

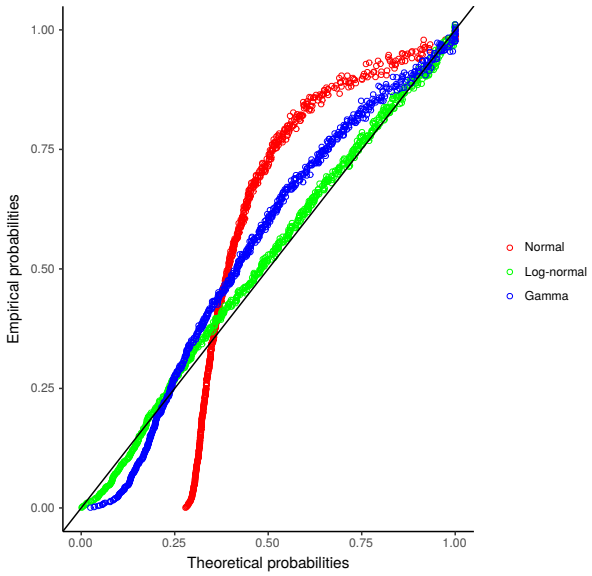

Figure 2.1 Goodness of fit for mean amplitude of calcium responses of neurons in PPC during darkness. Probability-probability (P-P) plot of the cumulative empirical values (experimental) in normal distribution, log-normal distribution, and gamma distribution against the theoretical cumulative distribution values. Closer the points to the straight line, indicates a better fit. Analysis by Dr. Owen Dando.

Calculating goodness-of-fit statistics:

```
## Goodness-of-fit criteria
##                                    norm      log-norm     gamma
## Akaike's Information Criterion   1264.879   -592.1635   -317.3748
## Bayesian Information Criterion   1274.383   -582.6589   -307.8702
```

Data fitting best a log-normal and a gamma distribution, so we proceed by fitting models using both.

2.1.1 Log-normal distribution (AIC= -592.1635)

Genotype main effect vs. no fixed effects (p=0.2083).

Movement main effect vs. no fixed effect (p<2.2e-16).

Genotype and movement main effects vs just movement (p=0.2083).

Genotype and movement main effects plus an interaction between the two vs just movement (p=0.3197).

Best fitting model by the log-normal LMM contains movement as fixed effect. However, modeling the data including genotype and the interaction between the allows us to calculate the sizes of the effects:

```
## Fixed effects:
##                                Estimate   Std. Error   t value
## (Intercept)                    -1.82915    0.15866    -11.529
## movement_typeloco               0.40824    0.04881      8.363
## genotypeHet                    -0.28675    0.24255     -1.182
## movement_typeloco:genotypeHet -0.06221    0.07445     -0.836
```

2.1.2 Gamma-distribution (AIC= -317.3748)

Genotype and movement main effects plus an interaction between the two vs just movement (p=0.06582).

```
## Fixed effects:
##                                 Estimate   Std. Error  t value   Pr(>|z|)
## (Intercept)                      -1.40270    0.22383   -6.267   3.68e-10 ***
## movement_typeloco                 0.36258    0.07792    4.653   3.27e-06 ***
## genotypeHet                      -0.45139    0.34200   -1.320   0.1869
## movement_typeloco:genotypeHet     0.25180    0.11854    2.124   0.0337*
```

2.2 Calcium responses in PPC during visual stimulation

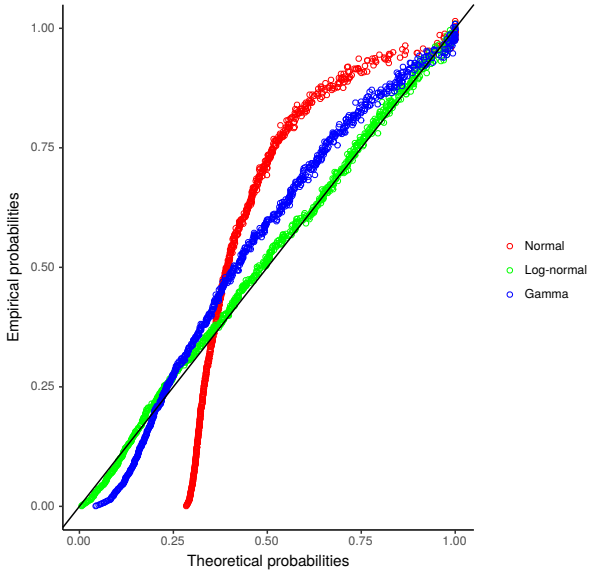

Figure 2.2 Goodness of fit for mean amplitude of calcium responses of neurons in PPC during visual stimulation. Probability-probability (P-P) plot of the cumulative empirical values (experimental) in normal distribution, log-normal distribution, and gamma distribution against the theoretical cumulative distribution values. Closer the points to the straight line, indicates a better fit. Analysis by Dr. Owen Dando.

Calculating goodness-of-fit statistics:

```
## Goodness-of-fit criteria
##                                   norm      log-norm    gamma
## Akaike's Information Criterion   1221.030   -643.6909   -375.8312
## Bayesian Information Criterion   1230.535   -634.1864   -366.3267
```

2.2.1 Log-normal distribution (AIC= -643.6909)

Genotype main effect vs. no fixed effects (p=0.4251).

Movement main effect vs. no fixed effect (p<2.2e-16).

Genotype and movement main effects vs just movement (p=0.4251).

Genotype and movement main effects plus an interaction between the two vs just movement (p=0.4447).

Best fitting model by the log-normal LMM contains movement as fixed effect. However, modeling the data including genotype and the interaction between the allows us to calculate the sizes of the effects:

```
## Fixed effects:
##                                Estimate   Std. Error   t value
## (Intercept)                    -1.91167    0.15736     -12.148
## movement_typeloco               0.39770    0.05419      7.338
## genotypeHet                    -0.23452    0.24057     -0.975
## movement_typeloco:genotypeHet   0.08206    0.08265      0.993
```

2.2.2 Gamma-distribution (AIC= -375.8312)

Genotype and movement main effects plus an interaction between the two vs just movement (p=0.009031).

```
Fixed effects:
##                                Estimate   Std. Error     t value    Pr(>|z|)
## (Intercept)                    -1.44095    0.20567       -7.006     2.45e-12 ***
## movement_typeloco              0.35619     0.08018       4.442      8.90e-06 ***
## genotypeHet                    -0.43668    0.31406       -1.390     0.16441
## movement_typeloco:genotypeHet   0.36091    0.12139       2.973      0.00295**
```

2.3 Calcium responses in wild type mice during darkness

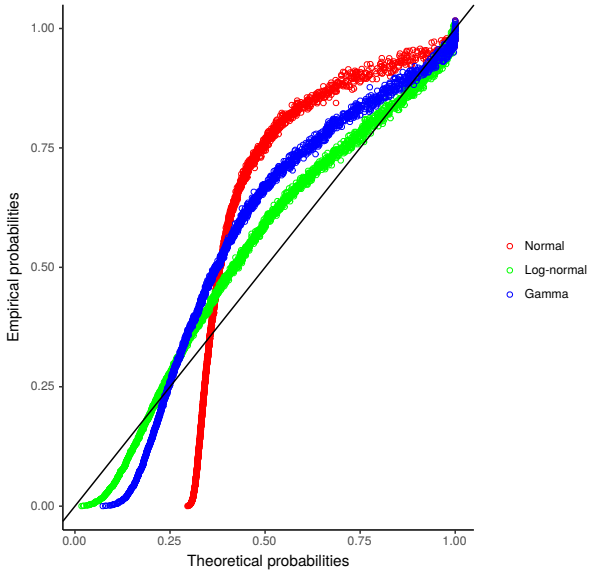

Figure 2.3 Goodness of fit for mean amplitude of calcium responses of wild type V1 dataset during darkness. Probability-probability (P-P) plot of the cumulative empirical values (experimental) in normal distribution, log-normal distribution, and gamma distribution against the theoretical cumulative distribution values. Closer the points to the straight line, indicates a better fit. Analysis by Dr. Owen Dando.

Calculating goodness-of-fit statistics:

```
## Goodness-of-fit criteria
##                                  norm      log-norm     gamma
## Akaike's Information Criterion   1689.092   -4102.108   -3019.523
## Bayesian Information Criterion   1700.716   -4090.484   -3007.899
```

2.3.1 Log-normal distribution (AIC= -4102.108)

Genotype main effect vs. no fixed effects (p=0.2551).

Movement main effect vs. no fixed effect (p<2.2e-16).

Genotype and movement main effects vs just movement (p=0.2551).

Genotype and movement main effects plus an interaction between the two vs just movement (p=<2.2e-16).

```
## Fixed effects:
##                                 Estimate Std. Error t value
## (Intercept)                     -2.36965    0.14480 -16.365
## movement_typeloco                0.23904    0.03182   7.513
## genotypeWTjax                   -0.05341    0.20517  -0.260
## movement_typeloco:genotypeWTjax  0.58578    0.04750  12.331
```

2.3.2 Gamma-distribution (AIC= -3019.523)

Genotype and movement main effects plus an interaction between the two vs just movement (p = 5.41e-13).

```
## Fixed effects:
##                                  Estimate   Std. Error  t value   Pr(>|z|)
## (Intercept)                     -2.09071    0.16158    -12.939    < 2e-16***
## movement_typeloco                0.48145    0.04602     10.463    < 2e-16***
## genotypeWTjax                   -0.08055    0.22895    -0.352     0.725
## movement_typeloco:genotypeWTjax  0.51520    0.06854     7.516     5.63e-4***
```

2.4 Calcium responses in wild type mice during visual stimulation with gratings

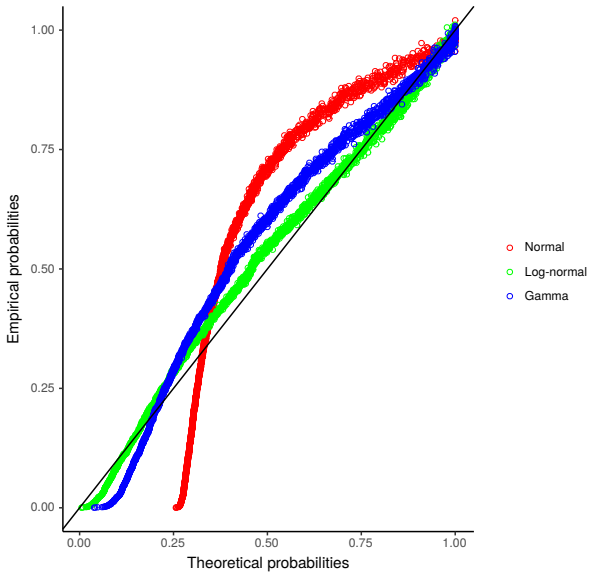

Figure 2.4 Goodness of fit for mean amplitude of calcium responses of wild type V1 dataset during presentation of gratings. Probability-probability (P-P) plot of the cumulative empirical values (experimental) in normal distribution, log-normal distribution, and gamma distribution against the theoretical cumulative distribution values. Closer the points to the straight line, indicates a better fit. Analysis by Dr. Owen Dando.

Calculating goodness-of-fit statistics:

```
## Goodness-of-fit criteria
##                                   norm      log-norm     gamma
## Akaike's Information Criterion   2014.246   -2580.652   -1893.076
## Bayesian Information Criterion   2025.870   -2569.028   -1881.452
```

2.4.1 Log-normal distribution (AIC= -2580.652)

Genotype main effect vs. no fixed effects (p=0.3498).

Movement main effect vs. no fixed effect (p<2.2e-16).

Genotype and movement main effects vs just movement (p=0.3498).

Genotype and movement main effects plus an interaction between the two vs just movement (p=2.851e-15).

```
## Fixed effects:
##                                 Estimate Std. Error    t value
## (Intercept)                     -2.41847    0.17203    -14.06
## movement_typeloco                0.92844    0.02130    43.58
## genotypeWTjax                    0.10026    0.24354     0.41
## movement_typeloco:genotypeWTjax  0.26210    0.03181     8.24
```

2.4.2 Gamma-distribution (AIC= -1893.076)

Genotype and movement main effects plus an interaction between the two vs just movement (p = 9.603e-07).

```
## Fixed effects:
##                                 Estimate   Std. Error  t value  Pr(>|z|)
## (Intercept)                     -2.20852    0.19028   -11.607   < 2e-16 ***
## movement_typeloco                0.99204    0.03644    27.226   < 2e-16 ***
## genotypeWTjax                    0.06874    0.27000    0.255    0.799
## movement_typeloco:genotypeWTjax  0.28364    0.05435    5.219    1.8e-07 ***
```

2.5 Calcium responses in wild type mice during grey screen illumination

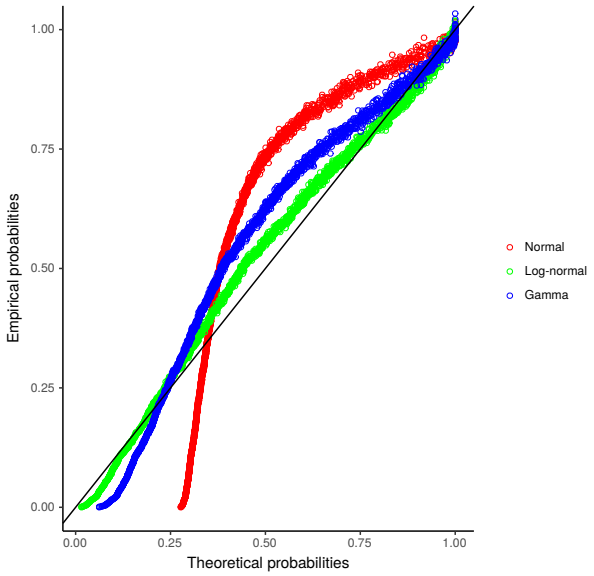

Figure 2.5 Goodness of fit for mean amplitude of calcium responses of wild type V1 dataset during presentation of grey screen. Probability-probability (P-P) plot of the cumulative empirical values (experimental) in normal distribution, log-normal distribution, and gamma distribution against the theoretical cumulative distribution values. Closer the points to the straight line, indicates a better fit. Analysis by Dr. Owen Dando.

Calculating goodness-of-fit statistics:

```
## Goodness-of-fit criteria
##                                  norm      log-norm      gamma
## Akaike's Information Criterion   1890.937    -3176.510   -2362.241
## Bayesian Information Criterion   1902.561    -3164.886   -2350.617
```

2.5.1 Log-normal distribution (AIC= -3176.510)

Genotype main effect vs. no fixed effects (p=0.5301).

Movement main effect vs. no fixed effect (p<2.2e-16).

Genotype and movement main effects vs just movement (p=0.5301).

Genotype and movement main effects plus an interaction between the two vs just movement (p<2.2e-16).

```
## Fixed effects:
##                                 Estimate   Std. Error  t value
## (Intercept)                    -2.38558    0.16804   -14.197
## movement_typeloco               0.69635    0.02418    28.796
## genotypeWTjax                  -0.09257    0.23792    -0.389
## movement_typeloco:genotypeWTjax  0.48545    0.03611    13.445
```

2.5.2 Gamma-distribution (AIC= -2362.241)

Genotype and movement main effects plus an interaction between the two vs just movement (p = 9.642e-15).

```
## Fixed effects:
##                                 Estimate    Std. Error  t value   Pr(>|z|)
## (Intercept)                    -2.16636    0.19036    -11.380    < 2e-16 ***
## movement_typeloco               0.79188    0.03861     20.507    < 2e-16 ***
## genotypeWTjax                  -0.09521    0.27111     -0.351    0.725
## movement_typeloco:genotypeWTjax  0.46410    0.05752     8.069     7.09e-16 ***
## ---
```

References

Aceti, M., Creson, T. K., Vaissiere, T., Rojas, C., Huang, W. C., Wang, Y. X., ... & Rumbaugh, G. (2015). Syngap1 haploinsufficiency damages a postnatal critical period of pyramidal cell structural maturation linked to cortical circuit assembly. *Biological psychiatry*, *77*(9), 805-815.

Agís-Balboa, R. C., Pinna, G., Pibiri, F., Kadriu, B., Costa, E., & Guidotti, A. (2007). Down-regulation of neurosteroid biosynthesis in corticolimbic circuits mediates social isolation-induced behavior in mice. *Proceedings of the National Academy of Sciences*, *104*(47), 18736-18741.

Aken, B. L., Ayling, S., Barrell, D., Clarke, L., Curwen, V., Fairley, S., ... & Howe, K. (2016). The Ensembl gene annotation system. *Database*, *2016*.

American Psychiatric Association. (2013). *Diagnostic and statistical manual of mental disorders (DSM-5®)*. American Psychiatric Pub.

Amodio, D. M., & Frith, C. D. (2006). Meeting of minds: the medial frontal cortex and social cognition. *Nature Reviews Neuroscience*, *7*(4), 268-277.

Andermann, M. L., Kerlin, A. M., Roumis, D. K., Glickfeld, L. L., & Reid, R. C. (2011). Functional specialization of mouse higher visual cortical areas. *Neuron*, *72*(6), 1025-1039.

Andersen, R. A., & Cui, H. (2009). Intention, action planning, and decision making in parietal-frontal circuits. *Neuron*, *63*(5), 568-583.

Araki, Y., Zeng, M., Zhang, M., & Huganir, R. L. (2015). Rapid dispersion of SynGAP from synaptic spines triggers AMPA receptor insertion and spine enlargement during LTP. *Neuron*, *85*(1), 173-189.

Arieli, A., Shoham, D. O. R. O. N., Hildesheim, R. I. N. A., & Grinvald, A. M. I. R. A. M. (1995). Coherent spatiotemporal patterns of ongoing activity revealed by real-time optical imaging coupled with single-unit recording in the cat visual cortex. *Journal of neurophysiology*, *73*(5), 2072-2093.

Arieli, A., Sterkin, A., Grinvald, A., & Aertsen, A. D. (1996). Dynamics of ongoing activity: explanation of the large variability in evoked cortical responses. *Science*, *273*(5283), 1868.

Asiminas, A. (2016). Modelling Fragile X Syndrome in rats: New directions in translational research.

Atsak, P., Orre, M., Bakker, P., Cerliani, L., Roozendaal, B., Gazzola, V., … Keysers, C. (2011). Experience modulates vicarious freezing in rats: A model for empathy. PLoS ONE, 6(7).

Auerbach, B. D., Osterweil, E. K., & Bear, M. F. (2011). Mutations causing syndromic autism define an axis of synaptic pathophysiology. *Nature*, *480*(7375), 63-68.

Avale, M. E., Chabout, J., Pons, S., Serreau, P., De Chaumont, F., Olivo-Marin, J. C., ... & Granon, S. (2011). Prefrontal nicotinic receptors control novel social interaction between mice. *The FASEB Journal*, *25*(7), 2145-2155.

Averbeck, B. B., Latham, P. E., & Pouget, A. (2006). Neural correlations, population coding and computation. *Nature reviews. Neuroscience*, *7*(5), 358.

Baeg, E. H., Kim, Y. B., Huh, K., Mook-Jung, I., Kim, H. T., & Jung, M. W. (2003). Dynamics of population code for working memory in the prefrontal cortex. *Neuron*, *40*(1), 177-188.

Bailey, D. B., Hatton, D. D., Skinner, M., & Mesibov, G. (2001). Autistic behavior, FMR1 protein, and developmental trajectories in young males with fragile X syndrome. *Journal of autism and developmental disorders*, *31*(2), 165-174.

Bailey, K. R., & Crawley, J. N. (2009). Anxiety-Related Behaviors in Mice. Methods of Behavior Analysis in Neuroscience, 13.

Bannerman, D.M., Grubb, M., Deacon, R.M., Yee, B.K., Feldon, J. & Rawlins, J.N. (2003) Ventral hippocampal lesions affect anxiety but not spatial learning. *Behav. Brain Res.*, **139**, 197–213.

Barkovich, A. J., Kuzniecky, R. I., Jackson, G. D., Guerrini, R., & Dobyns, W. B. (2005). A developmental and genetic classification for malformations of cortical development. *Neurology*, *65*(12), 1873-1887.

Barnes, A. S (2014). Convergence of synaptic pathophysiology in the hippocampus of Fmr1−/y and Syngap+/− mice.

Barnes, S. A., Wijetunge, L. S., Jackson, A. D., Katsanevaki, D., Osterweil, E. K., Komiyama, N. H., ... & Wyllie, D. J. (2015). Convergence of hippocampal pathophysiology in Syngap+/− and Fmr1−/y mice. *Journal of Neuroscience*, *35*(45), 15073-15081.

Barnett, M. W., Watson, R. F., Vitalis, T., Porter, K., Komiyama, N. H., Stoney, P. N., ... & Kind, P. C. (2006). Synaptic Ras GTPase activating protein regulates pattern formation in the trigeminal system of mice. *Journal of Neuroscience*, *26*(5), 1355-1365.

Barnett, S. A. (1976). The rat: a study in behavior. Australian National University Press.

Barnett, S. A. (2001). *The story of rats: their impact on us, and our impact on them*. Allen & Unwin.

Bartal, I. B. A., Decety, J., & Mason, P. (2011). Empathy and pro-social behavior in rats. *Science*, *334*(6061), 1427-1430.

Bast, T. & Feldon, J. (2003) Hippocampal modulation of sensorimotor processes. *Prog. Neurobiol.*, **70**, 319–345.

Bateup, H. S., Johnson, C. A., Denefrio, C. L., Saulnier, J. L., Kornacker, K., & Sabatini, B. L. (2013). Excitatory/inhibitory synaptic imbalance leads to hippocampal hyperexcitability in mouse models of tuberous sclerosis. *Neuron*, *78*(3), 510-522.

Baum, M. J., & Keverne, E. B. (2002). Sex difference in attraction thresholds for volatile odors from male and estrous female mouse urine. *Hormones and Behavior*, *41*(2), 213-219.

Baum, S. H., Stevenson, R. A., & Wallace, M. T. (2015). Behavioral, perceptual, and neural alterations in sensory and multisensory function in autism spectrum disorder. *Progress in Neurobiology*, *134*, 140-160.

Bauman, M. D., & Schumann, C. S. (2017). Advances in Nonhuman Primate Models of Autism: Integrating Neuroscience and Behavior. *Experimental Neurology*.

Bauman, M. D., Iosif, A. M., Ashwood, P., Braunschweig, D., Lee, A., Schumann, C. M., ... & Amaral, D. G. (2013). Maternal antibodies from mothers of children with autism alter brain growth and social behavior development in the rhesus monkey. *Translational psychiatry*, *3*(7), e278.

Baumgärtel, K., & Mansuy, I. M. (2012). Neural functions of calcineurin in synaptic plasticity and memory. *Learning & Memory*, *19*(9), 375-384.

Bear, M. F., Huber, K. M., & Warren, S. T. (2004). The mGluR theory of fragile X mental retardation. *Trends in neurosciences*, *27*(7), 370-377.

Belmonte, M. K., Allen, G., Beckel-Mitchener, A., Boulanger, L. M., Carper, R. A., & Webb, S. J. (2004). Autism and abnormal development of brain connectivity. *Journal of Neuroscience*, *24*(42), 9228-9231.

Belzung, C., & Lemoine, M. (2011). Criteria of validity for animal models of psychiatric disorders: focus on anxiety disorders and depression. *Biology of mood & anxiety disorders*, *1*(1), 9.

Bennett, C., Arroyo, S., & Hestrin, S. (2013). Subthreshold mechanisms underlying state-dependent modulation of visual responses. *Neuron*, *80*(2), 350-357.

Berry-Kravis, E. (2014). Mechanism-based treatments in neurodevelopmental disorders: fragile X syndrome. *Pediatric neurology*, *50*(4), 297-302.

Berryer, M. H., Chattopadhyaya, B., Xing, P., Riebe, I., Bosoi, C., Sanon, N., ... & Carmant, L. (2016). Decrease of SYNGAP1 in GABAergic cells impairs

inhibitory synapse connectivity, synaptic inhibition and cognitive function. *Nature communications*, *7*.

Berryer, M. H., Hamdan, F. F., Klitten, L. L., Møller, R. S., Carmant, L., Schwartzentruber, J., ... & Lacaille, J. C. (2013). Mutations in SYNGAP1 cause intellectual disability, autism, and a specific form of epilepsy by inducing haploinsufficiency. *Human mutation*, *34*(2), 385-394.

Besle, J., Fischer, C., Bidet-Caulet, A., Lecaignard, F., Bertrand, O., & Giard, M. H. (2008). Visual activation and audiovisual interactions in the auditory cortex during speech perception: intracranial recordings in humans. *Journal of Neuroscience*, *28*(52), 14301-14310.

Bevins, R. a, & Besheer, J. (2006). Object recognition in rats and mice: a one-trial non-matching-to-sample learning task to study "recognition memory". Nature Protocols, 1(3), 1306–1311.

Bisley, J. W., & Goldberg, M. E. (2010). Attention, intention, and priority in the parietal lobe. *Annual review of neuroscience*, *33*, 1-21.

Blair, H. T., Schafe, G. E., Bauer, E. P., Rodrigues, S. M., & LeDoux, J. E. (2001). Synaptic plasticity in the lateral amygdala: a cellular hypothesis of fear conditioning. *Learning & memory*, *8*(5), 229-242.

Blanchard, D. C., Blanchard, R. J., & Rodgers, R. J. (1991). Risk assessment and animal models of anxiety. In *Animal models in psychopharmacology* (pp. 117-134). Birkhäuser Basel.

Blanchard, D. C., Blanchard, R. J., Tom, P., & Rodgers, R. J. (1990). Diazepam changes risk assessment in an anxiety/defense test battery. *Psychopharmacology*, *101*(4), 511-518.

Blanchard, R. J., Flannelly, K. J., & Blanchard, D. C. (1988). Life-span studies of dominance and aggression in established colonies of laboratory rats. *Physiology & behavior*, *43*(1), 1-7.

Bolivar, V. J., Walters, S. R., & Phoenix, J. L. (2007). Assessing autism-like behavior in mice: variations in social interactions among inbred strains. *Behavioural brain research*, *176*(1), 21-26.

Bos, J. L., Rehmann, H., & Wittinghofer, A. (2007). GEFs and GAPs: critical elements in the control of small G proteins. *Cell*, *129*(5), 865-877.

Bouras, N. (Ed.). (1999). *Psychiatric and behavioural disorders in developmental disabilities and mental retardation*. Cambridge University Press.

Boutin, S., & Lane, J. E. (2014). Climate change and mammals: evolutionary versus plastic responses. *Evolutionary Applications*, *7*(1), 29-41.

Bovetti, S., Moretti, C., Zucca, S., Dal Maschio, M., Bonifazi, P., & Fellin, T. (2017). Simultaneous high-speed imaging and optogenetic inhibition in the intact mouse brain. *Scientific reports*, *7*.

Braff, D. L., Geyer, M. A., & Swerdlow, N. R. (2001). Human studies of prepulse inhibition of startle: normal subjects, patient groups, and pharmacological studies. *Psychopharmacology*, *156*(2-3), 234-258.

Brainard, D. H., & Vision, S. (1997). The psychophysics toolbox. *Spatial vision*, *10*, 433-436.

Buhl, E. H., & Lübke, J. (1989). Intracellular lucifer yellow injection in fixed brain slices combined with retrograde tracing, light and electron microscopy. *Neuroscience*, *28*(1), 3-16.

Buia, C. I., & Tiesinga, P. H. (2008). Role of interneuron diversity in the cortical microcircuit for attention. *Journal of neurophysiology*, *99*(5), 2158-2182.

Bunsey, M., & Eichenbaum, H. (1995). Selective damage to the hippocampal region blocks long-term retention of a natural and nonspatial stimulus-stimulus association. *Hippocampus*, *5*(6), 546-556.

Burgdorf, J., Moskal, J., Brudzynski, S., & Panksepp, J. (2013). Rats selectively bred for low levels of playinduced 50 kHz vocalizations as a model for autism spectrum disorders: a role for NMDA receptors. Behavioural Brain Research, 251, 18–24.

Burkhalter, A. (2008). Many specialists for suppressing cortical excitation. *Frontiers in neuroscience*, *2*(2), 155.

Buzsáki, G. Y., Bickford, R. G., Ponomareff, G., Thal, L. J., Mandel, R., & Gage, F. H. (1988). Nucleus basalis and thalamic control of neocortical activity in the freely moving rat. *Journal of neuroscience*, *8*(11), 4007-4026.

Buzsáki, G., & Watson, B. O. (2012). Brain rhythms and neural syntax: implications for efficient coding of cognitive content and neuropsychiatric disease. *Dialogues in clinical neuroscience*, *14*(4), 345.

Cardin, J. A., Carlén, M., Meletis, K., Knoblich, U., Zhang, F., Deisseroth, K., ... & Moore, C. I. (2009). Driving fast-spiking cells induces gamma rhythm and controls sensory responses. *Nature*, *459*(7247), 663.

Carlisle, H. J., & Kennedy, M. B. (2005). Spine architecture and synaptic plasticity. *Trends in neurosciences*, *28*(4), 182-187.

Carlisle, H. J., Manzerra, P., Marcora, E., & Kennedy, M. B. (2008). SynGAP regulates steady-state and activity-dependent phosphorylation of cofilin. *Journal of Neuroscience*, *28*(50), 13673-13683.

Carvill, G. L., Heavin, S. B., Yendle, S. C., McMahon, J. M., O'Roak, B. J., Cook, J., ... & Malone, S. (2013). Targeted resequencing in epileptic encephalopathies identifies de novo mutations in CHD2 and SYNGAP1. *Nature genetics*, *45*(7), 825-830.

Cauli, B., Audinat, E., Lambolez, B., Angulo, M. C., Ropert, N., Tsuzuki, K., ... & Rossier, J. (1997). Molecular and physiological diversity of cortical nonpyramidal cells. *Journal of Neuroscience*, *17*(10), 3894-3906.

Chafee, M. V., & Goldman-Rakic, P. S. (1998). Matching patterns of activity in primate prefrontal area 8a and parietal area 7ip neurons during a spatial working memorytask. *Journal of neurophysiology*, *79*(6), 2919-2940.

Chahrour, M. H., Timothy, W. Y., Lim, E. T., Ataman, B., Coulter, M. E., Hill, R. S., ... & Walsh, C. A. (2012). Whole-exome sequencing and homozygosity analysis implicate depolarization-regulated neuronal genes in autism. *PLoS genetics*, *8*(4), e1002635.

Chahrour, M., & Zoghbi, H. Y. (2007). The story of Rett syndrome: from clinic to neurobiology. *Neuron*, *56*(3), 422-437.

Chao, O. Y., Huston, J. P., Li, J. S., Wang, A. L., & de Souza Silva, M. A. (2016). The medial prefrontal cortex—lateral entorhinal cortex circuit is essential for episodic-like memory and associative object-recognition. *Hippocampus*, *26*(5), 633-645.

Cheal, M. L., & Sprott, R. L. (1971). Social olfaction: A review of the role of olfaction in a variety of animal behaviors. *Psychological Reports*, *29*(1), 195-243.

Chelly, J., & Mandel, J. L. (2001). Monogenic causes of X-linked mental retardation. *Nature reviews. Genetics*, *2*(9), 669.

Chelly, J., Khelfaoui, M., Francis, F., Chérif, B., & Bienvenu, T. (2006). Genetics and pathophysiology of mental retardation. *European journal of human genetics: EJHG*, *14*(6), 701.

Chen, H. J., Rojas-Soto, M., Oguni, A., & Kennedy, M. B. (1998). A synaptic Ras-GTPase activating protein (p135 SynGAP) inhibited by CaM kinase II. *Neuron*, *20*(5), 895-904.

Chen, T. W., Wardill, T. J., Sun, Y., Pulver, S. R., Renninger, S. L., Baohan, A., ... & Looger, L. L. (2013). Ultra-sensitive fluorescent proteins for imaging neuronal activity. *Nature*, *499*(7458), 295.

Chen, Y., Niu, Y., & Ji, W. (2016). Genome editing in nonhuman primates: approach to generating human disease models. *Journal of internal medicine*, *280*(3), 246-251.

Cheon, K. A., Kim, Y. S., Oh, S. H., Park, S. Y., Yoon, H. W., Herrington, J., ... & Leventhal, B. L. (2011). Involvement of the anterior thalamic radiation in boys with high functioning autism spectrum disorders: a diffusion tensor imaging study. *Brain research*, *1417*, 77-86.

Chez, M. G., Aimonovitch, M., Buchanan, T., Mrazek, S., & Tremb, R. J. (2004). Treating autistic spectrum disorders in children: utility of the cholinesterase inhibitor rivastigmine tartrate. *Journal of child neurology*, *19*(3), 165-169.

Chiang, C. Y. (2016). Cortical development & plasticity in the FMRP KO mouse.

Chklovskii, D. B., Schikorski, T., & Stevens, C. F. (2002). Wiring optimization in cortical circuits. *Neuron*, *34*(3), 341-347.

Chuang, S. C., Zhao, W., Bauchwitz, R., Yan, Q., Bianchi, R., & Wong, R. K. (2005). Prolonged epileptiform discharges induced by altered group I metabotropic glutamate receptor-mediated synaptic responses in hippocampal slices of a fragile X mouse model. *Journal of Neuroscience*, *25*(35), 8048-8055.

Clarke, L. E., & Barres, B. A. (2013). Emerging roles of astrocytes in neural circuit development. *Nature Reviews. Neuroscience*, *14*(5), 311.

Clement, J. P., Aceti, M., Creson, T. K., Ozkan, E. D., Shi, Y., Reish, N. J., ... & Xu, X. (2012). Pathogenic SYNGAP1 mutations impair cognitive development by disrupting maturation of dendritic spine synapses. *Cell*, *151*(4), 709-723.

Clement, J. P., Ozkan, E. D., Aceti, M., Miller, C. A., & Rumbaugh, G. (2013). SYNGAP1 links the maturation rate of excitatory synapses to the duration of critical-period synaptic plasticity. *Journal of Neuroscience*, *33*(25), 10447-10452.

Cohen, G. B., Ren, R., & Baltimore, D. (1995). Modular binding domains in signal transduction proteins. *Cell*, *80*(2), 237-248.

Cohen, M. R., & Maunsell, J. H. (2009). Attention improves performance primarily by reducing interneuronal correlations. *Nature neuroscience*, *12*(12), 1594-1600.

Compte, A., Brunel, N., Goldman-Rakic, P. S., & Wang, X. J. (2000). Synaptic mechanisms and network dynamics underlying spatial working memory in a cortical network model. *Cerebral Cortex*, *10*(9), 910-923.

Connor, C. E., Preddie, D. C., Gallant, J. L., & Van Essen, D. C. (1997). Spatial attention effects in macaque area V4. *Journal of Neuroscience*, *17*(9), 3201-3214.

Cooper, G. M., Coe, B. P., Girirajan, S., Rosenfeld, J. A., Vu, T. H., Baker, C., ... & Abdel-Hamid, H. (2011). A copy number variation morbidity map of developmental delay. *Nature genetics*, *43*(9), 838-846.

Coultrap, S. J., & Bayer, K. U. (2012). CaMKII regulation in information processing and storage. *Trends in neurosciences*, *35*(10), 607-618.

Courchesne, E., & Pierce, K. (2005). Why the frontal cortex in autism might be talking only to itself: local over-connectivity but long-distance disconnection. *Current opinion in neurobiology*, *15*(2), 225-230.

Covington, H. E., Lobo, M. K., Maze, I., Vialou, V., Hyman, J. M., Zaman, S., ... & Neve, R. L. (2010). Antidepressant effect of optogenetic stimulation of the medial prefrontal cortex. *Journal of Neuroscience*, *30*(48), 16082-16090.

Crawley JN. Translational animal models of autism and neurodevelopmental disorders. *Dialogues in Clinical Neuroscience*. 2012;14(3):293-305.

Crawley, J. N., Belknap, J. K., Collins, A., Crabbe, J. C., Frankel, W., Henderson, N., ... & Wehner, J. M. (1997). Behavioral phenotypes of inbred mouse strains: implications and recommendations for molecular studies. *Psychopharmacology*, *132*(2), 107-124.

Cressant, A., Besson, M., Suarez, S., Cormier, A., & Granon, S. (2007). Spatial learning in Long-Evans Hooded rats and C57BL/6J mice: Different strategies for different performance. Behavioural Brain Research, 177(1), 22–29.

Crochet, S., & Petersen, C. C. (2006). Correlating whisker behavior with membrane potential in barrel cortex of awake mice. *Nature neuroscience*, *9*(5), 608.

Crowe, D. A., Averbeck, B. B., & Chafee, M. V. (2010). Rapid sequences of population activity patterns dynamically encode task-critical spatial information in parietal cortex. *Journal of Neuroscience*, *30*(35), 11640-11653.

Cui X., Ji D., Fisher DA., Wu Y., Briner DM., Weinstein EJ. Targeted integration in rat and mouse embryos with zinc-finger nucleases. *Nat Biotechnol.* 2011;29:64–67.

Cullen, P. J., & Lockyer, P. J. (2002). Integration of calcium and Ras signalling. *Nature reviews. Molecular cell biology*, *3*(5), 339.

Curtis, C. E., & Lee, D. (2010). Beyond working memory: the role of persistent activity in decision making. *Trends in cognitive sciences*, *14*(5), 216-222.

da Silva, B. M., Bast, T., & Morris, R. G. (2014). Spatial memory: behavioral determinants of persistence in the watermaze delayed matching-to-place task. *Learning & Memory*, *21*(1), 28-36.

Dalland, T. (1970). Response and stimulus perseveration in rats with septal and dorsal hippocampal lesions. *Journal of Comparative and Physiological Psychology*, *71*(1), 114.

Dani, V. S., Chang, Q., Maffei, A., Turrigiano, G. G., Jaenisch, R., & Nelson, S. B. (2005). Reduced cortical activity due to a shift in the balance between excitation and inhibition in a mouse model of Rett syndrome. *Proceedings of the National Academy of Sciences of the United States of America*, *102*(35), 12560-12565.

Dantzer, R., & Bluthé, R. M. (1993). Vasopressin and behavior: from memory to olfaction. *Regulatory peptides*, *45*(1), 121-125.

De Ligt, J., Willemsen, M. H., Van Bon, B. W., Kleefstra, T., Yntema, H. G., Kroes, T., ... & del Rosario, M. (2012). Diagnostic exome sequencing in persons with severe intellectual disability. *New England Journal of Medicine*, *367*(20), 1921-1929.

De Rubeis, S., He, X., Goldberg, A. P., Poultney, C. S., Samocha, K., Cicek, A. E., ... & Singh, T. (2014). Synaptic, transcriptional and chromatin genes disrupted in autism. *Nature*, *515*(7526), 209-215.

De Vries, T. J., Schoffelmeer, A. N. M., Binnekade, R., Mulder, A. H., & Vanderschuren, L. J. M. J. (1998). Druginduced reinstatement of heroin- and cocaine-seeking behaviour following long-term extinction is associated with expression of behavioural sensitization. European Journal of Neuroscience, 10(11), 3565–3571.

Deacon, R. M. J., & Rawlins, J. N. P. (2006). T-maze alternation in the rodent. Nature Protocols, 1(1), 7–12.

Deacon, R. M., & Rawlins, J. N. P. (2006). T-maze alternation in the rodent. *Nature protocols*, *1*(1), 7.

Deacon, R.M., Bannerman, D.M. & Rawlins, J.N. (2002) Anxiolytic effects of cytotoxic hippocampal lesions in rats. *Behav. Neurosci.*, **116**, 494–497.

DECIPHER - DatabasE of genomiC varIation and Phenotype in Humans using Ensembl Resources.

DeFelipe, J. (1993). Neocortical neuronal diversity: chemical heterogeneity revealed by colocalization studies of classic neurotransmitters, neuropeptides, calcium-binding proteins, and cell surface molecules. *Cerebral cortex*, *3*(4), 273-289.

DeFelipe, J., & Fariñas, I. (1992). The pyramidal neuron of the cerebral cortex: morphological and chemical characteristics of the synaptic inputs. *Progress in neurobiology*, *39*(6), 563-607.

DeFelipe, J., Hendry, S. H., & Jones, E. G. (1989). Visualization of chandelier cell axons by parvalbumin immunoreactivity in monkey cerebral cortex. *Proceedings of the National Academy of Sciences*, *86*(6), 2093-2097.

Dember, W. N., & Fowler, H. (1958). Spontaneous alternation behavior. *Psychological bulletin*, *55*(6), 412.

Denman, D. J., & Contreras, D. (2013). The structure of pairwise correlation in mouse primary visual cortex reveals functional organization in the absence of an orientation map. *Cerebral Cortex*, *24*(10), 2707-2720.

Dielenberg, R. A., Carrive, P., & McGregor, I. S. (2001). The cardiovascular and behavioral response to cat odor in rats: unconditioned and conditioned effects. *Brain research*, *897*(1), 228-237.

Dombeck, D. A., Khabbaz, A. N., Collman, F., Adelman, T. L., & Tank, D. W. (2007). Imaging large-scale neural activity with cellular resolution in awake, mobile mice. *Neuron*, *56*(1), 43-57.

Dulcan, M. K., & Wiener, J. M. (Eds.). (2006). *Essentials of child and adolescent psychiatry*. American Psychiatric Pub.

Durand, S., Patrizi, A., Quast, K. B., Hachigian, L., Pavlyuk, R., Saxena, A., ... & Fagiolini, M. (2012). NMDA receptor regulation prevents regression of visual cortical function in the absence of Mecp2. *Neuron*, *76*(6), 1078-1090.

Dyer, E. L., Duarte, M. F., Johnson, D. H., & Baraniuk, R. G. (2010, September). Recovering spikes from noisy neuronal calcium signals via structured sparse approximation. In *International Conference on Latent Variable Analysis and Signal Separation* (pp. 604-611). Springer, Berlin, Heidelberg.

Dyment, D. A., Tetreault, M., Beaulieu, C. L., Hartley, T., Ferreira, P., Chardon, J. W., ... & Parboosingh, J. S. (2015). Whole-exome sequencing broadens the phenotypic spectrum of rare pediatric epilepsy: a retrospective study. *Clinical genetics*, *88*(1), 34-40.

Eacott, M. J., & Norman, G. (2004). Integrated memory for object, place, and context in rats: a possible model of episodic-like memory? *Journal of Neuroscience*, *24*(8), 1948-1953.

Ecker, A. S., Berens, P., Keliris, G. A., Bethge, M., Logothetis, N. K., & Tolias, A. S. (2010). Decorrelated neuronal firing in cortical microcircuits. *science*, *327*(5965), 584-587.

Engineer, C. T., Rahebi, K. C., Borland, M. S., Buell, E. P., Centanni, T. M., Fink, M. K., ... & Kilgard, M. P. (2015). Degraded neural and behavioral processing of speech sounds in a rat model of Rett syndrome. *Neurobiology of disease*, *83*, 26-34.

Ennaceur, A., & Delacour, J. (1988). A new one-trial test for neurobiological studies of memory in rats. 1: Behavioral data. *Behavioural brain research*, *31*(1), 47-59.

Erisken, S., Vaiceliunaite, A., Jurjut, O., Fiorini, M., Katzner, S., & Busse, L. (2014). Effects of locomotion extend throughout the mouse early visual system. *Current Biology*, *24*(24), 2899-2907.

Erlich, J. C., Bialek, M., & Brody, C. D. (2011). A cortical substrate for memory-guided orienting in the rat. *Neuron*, *72*(2), 330-343.

Esclassan, F., Francois, J., Phillips, K. G., Loomis, S., & Gilmour, G. (2015). Phenotypic characterization of nonsocial behavioral impairment in neurexin 1α knockout rats. *Behavioral neuroscience*, *129*(1), 74.

Felix-Ortiz, A. C., & Tye, K. M. (2014). Amygdala inputs to the ventral hippocampus bidirectionally modulate social behavior. *Journal of Neuroscience*, *34*(2), 586-595.

Ferreira, T. A., Blackman, A. V., Oyrer, J., Jayabal, S., Chung, A. J., Watt, A. J., ... & Van Meyel, D. J. (2014). Neuronal morphometry directly from bitmap images. *Nature methods*, *11*(10), 982-984.

Firth, H. V., & Wright, C. F. (2011). The deciphering developmental disorders (DDD) study. *Developmental Medicine & Child Neurology*, *53*(8), 702-703.

Firth, H. V., Richards, S. M., Bevan, A. P., Clayton, S., Corpas, M., Rajan, D., ... & Carter, N. P. (2009). DECIPHER: database of chromosomal imbalance and phenotype in humans using ensembl resources. *The American Journal of Human Genetics*, *84*(4), 524-533.

Fitzgerald, B., Morgan, J., Keene, N., Rollinson, R., Hodgson, A., & Dalrymple-Smith, J. (2000). An investigation into diet treatment for adults with previously untreated phenylketonuria and severe intellectual disability. *Journal of Intellectual Disability Research*, *44*(1), 53-59.

Fitzgerald, T. W., Gerety, S. S., Jones, W. D., van Kogelenberg, M., King, D. A., McRae, J., ... & Barrett, D. M. (2014). Large-scale discovery of novel genetic causes of developmental disorders. *Nature*, *519*(7542), 223-228.

Freedman, D. J., & Assad, J. A. (2011). A proposed common neural mechanism for categorization and perceptual decisions. *Nature neuroscience*, *14*(2), 143-146.

Frick, K. M., Stillner, E. T., & Berger-Sweeney, J. (2000). Mice are not little rats: species differences in a oneday water maze task. Neuroreport, 11(16), 3461–5.

Fries, P., Reynolds, J. H., Rorie, A. E., & Desimone, R. (2001). Modulation of oscillatory neuronal synchronization by selective visual attention. *Science*, *291*(5508), 1560-1563.

Fu, Y., Tucciarone, J. M., Espinosa, J. S., Sheng, N., Darcy, D. P., Nicoll, R. A., ... & Stryker, M. P. (2014). A cortical circuit for gain control by behavioral state. *Cell*, *156*(6), 1139-1152.

Fucile, S. (2004). Ca 2+ permeability of nicotinic acetylcholine receptors. *Cell calcium*, *35*(1), 1-8.

Fujisawa, S., Amarasingham, A., Harrison, M. T., & Buzsáki, G. (2008). Behavior-dependent short-term assembly dynamics in the medial prefrontal cortex. *Nature neuroscience*, *11*(7), 823-833.

Funk, A. J., Rumbaugh, G., Harotunian, V., McCullumsmith, R. E., & Meador-Woodruff, J. H. (2009). Decreased expression of NMDA receptor-associated proteins in frontal cortex of elderly patients with schizophrenia. *Neuroreport*, *20*(11), 1019.

Galbraith, J. A., Mrosko, B. J., & Myers, R. R. (1993). A system to measure thermal nociception. *Journal of neuroscience methods*, *49*(1), 63-68.

Gandhi, N. J., & Katnani, H. A. (2011). Motor functions of the superior colliculus. *Annual review of neuroscience*, *34*, 205-231.

Gaudissard, J., Ginger, M., Premoli, M., Memo, M., Frick, A., & Pietropaolo, S. (2017). Behavioral abnormalities in the Fmr1-KO2 mouse model of fragile X syndrome: The relevance of early life phases. *Autism Research*.

Gerlai, R., & Clayton, N. S. (1999). Analysing hippocampal function in transgenic mice: an ethological perspective. *Trends in neurosciences*, *22*(2), 47-51.

Gerstein, G. L., & Clark, W. A. (1964). Simultaneous studies of firing patterns in several neurons. *Science*, *143*(3612), 1325-1327.

Geschwind, D. H., & Levitt, P. (2007). Autism spectrum disorders: developmental disconnection syndromes. *Current opinion in neurobiology*, *17*(1), 103-111.

Gibbs, R. A., Weinstock, G. M., Metzker, M. L., Muzny, D. M., Sodergren, E. J., Scherer, S., ... & Okwuonu, G. (2004). Genome sequence of the Brown Norway rat yields insights into mammalian evolution. *Nature*, *428*(6982), 493-521.

Gilbert, C. D., & Sigman, M. (2007). Brain states: top-down influences in sensory processing. *Neuron*, *54*(5), 677-696.

Gillberg, C., Persson, E., Grufman, M., & Themnér, U. (1986). Psychiatric disorders in mildly and severely mentally retarded urban children and adolescents: epidemiological aspects. *The British journal of psychiatry*, *149*(1), 68-74.

Gkogkas, C. G., Khoutorsky, A., Ran, I., Rampakakis, E., Nevarko, T., Weatherill, D. B., ... & Major, F. (2013). Autism-related deficits via dysregulated eIF4E-dependent translational control. *Nature*, *493*(7432), 371.

Goard, M. J., Pho, G. N., Woodson, J., & Sur, M. (2016). Distinct roles of visual, parietal, and frontal motor cortices in memory-guided sensorimotor decisions. *Elife*, *5*, e13764.

Goard, M., & Dan, Y. (2009). Basal forebrain activation enhances cortical coding of natural scenes. *Nature neuroscience*, *12*(11), 1444-1449.

Gold, J. I., & Shadlen, M. N. (2007). The neural basis of decision making. *Annu. Rev. Neurosci.*, *30*, 535-574.

Golshani, P., Gonçalves, J. T., Khoshkhoo, S., Mostany, R., Smirnakis, S., & Portera-Cailliau, C. (2009). Internally mediated developmental desynchronization of neocortical network activity. *Journal of Neuroscience*, *29*(35), 10890-10899.

Gonçalves, J. T., Anstey, J. E., Golshani, P., & Portera-Cailliau, C. (2013). Circuit level defects in the developing neocortex of Fragile X mice. *Nature neuroscience*, *16*(7), 903-909.

Gonzalez-Sulser, A., Parthier, D., Candela, A., McClure, C., Pastoll, H., Garden, D., ... & Nolan, M. F. (2014). GABAergic projections from the medial septum selectively inhibit interneurons in the medial entorhinal cortex. *Journal of Neuroscience*, *34*(50), 16739-16743.

Gordon, J. A., & Stryker, M. P. (1996). Experience-dependent plasticity of binocular responses in the primary visual cortex of the mouse. *Journal of Neuroscience*, *16*(10), 3274-3286.

Gorski, J. A., Talley, T., Qiu, M., Puelles, L., Rubenstein, J. L., & Jones, K. R. (2002). Cortical excitatory neurons and glia, but not GABAergic neurons, are produced in the Emx1-expressing lineage. *Journal of Neuroscience*, *22*(15), 6309-6314.

Gottlieb, J. P., Kusunoki, M., & Goldberg, M. E. (1998). The representation of visual salience in monkey parietal cortex. *Nature*, *391*(6666), 481.

Grant, E.C. & MacIntosh, J.H. (1963) A comparison of the social postures of some common laboratory rodents. *Behaviour* **21**, 246–259.

Green, S. A., Hernandez, L. M., Bowman, H. C., Bookheimer, S. Y., & Dapretto, M. (2017). Sensory over-responsivity and social cognition in ASD: Effects of aversive sensory stimuli and attentional modulation on neural responses to social cues. *Developmental Cognitive Neuroscience*.

Green, S. A., Rudie, J. D., Colich, N. L., Wood, J. J., Shirinyan, D., Hernandez, L., ... & Bookheimer, S. Y. (2013). Overreactive brain responses to sensory stimuli in youth with autism spectrum disorders. *Journal of the American Academy of Child & Adolescent Psychiatry*, *52*(11), 1158-1172.

Greenberg, D. S., Houweling, A. R., & Kerr, J. N. (2008). Population imaging of ongoing neuronal activity in the visual cortex of awake rats. *Nature neuroscience*, *11*(7), 749-751.

Grewal, S. S., York, R. D., & Stork, P. J. (1999). Extracellular-signal-regulated kinase signalling in neurons. *Current opinion in neurobiology*, *9*(5), 544-553.

Griebel, G., Blanchard, D. C., & Blanchard, R. J. (1996). Evidence that the behaviors in the Mouse Defense Test Battery relate to different emotional states: a factor analytic study. *Physiology & behavior*, *60*(5), 1255-1260.

Grienberger, C., Rochefort, N. L., Adelsberger, H., Henning, H. A., Hill, D. N., Reichwald, J., ... & Konnerth, A. (2012). Staged decline of neuronal function in vivo in an animal model of Alzheimer's disease. *Nature Communications*, *3*, ncomms1783.

Gunaydin, L. A., Grosenick, L., Finkelstein, J. C., Kauvar, I. V., Fenno, L. E., Adhikari, A., ... & Tye, K. M. (2014). Natural neural projection dynamics underlying social behavior. *Cell*, *157*(7), 1535-1551.

Guo, X., Hamilton, P. J., Reish, N. J., Sweatt, J. D., Miller, C. A., & Rumbaugh, G. (2009). Reduced expression of the NMDA receptor-interacting protein SynGAP causes behavioral abnormalities that model symptoms of Schizophrenia. *Neuropsychopharmacology*, *34*(7), 1659-1672.

Guo, Z. V., Li, N., Huber, D., Ophir, E., Gutnisky, D., Ting, J. T., ... & Svoboda, K. (2014). Flow of cortical activity underlying a tactile decision in mice. *Neuron*, *81*(1), 179-194.

Gupta, A., Wang, Y., & Markram, H. (2000). Organizing principles for a diversity of GABAergic interneurons and synapses in the neocortex. *Science*, *287*(5451), 273-278.

Haberl, M. G., Zerbi, V., Veltien, A., Ginger, M., Heerschap, A., & Frick, A. (2015). Structural-functional connectivity deficits of neocortical circuits in the Fmr1−/y mouse model of autism. *Science advances*, *1*(10), e1500775.

Hagerman, R. J., & Polussa, J. (2015). Treatment of the psychiatric problems associated with fragile X syndrome. *Current opinion in psychiatry*, *28*(2), 107-112.

Hall, W. C., & Moschovakis, A. K. (Eds.). (2003). *The superior colliculus: new approaches for studying sensorimotor integration*. CRC Press.

Hamdan, F. F., Daoud, H., Piton, A., Gauthier, J., Dobrzeniecka, S., Krebs, M. O., ... & Wang, Z. (2011a). De novo SYNGAP1 mutations in nonsyndromic intellectual disability and autism. *Biological psychiatry*, *69*(9), 898-901.

Hamdan, F. F., Gauthier, J., Araki, Y., Lin, D. T., Yoshizawa, Y., Higashi, K., ... & Tomitori, H. (2011b). Excess of de novo deleterious mutations in genes associated with glutamatergic systems in nonsyndromic intellectual disability. *The American Journal of Human Genetics*, *88*(3), 306-316.

Hamdan, F. F., Gauthier, J., Spiegelman, D., Noreau, A., Yang, Y., Pellerin, S., ... & D'Anjou, G. (2009). Mutations in SYNGAP1 in autosomal nonsyndromic mental retardation. *New England Journal of Medicine*, *360*(6), 599-605.

Hamdan, F. F., Srour, M., Capo-Chichi, J. M., Daoud, H., Nassif, C., Patry, L., ... & Henrion, E. (2014). De novo mutations in moderate or severe intellectual disability. *PLoS genetics*, *10*(10), e1004772.

Hanks, T., Kopec, C. D., Brunton, B. W., Duan, C. A., Erlich, J. C., & Brody, C. D. (2015). Distinct relationships of parietal and prefrontal cortices to evidence accumulation. *Nature*, *520*(7546), 220.

Hardt, O., Migues, P. V., Hastings, M., Wong, J., & Nader, K. (2010). PKMζ maintains 1-day-and 6-day-old long-term object location but not object identity memory in dorsal hippocampus. *Hippocampus*, *20*(6), 691-695.

Harris, J. C. (2006). *Intellectual disability: Understanding its development, causes, classification, evaluation, and treatment*. Oxford University Press.

Harvey, C. D., Coen, P., & Tank, D. W. (2012). Choice-specific sequences in parietal cortex during a virtual-navigation decision task. *Nature*, *484*(7392), 62.

Hascoet, M., & Bourin, M. (2009). The Mouse Light–Dark Box Test. *Mood and anxiety related phenotypes in mice: Characterization using behavioral tests*, 197-223.

Haydon, P. G. (2000). Neuroglial networks: neurons and glia talk to each other. *Current biology*, *10*(19), R712-R714.

Hays, S. A., Huber, K. M., & Gibson, J. R. (2011). Altered neocortical rhythmic activity states in Fmr1 KO mice are due to enhanced mGluR5 signaling and involve changes in excitatory circuitry. *Journal of Neuroscience*, *31*(40), 14223-14234.

Hedrich, H. J. (2000). History, strains and models. In *The laboratory rat* (pp. 3-16).

Heidbreder, C. A., & Groenewegen, H. J. (2003). The medial prefrontal cortex in the rat: evidence for a dorso-ventral distinction based upon functional and anatomical characteristics. *Neuroscience & Biobehavioral Reviews*, *27*(6), 555-579.

Heifets, B. D., Chevaleyre, V., & Castillo, P. E. (2008). Interneuron activity controls endocannabinoid-mediated presynaptic plasticity through calcineurin. *Proceedings of the National Academy of Sciences*, *105*(29), 10250-10255.

Hensch, T. K. (2005). Critical period plasticity in local cortical circuits. *Nature reviews. Neuroscience*, *6*(11), 877.

Highley, J. R., Walker, M. A., Esiri, M. M., Crow, T. J., & Harrison, P. J. (2002). Asymmetry of the uncinate fasciculus: a post-mortem study of normal subjects and patients with schizophrenia. *Cerebral Cortex*, *12*(11), 1218-1224.

Hippenmeyer, S., Vrieseling, E., Sigrist, M., Portmann, T., Laengle, C., Ladle, D. R., & Arber, S. (2005). A developmental switch in the response of DRG neurons to ETS transcription factor signaling. *PLoS biology*, *3*(5), e159.

Hofer, S. B., Ko, H., Pichler, B., Vogelstein, J., Ros, H., Zeng, H., ... & Mrsic-Flogel, T. D. (2011). Differential connectivity and response dynamics of excitatory and inhibitory neurons in visual cortex. *Nature neuroscience*, *14*(8), 1045-1052.

Hohnadel, E., Bouchard, K., & Terry, A. V. (2007). Galantamine and donepezil attenuate pharmacologically induced deficits in prepulse inhibition in rats. *Neuropharmacology*, *52*(2), 542-551.

Hoischen, A., Krumm, N., & Eichler, E. E. (2014). Prioritization of neurodevelopmental disease genes by discovery of new mutations. *Nature neuroscience*, *17*(6), 764-772.

Hölter, S. M., Einicke, J., Sperling, B., Zimprich, A., Garrett, L., Fuchs, H., ... & Wurst, W. (2015). Tests for Anxiety-Related Behavior in Mice. *Current protocols in mouse biology*, 291-309.

Hood, K. E., & Cairns, R. B. (1989). A developmental-genetic analysis of aggressive behavior in mice: IV. Genotype-environment interaction. *Aggressive Behavior*, *15*(5), 361-380.

Hsiao, S. S., O'shaughnessy, D. M., & Johnson, K. O. (1993). Effects of selective attention on spatial form processing in monkey primary and secondary somatosensory cortex. *Journal of Neurophysiology*, *70*(1), 444-447.

Huber, D., Gutnisky, D. A., Peron, S., O'connor, D. H., Wiegert, J. S., Tian, L., ... & Svoboda, K. (2012). Multiple dynamic representations in the motor cortex during sensorimotor learning. *Nature*, *484*(7395), 473.

Huckins, L. M., Logan, D. W., & Sánchez-Andrade, G. (2013). Olfaction and olfactory-mediated behaviour in psychiatric disease models. *Cell and tissue research*, *354*(1), 69-80.

Huguet, G., Ey, E., & Bourgeron, T. (2013). The genetic landscapes of autism spectrum disorders. *Annual review of genomics and human genetics*, *14*, 191-213.

Hulbert, S. W., & Jiang, Y. H. (2016). Monogenic mouse models of autism spectrum disorders: common mechanisms and missing links. *Neuroscience*, *321*, 3-23.

Inglis, I. R., Langton, S., Forkman, B., & Lazarus, J. (2001). An information primacy model of exploratory and foraging behaviour. *Animal Behaviour*, *62*(3), 543-557.

Inlow, J. K., & Restifo, L. L. (2004). Molecular and comparative genetics of mental retardation. *Genetics*, *166*(2), 835-881.

Iossifov, I., Ronemus, M., Levy, D., Wang, Z., Hakker, I., Rosenbaum, J., ... & Kendall, J. (2012). De novo gene disruptions in children on the autistic spectrum. *Neuron*, *74*(2), 285-299.

Itsara, A., Cooper, G. M., Baker, C., Girirajan, S., Li, J., Absher, D., ... & Mefford, H. (2009). Population analysis of large copy number variants and hotspots of human genetic disease. *The American Journal of Human Genetics*, *84*(2), 148-161.

Jackson, J., Ayzenshtat, I., Karnani, M. M., & Yuste, R. (2016). VIP+ interneurons control neocortical activity across brain states. *Journal of neurophysiology*, *115*(6), 3008-3017.

Jacobs, S., Nathwani, M., & Doering, L. C. (2010). Fragile X astrocytes induce developmental delays in dendrite maturation and synaptic protein expression. *BMC neuroscience*, *11*(1), 132.

Jaramillo, S., & Zador, A. M. (2014). Mice and rats achieve similar levels of performance in an adaptive decision-making task. Frontiers in Systems Neuroscience, 8.

Jarrard, L. E. (1983). Selective hippocampal lesions and behavior: effects of kainic acid lesions on performance of place and cue tasks. *Behav Neurosci*, *97*(6), 873-889.

Jazrawi, S. P., & Horton, R. W. (1986). Brain adrenoceptor binding sites in mice susceptible (DBA/2J) and resistant (C57 Bl/6) to audiogenic seizures. *Journal of neurochemistry*, *47*(1), 173-177.

Jennings, C. G., Landman, R., Zhou, Y., Sharma, J., Hyman, J., Movshon, J. A., ... & Zhou, H. (2016). Opportunities and challenges in modeling human brain disorders in transgenic primates. *Nature neuroscience*, *19*(9), 1123-1130.

Jensen, T., & Edwards, J. G. (2012). Calcineurin is required for TRPV1-induced long-term depression of hippocampal interneurons. *Neuroscience letters*, *510*(2), 82-87.

Jeyabalan, N., & Clement, J. P. (2016). SYNGAP1: mind the Gap. *Frontiers in cellular neuroscience*, *10*.

Jiang, X., Shen, S., Cadwell, C. R., Berens, P., Sinz, F., Ecker, A. S., ... & Tolias, A. S. (2015). Principles of connectivity among morphologically defined cell types in adult neocortex. *Science*, *350*(6264), aac9462.

Johansen-Berg, H., & Lloyd, D. M. (2000). The physiology and psychology of selective attention to touch. *Front Biosci*, *5*, D894-D904.

Jonckers, E., Shah, D., Hamaide, J., Verhoye, M., & Van der Linden, A. (2015). The power of using functional fMRI on small rodents to study brain pharmacology and disease. *Frontiers in Pharmacology*, *6*, 231.

Jonckers, E., Van Audekerke, J., De Visscher, G., Van der Linden, A., & Verhoye, M. (2011). Functional connectivity fMRI of the rodent brain: comparison of functional connectivity networks in rat and mouse. *PloS one*, *6*(4), e18876.

Joosten, A. V., & Bundy, A. C. (2010). Sensory processing and stereotypical and repetitive behaviour in children with autism and intellectual disability. *Australian occupational therapy journal*, *57*(6), 366-372.

Just, M. A., Keller, T. A., Malave, V. L., Kana, R. K., & Varma, S. (2012). Autism as a neural systems disorder: a theory of frontal-posterior underconnectivity. *Neuroscience & Biobehavioral Reviews*, *36*(4), 1292-1313.

Kaidanovich-Beilin, O., Lipina, T., Vukobradovic, I., Roder, J., & Woodgett, J. R. (2011). Assessment of social interaction behaviors. *Journal of visualized experiments: JoVE*, (48).

Kaifosh, P., Zaremba, J. D., Danielson, N. B., & Losonczy, A. (2014). SIMA: Python software for analysis of dynamic fluorescence imaging data. *Frontiers in neuroinformatics*, *8*.

Kandel, E.R., Schwartz, J.H. and Jessell, T.M. eds., (2000). *Principles of neural science* (Vol. 4, pp. 1227-1246). New York: McGraw-hill.

Kaufman, L., Ayub, M., & Vincent, J. B. (2010). The genetic basis of non-syndromic intellectual disability: a review. *Journal of neurodevelopmental disorders*, *2*(4), 182.

Kawaguchi, Y., & Kubota, Y. (1997). GABAergic cell subtypes and their synaptic connections in rat frontal cortex. *Cerebral cortex (New York, NY: 1991)*, *7*(6), 476-486.

Kepecs, A., & Fishell, G. (2014). Interneuron Cell Types: Fit to form and formed to fit. *Nature*, *505*(7483), 318.

Kerr, J. N., Greenberg, D., & Helmchen, F. (2005). Imaging input and output of neocortical networks in vivo. *Proceedings of the National Academy of Sciences of the United States of America*, *102*(39), 14063-14068.

Kim, J. H., Lee, H. K., Takamiya, K., & Huganir, R. L. (2003). The role of synaptic GTPase-activating protein in neuronal development and synaptic plasticity. *Journal of Neuroscience*, *23*(4), 1119-1124.

Kim, J. H., Liao, D., Lau, L. F., & Huganir, R. L. (1998). SynGAP: a synaptic RasGAP that associates with the PSD-95/SAP90 protein family. *Neuron*, *20*(4), 683-691.

Kim, K. C., Kim, P., Go, H. S., Choi, C. S., Yang, S. I., Cheong, J. H., ... & Ko, K. H. (2011). The critical period of valproate exposure to induce autistic symptoms in Sprague–Dawley rats. *Toxicology letters*, *201*(2), 137-142.

Kimura, F. (2000). Cholinergic modulation of cortical function: a hypothetical role in shifting the dynamics in cortical network. *Neuroscience research*, *38*(1), 19-26.

Klitten, L. L., Møller, R. S., Nikanorova, M., Silahtaroglu, A., Hjalgrim, H., & Tommerup, N. (2011). A balanced translocation disrupts SYNGAP1 in a patient with intellectual disability, speech impairment, and epilepsy with myoclonic absences (EMA). *Epilepsia*, *52*(12).

Knapska, E., Macias, M., Mikosz, M., Nowak, A., Owczarek, D., Wawrzyniak, M., ... & Maren, S. (2012). Functional anatomy of neural circuits regulating fear and extinction. *Proceedings of the National Academy of Sciences*, *109*(42), 17093-17098.

Knuesel, I., Elliott, A., Chen, H. J., Mansuy, I. M., & Kennedy, M. B. (2005). A role for synGAP in regulating neuronal apoptosis. *European Journal of Neuroscience*, *21*(3), 611-621.

Knutson, B., Burgdorf, J., & Panksepp, J. (2002). Ultrasonic vocalizations as indices of affective states in rats. *Psychological bulletin*, *128*(6), 961.

Kogan, J. H., Frankland, P. W., & Silva, A. J. (2000). Long-term memory underlying hippocampus-dependent social recognition in mice. *Hippocampus*, *10*(1), 47-56.

Kolb, B., & Walkey, J. (1987). Behavioural and anatomical studies of the posterior parietal cortex in the rat. *Behavioural brain research*, *23*(2), 127-145.

Komiyama, N. H., Watabe, A. M., Carlisle, H. J., Porter, K., Charlesworth, P., Monti, J., ... & O'Dell, T. J. (2002). SynGAP regulates ERK/MAPK signaling, synaptic plasticity, and learning in the complex with postsynaptic density 95 and NMDA receptor. *Journal of Neuroscience*, *22*(22), 9721-9732.

Krapivinsky, G., Medina, I., Krapivinsky, L., Gapon, S., & Clapham, D. E. (2004). SynGAP-MUPP1-CaMKII synaptic complexes regulate p38 MAP kinase activity and NMDA receptor-dependent synaptic AMPA receptor potentiation. *Neuron*, *43*(4), 563-574.

Krepischi, A. C. V., Rosenberg, C., Costa, S. S., Crolla, J. A., Huang, S., & Vianna-Morgante, A. M. (2010). A Novel De Novo Microdeletion Spanning theSYNGAP1 Gene on the Short Arm of Chromosome 6 Associated With Mental Retardation.

Kroon, T., Sierksma, M. C., & Meredith, R. M. (2013). Investigating mechanisms underlying neurodevelopmental phenotypes of autistic and intellectual disability disorders: a perspective. *Frontiers in systems neuroscience*, *7*.

Kumar, S., & Hedges, S. B. (1998). A molecular timescale for vertebrate evolution. Nature, 392(6679), 917– 920.

Kwakye, L. D., Foss-Feig, J. H., Cascio, C. J., Stone, W. L., & Wallace, M. T. (2010). Altered auditory and multisensory temporal processing in autism spectrum disorders. *Frontiers in integrative neuroscience*, *4*.

La Fata, G., Gärtner, A., Domínguez-Iturza, N., Dresselaers, T., Dawitz, J., Poorthuis, R. B., ... & Dotti, C. G. (2014). FMRP regulates multipolar to bipolar transition affecting neuronal migration and cortical circuitry. *Nature neuroscience*, *17*(12), 1693-1700.

Langford, D. J., Crager, S. E., Shehzad, Z., Smith, S. B., Sotocinal, S. G., Levenstadt, J. S., ... & Mogil, J. S. (2006). Social modulation of pain as evidence for empathy in mice. *Science*, *312*(5782), 1967-1970.

Langford, D. J., Crager, S. E., Shehzad, Z., Smith, S. B., Sotocinal, S

Langston, R. F., & Wood, E. R. (2010). Associative recognition and the hippocampus: Differential effects of hippocampal lesions on object-place, object-context and object-place-context memory. *Hippocampus*, *20*(10), 1139-1153.

Langville, A. N., Meyer, C. D., Albright, R., Cox, J., & Duling, D. (2014). Algorithms, initializations, and convergence for the nonnegative matrix factorization. *arXiv preprint arXiv:1407.7299*.

Laviola, G., & Terranova, M. L. (1998). The developmental psychobiology of behavioural plasticity in mice: the role of social experiences in the family unit. *Neuroscience & Biobehavioral Reviews*, *23*(2), 197-213.

Lee, I., Hunsaker, M. R., & Kesner, R. P. (2005). The role of hippocampal subregions in detecting spatial novelty. *Behavioral neuroscience*, *119*(1), 145.

Leonard, A. S., Lim, I. A., Hemsworth, D. E., Horne, M. C., & Hell, J. W. (1999). Calcium/calmodulin-dependent protein kinase II is associated with the N-methyl-D-aspartate receptor. *Proceedings of the National Academy of Sciences*, *96*(6), 3239-3244.

Leonard, H., & Wen, X. (2002). The epidemiology of mental retardation: challenges and opportunities in the new millennium. *Developmental Disabilities Research Reviews*, *8*(3), 117-134.

Lever, C., Burton, S., & O'Keefe, J. (2006). Rearing on hind legs, environmental novelty, and the hippocampal formation. *Reviews in the neurosciences*, *17*(1-2), 111-134.

Li, S., Tian, X., Hartley, D. M., & Feig, L. A. (2006). Distinct roles for Ras-guanine nucleotide-releasing factor 1 (Ras-GRF1) and Ras-GRF2 in the induction of long-term potentiation and long-term depression. *Journal of Neuroscience*, *26*(6), 1721-1729.

Li, W., Okano, A., Tian, Q. B., Nakayama, K., Furihata, T., Nawa, H., & Suzuki, T. (2001). Characterization of a novel synGAP isoform, synGAP-β. *Journal of Biological Chemistry*, *276*(24), 21417-21424.

Li, W., Teng, F., Li, T., & Zhou, Q. (2013). Simultaneous generation and germline transmission of multiple gene mutations in rat using CRISPR-Cas systems. *Nature biotechnology*, *31*(8), 684-686.

Licata, A. M., Kaufman, M. T., Raposo, D., Ryan, M. B., Sheppard, J. P., & Churchland, A. K. (2017). Posterior parietal cortex guides visual decisions in rats. *Journal of Neuroscience*, *37*(19), 4954-4966.

Liebenauer, L. L., & Slotnick, B. M. (1996). Social organization and aggression in a group of olfactory bulbectomized male mice. *Physiology & behavior*, *60*(2), 403-409.

Lister, R. G. (1987). The use of a plus-maze to measure anxiety in the mouse. *Psychopharmacology*, *92*(2), 180-185.

Liu, D., Gu, X., Zhu, J., Zhang, X., Han, Z., Yan, W., ... & Chen, Z. (2014). Medial prefrontal activity during delay period contributes to learning of a working memory task. *Science*, *346*(6208), 458-463.

Liu, H., Chen, Y., Niu, Y., Zhang, K., Kang, Y., Ge, W., ... & Jing, B. (2014). TALEN-mediated gene mutagenesis in rhesus and cynomolgus monkeys. *Cell stem cell*, *14*(3), 323-328.

Liu, P., & Bilkey, D. K. (2001). The effect of excitotoxic lesions centered on the hippocampus or perirhinal cortex in object recognition and spatial memory tasks. *Behavioral neuroscience*, *115*(1), 94.

Liu, Z., Li, X., Zhang, J. T., Cai, Y. J., Cheng, T. L., Cheng, C., ... & Bian, W. J. (2016). Autism-like behaviours and germline transmission in transgenic monkeys overexpressing MeCP2. *Nature*, *530*(7588), 98.

Liu, Z., Zhou, X., Zhu, Y., Chen, Z. F., Yu, B., Wang, Y., ... & Zhang, Y. F. (2014). Generation of a monkey with MECP2 mutations by TALEN-based gene targeting. *Neuroscience bulletin*, *30*(3), 381-386.

Luongo, F. J., Horn, M. E., & Sohal, V. S. (2016). Putative microcircuit-level substrates for attention are disrupted in mouse models of autism. *Biological psychiatry*, *79*(8), 667-675.

Lyon, S., & Langston, R. F. (2014). Memory ontogeny in the juvenile rat. In *93.20/SS15*. SfN, Washington DC: Society for Neuroscience.

Maaswinkel, H., Baars, A. M., Gispen, W. H., & Spruijt, B. M. (1996). Roles of the basolateral amygdala and hippocampus in social recognition in rats. *Physiology & Behavior*, *60*(1), 55-63.

Macknin, J. B., Higuchi, M., Lee, V. M. Y., Trojanowski, J. Q., & Doty, R. L. (2004). Olfactory dysfunction occurs in transgenic mice overexpressing human τ protein. *Brain research*, *1000*(1), 174-178.

Madisen, L., Zwingman, T. A., Sunkin, S. M., Oh, S. W., Zariwala, H. A., Gu, H., ... & Lein, E. S. (2010). A robust and high-throughput Cre reporting and characterization system for the whole mouse brain. *Nature neuroscience*, *13*(1), 133-140.

Man, H. Y., Wang, Q., Lu, W. Y., Ju, W., Ahmadian, G., Liu, L., ... & Becker, L. E. (2003). Activation of PI3-kinase is required for AMPA receptor insertion during LTP of mEPSCs in cultured hippocampal neurons. *Neuron*, *38*(4), 611-624.

Maren, S., & Quirk, G. J. (2004). Neuronal signalling of fear memory. *Nature Reviews Neuroscience*, *5*(11), 844-852.

Mariusz, P. & Moryl, E. (1994) Antidepressant activity of non-competitive and competitive NMDA receptor antagonists in a chronic mild stress model of depression. *Eur. J. Pharmacol.*, **263**, 1–7.

Markram, H., Toledo-Rodriguez, M., Wang, Y., Gupta, A., Silberberg, G., & Wu, C. (2004). Interneurons of the neocortical inhibitory system. *Nature reviews. Neuroscience*, *5*(10), 793.

Markram, K., & Markram, H. (2010). The intense world theory–a unifying theory of the neurobiology of autism. *Frontiers in human neuroscience*, *4*.

Marshel, J. H., Garrett, M. E., Nauhaus, I., & Callaway, E. M. (2011). Functional specialization of seven mouse visual cortical areas. *Neuron*, *72*(6), 1040-1054.

Martin, L. A., Ashwood, P., Braunschweig, D., Cabanlit, M., Van de Water, J., & Amaral, D. G. (2008). Stereotypies and hyperactivity in rhesus monkeys exposed to IgG from mothers of children with autism. *Brain, behavior, and immunity*, *22*(6), 806-816.

Maski, K. P., Jeste, S. S., & Spence, S. J. (2011). Common neurological co-morbidities in autism spectrum disorders. *Current opinion in pediatrics*, *23*(6), 609.

Matochik, J. A. (1988). Role of the main olfactory system in recognition between individual spiny mice. *Physiology & behavior*, *42*(3), 217-222.

McGinley, M. J., Vinck, M., Reimer, J., Batista-Brito, R., Zagha, E., Cadwell, C. R., ... & McCormick, D. A. (2015). Waking state: rapid variations modulate neural and behavioral responses. *Neuron*, *87*(6), 1143-1161.

McHugh, S. B., Deacon, R. M. J., Rawlins, J. N. P., & Bannerman, D. M. (2004). Amygdala and ventral hippocampus contribute differentially to mechanisms of fear and anxiety. *Behavioral neuroscience*, *118*(1), 63.

McKibben, C. E., Reynolds, G. P., & Jenkins, T. A. (2014). Analysis of sociability and preference for social novelty in the acute and subchronic phencyclidine rat. *Journal of Psychopharmacology*, *28*(10), 955-963.

McMahon, A. C., Barnett, M. W., O'leary, T., Stoney, P. N., Collins, M. O., Papadia, S., ... & Wyllie, D. J. A. (2012). SynGAP isoforms exert opposing effects on synaptic strength. *Nature communications*, *3*, 900.

McNaughton, B. L., Mizumori, S. J. Y., Barnes, C. A., Leonard, B. J., Marquis, M., & Green, E. J. (1994). Cortical representation of motion during unrestrained spatial navigation in the rat. *Cerebral Cortex*, *4*(1), 27-39.

Mefford, H. C., Cooper, G. M., Zerr, T., Smith, J. D., Baker, C., Shafer, N., ... & Eichler, E. E. (2009). A method for rapid, targeted CNV genotyping identifies rare variants associated with neurocognitive disease. *Genome research*, *19*(9), 1579-1585.

Merali, Z., McIntosh, J., & Anisman, H. (2004). Anticipatory cues differentially provoke in vivo peptidergic and monoaminergic release at the medial prefrontal cortex. *Neuropsychopharmacology*, *29*(8), 1409.

Meredith, R. M., Dawitz, J., & Kramvis, I. (2012). Sensitive time-windows for susceptibility in neurodevelopmental disorders. *Trends in neurosciences*, *35*(6), 335-344.

Metherate, R., Cox, C. L., & Ashe, J. H. (1992). Cellular bases of neocortical activation: modulation of neural oscillations by the nucleus basalis and endogenous acetylcholine. *Journal of Neuroscience*, *12*(12), 4701-4711.

Meyers, E. M., Qi, X. L., & Constantinidis, C. (2012). Incorporation of new information into prefrontal cortical activity after learning working memory tasks. *Proceedings of the National Academy of Sciences*, *109*(12), 4651-4656.

Mignot, C., Von Stülpnagel, C., Nava, C., Ville, D., Sanlaville, D., Lesca, G., ... & Borggraefe, I. (2016). Genetic and neurodevelopmental spectrum of SYNGAP1-associated intellectual disability and epilepsy. *Journal of medical genetics*, *53*(8), 511-522.

Mikoshiba, K. (2006). Inositol 1, 4, 5-trisphosphate (IP3) receptors and their role in neuronal cell function. *Journal of neurochemistry*, *97*(6), 1627-1633.

Mirzaa, G. M., Millen, K. J., Barkovich, A. J., Dobyns, W. B., & Paciorkowski, A. R. (2014). The Developmental Brain Disorders Database (DBDB): a curated neurogenetics knowledge base with clinical and research applications. *American Journal of Medical Genetics Part A*, *164*(6), 1503-1511.

Mitchell, D., Maren, S., & Hwang, R. (1993). The effects of hippocampal lesions on two neotic choice tasks.

Mohan, H., de Haan, R., Mansvelder, H. D., & de Kock, C. P. (2017). The Posterior Parietal Cortex as Integrative Hub for Whisker Sensorimotor Information. *Neuroscience*.

Montagutelli, X. (2000). Effect of the genetic background on the phenotype of mouse mutations. *Journal of the American Society of Nephrology*, *11*(suppl 2), S101-S105.

Moon, I. S., Sakagami, H., Nakayama, J., & Suzuki, T. (2008). Differential distribution of synGAPα1 and synGAPβ isoforms in rat neurons. *Brain research*, *1241*, 62-75.

Morales, B., Choi, S. Y., & Kirkwood, A. (2002). Dark rearing alters the development of GABAergic transmission in visual cortex. *Journal of Neuroscience*, *22*(18), 8084-8090.

Moran, J., & Desimone, R. (1985). Selective attention gates visual processing in the extrastriate cortex. *Frontiers in cognitive neuroscience*, *229*, 342-345.

Morris, R. (1984). Developments of a water-maze procedure for studying spatial learning in the rat. *Journal of neuroscience methods*, *11*(1), 47-60.

Moy, S. S., Nadler, J. J., Perez, A., Barbaro, R. P., Johns, J. M., Magnuson, T. R., Piven, J. and Crawley, J. N. (2004), Sociability and preference for social novelty in five inbred strains: an approach to assess autistic-like behavior in mice. Genes, Brain and Behavior, 3: 287–302.

Muhia M., Yee B. K., Feldon J., Markopoulos F., Knuesel I. (2010). Disruption of hippocampus-regulated behavioural and cognitive processes by heterozygous constitutive deletion of SynGAP. Eur. J. Neurosci. 31, 529–543.

Mumby, D. G., Gaskin, S., Glenn, M. J., Schramek, T. E., & Lehmann, H. (2002). Hippocampal damage and exploratory preferences in rats: memory for objects, places, and contexts. *Learning & Memory*, *9*(2), 49-57.

Munger, S. D. (2009). Olfaction: noses within noses. *Nature*, *459*(7246), 521-522.

Nadler, J. J., Moy, S. S., Dold, G., Simmons, N., Perez, A., Young, N. B., ... & Crawley, J. N. (2004). Automated apparatus for quantitation of social approach behaviors in mice. *Genes, Brain and Behavior*, *3*(5), 303-314.

Nakamura, K. (1999). Auditory spatial discriminatory and mnemonic neurons in rat posterior parietal cortex. *Journal of Neurophysiology*, *82*(5), 2503-2517.

National Academies of Sciences, Engineering, and Medicine. (2015). *Mental disorders and disabilities among low-income children*. National Academies Press.

Nelson, R. J., & Trainor, B. C. (2007). Neural mechanisms of aggression. *Nature Reviews Neuroscience*, *8*(7), 536-546.

Nicolson, R., Craven-Thuss, B., & Smith, J. (2006). AProspective, Open-Label Trial of Galantamine in Autistic Disorder. *Journal of Child & Adolescent Psychopharmacology*, *16*(5), 621-629.

Niederhofer, H., Staffen, W., & Mair, A. (2002). Galantamine may be effective in treating autistic disorder. *BMJ: British Medical Journal*, *325*(7377), 1422.

Niell, C. M., & Stryker, M. P. (2010). Modulation of visual responses by behavioral state in mouse visual cortex. *Neuron*, *65*(4), 472-479.

Nimchinsky, E. A., Sabatini, B. L., & Svoboda, K. (2002). Structure and function of dendritic spines. *Annual review of physiology*, *64*(1), 313-353.

Nitz, D. A. (2006). Tracking route progression in the posterior parietal cortex. *Neuron*, *49*(5), 747-756.

O'keefe, J., & Nadel, L. (1978). *The hippocampus as a cognitive map*. Oxford: Clarendon Press.

O'roak, B. J., Deriziotis, P., Lee, C., Vives, L., Schwartz, J. J., Girirajan, S., ... & Rieder, M. J. (2011). Exome sequencing in sporadic autism spectrum disorders identifies severe de novo mutations. *Nature genetics*, *43*(6), 585-589.

O'roak, B. J., Stessman, H. A., Boyle, E. A., Witherspoon, K. T., Martin, B., Lee, C., ... & Bernier, R. (2014). Recurrent de novo mutations implicate novel genes underlying simplex autism risk. *Nature communications*, *5*, 5595.

Oddi, D., Subashi, E., Middei, S., Bellocchio, L., Lemaire-Mayo, V., Guzmán, M., ... & Pietropaolo, S. (2015). Early social enrichment rescues adult behavioral and brain abnormalities in a mouse model of fragile X syndrome. *Neuropsychopharmacology*, *40*(5), 1113-1122.

Oh, J. S., Manzerra, P., & Kennedy, M. B. (2004). Regulation of the neuron-specific Ras GTPase-activating protein, synGAP, by Ca2+/calmodulin-dependent protein kinase II. *Journal of Biological Chemistry*, *279*(17), 17980-17988.

Okun, M., Steinmetz, N., Cossell, L., Iacaruso, M. F., Ko, H., Barthó, P., ... & Harris, K. D. (2015). Diverse coupling of neurons to populations in sensory cortex. *Nature*, *521*(7553), 511.

Olcese, U., Iurilli, G., & Medini, P. (2013). Cellular and synaptic architecture of multisensory integration in the mouse neocortex. *Neuron*, *79*(3), 579-593.

Olshausen, B. A., & Field, D. J. (2004). Sparse coding of sensory inputs. *Current opinion in neurobiology*, *14*(4), 481-487.

Olton, D. S., Walker, J. A., & Wolf, W. A. (1982). A disconnection analysis of hippocampal function. *Brain research*, *233*(2), 241-253.

Oñativia, Jon, Simon R. Schultz, and Pier Luigi Dragotti. 2013. "A Finite Rate of Innovation Algorithm for Fast and Accurate Spike Detection from TwoPhoton Calcium Imaging." Journal of Neural Engineering 10 (4): 046017

Orsini, C. A., & Maren, S. (2012). Neural and cellular mechanisms of fear and extinction memory formation. *Neuroscience & Biobehavioral Reviews*, *36*(7), 1773-1802.

Orsini, C. A., Kim, J. H., Knapska, E., & Maren, S. (2011). Hippocampal and prefrontal projections to the basal amygdala mediate contextual regulation of fear after extinction. *Journal of Neuroscience*, *31*(47), 17269-17277.

Ozkan, E. D., Creson, T. K., Kramár, E. A., Rojas, C., Seese, R. R., Babyan, A. H., ... & Miller, C. A. (2014). Reduced cognition in Syngap1 mutants is caused by isolated damage within developing forebrain excitatory neurons. *Neuron*, *82*(6), 1317-1333.

Pacey, L. K., & Doering, L. C. (2007). Developmental expression of FMRP in the astrocyte lineage: implications for fragile X syndrome. *Glia*, *55*(15), 1601-1609.

Pakan, J. M., Lowe, S. C., Dylda, E., Keemink, S. W., Currie, S. P., Coutts, C. A., & Rochefort, N. L. (2016). Behavioral-state modulation of inhibition is context-dependent and cell type specific in mouse visual cortex. *Elife*, *5*, e14985.

Parker, M. J., Fryer, A. E., Shears, D. J., Lachlan, K. L., McKee, S. A., Magee, A. C., ... & Lederer, D. (2015). De novo, heterozygous, loss-of-function mutations in SYNGAP1 cause a syndromic form of intellectual disability. *American Journal of Medical Genetics Part A*, *167*(10), 2231-2237.

Parpura, V., Heneka, M. T., Montana, V., Oliet, S. H., Schousboe, A., Haydon, P. G., ... & Pekny, M. (2012). Glial cells in (patho) physiology. *Journal of neurochemistry*, *121*(1), 4-27.

Paukert, M., Agarwal, A., Cha, J., Doze, V. A., Kang, J. U., & Bergles, D. E. (2014). Norepinephrine controls astroglial responsiveness to local circuit activity. *Neuron*, *82*(6), 1263-1270.

Paxinos, G., & Franklin, K. B. (2004). *The mouse brain in stereotaxic coordinates*. Gulf Professional Publishing.

Peier, A. M., McIlwain, K. L., Kenneson, A., Warren, S. T., Paylor, R., & Nelson, D. L. (2000). (Over) correction of FMR1 deficiency with YAC transgenics: behavioral and physical features. *Human molecular genetics*, *9*(8), 1145-1159.

Pena, V., Hothorn, M., Eberth, A., Kaschau, N., Parret, A., Gremer, L., ... & Scheffzek, K. (2008). The C2 domain of SynGAP is essential for stimulation of the Rap GTPase reaction. *EMBO reports*, *9*(4), 350-355.

Perna, J. C., & Engelmann, M. (2015). Recognizing others: rodent's social memories. In *Social Behavior from Rodents to Humans* (pp. 25-45). Springer International Publishing.

Petersen, C. C., & Crochet, S. (2013). Synaptic computation and sensory processing in neocortical layer 2/3. *Neuron*, *78*(1), 28-48.

Pfeffer, C. K., Xue, M., He, M., Huang, Z. J., & Scanziani, M. (2013). Inhibition of inhibition in visual cortex: the logic of connections between molecularly distinct interneurons. *Nature neuroscience*, *16*(8), 1068-1076.

Pinto, L., Goard, M. J., Estandian, D., Xu, M., Kwan, A. C., Lee, S. H., ... & Dan, Y. (2013). Fast modulation of visual perception by basal forebrain cholinergic neurons. *Nature neuroscience*, *16*(12), 1857-1863.

Polack, P. O., Friedman, J., & Golshani, P. (2013). Cellular mechanisms of brain state-dependent gain modulation in visual cortex. *Nature neuroscience*, *16*(9), 1331-1339.

Porter, K., Komiyama, N. H., Vitalis, T., Kind, P. C., & Grant, S. G. (2005). Differential expression of two NMDA receptor interacting proteins, PSD-95 and SynGAP during mouse development. *European Journal of Neuroscience*, *21*(2), 351-362.

Portera-Cailliau, C. (2012). Which comes first in fragile X syndrome, dendritic spine dysgenesis or defects in circuit plasticity?. *The Neuroscientist*, *18*(1), 28-44.

Pouille, F., & Scanziani, M. (2001). Enforcement of temporal fidelity in pyramidal cells by somatic feed-forward inhibition. *Science*, *293*(5532), 1159-1163.

Poulet, J. F., & Petersen, C. C. (2008). Internal brain state regulates membrane potential synchrony in barrel cortex of behaving mice. *Nature*, *454*(7206), 881.

Prchalova, D., Havlovicova, M., Sterbova, K., Stranecky, V., Hancarova, M., & Sedlacek, Z. (2017). Analysis of 31-year-old patient with SYNGAP1 gene defect points to importance of variants in broader splice regions and reveals developmental trajectory of SYNGAP1-associated phenotype: case report. *BMC Medical Genetics*, *18*(1), 62.

Provenzano, G., Chelini, G., & Bozzi, Y. (2017). Genetic control of social behavior: Lessons from mutant mice. *Behavioural brain research*, *325*, 237-250.

Purcell, S. M., Moran, J. L., Fromer, M., Ruderfer, D., Solovieff, N., Roussos, P., ... & Duncan, L. (2014). A polygenic burden of rare disruptive mutations in schizophrenia. *Nature*, *506*(7487), 185.

Quintana, J., & Fuster, J. M. (1999). From perception to action: temporal integrative functions of prefrontal and parietal neurons. *Cerebral Cortex*, *9*(3), 213-221.

Rama, S., Krapivinsky, G., Clapham, D. E., & Medina, I. (2008). The MUPP1–SynGAPα protein complex does not mediate activity-induced LTP. *Molecular and Cellular Neuroscience*, *38*(2), 183-188.

Ramocki, M. B., Peters, S. U., Tavyev, Y. J., Zhang, F., Carvalho, C., Schaaf, C. P., ... & Zoghbi, H. Y. (2009). Autism and other neuropsychiatric symptoms are prevalent in individuals with MeCP2 duplication syndrome. *Annals of neurology*, *66*(6), 771-782.

Randrup, A., & Munkvad, I. (1974). Pharmacology and physiology of stereotyped behavior. *Journal of psychiatric research*, *11*, 1-10.

Rane, P., Cochran, D., Hodge, S. M., Haselgrove, C., Kennedy, D., & Frazier, J. A. (2015). Connectivity in autism: A review of MRI connectivity studies. *Harvard review of psychiatry*, *23*(4), 223.

Raposo, D., Kaufman, M. T., & Churchland, A. K. (2014). A category-free neural population supports evolving demands during decision-making. *Nature neuroscience*, *17*(12), 1784-1792.

Ratering D., Baltes C., Nordmeyer-Massner J., Marek D., Rudin M. (2008). Performance of a 200-MHz cryogenic RF probe designed for MRI and MRS of the murine brain. *Magn. Reson. Med.* 591440–1447.

Rauch, A., Wieczorek, D., Graf, E., Wieland, T., Endele, S., Schwarzmayr, T., ... & Dufke, A. (2012). Range of genetic mutations associated with severe non-syndromic sporadic intellectual disability: an exome sequencing study. *The Lancet*, *380*(9854), 1674-1682.

Redin, C., Gérard, B., Lauer, J., Herenger, Y., Muller, J., Quartier, A., ... & Le Gras, S. (2014). Efficient strategy for the molecular diagnosis of intellectual disability using targeted high-throughput sequencing. *Journal of medical genetics*, *51*(11), 724-736.

Reep, R. L., Chandler, H. C., King, V., & Corwin, J. V. (1994). Rat posterior parietal cortex: topography of corticocortical and thalamic connections. *Experimental Brain Research*, *100*(1), 67-84.

Reimer, J., Froudarakis, E., Cadwell, C. R., Yatsenko, D., Denfield, G. H., & Tolias, A. S. (2014). Pupil fluctuations track fast switching of cortical states during quiet wakefulness. *Neuron*, *84*(2), 355-362.

Renart, A., De La Rocha, J., Bartho, P., Hollender, L., Parga, N., Reyes, A., & Harris, K. D. (2010). The asynchronous state in cortical circuits. *science*, *327*(5965), 587-590.

Renaud, S., Michaux, J., Schmidt, D. N., Aguilar, J. P., Mein, P., & Auffray, J. C. (2005). Morphological evolution, ecological diversification and climate change in rodents. *Proceedings of the Royal Society of London B: Biological Sciences*, *272*(1563), 609-617.

Resendez, S. L., Jennings, J. H., Ung, R. L., Namboodiri, V. M. K., Zhou, Z. C., Otis, J. M., ... & Stuber, G. D. (2016). Visualization of cortical, subcortical, and deep brain neural circuit dynamics during naturalistic mammalian behavior with head-mounted microscopes and chronically implanted lenses. *Nature protocols*, *11*(3), 566.

Restivo, L., Ferrari, F., Passino, E., Sgobio, C., Bock, J., Oostra, B. A., ... & Ammassari-Teule, M. (2005). Enriched environment promotes behavioral and morphological recovery in a mouse model for the fragile X syndrome. *Proceedings of the National Academy of Sciences of the United States of America*, *102*(32), 11557-11562.

Ricceri, L., Moles, A., & Crawley, J. (2007). Behavioral phenotyping of mouse models of neurodevelopmental disorders: relevant social behavior patterns across the life span. *Behavioural brain research*, *176*(1), 40-52.

Riehle, A., Grün, S., Diesmann, M., & Aertsen, A. (1997). Spike synchronization and rate modulation differentially involved in motor cortical function. *Science*, *278*(5345), 1950-1953.

Rippon, G., Brock, J., Brown, C., & Boucher, J. (2007). Disordered connectivity in the autistic brain: challenges for the 'new psychophysiology'. *International journal of psychophysiology*, *63*(2), 164-172.

Riva, D., Bulgheroni, S., Aquino, D., Di Salle, F., Savoiardo, M., & Erbetta, A. (2011). Basal forebrain involvement in low-functioning autistic children: a voxel-based morphometry study. *American Journal of Neuroradiology*, *32*(8), 1430-1435.

Rochefort, N. L., Garaschuk, O., Milos, R. I., Narushima, M., Marandi, N., Pichler, B., ... & Konnerth, A. (2009). Sparsification of neuronal activity in the visual cortex at eye-opening. *Proceedings of the National Academy of Sciences*, *106*(35), 15049-15054.

Rodriguez, R., Kallenbach, U., Singer, W., & Munk, M. H. (2004). Short-and long-term effects of cholinergic modulation on gamma oscillations and response synchronization in the visual cortex. *Journal of Neuroscience*, *24*(46), 10369-10378.

Ropers, H. H. (2008). Genetics of intellectual disability. *Current opinion in genetics & development*, *18*(3), 241-250.

Ropers, H. H. (2010). Genetics of early onset cognitive impairment. *Annual review of genomics and human genetics*, *11*, 161-187.

Rosenkranz, J. A., Frick, A., & Johnston, D. (2009). Kinase-dependent modification of dendritic excitability after long-term potentiation. *The Journal of physiology*, *587*(1), 115-125.

Roth, M. M., Helmchen, F., & Kampa, B. M. (2012). Distinct functional properties of primary and posteromedial visual area of mouse neocortex. *Journal of Neuroscience*, *32*(28), 9716-9726.

Rothschild, Gideon, Israel Nelken, and Adi Mizrahi. "Functional organization and population dynamics in the mouse primary auditory cortex." *Nature neuroscience* 13.3 (2010): 353-360.

Roy, A., Roy, M., & Clarke, D. (2016). *The psychiatry of intellectual disability*. CRC Press.

Rudie, J. D., & Dapretto, M. (2013). Convergent evidence of brain overconnectivity in children with autism?. *Cell reports*, *5*(3), 565-566.

Rumbaugh, G., Adams, J. P., Kim, J. H., & Huganir, R. L. (2006). SynGAP regulates synaptic strength and mitogen-activated protein kinases in cultured neurons. *Proceedings of the National Academy of Sciences of the United States of America*, *103*(12), 4344-4351.

Saglietti, L., Dequidt, C., Kamieniarz, K., Rousset, M. C., Valnegri, P., Thoumine, O., ... & Sheng, M. (2007). Extracellular interactions between GluR2 and N-cadherin in spine regulation. *Neuron*, *54*(3), 461-477.

Sahay, A., Scobie, K. N., Hill, A. S., O'carroll, C. M., Kheirbek, M. A., Burghardt, N. S., ... & Hen, R. (2011). Increasing adult hippocampal neurogenesis is sufficient to improve pattern separation. *Nature*, *472*(7344), 466-470.

Salinas, E., & Sejnowski, T. J. (2001). Correlated neuronal activity and the flow of neural information. *Nature reviews. Neuroscience*, *2*(8), 539.

San Martín, A., & Pagani, M. R. (2014). Understanding intellectual disability through RASopathies. *Journal of Physiology-Paris*, *108*(4), 232-239.

Saneyoshi, T., Wayman, G., Fortin, D., Davare, M., Hoshi, N., Nozaki, N., ... & Soderling, T. R. (2008). Activity-dependent synaptogenesis: regulation by a CaM-kinase kinase/CaM-kinase I/βPIX signaling complex. *Neuron*, *57*(1), 94-107.

Sato, N., Tan, L., Tate, K., & Okada, M. (2015). Rats demonstrate helping behavior toward a soaked conspecific. Animal Cognition, 1039–1047.

Save, E., & Poucet, B. (2009). Role of the parietal cortex in long-term representation of spatial information in the rat. *Neurobiology of learning and memory*, *91*(2), 172-178.

Save, Y. (2000). Diagnostic and statistical manual of mental disorders. *American Psychiatric Association, 4th ed, text rev, Washington, DC: Author; Burket, RC, Schramm, LL, Therapists' attitudes about treating patients with eating disorders (1995) Southern Medical Journal*, *88*, 813-818.

Sawtell, N. B., Frenkel, M. Y., Philpot, B. D., Nakazawa, K., Tonegawa, S., & Bear, M. F. (2003). NMDA receptor-dependent ocular dominance plasticity in adult visual cortex. *Neuron*, *38*(6), 977-985.

Schafe, G. E., Doyère, V., & LeDoux, J. E. (2005). Tracking the fear engram: the lateral amygdala is an essential locus of fear memory storage. *Journal of Neuroscience*, *25*(43), 10010-10014.

Schneider, T., & Przewlocki, R. (2005). Behavioral alterations in rats prenatally exposed to valproic acid: animal model of autism. *Neuropsychopharmacology*, *30*(1), 80.

Schneider, T., Roman, A., Basta-Kaim, A., Kubera, M., Budziszewska, B., Schneider, K., & Przewłocki, R. (2008). Gender-specific behavioral and immunological alterations in an animal model of autism induced by prenatal exposure to valproic acid. *Psychoneuroendocrinology*, *33*(6), 728-740.

Semple, B. D., Blomgren, K., Gimlin, K., Ferriero, D. M., & Noble-Haeusslein, L. J. (2013). Brain development in rodents and humans: Identifying benchmarks of maturation and vulnerability to injury across species. *Progress in neurobiology*, *106*, 1-16.

Semple, B. D., Canchola, S. A., & Noble-Haeusslein, L. J. (2012). Deficits in social behavior emerge during development after pediatric traumatic brain injury in mice. *Journal of neurotrauma*, *29*(17), 2672-2683.

Senn, V., Wolff, S. B., Herry, C., Grenier, F., Ehrlich, I., Gründemann, J., ... & Lüthi, A. (2014). Long-range connectivity defines behavioral specificity of amygdala neurons. *Neuron*, *81*(2), 428-437.

Shadlen, M. N., & Newsome, W. T. (2001). Neural basis of a perceptual decision in the parietal cortex (area LIP) of the rhesus monkey. *Journal of neurophysiology*, *86*(4), 1916-1936.

Shen, J. X., & Yakel, J. L. (2009). Nicotinic acetylcholine receptor-mediated calcium signaling in the nervous system. *Acta pharmacologica Sinica*, *30*(6), 673.

Sheng, M., & Kim, M. J. (2002). Postsynaptic signaling and plasticity mechanisms. *Science*, *298*(5594), 776-780.

Sherman, S. M., & Guillery, R. W. (2002). The role of the thalamus in the flow of information to the cortex. *Philosophical Transactions of the Royal Society of London B: Biological Sciences*, *357*(1428), 1695-1708.

Siddiqui, T. J., Pancaroglu, R., Kang, Y., Rooyakkers, A., & Craig, A. M. (2010). LRRTMs and neuroligins bind neurexins with a differential code to cooperate in glutamate synapse development. *Journal of Neuroscience*, *30*(22), 7495-7506.

Silva, A. J., & Ehninger, D. (2009). Adult reversal of cognitive phenotypes in neurodevelopmental disorders. *Journal of neurodevelopmental disorders*, *1*(2), 150.

Silverman, J. L., Yang, M., Lord, C., & Crawley, J. N. (2010). Behavioural phenotyping assays for mouse models of autism. *Nature Reviews Neuroscience*, *11*(7), 490-502.

Silvestre, J.S., Nadal, R., Pallares, M. & Ferre, N. (1997) Acute effects of ketamine in the holeboard, the elevated-plus maze, and the social interaction test in Wistar rats. *Depress. Anxiety*, **5**, 29–33.

Simonoff, E., Pickles, A., Charman, T., Chandler, S., Loucas, T., & Baird, G. (2008). Psychiatric disorders in children with autism spectrum disorders: prevalence, comorbidity, and associated factors in a population-derived sample. *Journal of the American Academy of Child & Adolescent Psychiatry*, *47*(8), 921-929.

Sippy, T., & Yuste, R. (2013). Decorrelating action of inhibition in neocortical networks. *Journal of Neuroscience*, *33*(23), 9813-9830.

Siviy, S. M., & Panksepp, J. (2011). In search of the neurobiological substrates for social playfulness in mammalian brains. Neuroscience and Biobehavioral Reviews.

Siviy, S. M., & Panksepp, J. (2011). In search of the neurobiological substrates for social playfulness in mammalian brains. *Neuroscience & Biobehavioral Reviews*, *35*(9), 1821-1830.

Smith, M. A., & Kohn, A. (2008). Spatial and temporal scales of neuronal correlation in primary visual cortex. *Journal of Neuroscience*, *28*(48), 12591-12603.

Smith, M. A., Jia, X., Zandvakili, A., & Kohn, A. (2013). Laminar dependence of neuronal correlations in visual cortex. *Journal of neurophysiology*, *109*(4), 940-947.

Sohal, V. S. (2012). Insights into cortical oscillations arising from optogenetic studies. *Biological psychiatry*, *71*(12), 1039-1045.

Sohal, V. S., Zhang, F., Yizhar, O., & Deisseroth, K. (2009). Parvalbumin neurons and gamma rhythms enhance cortical circuit performance. *Nature*, *459*(7247), 698.

Song, Y. H., Kim, J. H., Jeong, H. W., Choi, I., Jeong, D., Kim, K., & Lee, S. H. (2017). A neural circuit for auditory dominance over visual perception. *Neuron*, *93*(4), 940-954.

Specht, C. G., & Schoepfer, R. (2001). Deletion of the alpha-synuclein locus in a subpopulation of C57BL/6J inbred mice. *BMC neuroscience*, *2*(1), 11.

Spencer, C. M., Alekseyenko, O., Hamilton, S. M., Thomas, A. M., Serysheva, E., Yuva-Paylor, L. A., & Paylor, R. (2011). Modifying behavioral phenotypes in Fmr1KO mice: Genetic background differences reveal autistic-like responses. Autism Research, 4(1), 40–56.

Srinivasan, R., Huang, B. S., Venugopal, S., Johnston, A. D., Chai, H., Zeng, H., ... & Khakh, B. S. (2015). Ca2+ signaling in astrocytes from Ip3r2-/-mice in brain slices and during startle responses in vivo. *Nature neuroscience*, *18*(5), 708-717.

Steiner, A. P., & Redish, A. D. (2014). Behavioral and neurophysiological correlates of regret in rat decisionmaking on a neuroeconomic task. Nature Neuroscience, 17(7), 995–1002.

Stevens, B. (2008). Neuron-astrocyte signaling in the development and plasticity of neural circuits. *Neurosignals*, *16*(4), 278-288.

Stornetta, R. L., & Zhu, J. J. (2011). Ras and Rap signaling in synaptic plasticity and mental disorders. *The Neuroscientist*, *17*(1), 54-78.

Stranahan, A. M. (2011). Similarities and differences in spatial learning and object recognition between young male C57Bl/6J mice and Sprague-Dawley rats. Behavioral Neuroscience, 125(5), 791–795.

Su, A. I., Cooke, M. P., Ching, K. A., Hakak, Y., Walker, J. R., Wiltshire, T., ... & Patapoutian, A. (2002). Large-scale analysis of the human and mouse transcriptomes. *Proceedings of the National Academy of Sciences*, *99*(7), 4465-4470.

Swerdlow, N. R., Braff, D. L., & Geyer, M. A. (2000). Animal models of deficient sensorimotor gating: what we know, what we think we know, and what we hope to know soon. *Behavioural pharmacology*.

Swerdlow, N. R., Karban, B., Ploum, Y., Sharp, R., Geyer, M. A., & Eastvold, A. (2001). Tactile prepuff inhibition of startle in children with Tourette's syndrome: in search of an "fMRI-friendly" startle paradigm. *Biological psychiatry*, *50*(8), 578-585.

Sztainberg, Y., & Zoghbi, H. Y. (2016). Lessons learned from studying syndromic autism spectrum disorders. *Nature neuroscience*, *19*(11), 1408-1417.

Taniguchi, H., He, M., Wu, P., Kim, S., Paik, R., Sugino, K., ... & Miyoshi, G. (2011). A resource of Cre driver lines for genetic targeting of GABAergic neurons in cerebral cortex. *Neuron*, *71*(6), 995-1013.

Thomson, A. M., & Deuchars, J. (1994). Temporal and spatial properties of local circuits in neocortex. *Trends in neurosciences*, *17*(3), 119-126.

Till, S. M., Asiminas, A., Jackson, A. D., Katsanevaki, D., Barnes, S. A., Osterweil, E. K., … Kind, P. C. (2015). 227 Conserved hippocampal cellular pathophysiology but distinct behavioural deficits in a new rat model of FXS. Human Molecular Genetics, 24(21), 5977–5984.

Tønnesen, J., Katona, G., Rózsa, B., & Nägerl, U. V. (2014). Spine neck plasticity regulates compartmentalization of synapses. *Nature neuroscience*, *17*(5), 678-685.

Tsiola, A., Hamzei-Sichani, F., Peterlin, Z., & Yuste, R. (2003). Quantitative morphologic classification of layer 5 neurons from mouse primary visual cortex. *Journal of Comparative Neurology*, *461*(4), 415-428.

Uhlmann, E. J., Wong, M., Baldwin, R. L., Bajenaru, M. L., Onda, H., Kwiatkowski, D. J., ... & Gutmann, D. H. (2002). Astrocyte-specific TSC1 conditional knockout mice exhibit abnormal neuronal organization and seizures. *Annals of neurology*, *52*(3), 285-296.

Urban-Ciecko, J., & Barth, A. L. (2016). Somatostatin-expressing neurons in cortical networks. *Nature Reviews Neuroscience*, *17*(7), 401-409.

van Blarikom, W., Tan, I. Y., Aldenkamp, A. P., & van Gennep, A. T. G. (2006). Epilepsy, intellectual disability, and living environment: a critical review. *Epilepsy & Behavior*, *9*(1), 14-18.

Van Bokhoven, H. (2011). Genetic and epigenetic networks in intellectual disabilities. *Annual review of genetics*, *45*, 81-104.

Van Den Heuvel, M. P., Mandl, R. C., Kahn, R. S., Pol, H., & Hilleke, E. (2009). Functionally linked resting-state networks reflect the underlying structural connectivity architecture of the human brain. *Human brain mapping*, *30*(10), 3127-3141.

Van der Linden A, Van Camp N, Ramos-Cabrer P, Hoehn M. (2007) Current status of functional MRI on small animals: application to physiology, pathophysiology, and cognition. NMR Biomed, *20*(5):522-45.

Vazquez, L. E., Chen, H. J., Sokolova, I., Knuesel, I., & Kennedy, M. B. (2004). SynGAP regulates spine formation. *Journal of Neuroscience*, *24*(40), 8862-8872.

Vialou, V., Bagot, R. C., Cahill, M. E., Ferguson, D., Robison, A. J., Dietz, D. M., ... & Winstanley, C. A. (2014). Prefrontal cortical circuit for depression-and anxiety-related behaviors mediated by cholecystokinin: role of ΔFosB. *Journal of Neuroscience*, *34*(11), 3878-3887.

Vissers, L. E., de Ligt, J., Gilissen, C., Janssen, I., Steehouwer, M., de Vries, P., ... & van Bon, B. W. (2010). A de novo paradigm for mental retardation. *Nature genetics*, *42*(12), 1109-1112.

Vogel-Ciernia, A., & Wood, M. A. (2014). Examining object location and object recognition memory in mice. *Current protocols in neuroscience*, 8-31.

Vogelstein, J. T., Packer, A. M., Machado, T. A., Sippy, T., Babadi, B., Yuste, R., & Paninski, L. (2010). Fast nonnegative deconvolution for spike train inference from population calcium imaging. *Journal of neurophysiology*, *104*(6), 3691-3704.

von Stülpnagel, C., Funke, C., Haberl, C., Hörtnagel, K., Jüngling, J., Weber, Y. G., ... & Kluger, G. (2015). SYNGAP1 mutation in focal and generalized epilepsy: a literature overview and a case report with special aspects of the EEG. *Neuropediatrics*, *46*(04), 287-291.

Walkup, W. G., Mastro, T. L., Schenker, L. T., Vielmetter, J., Hu, R., Iancu, A., ... & Kennedy, M. B. (2016). A model for regulation by SynGAP-α1 of binding of synaptic proteins to PDZ-domain'Slots' in the postsynaptic density. *Elife*, *5*, e16813.

Walkup, W. G., Washburn, L., Sweredoski, M. J., Carlisle, H. J., Graham, R. L., Hess, S., & Kennedy, M. B. (2015). Phosphorylation of synaptic GTPase-activating protein (synGAP) by Ca2+/calmodulin-dependent protein kinase II (CaMKII) and cyclin-dependent kinase 5 (CDK5) alters the ratio of its GAP activity toward Ras and Rap GTPases. *Journal of Biological Chemistry*, *290*(8), 4908-4927.

Wallace, M. T., Ramachandran, R., & Stein, B. E. (2004). A revised view of sensory cortical parcellation. *Proceedings of the National Academy of Sciences*, *101*(7), 2167-2172.

Wang, F., Kessels, H. W., & Hu, H. (2014). The mouse that roared: neural mechanisms of social hierarchy. *Trends in Neurosciences*, *37*(11), 674-682.

Wang, X. B., Yang, Y., & Zhou, Q. (2007). Independent expression of synaptic and morphological plasticity associated with long-term depression. *Journal of Neuroscience*, *27*(45), 12419-12429.

Wang, X. J. (2001). Synaptic reverberation underlying mnemonic persistent activity. *Trends in neurosciences*, *24*(8), 455-463.

Wang, Y., Gupta, A., Toledo-Rodriguez, M., Wu, C. Z., & Markram, H. (2002). Anatomical, physiological, molecular and circuit properties of nest basket cells in the developing somatosensory cortex. *Cerebral Cortex*, *12*(4), 395-410.

Watabe, A. M., Zaki, P. A., & O'Dell, T. J. (2000). Coactivation of β-adrenergic and cholinergic receptors enhances the induction of long-term potentiation and synergistically activates mitogen-activated protein kinase in the hippocampal CA1 region. *Journal of Neuroscience*, *20*(16), 5924-5931.

White, E. L., & Keller, A. (1989). *Cortical circuits: synaptic organization of the cerebral cortex: structure, function, and theory* (pp. xvi-223). Boston: Birkhäuser.

Whitlock, J. R., Pfuhl, G., Dagslott, N., Moser, M. B., & Moser, E. I. (2012). Functional split between parietal and entorhinal cortices in the rat. *Neuron*, *73*(4), 789-802.

Whitlock, J. R., Sutherland, R. J., Witter, M. P., Moser, M. B., & Moser, E. I. (2008). Navigating from hippocampus to parietal cortex. *Proceedings of the National Academy of Sciences*, *105*(39), 14755-14762.

Wijetunge, L. S., Angibaud, J., Frick, A., Kind, P. C., & Nägerl, U. V. (2014). Stimulated emission depletion (STED) microscopy reveals nanoscale defects in the developmental trajectory of dendritic spine morphogenesis in a mouse model of fragile X syndrome. *Journal of Neuroscience*, *34*(18), 6405-6412.

Wijetunge, L. S., Chattarji, S., Wyllie, D. J., & Kind, P. C. (2013). Fragile X syndrome: from targets to treatments. *Neuropharmacology*, *68*, 83-96.

Wiley, J.L., Cristello, A.F. & Balster, R.L. (1995) Effects of site-selective NMDA receptor antagonists in an elevated plus-maze model of anxiety in mice. *Eur. J. Pharmacol.*, **294**, 101–107.

Willner, P. (1984). The validity of animal models of depression. *Psychopharmacology*, *83*(1), 1-16.

Winocur, G. (1990). Anterograde and retrograde amnesia in rats with dorsal hippocampal or dorsomedial thalamic lesions. *Behavioural brain research*, *38*(2), 145-154.

Winters, B. D., Bartko, S. J., Saksida, L. M., & Bussey, T. J. (2007). Scopolamine infused into perirhinal cortex improves object recognition memory by blocking the acquisition of interfering object information. *Learning & Memory*, *14*(9), 590-596.

Wolfer, D. P., Crusio, W. E., & Lipp, H. P. (2002). Knockout mice: simple solutions to the problems of genetic background and flanking genes. *Trends in neurosciences*, *25*(7), 336-340.

Wood, E. R., Dudchenko, P. A., & Eichenbaum, H. (1999). The global record of memory in hippocampal neuronal activity. *Nature*, *397*(6720), 613-616.

Woodley, S. K., & Baum, M. J. (2003). Effects of sex hormones and gender on attraction thresholds for volatile anal scent gland odors in ferrets. *Hormones and behavior*, *44*(2), 110-118.

Wotjak, C. T. (2003). C57BLack/BOX? The importance of exact mouse strain nomenclature. *Trends in Genetics*, *19*(4), 183-184.

Wrenn, C. C., Harris, A. P., Saavedra, M. C., & Crawley, J. N. (2003). Social transmission of food preference in mice: methodology and application to galanin-overexpressing transgenic mice. *Behavioral neuroscience*, *117*(1), 21.

Writzl, K., & Knegt, A. C. (2013). 6p21. 3 microdeletion involving the SYNGAP1 gene in a patient with intellectual disability, seizures, and severe speech impairment. *American journal of medical genetics Part A*, *161*(7), 1682-1685.

Xu, B., Ionita-Laza, I., Roos, J. L., Boone, B., Woodrick, S., Sun, Y., ... & Karayiorgou, M. (2012). De novo gene mutations highlight patterns of genetic and neural complexity in schizophrenia. *Nature genetics*, *44*(12), 1365-1369.

Xu, Q., Tam, M., & Anderson, S. A. (2008). Fate mapping Nkx2. 1-lineage cells in the mouse telencephalon. *Journal of Comparative Neurology*, *506*(1), 16-29.

Yamamuro, K., Kimoto, S., Rosen, K. M., Kishimoto, T., & Makinodan, M. (2015). Potential primary roles of glial cells in the mechanisms of psychiatric disorders. *Frontiers in cellular neuroscience*, *9*.

Yang, M., & Crawley, J. N. (2009). Simple behavioral assessment of mouse olfaction. *Current protocols in neuroscience*, 8-24.

Yang, Y., Tao-Cheng, J. H., Bayer, K. U., Reese, T. S., & Dosemeci, A. (2013). Camkii-Mediated Phosphorylation Regulates Distributions of Syngap-α1 and–α2 at the Postsynaptic Density. *PLoS One*, *8*(8), e71795.

Yang, Y., Tao-Cheng, J. H., Reese, T. S., & Dosemeci, A. (2011). SynGAP moves out of the core of the postsynaptic density upon depolarization. *Neuroscience*, *192*, 132-139.

Yates, A., Akanni, W., Amode, M. R., Barrell, D., Billis, K., Carvalho-Silva, D., ... & Girón, C. G. (2015). Ensembl 2016. *Nucleic acids research*, *44*(D1), D710-D716.

Yatsenko, D., Josić, K., Ecker, A. S., Froudarakis, E., Cotton, R. J., & Tolias, A. S. (2015). Improved estimation and interpretation of correlations in neural circuits. *PLoS computational biology*, *11*(3), e1004083.

Ye, X., & Carew, T. J. (2010). Small G protein signaling in neuronal plasticity and memory formation: the specific role of ras family proteins. *Neuron*, *68*(3), 340-361.

Yizhar, O., Fenno, L. E., Prigge, M., Schneider, F., Davidson, T. J., O'Shea, D. J., ... & Stehfest, K. (2011). Neocortical excitation/inhibition balance in information processing and social dysfunction. *Nature*, *477*(7363), 171-178.

Yuste, R. (2013). Electrical compartmentalization in dendritic spines. *Annual review of neuroscience*, *36*, 429-449.

Zhang, W., Vazquez, L., Apperson, M., & Kennedy, M. B. (1999). Citron binds to PSD-95 at glutamatergic synapses on inhibitory neurons in the hippocampus. *Journal of Neuroscience*, *19*(1), 96-108.

Zheng, J., Winkeler, A., Peyronneau, M.-A., Dollé, F., & Boisgard, R. (2016). Evaluation of PET Imaging Performance of the TSPO Radioligand [^{18}F]DPA-714 in Mouse and Rat Models of Cancer and Inflammation. *Molecular Imaging and Biology*, *18*, 127–134.

Zilles, K., Schröder, H., Schröder, U., Horvath, E., Werner, L., Luiten, P. G. M., ... & Strosberg, A. D. (1989). Distribution of cholinergic receptors in the rat and human neocortex. In *Central cholinergic synaptic transmission* (pp. 212-228). Birkhäuser Basel.

Zollino, M., Gurrieri, F., Orteschi, D., Marangi, G., Leuzzi, V., & Neri, G. (2011). Integrated analysis of clinical signs and literature data for the diagnosis and therapy of a previously undescribed 6p21. 3 deletion syndrome. *European Journal of Human Genetics*, *19*(2), 239.

Zupan, B. (2012). Nimfa: A python library for nonnegative matrix factorization. *Journal of Machine Learning Research*, *13*(Mar), 849-853.